CHAPTER 24

Mechanical Properties

Witold Brostow

Department of Materials Science and Engineering and Department of Physics,
University of North Texas, POBox 305310, Denton, TX 76203-5310, USA;
http://www.unt.edu/LAPOM/; brostow@unt.edu

24.1 RELAXATIONAL AND DESTRUCTIVE PROCESSES

24.1.1 Introduction; Service Performance and Reliability

Service performance and reliability constitute the bottom line of the entire polymer science and engineering. Since this statement might appear an exaggeration, let me immediately explain why. Synthesis of macromolecules is of interest primarily to synthetic chemists; polymer rheology is of interest to polymer rheologists; rotational injection molding is of interest to rotational injection molders; and so on. There is, however, an exception: reliability of polymeric materials and components is of interest to everybody—polymer scientists, polymer engineers, and all laymen including those who do not even know what the word "polymer" means. A very good example provides a little girl playing with a plastic doll. If the doll will break into pieces, the girl will certainly cry first. Somewhat later, however, some captains of industry might cry also.

Given this situation, let us formulate two highly pertinent and often asked questions:

1. Will a given polymeric material or component serve for a reasonable amount of time, or will it fail prematurely?
2. Can we get a material or component with better properties?

While both questions are often asked simultaneously, the second question deals with development of new materials and will not be considered per se in this Chapter; some answers are provided in Chapter 41 on polymer liquid crystals. The first question shows that failure is related to prediction of performance under given service conditions, and this is the way we are going to tackle this problem. More specifically, we need prediction of long-term performance from short-term tests, and this will be one of the leitmotivs of the present chapter.

The subject of this chapter is a vast one. There exist entire books devoted to it, including classical books by Ferry [1] and Aklonis and McKnight [2] as well as more recent ones [3,4].

24.1.2 The Chain Relaxation Capability (CRC)

Polymeric materials are all viscoelastic. The "face" each polymer shows to the observer—elastic, viscous flow, a combination of both—depends on the rate and duration of force application as well as on the nature of the material and external conditions including the temperature T. We discuss the nature of viscoelasticity below and additionally in Section 5. In general, properties of viscoelastics depend on *time*, in contrast to metals and ceramics.

To get a clear picture of the problem we are about to tackle, let us return to the girl with her plastic doll. Playing with the doll, the girl applies forces with various duration, direction(s) and application rate(s). For instance, the girl applied a tensile force to the head and both legs of the doll. The doll is a physical system which thus received energy U_0 from outside. Important for the girl—and for us—is the question number 1 formulated above. Will the energy U_0 be spent on destruction and eventual fracture of the doll, or will it get somehow dissipated and the doll will "live long"? We can write a general equation [5–7]

$$U = U_0 - U_b - U_r, \tag{24.1}$$

here U is the energy furnished from outside which at a given time has not yet been spent one way or the other; U_b (b for bond breaking) at the same time has been spent on destructive processes (such as crack formation or propagation); U_r at the given time has been dissipated, that is spent on nondestructive processes. Dissipation in a viscoelastic material is largely related to relaxational processes; the subscript r stands for relaxation. The quantities in Eq. (24.1) may refer to the material as a whole, but it is usually convenient to take them per unit weight of the polymer such as 1 g. U_r is quite important. It will be related soon to the chain relaxation capability (CRC) which has been defined [5–7] as follows:

CRC is the amount of external energy dissipated by relaxation in a unit of time per unit weight of polymer. In the following we shall use the abbreviation CRC for the concept and the symbol U_{CRC} for the, respective, amount of energy. Thus, at a given time t

$$U_r = \int_0^t U_{CRC} \mathrm{d}t. \tag{24.2}$$

The main reason why the concept of CRC is so useful is the following fact: it takes approximately 1,000 times more energy to break a primary chemical bond such as a carbon–carbon bond in a carbonic chain (what contributes to U_b and to crack propagation) than to execute a conformational rearrangement around the same bond. This is the basis of the following key statement [5–7]:

Relaxational processes have priority in the utilization of external energy. The excess energy which cannot be dissipated by such processes goes into destructive processes.

Nature is very kind to us! A viscoelastic material will relax rather than fracture—as long as it can go on relaxing. Unless there is a high concentration of external energy at a particular location, and as a consequence a number of primary bonds will break starting a crack, that energy will be dissipated. In contrast to nonchain materials, when we pull at a polymeric chain we gradually engage all segments of it; this by itself lowers the probability of local concentration of external energy and of destruction. Of course, there exist local energy concentrators and we shall discuss them below. There exist a number of constituents of CRC; we have just named one of them, but let us list them together:

1. Transmission of energy across the chain producing intensified vibrations of the segments.
2. Transmission—mainly by entanglements but also by segment motions—of energy from the chain to its neighbors.
3. Conformational rearrangements (such as *cis* into *trans* in carbonic macromolecules) executed by the chains.
4. Elastic energy storage resulting from bond stretching and angle changes.
5. Phase transformation toughening first observed by Kim and Robertson [8] and also studied by Karger-Kocsis [9].

Incidentally, fairly often the penultimate factor is excluded—with bad consequences for models based on such an assumption.

24.1.3 Correspondence Principles

Given the conclusions from the previous section, we naturally ask: when will a given polymeric material or component have high CRC—so that we can expect a reasonable service time? We need to answer this question before dealing with specific properties and specific classes of materials.

Paul Flory has shown how free volume v^f is important for thermophysical properties of materials—and not only polymeric ones [10,11]; see also a chapter by Orwoll in this Handbook [12]. There are also seminal papers by Litt and Tobolsky [13] and Tschoegl [14–16] showing importance of v^f for mechanical properties of viscoelastic materials. Consider now our CRC from this point of view. It is easy to envisage that the larger v^f is, the larger is the maneuvering ability of the chains—what means the higher is CRC. Using specific quantities (typically per 1 g), we write

$$v = v^* + v^f. \tag{24.3}$$

Here v is the total specific volume and v^* is the characteristic (hard-core, incompressible) volume. The last two names are based on the concept of "squeezing out" the whole free volume by applying a very high pressure so that only v^* remains. Instead of free volume, some people work with the reduced volume

$$\tilde{v} = v/v^* = 1 + v^f/v^*. \tag{24.4}$$

Equations such as (3) or (4) are not usable until a specific equation of state of the general form $\tilde{v} = \tilde{v}(\tilde{P}, \tilde{T})$ or $\tilde{P} = \tilde{P}(\tilde{v}, \tilde{T})$ is assumed. Here P is the pressure and we need two more reduced quantities:

$$\tilde{P} = P/P^* \text{ and } \tilde{T} = T/T^*. \tag{24.5}$$

The idea of reduced quantities goes all the way back to Johannes D. van der Waals in the eighteenth century. Thus, an equation of state requires three reducing quantities, v^*,P^*, and T^*. We have found repetitively good results using the Hartmann equation of state [17–19]

$$\tilde{P}\tilde{v}^5 = \tilde{T}^{3/2} - \ln \tilde{v}. \tag{24.6}$$

Since experiments are often conducted at the atmospheric pressure $P \approx 0.1\ \mathrm{J\ cm^{-3}}$, then the term containing $\tilde{P}$ in Eq. (24.6) is negligible, and we have simply

$$\tilde{v} = \exp[\tilde{T}^{3/2}]. \tag{24.7}$$

The pressure unit of $\mathrm{J\ cm^{-3}}$ has been used for instance by Flory [11] and in contrast to Pa saves our time in calculations. Fortunately $1\ \mathrm{J\ cm^{-3}} = 1\ \mathrm{MPa} = 1\ \mathrm{MN\ m^{-2}} = 10^7\ \mathrm{erg\ cm^{-3}} = 10^7\ \mathrm{dyne\ cm^{-2}} = 10\ \mathrm{bar} = 145.04\ \mathrm{psi} = 9.86923$ atm.; the last number depends on the geographic location.

Given Eqs. (24.6) and (24.7), we need to evaluate the characteristic parameters v^*, T^* and if we deal not only with the atmospheric pressure also P^*. One can use the *thermomechanical analysis* (TMA) in the expansion mode to determine at the atmospheric pressure the dependence of specific volume v on temperature T. By fitting the experimental results to Eq. (24.7) one obtains the characteristic parameters v^* and T^*. Zoller and coworkers have long ago developed a so-called Gnomix apparatus which performs full P–V–T determination [20]. There are several machines around the world based on the Zoller invention. We have used a Gnomix to advantage for organic polymers [21,22] as well as for inorganic ones [23]. One then represents experimental results by Eq. (24.6) and one calculates by a least-squares procedure the parameters P^*, v^*, and T^*.

To connect free volume to mechanical properties, we now need the classical Doolittle equation

$$\ln \eta = A' + Bv^*/v^{\mathrm{f}}, \tag{24.8}$$

where η is the viscosity. The connection can be made through *correspondence principles* which now we are going to discuss. Consider first a conformational rearrangement in a polymeric chain so fast that one cannot record it at room temperature. Clearly the total volume decreases when the temperature decreases, and along with it the free volume becomes smaller too. Thus, we can reach a temperature low enough to "catch" the process under investigation. This idea works also in the opposite direction. Instead of conducting experiments for 100 years at the ambient temperature, we can go to a higher temperature, thus produce higher free volume v^{f} in the material, and "catch" within, say, 10 hours the same series of events. This is the basis for the *time–temperature correspondence*. Clearly we now have what we have been looking for: the capability to predict long-term behavior from short term tests. One performs experiments at a series of temperatures. There exists a temperature of particular interest, for instance 20 °C. There is also at least one parameter of particular interest, such as the tensile compliance $D(t)$. In elastic materials we simply have $D(t) = \varepsilon(t)/\sigma = 1/E$, where E is the tensile modulus. However, our strain depends on time t; at constant T and σ we have generally

$$D(t) = \varepsilon(t)/\sigma = 1/E(t). \tag{24.9}$$

We now create a large diagram of $D = D(t)$ (or more often of $\log D = \log d(\log t)$. We begin with results for 20 °C and also include isothermal results for all other temperatures. Then, without moving the curve for 20 °C, we shift results for all other temperatures so that they would form a single curve. We shall show below examples of such diagrams, often called master curves, an approach advocated for a long time by Ferry and his coworkers [27,1]. Each $D(t)$ isotherm is moved left or right by a distance a_T called the shift factor; clearly a_T is different for each temperature. The whole procedure is also known as the method of reduced variables and means that

$$D(t, T; \sigma = \text{const.}) = D(t/a_T, T_{\mathrm{ref}}; \sigma = \text{const.}). \tag{24.10}$$

Here T_{ref} (often also denoted by T_0) is the temperature to which the master curve pertains. Thus, in our case $T_{\mathrm{ref}} = 20\,^\circ\mathrm{C}$ while in general $a_{\mathrm{T}}(T_{\mathrm{ref}}) = 1$.

Changing the temperature is not the only option. By varying stress we can also change the free volume. *Time–stress correspondence* has been demonstrated experimentally already in 1948 by O'Shaughnessy [24]. Little attention has been paid to it, except for work in Latvia summarized by Goldman [25]. Only in 2000 an equation which makes possible quantitative predictions has been developed [26].

We can also apply an oscillating (typically sinusoidal) force to a polymeric component. If the frequency ν of the oscillations is low, the chains will be able to adjust better to the externally imposed field, just as they do at higher temperatures. The inverse is true as well: high frequencies will give little opportunity for such rearrangements—as if the free volume and the temperature were low. Thus, we have time–frequency correspondence. We can write a series of approximate proportionalities [7]

$$\mathrm{CRC} \sim v^{\mathrm{f}} \sim T - \nu \sim \rho^{-1} \tag{24.11}$$

Here $\rho = v^{-1}$ is the mass density.

The correspondence principles allow us to achieve our goal: prediction of long-term mechanical properties—and thus performance and reliability—from short-term tests. It is possible to predict behavior for, say, 16 decades of time from experiments each of which was made over four decades only; examples will be given below. It is easy to see that, when using the time–temperature correspondence, essential is the capability to predict the temperature shift factor $a_T(T)$. Similarly, when using the time–stress correspondence one needs the stress shift factor $a_\sigma(\sigma)$. Starting from the Doolittle equation (24.8), it was possible to obtain a general equation [26]

$$\begin{aligned}\ln a_{T,\sigma} = {} & A_{T,\sigma} + \ln T_{\mathrm{ref}}/T + \ln[v(T, \sigma)/v_{\mathrm{ref}}] \\ & + B/(\tilde{v} - 1) + C(\sigma - \sigma_{\mathrm{ref}}).\end{aligned} \tag{24.12}$$

Here v_{ref} pertains to the stress level of interest and is thus similar to T_{ref}. If we assume a constant stress level, we obtain an equation which allows us to apply the time–temperature correspondence:

$$\ln a_T = A_T + B/(\tilde{v} - 1). \quad (24.13)$$

Similarly, if we assume a constant temperature and perform experiments at several stress levels, from Eq. (24.12) we obtain

$$\ln a_s = A_s + \ln T_{\text{ref}}/T + \ln[v(\sigma)/v_{\text{ref}}] + B/(\tilde{v} - 1) + C(\sigma - \sigma_{\text{ref}}). \quad (24.14)$$

Later in this Chapter we shall show applications of these concepts. Before doing so, however, we need to deal with the essential concepts of fracture mechanics.

24.2 FRACTURE MECHANICS FOR POLYMERIC MATERIALS

24.2.1 Stress Concentrators and Stress Concentration Factor

As noted in the beginning of this Chapter, fracture is the bottom line of polymer science and engineering, and indeed of the entire materials science and engineering. As a result of the processing procedures used, plus handling in transport, etc., polymeric materials and components exhibit structure imperfections at various levels. Thus, there exist knit lines: areas in injection-molded parts of thermoplastics in which separate polymer melt flows arise, meet, and then to some extent—but not quite—combine together during manufacturing. Consequences of the presence of knit lines on mechanical properties are discussed by Criens and Moslé [28]. Due to the presence of crazes, scratches, cracks and other imperfections, mechanical properties of real polymeric materials are not as good as they theoretically could be. In this section we shall deal particularly with stress concentrators such as *cracks* (which appear although we did not want them) and *notches* (which are well-defined cracks introduced deliberately).

The deteriorating effects of cracks and notches on material properties are represented by *the stress concentration factor*

$$K_t = 1 + 2(h/r)^{1/2}. \quad (24.15)$$

Here h is the depth (length) of the crack or notch, or one-half of the length of the major axis in an elliptical hole; r is the radius of curvature at the tip of the notch, or at each end of the major axis of an elliptical crack. The name stress concentration factor is very appropriate. Consider again a tensile test with the stress σ applied to the ends of the specimen (for details see below Section 3). The lines of force applied to these ends cannot go through the air; they must go through the material, and thus around the crack. As a consequence, when the lines meet (or separate, depending on the direction) at the crack tip, that tip is subjected not to the stress σ, but to the stress $\sigma \times K_t$. The phenomenon is well known to anybody who wanted to make two smaller sheets from a plastic sheet and found that his or her own hands are not strong enough for this operation. However, a small incision with a pair of scissors on one side of the sheet led to success. The incision was in fact a notch—and created stress concentration defined by Eq. (24.15).

Equation (24.15) corresponds to our intuitive notions about the deterioration produced by a crack. The deeper the crack is (h larger) the more "evil" it can produce. The more blunt the crack is (less sharp, larger r), the more "benign" it will turn out to be when external forces "attack" the component.

24.2.2 Stress Intensity Factor

To account for differences on the loading modes (tensile, shear or tearing), a somewhat different measure of the "evil" produced by a crack or notch called the *stress intensity factor* is used

$$K_{\text{I}} = \alpha^* \pi^{1/2} \sigma h^{1/2}. \quad (24.16)$$

K_{I} characterizes the stress distribution field near the crack tip; the subscript Roman one, I, refers to the opening or tensile mode of crack extension; α^* is a geometric factor appropriate to a particular crack and component shape; the remaining symbols are the same as in Eq. (24.15). Unfortunately, K_t and K_{I} have similar symbols, similar names, and are expressed in terms of the same quantities. However, our effort to change this situation would largely be wasted.

For an infinite plate in plane stress, the geometric factor $\alpha^* = 1$. Plane stress means that the stress s_z along the z axis perpendicular to the plane surface is equal to zero; in practice this is not exactly true, but represents a reasonable approximation. For other geometries there exist tabulations of α^* values [29].

24.2.3 Griffith's Theory of Fracture

Entire books have been written on fracture of polymers, so here we shall quote the most important results. We go back to the story of the girl with her plastic doll. Griffith [30,31] considered for elastic bodies the question: when will a crack propagate? His answer was: this will happen if the crack growth will lower the overall energy. He considered three contributions: (1) the potential energy of the external forces which are doing work on the body deforming it, (2) the stored elastic strain energy, and (3) the work done against the cohesive forces as new crack surfaces are formed. He thus derived an equation which we can write as

$$\sigma_{\text{cr}} = (2\Gamma E/\pi h)^{1/2}. \quad (24.17)$$

Here σ_{cr} is the stress level at and above which the crack will propagate; Γ is the surface energy per unit area (corresponds to the last of the three factors): E is the elastic modulus (also often called the Young modulus); h is the same as before. Thus, if the actual stress imposed is $\sigma < \sigma_{\text{cr}}$, the material will sustain the stress without the crack growing. The equation is the same for both constant load and constant displacement conditions, hence it should work also for any intermediate conditions.

Equation (24.17) has been the inspiration for much further work—some pertinent and some just rewriting it introducing new symbols and new names. One of these reformulations is

$$G_{\mathrm{r}} = \pi h \sigma^2 / E, \tag{24.18}$$

where G_{r} is known as the *elastic energy release rate*. Another such quantity is

$$R = 2\Gamma \tag{24.19}$$

Which is called the *crack resistance*. Substituting into Eq. (24.19) the value of 2Γ from Eq. (24.17), we get

$$R = \pi h \sigma_{\mathrm{cr}} / E, \tag{24.20}$$

where the right hand sides of Eqs. (24.18) and (24.20) are similar. This leads to a new concept of

$$G_{\mathrm{cr}} = \pi h \sigma_{\mathrm{cr}}^2 / E, \tag{24.21}$$

where G_{cr} is called the *critical energy release rate*. This is followed by a statement such as: when the elastic energy release rate G_{r} given by Eq. (24.18) becomes equal to the crack resistance R, then G_{r} acquires the critical value G_{cr} and a crack will propagate. It is amazing how many people are investing their efforts into rewording knowledge created by others! The whole story from Eq. (24.18) to (24.21) is nothing new beyond what we have learned already from the Griffith Eq. (24.17). We are mentioning this only because quantities such as the energy release rate are in use. For the same reason we still need to mention connections resulting from Eqs. (24.18), and (24.21) and the definition (16) of K_{I}. Making pairwise comparisons, we immediately find

$$K_{\mathrm{I}} = \alpha^* (G_{\mathrm{r}} E)^{1/2} \tag{24.22}$$

and

$$K_{\mathrm{Ic}} = \alpha^* (G_{\mathrm{cr}} E)^{1/2}, \tag{24.23}$$

where, as expected, K_{Ic} is called the *critical stress intensity factor*; it is also known as *fracture toughness*. Important, however, is the following generalization of Eq. (24.17):

$$\sigma_{\mathrm{cr}} = [2[\Gamma + \Gamma_{\mathrm{p}})E/\pi h]^{1/2}. \tag{24.24}$$

Recall that the whole theory of Griffith has been developed for elastic bodies—what applies to metals within a certain range of imposed stresses. Thus, Eqs. (24.17)–(24.23) form the essence of linear elastic fracture mechanics (LEFM). In Eq. (24.24) a "plastic" term Γ_{p} has been added to the elastic term Γ; metals exhibit also plasticity, hence the improvement displayed in Eq. (24.24). If we make a further step and assume that Γ_{p} includes all nonelastic contributions, we shall have an equation usable also for viscoelastic materials. We, therefore, have to use Eq. (24.24) instead of (24.17) while in Eqs. (24.18)–(24.23) we need to put $\Gamma + \Gamma_{\mathrm{p}}$ instead of just Γ. Values of K_{Ic} for a number of polymers are listed in Table 24.1. The impact strength values listed at the end of this chapter are also pertinent since they represent a different measure of fracture toughness.

TABLE 24.1. *Fracture toughness K_{Ic} values for selected polymers.*

Polymer	$K_{\mathrm{Ic}}/(\mathrm{J\ cm^{-3}\ m^{1/2}})$
Epoxy	0.6
Polyester thermoset	0.6
Polystyrenes	0.7–1.1
high-impact polystyrenes	1–2
Poly(methyl methacrylate)s	0.7–1.6
Poly(ether sulfone)	1.2
Acrylonitrile-butadiene-styrene	2.0
Polycarbonate	2.2
Poly(vinyl chloride)s	2–4
Polyamide (nylon 6,6)	2.5–3
Polyethylenes	1–6
Polypropylenes	3–4.5
Polyoxymethylene	4
Poly(ethylene terephthalate)	5

Note: $\mathrm{J\ cm^{-3}\ m^{1/2} = MPa\ m^{1/2}} = 0.9100$ ksi in.$^{1/2}$

24.2.4 Crazes and Shear Yielding

We need to consider the problem of the origin of the cracks. Crazes constitute one source of cracks. They are observed in glassy thermoplastics. Originally, crazes were thought to be just tiny cracks, but this turned out not to be true. We now recognize three kinds of these structures: surface crazes, internal crazes, and crazes at the crack tip. All three kinds consist of elongated voids and fibrils. The fibrils consist of highly oriented chains while each fibril is oriented at approximately 90° to the craze axis. The fibrils span the craze top-to-bottom, resulting in an internal sponge-like structure. Extensive studies of crazes and their behavior under loads have been conducted by Kramer and his school [32–42] and have been reviewed by Donald [43]. We know from their work that there are two unique regions within a craze: (1) the craze/bulk interface, a thin (10–25 nm) strain-softened polymer layer in in which the fibrillation (and thus craze widening) takes place; and (2) the craze midrib, a somewhat thicker (50–100 nm wide) layer in the craze center which forms immediately behind the advancing craze. The relative position of the midrib does not change as the craze widens. By contrast, as the phase boundaries advance, new locally strain-softened regions are continuously generated, while strain-hardened craze fibrils are left behind.

We already know that cracks are more dangerous than crazes. The latter are capable of bearing significant loads thanks to the fibrils. Therefore, we need to know under what conditions can crazes transform into cracks? Kramer, Donald, and coworkers have established that the craze fibril stability depends on the average number of effectively entangled strands n_e that survive the formation of fibril surfaces. Equations for calculating the original number of strands n_0 as well as the number n_e have been developed by Kramer and Berger [38]. It turns out that polymers with $n_e > 11.0 \times 10^{25}$ strands m^{-3} and concomitantly a short entanglement length l_e are ductile and deform by shear yielding. Such materials exhibit engineering strains up to $\varepsilon = 0.25$ or even more prior to macroscopic fracture. Polymers with $n_e < 11.0 \times 10^{25}$ strands m^{-3} and thus with large l_e are brittle and deform by crazing only. For polymers with intermediate values of n_e and l_e there is a competition between shear deformation and crazing.

In Fig. 24.1 we show a part of a craze. The parameter D is the (mean) craze fibril diameter while D_0 is the craze fibril spacing. Both D and D_0 increase somewhat with increasing n_e. Berger [42] traced the craze fibril breakdowns to the formation of small pear-shaped voids at the craze/bulk interface. The results in [42] confirm the microscopic model of Kramer and Berger [38] which we see in Fig. 24.1.

In general, providing from outside energy in excess of CRC may result in crazing, shear yielding, or cracking. In *shear yielding* oriented regions are formed at 45° angles to the stress. The shear bands are birefringent; in contrast to crazes, no void spaces are produced. Thus, crazing—created by tensile fields—is accompanied by volume dilation while shear yielding—created by compressive fields—is not. Combined fields result in mixed responses.

The presence of liquids or vapors in the environment of a polymeric component affects the response to external mechanical forces. Thus, for instance polyarylate (Par) under uniaxial extension exhibits exclusively shear yielding without crazing. However, exposure to organic vapor (methylethyl ketone) results in crystallization, embrittlement, and conversion of the response to deformation from shear yielding to crazing [42].

Finally, let us mention that *crack healing* is possible. This phenomenon has been investigated by Kausch and also by Wool and reviewed by these authors [44,45].

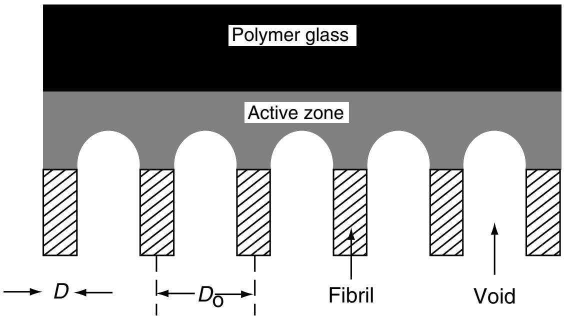

FIGURE 24.1. A schematic of a fraction of one side of a craze.

24.2.5 Rapid Crack Propagation and Its Prevention

The general definition of CRC in Subsection 24.1.2 does not specify a quantitative measure. Such a measure has to be defined for each specific problem. As an example, we shall now consider rapid crack propagation (RCP). RCP is a dangerous process. Velocities of 100–400 m s^{-1} (that is 300–1,400 feet s^{-1}) have been observed in polyethylene (PE) pipes. Since such pipes are being used for fuel gas distribution within localities; RCP might be accompanied by an explosion of the gas pressurized inside.

Given the importance of the problem, studies were made with the objective of connecting the crack length L with a variety of parameters: fuel pressure inside, pipe fatigue, tensile behavior of the piping material, and so on. L was determined by a standard procedure of Greig and Smith [46] such that a knife is pushed through a pressurized pipe by falling weight; given the rate at which RCP takes place, the length L is achieved almost instantaneously. However, no such connections were found—until Gaube and Müller [47] found a correspondence between the notch impact energy U_l (see Section 24.4.2) and L. An analysis of the problem [48] led to the following equation:

$$L = L_0 + L_1/U_l, \qquad (24.25)$$

where L_0 is a material constant with the dimensions of length, L_1 is another constant with the dimensions of length and energy, and U_l is the notch impact energy. What is required here is a criterion showing when RCP will *not* occur. Since the notch impact energy U_l is the independent variable in Eq. (24.25), it constitutes the appropriate measure of CRC for the problem under consideration. U_l can be determined by an independent and fairly widely available experimental procedure. L can be measured in an outdoor 14 m long stand at Hoechst AG in Frankfurt-on-the-Main (although such facilities are not widely available). Therefore, CRC will be represented here by a limiting impact energy $U_{l\text{-lim}}$ defined as

$$L(U_l > U_{l\text{-lim}}) = 0. \qquad (24.26)$$

Now we simply substitute the definition of $U_{l\text{-lim}}$ from Eq. (24.26) into Eq. (24.25), with the result

$$U_{l\text{-lim}} = -L_1/L_0. \qquad (24.27)$$

An example of the application of the criterion just defined is shown in Fig. 24.2. The coordinates are L and U_l, as defined by Eq. (24.25). The criterion applies to all classes of materials; if all plastic pipes were identical, we would have only one point on the diagram, so here again differences in processing, handling, transport etc. appear. Each pipe is slightly different, and there is a certain scatter due to the limited accuracy of the two kinds of experiments, but it is clear that Eq. (24.25) is obeyed. Therefore, the criterion Eq. (24.27) derived from (24.25) is valid. For the data shown in Fig. 24.2 we have $L_0 = -896\,mm$, $L_1 = 269$ J mm,

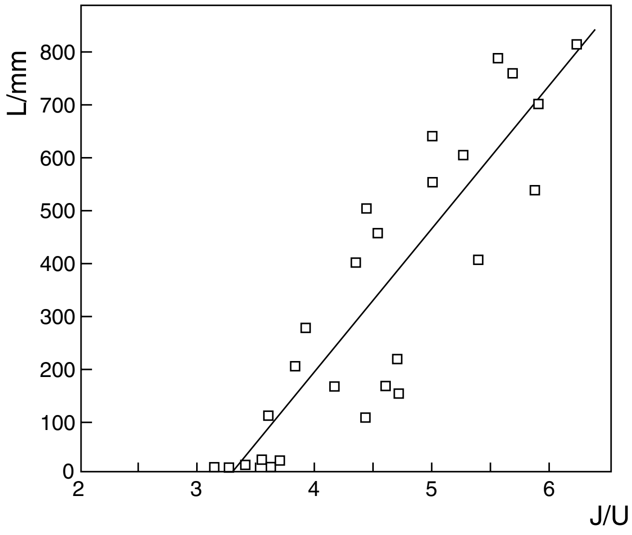

FIGURE 24.2. Length L/mm of the cracks in PE pipes determined by the Greig-Smith test 50 vs. the reciprocal Charpy impact energy $(U/J)^{-1}$; after [48].

therefore $U_{\text{I-lim}} = 0.300\,\text{J}$. If the impact energy determined in the Charpy test (see the section on impact behavior) is higher than this value, rapid crack propagation will not occur. Since the criterion is defined for a class of polyethylenes, a safety factor somewhat larger than unity may be introduced.

24.2.6 Slow Crack Propagation and Its Prediction

The slow crack propagation (SCP) is vastly different from RCP, not at all spectacular but in fact "quiet" and insidious. The crack propagation rate dh/dt might be only, say, 1 mm per month; an observation for instance two weeks after installing a polymeric component might reveal nothing. Experimentalists customarily present the dh/dt rates as a function of the logarithmic stress intensity factor K_I as defined by Eq. (24.16); we now use h as the crack length (as we did before) to differentiate it from the length L which pertained to RCP. The problem clearly consisted in relating dh/dt to K_I. It was solved [49] by using the CRC approach in conjunction with the Eq. (24.17) of fracture mechanics. The problem was different than that of Griffith. He needed the critical stress σ_{cr} above which crack propagation occurs for a given crack length h. In our problem we need to know whether the crack length is below a certain value, call it h_{cr}, so that the crack will not propagate [49]. We therefore reformulate the Griffith Eq. (24.17) as

$$h_{cr} = 2\Gamma E/\pi\sigma^3. \qquad (24.28)$$

By definition, the crack will propagate only when $h > h_{cr}$. This is not only a consequence of the CRC concept but also supported by the molecular dynamics computer simulations [50,51] showing that a crossover exists from the force field region dominated by chain relaxation to one in which crack propagation occurs.

Since notches with $h < h_{cr}$ do not cause crack propagation, it was only natural to assume

$$\frac{dh}{dt} = \beta(h - h_{cr}) \text{ for } h \geq h_{cr}, \qquad (24.29)$$

where β is a time-independent proportionality factor characteristic for the material since it depends on CRC. We do not have space here to provide details of the derivation; the final result [49] is

$$\log K_I = (1/2)\log(\alpha^{*2}2\Gamma E) + (1/2)\log[1 + (1/\beta h_{cr})]dh/dt. \qquad (24.30)$$

Equation (24.30) provides the desired connection between K_I and dh/dt. In the derivation both the stress level σ and the original crack length h_0 were used but both canceled out, with the unexpected result that the crack propagation rate is independent of both! The experimental results support Eq. (24.30) as shown for instance in Fig. 24.3 for Hoechst PEs studied under uniaxial tension in water medium at 60 °C. Each symbol pertains to a different stress level and a different original notch length. It is clear that all polyethylenes with the molecular mass M_A form a common curve, and the same is true for the other molecular masses. Moreover, we see that a higher M results in a lower crack propagation rate; this result is related to the constituents of CRC listed at the end of Section 24.1.3, particularly the first two of them.

In the beginning we have called SCP "insidious". The lowest experimental crack propagation rate value in Fig. 24.3 is $dh/dt = 10^{-8}\,cm\,s^{-1}$; this is only 0.315 cm per year, but the crack does grow. This fact gives us an idea on the utility of Eq. (24.30).

24.3 QUASISTATIC TESTING AND TRANSIENT TESTING

24.3.1 Types of Testing Procedures

We have already referred to various kinds of data on mechanical behavior of polymers. We are now going to consider methods of acquisition of such information. The most frequently used are the so-called *quasistatic* methods which involve relatively slow loading. *Tension, compression, and flexure* belong here. The quasistatic methods have to be distinguished from so-called *transient tests* which include *stress relaxation* and *creep*. There are also impact tests and dynamic mechanical procedures which will be defined later.

Specimens for testing may be produced by processing operations such as injection molding, compression molding, or machining from sheets. Machined surfaces have to be smoothed in their long axis direction with abrasive paper. Any flash on molded specimens shall be removed; the cross-sectional area has to be uniform along the whole length subjected to testing. Consequences of any nonuniformity would show up as stress concentrators discussed above.

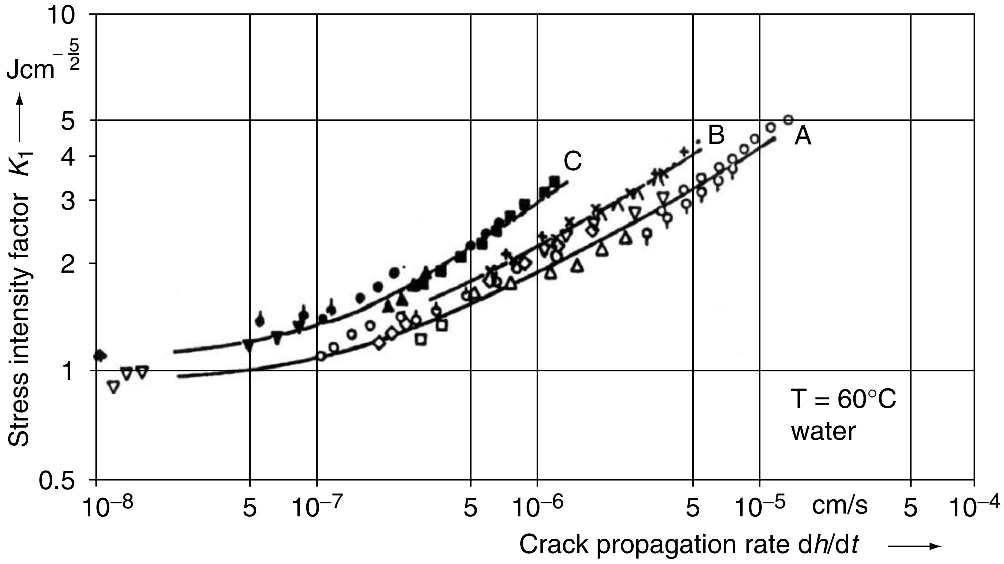

FIGURE 24.3. Crack propagation rate vs. the stress intensity factor for Hoechst polyethylenes. Each PE class such as A has the same molecular mass, with $M_A < M_B < M_C$; after [49].

The recommended number of tests on each sample is at least five, 10 or more are preferred. If producing design data for a particular application is the objective, the samples must be prepared by the same method as the part in question.

Testing of materials is governed by standards. We shall often refer below to those of the American Society for Testing and Materials (ASTM), West Conshohocken, PA. However, as national economies become more and more connected into a global economy, the use of standards defined by the International Standards Organization (ISO) is on the increase. In Table 24.2 we list several ISO and ASTM tests.

24.3.2 Tensile Properties

Tensile testing is the most frequently used method to characterize the material strength. The machine used is presented schematically in Fig. 24.4. It should be of the constant-rate-of-crosshead-movement type, consisting of one fixed and one movable member, both carrying self-aligning grips. The movable member shall move with a uniform, controlled velocity with respect to the stationary one. An extensometer is used to determine the distance between two designated points within the gage length of the test specimen as this is stretched. Speed of testing is defined as the relative rate of motion of the grips or test fixtures. It is specified for different types of specimens, varying typically from 1 to 500 mm/min (0.2–20 in. min^{-1}). The lowest speed that produces rupture in the time range 0.5–5 min for the specimen geometry used is to be selected.

One tests dumbbell-shaped or straight-sided specimens under defined conditions of pretreatment, temperature, humidity, and deformation rate. The former specimens are shown in Fig. 24.5.

There are two essential properties determined each time. The first is the *engineering stress*

$$\sigma = F/A_0, \qquad (24.31)$$

where F is the applied force and A_0 is the initial cross-sectional area. Determination of the *true stress* based on the actual cross-sectional area A which changes during the

TABLE 24.2. *ISO and ASTM tests for important mechanical properties.*

Property	ISO standard	ASTM standard
Tensile modulus	527-1 & 2	D 638
Yield stress	527-1 & 2	D 638
Yield strain	527-1 & 2	D 638
Nominal strain at break	527-1 & 2	—
Elongation at break	527	D 638
Stress at 50% strain	527-1 & 2	—
Stress at break	527-1 & 2	D 638
Strain at break	527-1 & 2	D 638
Flexural modulus	178	D 790
Flexural strength	178	D 790
Charpy impact strength at −30 °C	179	D 256
Charpy impact strength at +23 °C	179	D 256
Charpy notched impact strength at −30 °C	179	D 256
Tensile impact	8256	D 1822
Izod impact strength at −30 °C	180	D 4812
Izod impact strength at +23 °C	180	D 4812
Izod notched impact strength at −30 °C	180	D 256
Izod notched impact strength at +23 °C	180	D 256

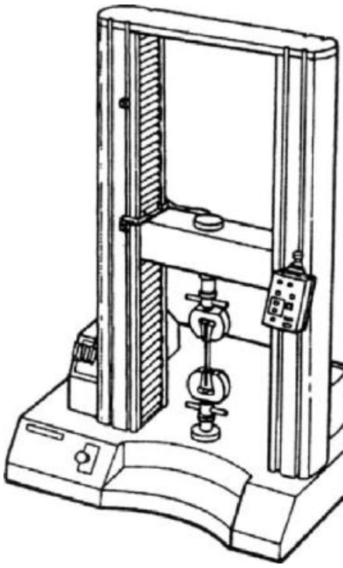

FIGURE 24.4. The machine for quasistatic testing—including tension, compression, 3-point bending and/or 4-point bending.

experiment is possible but more difficult. The other key property is the *engineering strain* (also known as the nominal tensile strain)

$$\varepsilon = (l - l_0)/l_0 = \Delta l/l_0. \qquad (24.32)$$

Here l is the current length of the specimen while l_0 is the original length.

The quantities obtained most often from tensile testing are:

Tensile strength: The maximum load divided by A_0.

Percent elongation: If the specimen gives a yield load larger than the load at break, calculate *percent elongation at yield*. Otherwise, *percent elongation at break* is reported.

Modulus of elasticity: It is the proportionality factor E appearing in *Hooke's law*:

$$\sigma = E\varepsilon \qquad (24.33)$$

and is also often called *Young's modulus*. It is calculated from the initial linear portion of the load vs. extension curve giving us the stress vs. strain curve. For materials where there is no clear linearity of the initial portion of the stress–strain curve, the modulus is calculated by dividing the nominal (= engineering) stress value by the corresponding designated strain (secant modulus).

In Fig. 24.6 we show several types of behavior seen in tensile testing of polymers. For performing a specific test, consult one of the standards listed in Table 24.2.

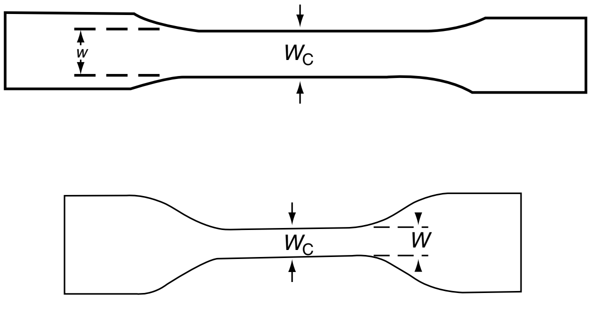

FIGURE 24.5. The dumbbell ("dogbone") specimens for tensile testing.

24.3.3 Compressive Properties

Of course, in compressive testing the strain defined by Eq. (24.32) is negative, but the definitions (31)–(33) are applicable. Basically two different testing methods are available here. In the first one the sample is deformed at a constant rate under simultaneous recording of the stress and deformation. This method, in essence a mirror image of the tensile test, is defined in ASTM D 695M. According to the second method, a constant load is applied to the specimen, the deformation of which is recorded after a given period of time with additional reading of the recovery of the specimen following unloading. This method, basically a compressive creep recovery test, is the subject of ASTM D 621.

Compression is an important mode of load application. An example of compressive loading is assemblies of conductors and insulators held together by suitable fastening devices. However, the compressive strength as such has a rather limited design value, since this type of loading apart from exceptions, such as collapsing foams or shatter of brittle plastics, seldom results in failure.

Testing of flexible materials, like rubbers, may involve complications due to their deformability. For instance, one finds that compressive stiffness is markedly dependent on contact surface constraints and specimen shape.

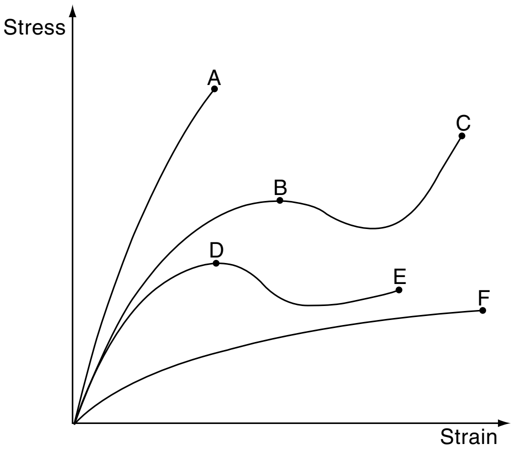

FIGURE 24.6. Typical engineering tensile stress vs. engineering strain curves. Points A, C, E, and F correspond to the tensile strength and elongation at break, D and B at yield. The curve ending at A represents a brittle material, those with C and E tough materials each with a yield point, while the curve ending at F shows a tough material without a yield point.

24.3.4 Flexure and Bending

We already mentioned that the machine shown in Fig. 24.4 serves also for bending. Most popular are two kinds, 3 point and 4 point, shown in Fig. 24.7, and described in standards D 790, D 790 M (=metric) and ISO 178. There are also less used but more specific standards: ASTM D 747 for apparent bending modulus of plastics by means of a cantilever beam and D 648 for deflection temperature of plastics under flexural load.

For brittle materials, flexure testing is believed to yield more reliable strength, modulus, and other data than the tensile method, this primarily by reducing the pronounced effects of misalignment in tension. For sheet materials (except laminated thermosets, high-strength reinforced composites) the dimensions of the specimens depend on whether tested flatwise or edgewise; the thickness of the sheet is the depth, or width, respectively. The depth shall not exceed the width in the latter case. ASTM standards specify also that, for sheets less than 1.5 mm in thickness, a specimen 50 mm long by 10 mm wide shall be tested flatwise on a 25 mm support span. Molding materials shall be 80 by 10 by 4 mm tested flatwise on a 64 mm support span. Special rules apply to laminated thermosets and highly anisotropic composites, which shall be tested with a larger span-to-thickness ratio (up to 60:1). Anisotropic materials require four different specimens, tested edgewise and flatwise, and cut in lengthwise and crosswise directions.

24.3.5 Stress Relaxation

Stress relaxation is typically determined in the uniaxial mode in a specimen or part kept at constant deformation. This pertains to parts in service such as fasteners, seals, or screws. An example of results of such a test are shown in Fig. 24.8. The relaxing stress could conceivably fall to zero (curve a in the bottom part of Fig. 24.8) but in practice the behavior displayed as curve b is observed, so that a certain level of *internal stress* σ_i is established.

The concept of internal stress is very useful for bringing out common features of stress relaxation behavior of different kinds of materials. Instead of plotting stress vs. time t, let us plot $(\sigma - \sigma_i)/(\sigma_0 - \sigma_i) = \sigma_i^*/\sigma_0^*$ vs. t. Here σ_0 pertains to the time of strain imposition. Such a plot was proposed by Kubát already in 1965 [52]. An example is shown in Fig. 24.9. We see that curves for ostensibly very different materials have similar shapes. A large central part of each curve has almost the same slope s as the other curves, so that

$$s = (-\mathrm{d}\sigma/\mathrm{d}\ln t)_{\max} = (0.1 \pm 0.01)(\sigma_0 - \sigma_i). \quad (24.34)$$

To explain the situation displayed in Fig. 24.8, Kubát has proposed a cooperative theory of stress relaxation [53,54]. He assumed that single units (metal atoms, polymer chain segments) do not relax individually but clusters of such units relax together. Thus, the Kubát theory is quite general an explains the observed behavior of metals and polymers alike. Molecular dynamics computer simulations have confirmed that indeed cluster relaxations prevail over individual relaxation, and this both for metals [55] and for polymers [56,57].

In Section 24.1.3 we have discussed among others the time–temperature correspondence principle. An example of application of that principle is shown in Fig. 24.10. The results pertain to high density polyethylene (HDPE) subjected to different levels of predrawing [58]. The draw ratio is defined as

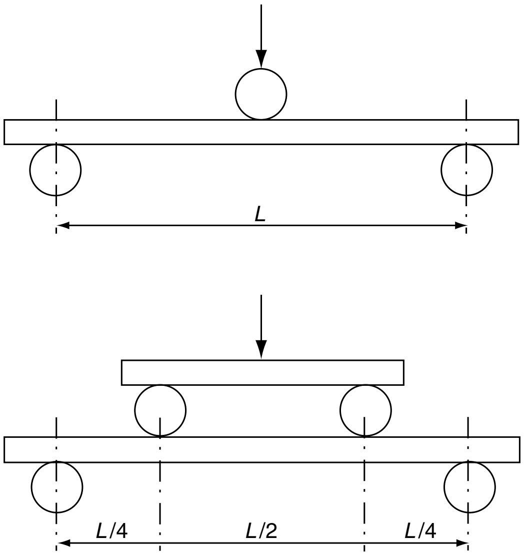

FIGURE 24.7. 3-point and 4-point loading modes in bending.

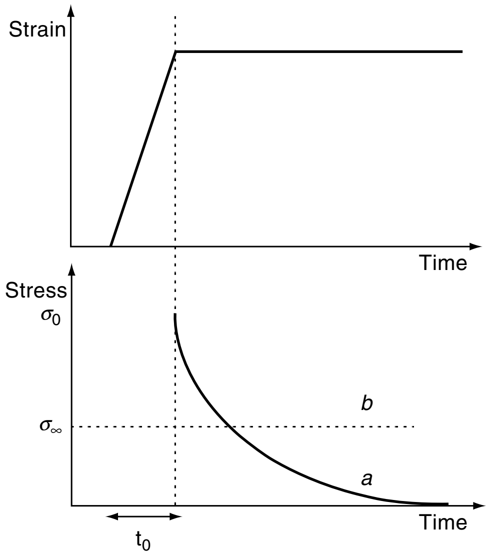

FIGURE 24.8. Stress relaxation represented by strain vs. time and stress vs. time curves. Explanation in text.

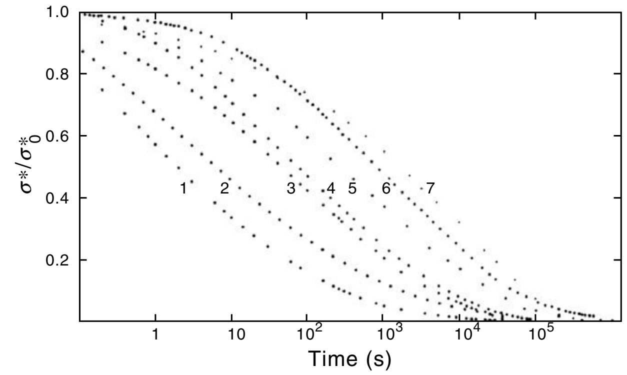

FIGURE 24.9. Stress relaxation curves—as explained in the text—for polyisoprene (natural rubber, 1), oriented low density polyethylene (LDPE) with the draw ratio $\lambda = 1.8$ (curve 2), indium (3), unoriented LDPE (4), cadmium (5), polyisobutylene (6), and lead (7).

$$\lambda = \varepsilon + 1, \tag{24.35}$$

where ε is the engineering strain defined by Eq. (24.32). The curves in Fig. 24.10 have the same shape as those in Fig. 24.9. The final horizontal parts are fairly long in Fig. 24.10, a consequence of prediction over 16 decades of time. The necessary shift factor values have been calculated from

$$\ln a_T = 1/(a + c\lambda) + B/(\tilde{v} - 1). \tag{24.36}$$

Equation (24.36) reduces to Eq. (24.13) for $\lambda = 1$. Equation (24.7) has been also used along with a representation of T^* as a quadratic function of λ. We see that indeed predict of long-term behavior from short-term tests can be accomplished.

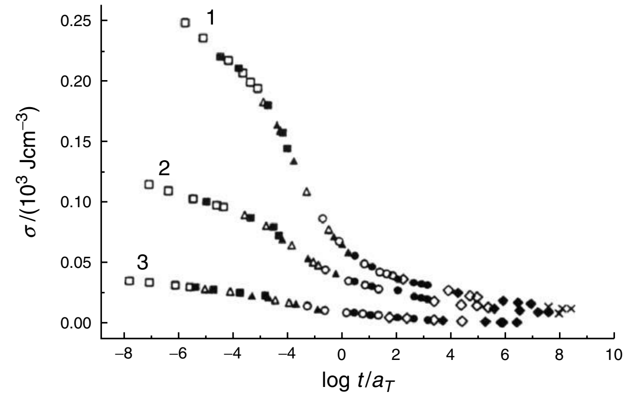

FIGURE 24.10. Master stress relaxation curves for HDPE at the reference temperature $T = 313.2$ K ($= 40$ °C), the constant tensile strain $\varepsilon = 0.025$ and at different values of the draw ratio: $\lambda = 12.2$ in the top (1) curve; $\lambda = 5.5$ in the middle (2) curve; and the material without predeformation ($\lambda = 1$) in the bottom (3) curve. The symbols pertaining to the experiment temperatures are the same in all three curves: □ for −50 °C; ■ for − 30 °C; △ for − 10 °C; ▲ for 0 °C; ○ for + 20 °C; ● for + 40 °C; ◇ for + 60 °C; ◆ for + 80 °C; and × for + 100 °C. The vertical coordinate is the tensile stress σ, the horizontal is log t/a_T; after [58].

24.3.6 Creep

Creep denotes the time-dependent elongation of a specimen or part subjected to a constant stress. Normally, the deformation range is relatively limited; the stress provided by a dead-weight can thus be considered as fairly constant and the change in the cross-section during the process neglected. Such a loading mode emulates the loading situations normally encountered in engineering practice. The pertinent standards include ASTM D 2990.

Figure 24.11 shows a schematic picture of a creep curve plotted as strain vs. time. There is an initial elastic deformation which at higher stress levels may also include a plastic component. This is followed by the primary creep stage characterized by a decreasing creep rate—stabilizing at a level corresponding to the secondary or stationary creep stage. In the end phase of the process, called tertiary creep, the rate becomes higher again, eventually resulting in creep rupture. It is to be noted that *long-term failure may occur at significantly lower stresses than those determined in normal tensile testing*. The logarithm of the time to rupture is often found to decrease linearly with the applied load.

Primary (transient) creep can be considered as a consolidation process during which the structure of the material adjusts itself to the following steady-state creep stage. In some instances, like in cross-linked elastomers at low stresses, the steady state is absent, with the creep rate decreasing to zero, and the total creep strain remaining constant. In this case, primary creep is a delayed response of the material to the applied stress. At higher stress levels, chain scission, oxidation effects etc. may influence this simple behavior.

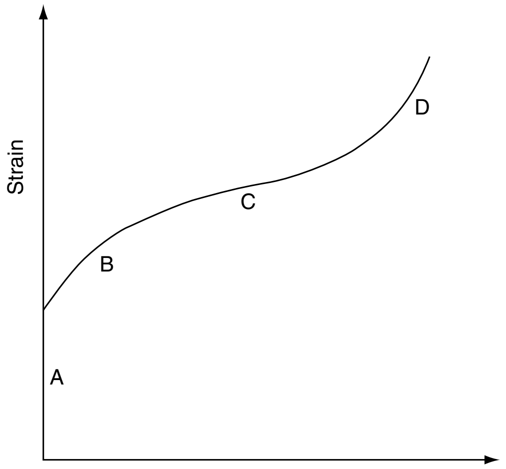

FIGURE 24.11. A schematic of a creep curve. A = instantaneous initial deformation which may contain a plastic component; B = primary, C = secondary and D = tertiary creep stage.

During the steady-state stage the material flows in a viscous (plastic) manner. In some instances, this stage may not be clearly discernible, constituting only a transition between the primary and tertiary portions of the creep curve. It may be noted that the acceleration of the creep rate in the latter part is not due entirely to a decrease in the cross-section of the specimen and thus to an increase in the stress level in tests where the specimen is loaded with a dead-weight.

We have already mentioned *creep recovery*. An example including the recovery stage is shown in Fig. 24.12.

We observe that the recovery curve is almost a mirror image of the primary creep stage.

In Section 24.1 we have defined ways of prediction of long-term behavior from short-term tests. Let us now provide more examples of application of these concepts. Creep and stress relaxation have been determined for PET/0.6PHB, where PET is the poly(ethylene terephthalate), PHB, the p-hydroxybenzoic acid, and 0.6 is the mole fraction of the latter in the copolymer [58]. PET/0.6PHB is a polymer liquid crystal, see chapter 41 on PLCs in this Handbook. In temperature ranges of interest it forms 4 coexisting phases [60]. Conventional wisdom said that prediction methods work only for so-called rheologically simple materials, practically for one-phase polymers. Therefore, we have decided to apply as severe a test as possible to our prediction methods and a multiphase PLC is a good choice.

In Fig. 24.13 we show several isotherms of tensile creep compliance (see Eq. (24.9)) for PET/0.6PHB [58]. In Fig. 24.14 we show a master curve for $T_{\mathrm{ref}} = 62$ °C (the glass transition temperature of PET, the nonliquid crystalline component of the PLC) based on the curves from Fig. 24.13. We see a successful prediction over 16 decades of time.

Important here of course is whether the shift factor a_{T} values calculated from Eq. (24.13) agree with the experimental ones. These results are displayed in Fig. 24.15. The continuous line is calculated from our Eq. (24.13). The dotted line is from an equation proposed in 1955 by Williams, Landel, and Ferry (WLF) [27], a pioneering $a_{\mathrm{T}}(T)$ formula at that time. We see that the WLF equation works well in a certain temperature range—this seems the reason it is still in use—but fails miserably outside of that range. Nobody else but Ferry [1] stated that range of application of WLF amounts to 50 K or so, not more. If one makes a primitive and unfounded assumption in our Eq. (24.13), one gets from it the WLF equation as a special case [6]. The problem is when people use the WLF equation blindly in wide temperature ranges, obtain bad results, and draw a false conclusion that the time—temperature correspondence principle does not work.

As already mentioned, stress relaxation was also determined for PET/0.6PHB [59]. We do not present the results here, although also in this case one obtains a master curve which covers 16 decades of time. Important, however, is the comparison of $a_{\mathrm{T}}(T)$ values from creep and stress relaxation. This is made in Fig. 24.16. The continuous line is again obtained from Eq. (24.13). We see that the a_{T} values obtained from these two kinds of experiments practically coincide. Thus, Eq. (24.13) serves to predict a true material property rather than a property related to just one kinds of experiments.

The time—stress correspondence principle as embodied by Eq. (24.14) has also been used successfully [61]. We do not include such results for brevity. One could argue that the use of equations discussed in Section 24.1 requires fairly large amounts of experimentation. This impression might be

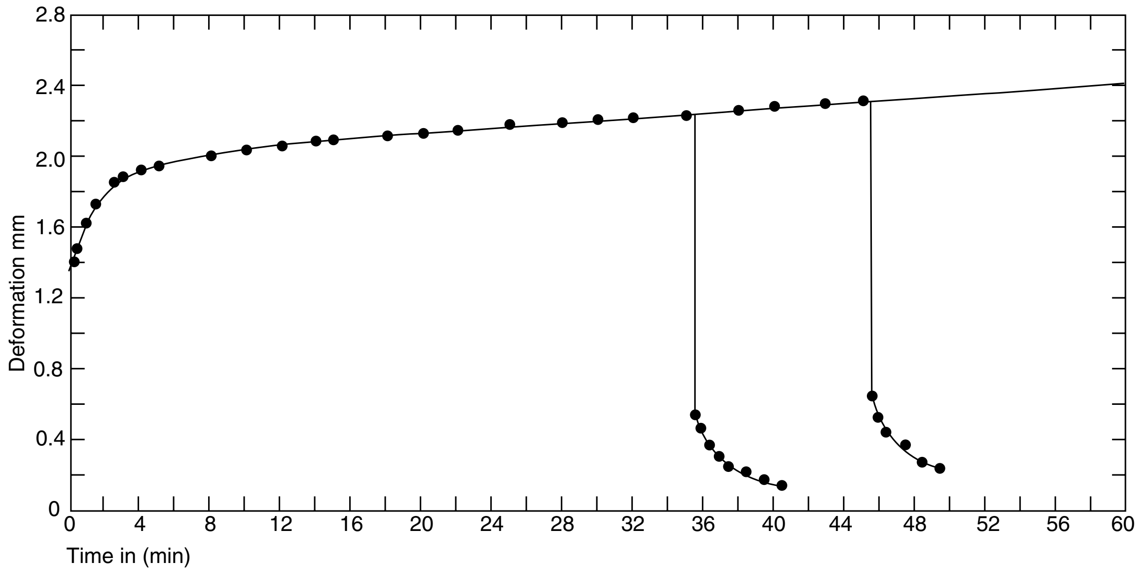

FIGURE 24.12. Creep and creep recovery of an oriented polypropylene monofilament with 0.35 mm in radius at 60.7 °C and stress level $\sigma = 36\,\mathrm{J\,cm^{-3}}$ unloaded at 35.5 and 45.5 min. Deformation in mm relates to a specimen length $l_0 = 100\,\mathrm{mm}$.

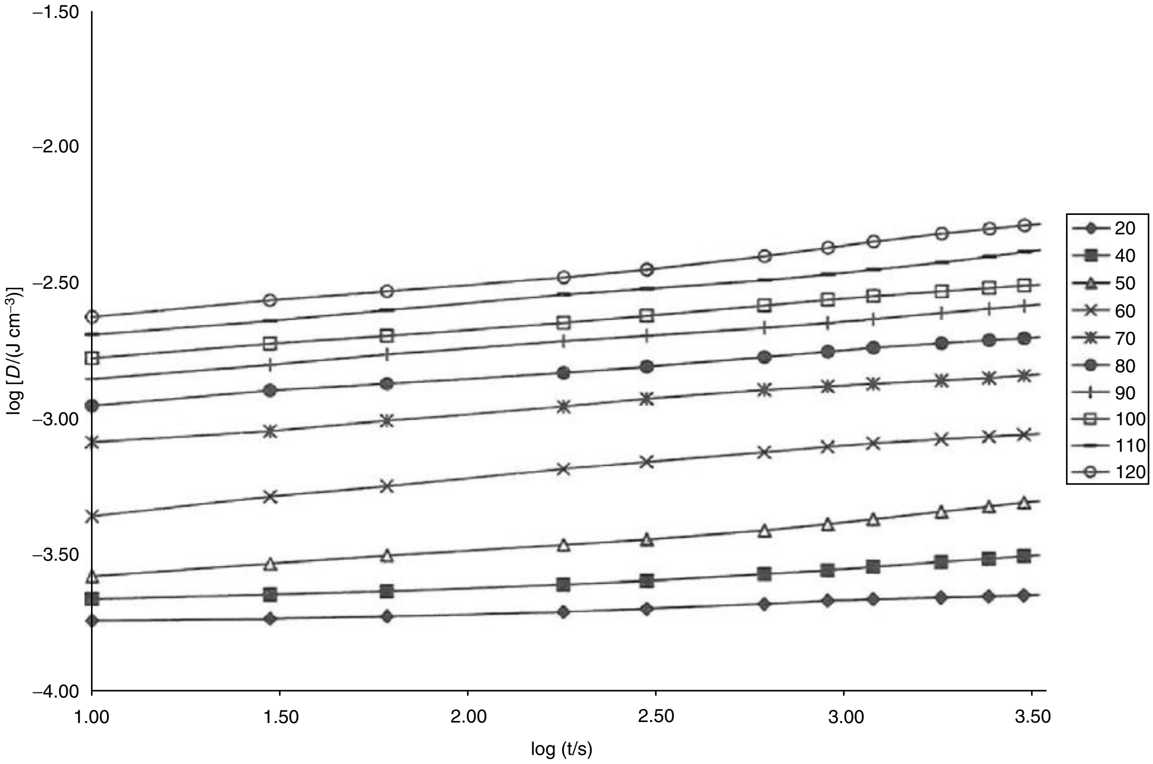

FIGURE 24.13. Experimental tensile creep compliance for PET/0.6PHB in logarithmic coordinates at 20 °C (the bottom curve) and other temperatures indicated in the insert; after [59].

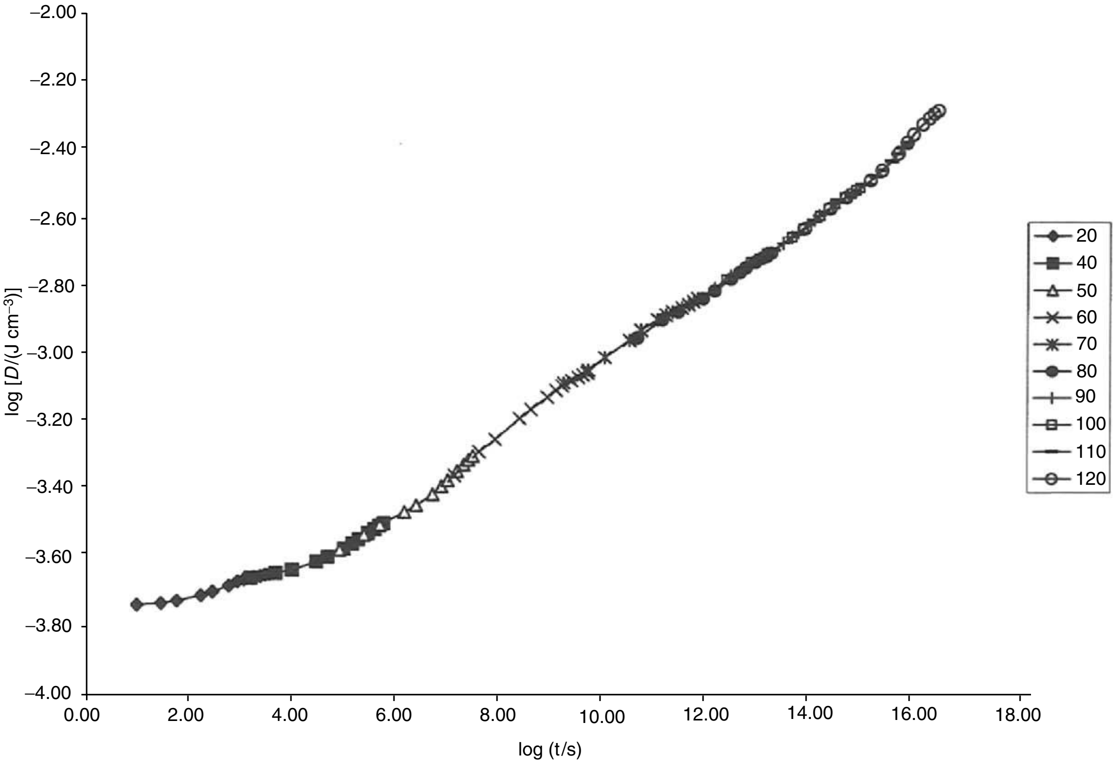

FIGURE 24.14. Tensile creep compliance for PET/0.6PHB in logarithmic coordinates as the master curve for 62 °C; after [59].

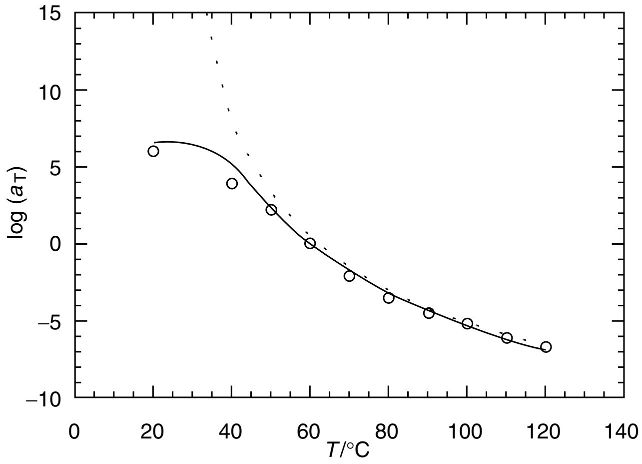

FIGURE 24.15. The temperature shift factor $a_T(T)$ for PET/0.6PHB for 62 °C. Circles are experimental values, the dotted line from the WLF equation and the continuous line from Eq. (24.13) in conjunction with Eq. (24.7); after [59].

confirmed for instance by our Fig. 24.13 which contains 10 isotherms. Therefore, methods of prediction of long-term behavior from short-term tests based on our Eqs. (24.12)–(24.14) have been developed [62, 63] such that one uses two or three experimental isotherms or results for two or three stress levels. Again, we are not going to discuss these results here for brevity.

24.4 IMPACT BEHAVIOR

24.4.1 Rates of Force Application

We have noted in Subsection 24.2.5 that a measure of CRC has to be defined for each specific problem. Imagine a slow-loading process, such as a part (an early stage) of quasistatic loading by compression. Then U_{CRC} featured in Eq. (24.2) might be relatively low; as a consequence U_r will be low too, but still $U_r > U_0$, and the material or component will "survive an attack". However, if the loading occurs at a fast rate, the same external energy U_0 will exceed U_r because relaxational processes take time, and fracture will occur. We shall now consider impact testing with this situation in mind.

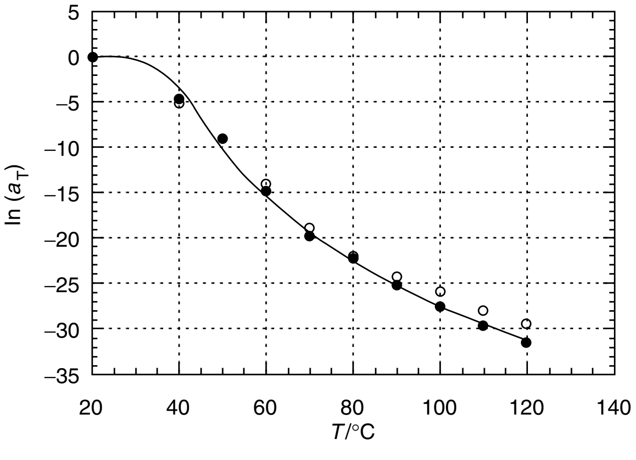

FIGURE 24.16. Experimental shift factors $a_T(T)$ from creep (full circles) and from stress relaxation (empty circles). The continuous line is from Eq. (24.13) in conjunction with Eq. (24.7); after [59].

24.4.2 Impact Testing

The most frequently applied impact tests are shown in Fig. 24.17 A and B. A pendulum (shown as a filled arrow) falls from a certain height; the loss in the potential energy of the pendulum is assumed equal (with a correction for losses such as friction) to the energy U_0 absorbed by the specimen; see Eq. (24.1). The Charpy test is described by the ASTM D 256 standard method B, the lzod test by the same standard method A. We see (Fig. 24.17 A) that in the Charpy test there is a symmetry with respect to the center of the specimen. By contrast, in the lzod test (Fig. 24.17 B) the bottom half of the specimen remains "untouched" while the top part is broken off. We—and more and more laboratories around the world—perform now both tests with a sensor installed on the pendulum and connected to a computer. Thus, not only a single value of the energy but a whole curve is obtained. For convenience single values of impact strength (IS) for a number of polymers are listed in Tables at the end of this chapter.

There is also a combination of tension with impact shown schematically in Fig. 24.17 C. This test is also symmetric with respect to the center, just as the Charpy procedure.

24.4.3 Impact Transition Temperature: Determination and Prediction

Traditionally—and that started with metals—one distinguishes two types of mechanical behavior of polymers: brittle and ductile. It will be clear to us after discussion of the free volume concept in Subsection 24.1.3 that brittle behavior will dominate at low temperatures when the free

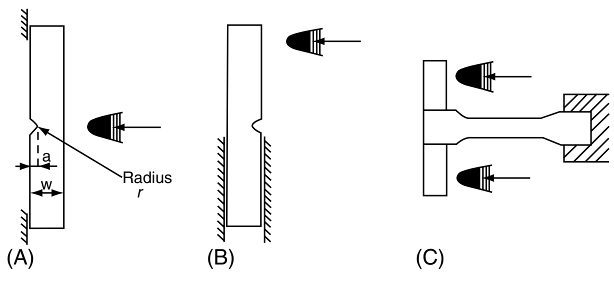

FIGURE 24.17. Schematics of impact tests showing geometry, loading mechanisms, and clamping modes.

volume is low. Therefore, there is a transition temperature T_I above which the material will be ductile. We shall discuss the CRC connections and a way to predict T_I in the next Subsection. Now we shall define a procedure of experimental determination of T_I. It should be noted immediately that the index I refers to impact; determination of brittle-to-ductile transition by loading at a rate slower than impact will result in finding not a single temperature, but a temperature range; the range might be as large as 10 K [64].

In view of this, we define T_I as the temperature at which the response of the material changes from brittle to ductile under high-impact conditions. The Charpy test described above can be used to achieve those conditions [6]. As discussed in Subsection 24.2.5, two specimens are hardly ever identical. At T_I we have, therefore, 50% failing in the brittle way and the other half in the ductile way.

The difference between the two kinds of failure are easily visible when one compares fracture surfaces, macroscopically as well as in micrographs obtained by scanning electron microscopy (SEM). Macroscopically, the fracture surface of a brittle failure appears smooth. SEM micrographs show in this case a "flaky" surface. By contrast, ductile failure is characterized by "hills and valleys" with deformed strands coming out from the surface, as well as holes in the surface left by strands which at break time have "joined" the other surface. Examples of the two types of micrographs are shown, respectively, in Figs. 24.18 and 24.19. There is a whole book by Michler [65] on polymer micromechanics which contains many instructive SEM micrographs of fracture surfaces as well as crazes, shear yielding, and also combinations such as crazes crossing shear bands.

Using the concepts discussed in Sections 24.1 and 24.2, the following equation [6] was derived:

$$K_t = F \times \mathrm{e}^{-B/(\tilde{v}_I - 1)} \tag{24.37}$$

here K_t is the stress concentration factor as defined by Eq. (24.15); B is the Doolittle constant from Eq. (24.8); and the reduced volume $\tilde{v}_I$ is that at the impact-transition temperature T_I. Thus, we have an implicit formula for T_I which can be related to $\tilde{v}_I$ by an equation of state such as Eq. (24.6) or (24.7); there is a T_I value corresponding to each stress concentration factor.

Equation (24.37) was tested for LDPE for which sufficient data were available. The results are shown in Fig. 24.20. We see that the equation is obeyed within the limits of the experimental accuracy. Thus, two pairs of T_I and K_t values are sufficient for the calculation of the parameters F and B and for subsequent prediction of the entire diagram.

24.4.4 Prediction of Volumetric Properties from Impact Data

We have used above free volume to explain mechanical properties. Since we have at our disposal quantitative relationships which work well, it was tempting to see whether the relationships can be used also in the opposite direction: going from mechanical properties toward volumetric ones. Thus, Eq. (24.37) was used in this opposite direction [66]:

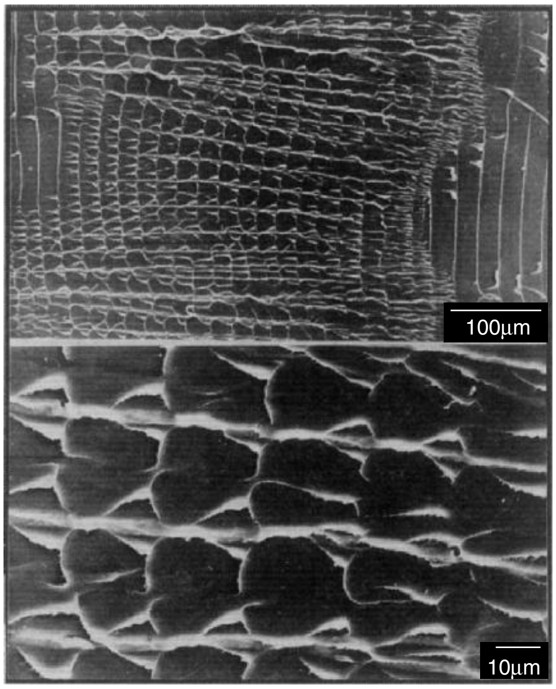

FIGURE 24.18. SEMicrograph of a brittle fracture surface; after [65].

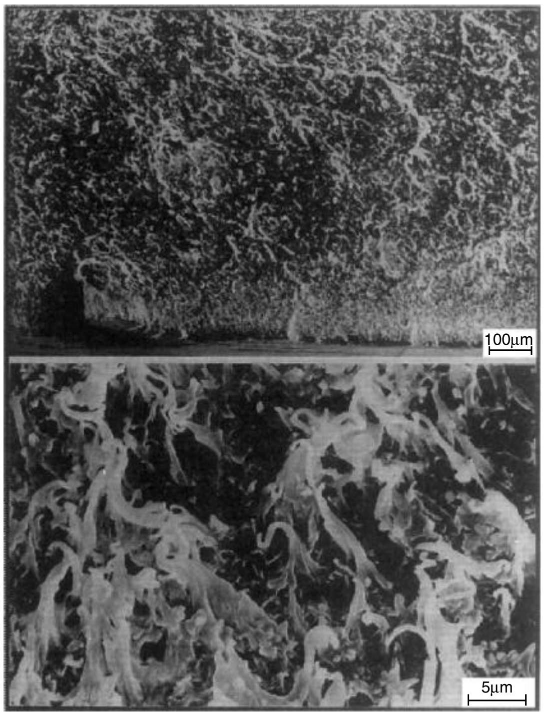

FIGURE 24.19. SEMicrograph of a ductile fracture surface; after [65].

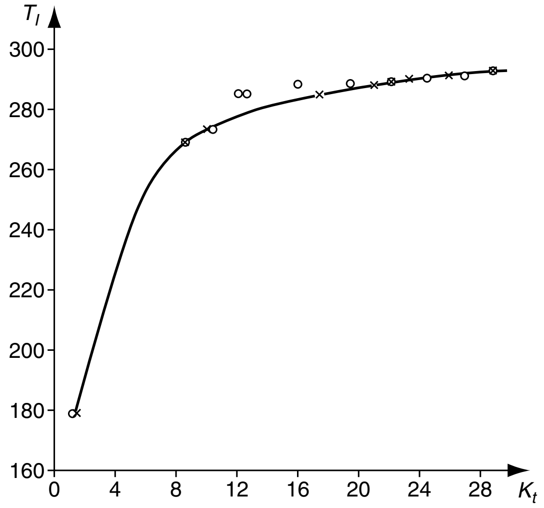

FIGURE 24.20. Relation between the stress concentration factor K_t and the impact transition temperature T_l in K for LDPE. Circles represent experimental values obtained by the Charpy method and crosses those calculated from Eq. (24.37).

specific volume v was obtained for the first time from mechanical parameters—the impact transition data—via an equation of state. The result was prediction of v over a temperature range of 100 K. The average difference between calculated and experimental specific volume values was only 0.092%. This constitutes one more confirmation—and of a different type—of the physical significance of the CRC concept and of the relations based on that concept.

24.5 VISCOELASTICITY AND DYNAMIC MECHANICAL TESTING

24.5.1 Objectives and Definitions

As noted in Subsection 24.1.2, viscoelasticity of polymers represents a combination of elastic and viscous flow material responses. Dynamic mechanical analysis (DMA, also called dynamic mechanical thermal analysis, DMTA) enables simultaneous study of both elastic (symbol $'$) and viscous flow (symbol $''$) types of behavior. One determines the response of a specimen to periodic deformations or stresses. Normally, the specimen is loaded in a sinusoidal fashion in shear, tension, flexion, or torsion. If, say, the experiment is performed in tension, one determines the elastic tensile modulus E' called *storage modulus* and the corresponding viscous flow quantity E'' called the *loss modulus*.

Diagrams showing the temperature or frequency dependence of storage and loss modulae can be used to locate the thermal transition regions such as the glass transition—although other methods such as differential scanning calorimetry (DSC) can be used for that purpose as well. At the same time, the dynamic mechanical methods constitute the primary technique for the study of dissipation mechanisms, and thus of CRC. Clearly DMA data are of importance in designing products to be used in, for instance, vibration isolation, where the mechanical damping properties are used to convert mechanical vibrations into heat. Methods of this type are also highly useful in studies of phase separation in multicomponent systems, effects of fillers and other additives, different processing variables, degree of crystallinity, molecular orientation, internal stresses, etc.

Consider a material subjected to an oscillating load of small amplitude that is in the linear viscoelastic range. The angular frequency of the sinusoidal oscillation is ω. A sinusoidal stress σ will produce a sinusoidal strain ε, and vice versa. However, because of the viscous component of the deformation, there will be a phase shift between stress and strain. The pertinent quantities can be represented as follows:

$$\varepsilon = \varepsilon_0 \sin \omega t \tag{24.38}$$

$$\begin{aligned}\sigma &= \sigma_0 \sin(\omega t + \delta) \\ &= \sigma_0 \sin \omega t \cos \delta + \sigma_0 \cos \omega t \sin \delta.\end{aligned} \tag{24.39}$$

Here σ_0 and ε_0 denote, respectively, the amplitudes of stress and strain, t the time, and δ the phase shift between stress and strain. An illustration is provided in Fig. 24.21.

As already mentioned, the description of the response of a viscoelastic material to a sinusoidal tensile strain requires the introduction of two modulae; they are defined as

$$E' = \frac{\sigma_0}{\varepsilon_0} \cos \delta = E_\mathrm{d} \cos \delta \tag{24.40}$$

$$E'' = \frac{\sigma_0}{\varepsilon_0} \sin \delta = E_\mathrm{d} \sin \delta, \tag{24.41}$$

E_d is named the absolute value of the dynamic modulus. Obviously,

$$E_\mathrm{d} = [(E')^2 + (E'')^2]^{1/2}. \tag{24.42}$$

The introduction of E' and E'' enables us to write Eq. (24.39) as

$$\sigma = \varepsilon_0 E' \sin \omega t + \varepsilon_0 E'' \cos \omega t. \tag{24.43}$$

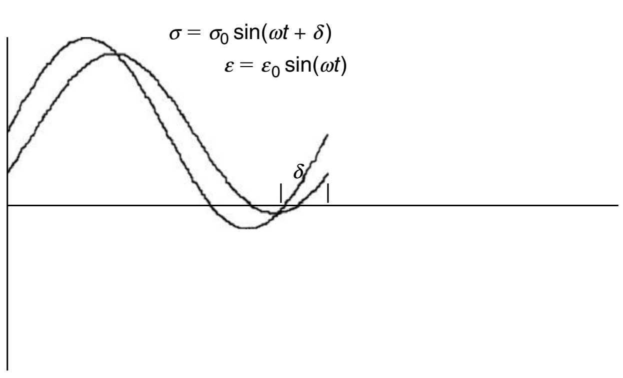

FIGURE 24.21. The phase lag of the strain ε resulting from an applied sinusoidal stress σ.

The ratio

$$\frac{E''}{E'} = \tan\delta \tag{24.44}$$

is the mechanical loss factor. It is a measure of the energy dissipated during a loading cycle relative the energy stored elastically in the material. Sometimes the term internal friction is used instead.

Another way of describing this type of response is to use the similarity between Eq. (24.42) and the decomposition of a number in the complex plane into its real and imaginary components. We can thus define a complex dynamic modulus E^* in the following way

$$E^* = E' + iE'' = E_\mathrm{d}\mathrm{e}^{\mathrm{i}\delta}, \tag{24.45}$$

where E_d is the absolute value of the dynamic modulus introduced in Eqs. (24.40) and (24.41) and equal to σ_0/ε_0.

Figure 24.22 illustrates the decomposition of E^* into its components according to Eq. (24.45). As can be seen, the complex representation is equivalent to that introduced above; see Eqs. (24.40) and (24.41). The modulae relating to dynamic shear and hydrostatic compression, that is G and K, respectively, are defined in the same way as E in the above equations.

In some cases, the inverse values of the complex modulae named compliances are used; these are similar to the transient modulae and compliances such as seen in Eq. (24.9). The complex tensile compliance D^* is thus defined as

$$D^* = \frac{1}{E^*}, \tag{24.46}$$

and the complex shear compliance J^* as

$$J^* = \frac{1}{G^*}. \tag{24.47}$$

The following equations relate the components of D and E:

$$E' = \frac{D'}{D_\mathrm{d}^2},\ E'' = \frac{D''}{D_\mathrm{d}^2}, \tag{24.48}$$

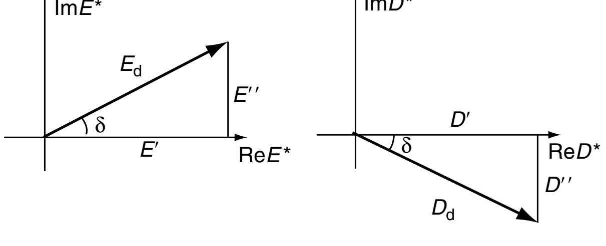

FIGURE 24.22. Graphical representation of the storage and loss moduli E' and E'' as components of a vector E_d in the complex plane. E_d is the absolute value of the dynamic modulus. The corresponding compliances are shown in the right hand part of the figure.

$$D' = \frac{E'}{E_\mathrm{d}^2},\ D' = \frac{E'}{E_\mathrm{d}^2}, \tag{24.49}$$

where D_d is given by $D_\mathrm{d}E_\mathrm{d} = 1$. Similar relations apply to the other moduli and the corresponding compliances. The graphical visualization of the compliance components using the complex plane is shown also in Fig. 24.22.

It should be remembered that the moduli and compliances under discussion are functions of frequency. The quantities E', D' etc. should thus be written $E'(\omega)$, $D'(\omega)$, and so forth. The frequency dependence of these quantities is governed by the same distribution of relaxation or retardation times as is stress relaxation, creep or other time-dependent mechanical phenomena. Single relaxation or retardation times cannot depict the frequency dependence of the dynamic mechanical behavior of polymers.

There is just one book in the world literature on the subject of dynamic mechanical analysis (DMA) which discusses the quantities briefly defined above, namely by Menard [67]. A summary is provided also by Menard in a book chapter [68].

24.5.2 Experimental Procedures

Dynamic mechanical testing allows the use of a variety of instrument types and a wide range of experimental conditions. The temperature may range from practically obtainable subambient up to levels where thermal degradation occurs, the frequencies typically from 0.01 to 1,000 Hz. The results should be examined for possible self-resonances. The elastic modulus of the material to be examined may range from $0.1\,\mathrm{J\,cm^{-3}}$ to $100\,\mathrm{J\,cm^{-3}}$ depending on type of polymer, temperature, and frequency.

The different techniques available for the determination of dynamic mechanical properties include several modes of load application and a number of dependent variables (temperature, frequency, and time). ASTM D 4092 provides a collection of definitions and terms, the most important of them described in Section 24.5.1. ASTM D 4065 describes standard practice in determining dynamic mechanical properties according to a variety of experimental methods; see Fig. 24.23.

24.5.3 Fatigue Determination

Plastics parts subjected to repeated loading may undergo failure by so-called dynamic fatigue. The term dynamic intends to distinguish this type of failure from that mentioned in static loading—as for instance in creep where the term static fatigue is sometimes used; see Section 24.3.6. The stress levels leading to failure are in both cases lower than those recorded in short-term tests. In dynamic fatigue, it is often observed that no failure occurs when the stress amplitude is lower than a certain value, the so-called fatigue or endurance limit, often characteristic of the material being studied.

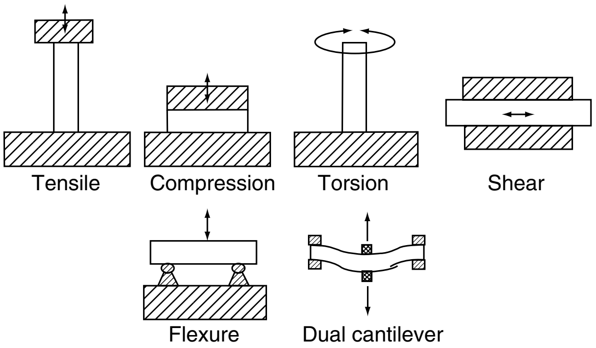

FIGURE 24.23. Schematic picture of various loading modes used in dynamic mechanical testing.

Fatigue testing of polymers cannot be accelerated by simply increasing the loading frequency. The reason is the relatively high level of mechanical damping (internal friction) in common polymers which would produce an excessive heating of the specimen.

Fatigue tests provide data on the number of loading cycles producing certain types of deterioration of the material (crack initiation and propagation, fatigue failure, softening due to energy dissipation). The ASTM test D 671, based on a constant force amplitude, allows these effects to be studied at varying stress levels and environmental conditions. When used for design purposes, the testing and end-use conditions are to be similar. Differences in the fatigue behavior may also be noted when employing testing equipment different from that described in the standard.

There exists a related but different German Standard DIN 53 442 which uses dumb-bell-shaped specimens differing from those used for tensile testing by a rounded middle section. Another difference in comparison with the above ASTM method is the use of constant deformation amplitude of the vibrations. This results in a stress amplitude decreasing with time due to stress relaxation. Apart from this, the stress amplitude diminishes also due to the heating of the specimen. The results are reported in a similar manner as required by the ASTM standard with the stress amplitude relating to the first cycle.

24.5.4 Application of Time–Frequency Correspondence Principle

We have explained the correspondence principles in Section 24.1.3, including the time—frequency correspondence. We were not able to apply this particular principle before becoming familiar with dynamic mechanical experiments. We need to provide at least an example of the application of the correspondence in the frequency domain. In Fig. 24.24 we show results from [58] pertaining to HDPE. The shift factors used to obtain that diagram have been calculated from equations in Section 24.1.3. More examples can be found for instance in the same paper [58].

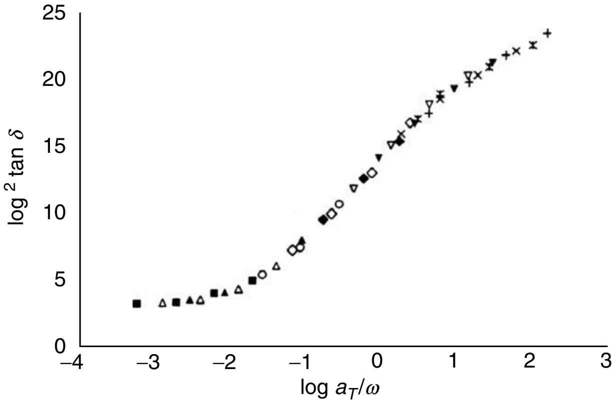

FIGURE 24.24. The master curve for HDPE of tan δ vs. log a_T/ω for 40°C and $\lambda = 1$; after [58].

24.6 ELASTOMERS

24.6.1 Mechanical Behavior as a Function of Temperature

The most amazing thing about elastomeric polymers is the fact that they can be stretched by several hundreds of percent and still behave elastically; that is the engineering stress σ (Eq. (24.31) will still be directly proportional to the engineering strain ε (Eq. (24.32)). This in contrast to other polymers, and in an even sharper contrast to metals and ceramics in which the elastic region ends at one percent elongation or even less. As a result, the elastic tensile modulus E (see Eq. (24.33)) is $1.1 \times 10^5 \mathrm{J\,cm^{-3}}$ for copper, $7.2 \times 10^4 \mathrm{J\,cm^{-3}}$ for clear fused quartz, $2 \times 10^3 \mathrm{J\,cm^{-3}}$ for nylon (that is a nonelastomeric polymer) and only about $1 \mathrm{J\,cm^{-3}}$ for gum rubber.

The explanation of the behavior which is ordinarily called rubbery lies in the huge number of possible conformations in elastomeric chains. When a copper wire is drawn, we soon come to weakening and eventual destruction of primary chemical bonds between Cu atoms. When a rubber band is drawn, rotations and other changes results in new conformations, but the primary bonds are preserved. This can be described as *unkinking* and *straightening out* of kinked and "mixed up spaghetti-like" elastomeric chains.

It is essential to note that elastomers do *not* always behave in the manner known from stretching a rubber band at room temperature. Some of us might have seen an experiment when such a rubber band was put into liquid nitrogen, became brittle, and when stretching was attempted the band broke into little fragments. Thus, in general the type of behavior of an elastomer depends on the *temperature*. This is shown in Fig. 24.25: the elastic modulus E (for a certain fixed time after the imposition of a force) as a function of temperature T. At low temperatures we have the brittle behavior—as the rubber band in liquid nitrogen;

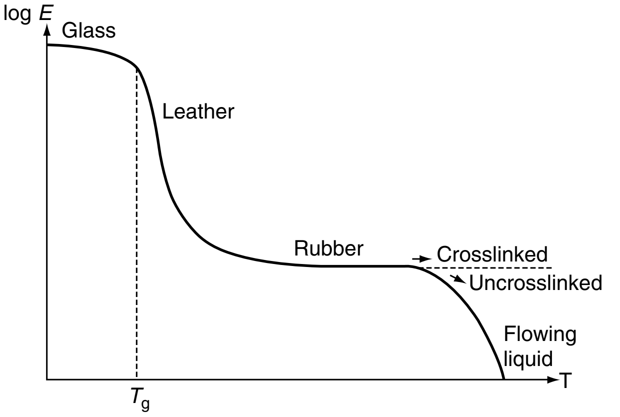

FIGURE 24.25. Dependence of the tensile modulus E (for a fixed time t since the imposition of a force) on temperature T for an elastomer.

the modulus E is relatively high. Then from the glass transition temperature T_g up to approximately $T_g + 30K$ we have the *leathery* state—with *retarded* high elasticity. Then comes the *rubbery* behavior known to us from stretching the elastomeric band at room temperature: *instantaneous* high elasticity. Finally, if the elastomer is not cross-linked, we have melting and liquid flow. If the elastomer is cross-linked, the rubbery plateau persists. We conclude that an elastomer might exhibit glassy, leathery, rubbery, or liquid flow behavior.

24.6.2 Thermodynamic and Molecular Behavior

We have already referred to the fact that the explanation for the instantaneous high elasticity lies at the molecular level. This is a vast area of active research, and we do not have space to discuss details, but we can recommend to the reader a book by Mark and Erman [69] which covers precisely that field.

Here we shall mention only two facts. First, the behavior at the molecular level can be related to the macroscopic *thermodynamic* description. For the simple uniaxial tension we have

$$dU = TdS - PdV + Fdl \tag{24.50}$$

$$dA = -SdT - PdV + Fdl, \tag{24.51}$$

where the symbols have the same meaning as before: U is energy; S, entropy; F, force; and l is the length while A is the Helmholtz function. Second, Eqs. (24.50) and (24.51) can be used in conjunction with the analysis of a *memoryless* system (also known as the story of the drunkard walk) to obtain the following relation:

$$F = kTl/Nh^2, \tag{24.52}$$

where N is a constant proportional to the degree of polymerization, k is the Boltzmann constant while h is the length of one segment. We can easily verify that the last result is true: when we put a stretched piece of rubber between our lips, under given tension the specimen shrinks when warmed. In other words, since F, N, and h^2 are all constant, an increase in T must produce a decrease in l. Other cases such as biaxial extension and shear are treated in the already quoted book of Mark and Erman [69].

24.6.3 Swelling of Networks

Some polymeric materials are water-repellent and thus used for instance as impregnation of overcoats, but some elastomeric and other networks absorb liquid penetrants avidly and swell—until an equilibrium degree of swelling is reached. Since this is only one chapter in the Handbook, of limited length, again we shall take the same short-cut as in the preceding Subsection: we recommend to the reader the book by Mark and Erman [69]. Since the behavior of elastomers is characterized in terms of energy and Helmholtz function, as in our Eqs. (24.50) and (24.51), we need a relation for the calculation of change of A caused by swelling [70]:

$$\Delta A_{\text{swelling}} = \Delta A_{\text{el}} + \Delta A_{\text{mix}}. \tag{24.53}$$

That is, the change in the Helmholtz function on swelling consists of an elastic ("mechanical") contribution ΔA_{el} resulting from the change of dimensions of the network caused by the solvent penetration and also from the "thermodynamic" contribution ΔA_{mix} caused by polymer + solvent interactions upon mixing. The latter can be calculated for the swelling process by similar procedures as for polymer + polymer or liquid + liquid systems. Equation (24.53) is thus the starting point for dealing with mechanical, thermodynamic, and molecular behavior of swollen networks. The assumption that there is no mixed term, that is mechanical effects do not affect thermodynamic ones nor vice versa, has been supported by results for several systems [70].

24.6.4 Filled Elastomers

Natural rubber crystallizes on elongation—a phenomenon called *strain-induced crystallization*—what enhances mechanical properties. However, a filler in the form of carbon black is typically added to natural rubber to additionally modify the mechanical properties. Elastomers which cannot undergo strain-induced crystallization contain even more fillers. Carbon black is used in such cases also, but silicone rubbers are filled with silica.

Automotive tires constitute the classic example of carbon-black reinforced elastomers. The elastomer can be either natural rubber—as typically is the case of truck and aircraft tires, or else a synthetic rubber—as is typical for automobile tires. However, reinforcing fillers constitute only one of many additives. There are also antioxidants, light stabilizers, plasticizers, antiplasticizers, impact modifiers, processing aids, colorants, flame retardants, crosslinking agents etc. There exists a thorough collective book edited by Zweifel [71] on polymer additives, which discusses filers and reinforcements in some detail.

24.7 OTHER ISSUES

24.7.1 Brittleness and Aging

There is still a number of topics related to mechanical properties of polymers which we did not cover. One of them is *aging* in the glassy state: tending toward equilibrium, the material increases its density, and thus lowers its free volume. We do not have space for it, but aging is understandable in terms of CRC as explained in Section 24.1, and is discussed in some detail by Robertson and Kim [72].

An important result of aging *is brittleness*. Of course, there are also materials which are brittle even without aging. Brittleness is not a simple inverse of ductility (for which there is more than one definition) nor of toughness. Brittleness has been defined [73] as

$$B = 1/(\varepsilon_b \cdot E') \tag{24.54}$$

where ε_b is the elongation at break in tensile testing (along with the stress at break σ_b and other quantities, see Tables below) while E′ is known to us From Section 24.5.1. Thus, the first term in the denominator comes from quasi-static tensile testing and the second from DMA. Application of Eq. (24.54) shows that polystyrene is highly brittle, what explains odd behavior of PS in a variety of circumstances [73].

24.7.2 Nanoindentation

Nanoindentation is a technique gaining increasing popularity [74–76]. Actually, the technique is sometimes abused by attempts to calculate the elastic modulus E on the basis of a model valid for fully elastic materials only [74]. While such attempts fail, a connection has been found by Fujisawa and Swain between E and the unloading strain rate [75]. As shown by Tweedie and Van Vliet [76], spherical indentation provides lower contact strains and more reliable results than conical indentation. A modification providing repetitive indenter hits perpendicular to the specimen surface at the same spot and thus nanoindentation fatigue testing (NIFT) exists also [77].

24.7.3 Tribology

Another important area is *tribology* which includes friction, scratch resistance, wear and design of interactive surfaces in relative motion [78]. Rabinowicz [78] describes vividly huge annual losses to industry caused by wear. Some tribologists claim that their discipline is not a part of mechanics but independent and comparable to mechanics in its importance. A review of polymer tribology which includes fundamental definitions is available [79]. Similarly as mechanical properties, tribological properties of polymers can be varied by using additives; thus, carbon black can be used for the purpose [80]. By contrast, using external liquid lubricants—which work so well for metal surfaces—is in many cases dangerous because of swelling described above. Another option is application of magnetic fields which cause polymer orientation and thus can improve scratch resistance [81].

24.8 TABLES OF SELECTED MECHANICAL DATA

Following are selected data for the most often used polymers. They have been divided (partly arbitrarily, because of the overlap in definitions) into four tables, numbered from 24.3 to 24.6 respectively, for general purpose polymers, engineering polymers, thermosets, and elastomers. The third column in each of these tables shows the values of density, the fourth of the tensile modulus, the fifth the stress at break, the sixth the elongation at break; IS denotes the Izod impact strength for notched specimens. The letters *A* and *C* in the last column in Tables 24.3 and 24.4 pertain respectively to amorphous and crystalline thermoplastic polymers.

ACKNOWLEDGMENTS

Professor Josef Kubát of the Chalmers University of Technology in Gothenburg and Dr. Michael J. Kubát of the Royal Institute of Technology in Stockholm have participated in writing this chapter for the first Handbook edition. Thanks are due to Professor G.H. Michler of the Institute of Materials Science of the Martin Luther University in Merseburg for providing us with the micrographs used in Section 24.4. I appreciate discussions with: Professor Michael Bratychak, Lvivska Politechnika National University; Dr. Georg Broza, Technical University of Hamburg; Dr. Rimantas Levinskas, Lithuanian Energy Institute, Kaunas; Professor Robert Maksimov, Institute of Polymer Mechanics, the Latvian National University, Riga; Professor Moshe Narkis, Technion, Haifa, Dr. Dorota Pietkiewicz, LAPOM, University of North Texas, Denton; and Professor Anuvat Sirivat, Chulalongkorn University, Bangkok.

TABLE 24.3. *Mechanical properties of thermoplastics: commodity (general purpose) plastics.*

Polymer	Grade	$\rho/(\mathrm{g/cm^3})$	E/(GPa)	σ_b/(MPa)	ε_b/(%)	IS/(J/m)	Structure
PE LD, LDPE Polyethylene, low density		0.915–0.93	0.14–0.3	7–17	200–900	NB	C
PE HD, HDPE Polyethylene, high density		0.94–0.97	0.7–1.4	20–40	100–1000	30–200	C
PE UHMW, UHMW PE Polyethylene, ultra-high molecular weight		0.93–0.94	0.1–0.7	20–40	200–500	NB	C
PP polypropylene	Homopolymer	0.90–0.91	1.1–2	30–40	100–600	20–75	C
PP polypropylene	−40% glass fiber filled	1.22–1.23	6.8–7.2	60–110	1.5–4	75–110	
PP	Copolymer	0.89–0.905	0.9–1.2	28–40	200–500	60–750	C
PVC Poly(vinyl chloride)	Rigid (RPVC)	1.32–1.58	1–3.5	40–75	30–80	20–1000	A
PVC	Flexible (FPVC, plasticized)	1.16–1.70	0.05–0.15	6–25	150–400	—	A
PS Polystyrene		1.04–1.05	2.4–3.2	30–60	1–4	13–25	A
SB Styrene-butadiene	Rubber-modified PS High-impact PS, HIPS	0.98–1.10	1.5–2.5	15–40	15–60	50–400	A
ABS Acrylonitrile-butadiene-styrene	Medium IS	1.03–1.06	2–2.8	30–50	15–30	130–320	A
ABS Acrylonitrile-butadiene-styrene	High IS	1.01–1.04	1.6–2.5	30–40	5–70	350–600	A
SAN Styrene-acrylonitrile		1.07–1.09	3.4–3.7	55–75	2–5	15–30	A
ASA Acrylate-styrene-acrylonitrile		1.05–1.07	2.2–2.4	30–50	20–40	450–600	A

TABLE 24.4. *Mechanical properties of thermoplastics: engineering plastics.*

Polymer	Grade	$\rho/(\mathrm{g/cm^3})$	E/(GPa)	σ_b/(MPa)	ε_b/(%)	IS/(J/m)	Structure
PA 6 Polyamide 6 (Polycaprolactam)	[a]	1.13	3	80	50–120	30–120	C
PA 6 Polyamide 6 (Polycaprolactam)	[b]		1.5	50	160–200	160	
PA 6 Polyamide 6 (Polycaprolactam)	[a] 30–35% glass fiber	1.35–1.42	8–10	170–180	2–4	50	C
PA 6 Polyamide 6 (Polycaprolactam)	[b] 30–35% glass fiber		5.5	110		95	
PA 66 Polyamide 66 [Poly(hexamethyleneadipamide)]	[a]	1.14	3.4	75–90	20	30–55	C
PA 66 Polyamide 66 [Poly(hexamethyleneadipamide)]	[b]		17–2	50	80	50–110	C
PA 11 Polyamide 11 [Poly(11-aminoundecanoic acid)]	[a]	1.04	1.5	45–50	400–500	100–NB	C
POM Polyacetal Polyoxymethylene	Homopolymer	1.42	3.1	65–70	25–75	60–120	C
POM Polyacetal Polyoxymethylene	Copolymer	1.41	2.8	65–72??	40–75	50–80	C
PET Poly(ethylene terephthalate)		1.29–1.40	3	50	50–300	12–40	C
PBT Poly(butylene terephthalate)		1.31	2.3–2.5	50–60	120–200	40–55	C
PBT Poly(butylene terephthalate)	+30% glass fiber	1.52	10	100–140	2–4	80–130	
PC Polycarbonate		1.2	2.1–2.4	70–90	100–120	650–1000[c]	A
CA Cellulose acetate		1.27–1.32	1.5–2.5	25–45	10–70	100–450	A
CAB Cellulose acetate butyrate		1.18	1.4–1.8	30–35	30–100	50–500	A
PMMA Poly(methyl methacrylate)		1.17–1.20	2.5–3.3	55–75	3–5	10–20	A
PTFE Polytetrafluoroethylene		2.15–2.20	0.41	7–30	200–400	150	C
PSU (PSO) Polysulfone		1.25	2.5–2.6	70	50–100	65–70	A
PES Polyethersulfone		1.37	2.5	80–90	40–80	75–120	A
PPS Poly(phenylene sulfide)		1.35	3.6	65–75	1–2	70	C
PPO (PPE) Poly(phenylene oxide) or -ether	Modified with PS	1.06–1.08	2.2–2.7	50–60	200–350	200–370	A
PEEK Polytetheretherketone		1.32	3.6	90–200	50	80	C
PEEK Polyetheretherketone	30% glass fiber	1.49	10	100	2	100	C

[a] dry as molded.
[b] at 50% relative humidity.
[c] thickness 3.2 mm.

TABLE 24.5. *Mechanical properties: thermosets.*

Polymer	Grade	$\rho/(\mathrm{g/cm^3})$	$E/(\mathrm{GPa})$	$\sigma_b/(\mathrm{MPa})$	$\varepsilon_b/(\%)$	IS/(J/m)
PF Phenol-formaldehyde resin	Wood-flour (ca. 50%) filled molding compound	1.37–1.46	5.5–12	30–60	0.4–0.8	10–30
PF Phenol-formaldehyde resin	Impact modified, cellulose filled (ca. 50%)	1.38–1.42		25–45	1–2	20–60
MF Melamine-formaldehyde resin	Cellulose filled (ca. 50%)	1.47–1.52	8–10	35–100	0.5–1	10–20
UF Urea-formaldehyde resin	Cellulose filled (ca. 50%)	1.46–1.48	7–9	40–60	0.4–0.8	10–20
Polyester thermosetting resin	Cast, rigid	1.04–1.46	2–4.5	30–40	1.5–2.5	10–20
Polyester thermosetting resin	Premix, chopped glass	1.65–2.30	7–17	20–60	1	80–320
Polyester thermosetting resin	Woven glass cloth	1.5–2.1	10–30	200–350	1–2	300–1600
Epoxy resin	Unfilled	1.2–1.3	3–5	30–90	1–2	10–50
SMC Sheet molding compound	Glass fiber reinforced SMC	1.6–2	15–30	140–250	0.5–2	1600–2100

TABLE 24.6. *Mechanical properties: elastomers.*

Polymer	Grade	$\rho/(\mathrm{g/cm^3})$	$E/(\mathrm{MPa})$	$\sigma_b/(\mathrm{MPa})$	ε_b
NR (Natural rubber) *Cis*-polyisoprene	Unfilled vulcanisate	0.93	1–2	17–30	650–900
	50 pph CB, vulc.[a]		3.5–6	14–28	450–600
SBR Styrene-butadiene rubber	Unfilled, vulc. (23–25% styrene)	0.93–1.0	1–2	1.4–2.8	450–600
	50 pph CB, vulc.[a]		14–19	14–27	400–650
IIR (Butyl rubber) Isobutylene-isoprene rubber	Unfilled, vulc.	0.91–0.98	—	17–21	750–950
	50 pph CB, vulc.[a]		4–10	9–21	300–700
NBR (Nitrile rubber) Acrylonitrile-butadiene rubber	Unfilled, vulc. (AN content 26–27%)	0.92	—	4–7	350–800
	50 pph CB, vulc.[a]		8–18	10–30	350–800
CR (Chloroprene rubber) Poly(2-chloro-1,3-butadiene)	Unfilled, vulc.	1.2–1.25	1–3	13–22	800–1000
	50 pph CB, vulc.[a]		3–5	23–25	200–450
EPDM Ethylene-propylene rubber	Unfilled, vulc.	0.85–0.87	—	1.2	400
	50 pph CB, vulc.[a]		5–10	10–16	250–750

[a] pph=parts per hundred; CB=carbon black.

REFERENCES

1. J.D. Ferry, *Viscoelastic Properties of Polymers*, 3rd edition (Wiley, New York 1980).
2. J.J. Aklonis and W.J. MacKnight, *Introduction to Polymer Viscoelasticity*, 2nd edition (Wiley, New York 1983).
3. *Failure of Plastics*, edited by W. Brostow and R.D. Corneliussen (Hanser, Munich, Vienna, New York 1986, 1989, 1992).
4. *Performance of Plastics*, edited by W. Brostow (Hanser, Munich, Cincinnati 2000).
5. W. Brostow, *Mater. Chem. Phys.* **13,** 47 (1985).
6. W. Brostow, Chapter 10 in Ref. 3.
7. W. Brostow, Chapter 5 in Ref. 4.
8. J. Kim and R.E. Robertson, *J. Mater. Sci.* **27,** 300 (1992).
9. J. Karger-Kocsis, *Polym. Eng. Sci.* **36,** 203 (1996).
10. P.J. Flory, *Statistical Mechanics of Chain Molecules* (Wiley, New York 1969).
11. P.J. Flory, *Faraday Soc. Disc.* **49,** 7 (1970).
12. R.A. Orwoll, Chapter 7 in this Handbook.
13. M.H. Litt and A.V. Tobolsky, *J. Macromol. Sci. Phys.* **1,** 433 (1967).
14. D.G. Fesko and N.W. Tschoegl, *J. Polymer Sci. C* **35,** 51 (1971).
15. R.W. Fillers and N.W. Tschoegl, *Trans. Soc. Rheol.* **21,** 51 (1977).
16. W.K. Moonan and N.W. Tschoegl, *Internat. J. Polym. Mater.* **10,** 199 (1984).
17. B. Hartmann, *Proc. Can. High Polym. Forum* **22,** 20 (1983).
18. B. Hartmann and M.A. Haque, *J. Appl. Phys.* **58,** 2831 (1985).
19. B. Hartmann and M.A. Haque, *J. Appl. Polym. Sci.* **30,** 1553 (1985).
20. P. Zoller, P. Bolli, V. Pahud and H. Ackermann, *Rev. Sci. Instrum.* **47,** 948 (1976).
21. J.M. Berry, W. Brostow, M. Hess and E.G. Jacobs, *Polymer* **39,** 4081 (1998).
22. W. Brostow, V.M. Castaño, G. Martinez-Barrera and D. Pietkiewicz, *Physica B* **344,** 206 (2004).
23. W. Brostow, V.M. Castaño, G. Martinez-Barrera and D. J.-M. Saiter, *Physica B* **334,** 436 (2003).
24. M.T. O'Shaughnessy, *Textile Res. J.* **18,** 263 (1948).
25. A.Y. Goldman, Prediction of Deformation Properties of Polymeric and Composite Materials (American Chemical Society, Washington, DC 1994).
26. W. Brostow, *Mater. Res. Innovat.* **3,** 347 (2000).
27. M.L. Williams, R.F. Landel and J.D. Ferry, *J. Am. Chem. Soc.* **77,** 3701 (1955).
28. R.M. Criens and H.-G. Moslé, Chapter 21 in Ref. 3.
29. J.E. Shigley and C.R. Mischke, *Mechanical Engineering Design* (McGrawHill, New York 1989).
30. A.A. Griffith, *Phil. Trans. R. Soc.* **A211,** 163 (1921).
31. A.A. Griffith, *Proc. 1st Int. Congress Appl. Mech.* p. 55 (Delft 1924).
32. A.M. Donald and E.J. Kramer, *J. Mater. Sci.* **17,** 1871 (1982).
33. E.J. Kramer, *Adv. Polym. Sci.* **52/53,** 1 (1983).
34. E.J. Kramer, *Polym. Eng. Sci.* **24,** 761 (1984).

35. C.S. Henkee and E.J. Kramer, *J. Mater. Sci.* **21,** 1398 (1986).
36. L.L. Berger and E.J. Kramer, *J. Mater. Sci.* **22,** 2739 (1987).
37. L.L. Berger and E.J. Kramer, *J. Mater. Sci.* **23,** 3536 (1988).
38. E.J. Kramer and L.L. Berger, *Adv. Polym. Sci.* **91/92,** 1 (1990).
39. L.L. Berger, *Macromolecules* **22,** 3162 (1989).
40. L.L. Berger, *Macromolecules* **23,** 2926 (1990).
41. C.J.G. Plummer and A.M. Donald, *Polymer* **32,** 409 (1991).
42. L.L. Berger, *J. Polym. Sci. Phys.* **27,** 1629 (1989).
43. A.M. Donald, Chapter 13 in Ref. 4.
44. H.H. Kausch, Chapter 5 in Ref. 3.
45. R.P. Wool, Chapter 15 in Ref. 4.
46. J.M. Greig and T.R. Smith, *Paper 3 at the Conference on Designing to Avoid Mechanical Failure*, Plastics Institute of London, Cranfield Institute of Technology, 8–10 January 1973.
47. E. Gaube and W.F. Müller, *Kunststoffe* **70,** 72 (1980).
48. W. Brostow and W.F. Müller, *Polymer* **27,** 76 (1986).
49. W. Brostow, M. Fleissner and W.F. Müller, *Polymer* **32,** 419 (1991).
50. R. Simoes, A.M. Cunha and W. Brostow, e-Polymers 2004, no. 067.
51. R. Simoes, A.M. Cunha and W. Brostow, *Model. & Simul. Mater. Sci. & Eng.* **14,** 157 (2006); R. Simoes, A.M. Cunha and W. Brostow, *Comput. Mater. Sci.* **36,** 319 (2006).
52. J. Kubát, *Nature* **204,** 378 (1965).
53. J. Kubát, *Phys. Status Solidi B* **111,** 599 (1982).
54. J. Kubát and M. Rigdahl, Chapter 4 in Ref. 3.
55. W. Brostow and J. Kubát, *Phys. Rev. B* **47,** 7659 (1993).
56. W. Brostow, J. Kubát and M.J. Kubát, *Mater. Res. Soc. Symp.* **321,** 99 (1994).
57. S. Blonski, W. Brostow and J. Kubát, *Phys. Rev. B* **49,** 6494 (1994).
58. Yu. M. Boyko, W. Brostow, A. Ya. Goldman and A.C. Ramamurthy, *Polymer* **36,** 1383 (1995).
59. W. Brostow, N.A. D'Souza, J. Kubát and R. Maksimov, *J. Chem. Phys.* **110,** 9706 (1999).
60. W. Brostow, M. Hess and B.L. López, *Macromolecules* **27,** 2262 (1994).
61. A.E. Akinay, W. Brostow and R. Maksimov, *Polym. Eng. Sci.* **41,** 977 (2001).
62. A.E. Akinay and W. Brostow, *Polymer* **42,** 4527 (2001).
63. A.E. Akinay, W. Brostow, V.M. Castaño, R. Maksimov and P. Olszynski, *Polymer* **43,** 3593 (2002).
64. E.H. Andrews, *Fracture in Polymers* (American Elsevier, New York 1968).
65. G.H. Michler, *Kunststoff-Mikromechanik* (Carl Hanser Verlag, München, Wien 1992).
66. W. Brostow and M.A. Macip, *Macromolecules* **22,** 2761 (1989).
67. K.P. Menard, *Dynamic Mechanical Analysis – An Introduction* (CRC Press, Boca Raton – London, 1999).
68. K.P. Menard, Chapter 8 in Ref. 4.
69. J.E. Mark and B. Erman, *Rubberlike Elasticity - A Molecular Primer* 2nd edn. (Cambridge University Press, 2000).
70. W. Brostow, *Macromolecules* **4,** 742 (1971).
71. *Plastics Additives Handbook*, edited by H. Zweifel (Hanser, Munich, Cincinnati 2000).
72. R.E. Robertson and J.-H. Kim, Chapter 14 in Ref. 4.
73. W. Brostow, H.E. Hagg Lobland and M. Narkis, *J. Mater. Res.* **21,** 2422 (2006).
74. W.C. Oliver and G.M. Pharr, *J. Mater. Res.* **7,** 1564 (1992); W.C. Oliver and G.M. Pharr, *J. Mater. Res.* **19,** 3 (2004).
75. N. Fujisawa and M.V. Swain, *J. Mater. Res.* **21,** 708 (2006).
76. C.A. Tweedie and K.J. Van Vliet, *J. Mater. Res.* **21,** 1576 (2006).
77. B.D. Beake, B. Bilyeu, W. Brostow and W. Chonkaew, *Polymer Internat.* 56 (2007) to be published.
78. E. Rabinowicz, *Friction and Wear of Materials*, 2nd edn. (Wiley, New York, 1995).
79. W. Brostow, J.-L. Deborde, M. Jaklewicz and P. Olszynski, *J. Mater. Ed.* **24,** 119 (2003).
80. W. Brostow, M. Keselman, I. Mironi-Harpaz, M. Narkis and R. Peirce, *Polymer* **46,** 5058 (2005).
81. W. Brostow and M. Jaklewicz, *J. Mater. Res.* **19,** 1038 (2004).

CHAPTER 25

Chain Dimensions and Entanglement Spacings

L. J. Fetters*, D. J. Lohse†, and R. H. Colby‡

*Chemical and Biomedical Engineering, Cornell University, Ithaca, NY 14853-5201; †ExxonMobil Research and Engineering Company, Annandale, NJ 08801-0998; ‡Materials Science and Engineering, Penn State University, University Park, PA 16802

This chapter summarizes data on chain dimensions and entanglement spacings for a number of linear flexible polymers. The polymers are listed in the Appendix along with their abbreviations used in the Tables. The equations relating various important parameters are from the literature [1–3]. While polymer chain entanglement is far from being understood [4–6], one natural idea based on overlap [7] appears useful for thinking about entanglement effects in polymer melts. This concept leads to the entanglement criterion: *a fixed number of entanglement strands (P_e) share a volume equal to the cube of the tube diameter (a^3)* [8–12]. One of the main purposes of this chapter is to test this criterion using literature data on flexible polymer melts and evaluate this universal number. Empirical relations useful for estimating the plateau modulus and entanglement molar mass of polymer melts emerge from this analysis. Chain entanglement is important, not merely for melt rheology, but also for mechanical properties of glassy [13] and semicrystalline polymers [14]. This chapter first discusses chain dimensions of polymers and then discusses chain entanglement and the tube diameter. The critical molar mass for entanglement effects in melt viscosity is then discussed, followed by the temperature dependence of chain dimensions.

25.1 CHAIN DIMENSIONS

In either the melt state or in a θ-solvent solution, linear flexible polymers adopt Gaussian statistics, and their average conformation is described as a random walk. Consequently, the ratio of their unperturbed mean-square end-to-end distance $<R^2>_0$ and their molar mass M is a constant, for large M, that characterizes their chain dimensions. In practice, the ratio $<R^2>_0/M$ depends weakly on temperature in the melt and the specific choice of θ-solvent, imparting a weak temperature dependence to various quantities calculated from that ratio.

The Kuhn length b of a polymer is the ratio of the mean-square end-to-end distance $<R^2>_0$ and the fully extended size $R_{\max}$

$$b \equiv \frac{\langle R^2 \rangle_0}{R_{\max}}. \tag{25.1}$$

Aliphatic backbone polymers have n backbone bonds, with a well-defined average backbone bond length l, and known backbone bond angle θ, making $R_{\max} = nl\cos(\theta/2)$ in the all-*trans* conformation. Flory defined [15] the characteristic ratio C_∞ as the ratio of the actual unperturbed mean-square end-to-end distance $<R^2>_0$ and that of a freely jointed chain nl^2, which is a polymer-specific constant at large M

$$C_\infty \equiv \frac{\langle R^2 \rangle_0}{nl^2} = \frac{m_b \langle R^2 \rangle_0}{l^2 M}. \tag{25.2}$$

The second equality uses the equation $n = M/m_b$, where m_b is the average molar mass per backbone bond. Using this definition of C_∞, the Kuhn length can be rewritten as:

$$b = \frac{C_\infty nl^2}{nl\cos(\theta/2)} = \frac{C_\infty l}{\cos(\theta/2)}. \tag{25.3}$$

It is common to assume the fully extended conformation is a linear chain (ignoring bond angles) and hence $R'_{\max} = nl$, and $b' = C_\infty l$. Since the bond angle of a polyethylene chain is $\theta = 68°$, $b'/b = \cos(\theta/2) = 0.83$. In principle, either convention may be utilized; here we use Eq. (25.3) to calculate the Kuhn length.

The Kuhn length is the effective monomer size for the equivalent freely jointed chain (N Kuhn monomers of length b instead of n backbone bonds of length l)

$$\langle R^2 \rangle_0 = C_\infty n l^2 = N b^2, \quad R_{\max} = Nb. \tag{25.4}$$

The molar mass of a Kuhn monomer is $M_0 = M/N$ and the volume occupied by the Kuhn monomer is $\nu_0 = M_0/\rho N_{\mathrm{Av}}$, where ρ is the density and N_{Av} is Avogadro's number. This description of chain dimensions can be used to calculate many quantities. For example, combining Eqs. (25.3) and (25.4) yields the number of main chain bonds in a Kuhn monomer $n/N = C_\infty / \cos^2(\theta/2)$.

Witten *et al.* [16] define the packing length p as the ratio of the occupied volume of a chain $M/\rho N_{\mathrm{Av}}$ and the mean-square end-to-end distance

$$p \equiv \frac{M}{\langle R^2 \rangle_0 \, \rho N_{\mathrm{Av}}} = \frac{M_0}{b^2 \rho N_{\mathrm{Av}}} = \frac{\nu_0}{b^2}. \tag{25.5}$$

25.2 CHAIN ENTANGLEMENT AND TUBE DIAMETER

The plateau modulus G_{e} defines the entanglement spacing of a polymer melt, and the entanglement molar mass M_{e}[17]

$$M_{\mathrm{e}} \equiv \frac{\rho R T}{G_{\mathrm{e}}} = V_{\mathrm{e}} \rho N_{\mathrm{Av}}, \tag{25.6}$$

where $R = kN_{\mathrm{Av}}$ is the ideal gas constant (k is the Boltzmann constant), T is the absolute temperature, and $V_{\mathrm{e}} \equiv kT/G_{\mathrm{e}} = M_{\mathrm{e}}/(\rho N_{\mathrm{Av}})$ is the entanglement volume. The length scale associated with the entanglement spacing is the tube diameter a [3]. Since a chain in the melt is Gaussian on all scales larger than the Kuhn length, and for flexible chains $a \gg b$, the tube diameter is related to the entanglement molar mass through the chain dimensions

$$a = \sqrt{\frac{\langle R^2 \rangle_0 \, M_{\mathrm{e}}}{M}} = b\sqrt{N_{\mathrm{e}}}, \tag{25.7}$$

where N_{e} is the number of Kuhn monomers in an entanglement strand (of molar mass M_{e}). The occupied volume of an entanglement strand is V_{e}

$$V_{\mathrm{e}} = \nu_0 N_{\mathrm{e}} = \nu_0 \left(\frac{a}{b}\right)^2 = a^2 p. \tag{25.8}$$

In analogy to polymer networks (where the equilibrium modulus is kT per network strand) the plateau modulus is kT per entanglement strand

$$G_{\mathrm{e}} = \frac{kT}{V_{\mathrm{e}}} = \frac{b^2 kT}{\nu_0 a^2} = \frac{kT}{a^2 p}. \tag{25.9}$$

The number of entanglement strands P_{e} within the confinement volume a^3 is determined as the ratio of confinement volume and entanglement strand volume (an overlap parameter [3] for entanglement)

$$P_{\mathrm{e}} \equiv \frac{a^3}{V_{\mathrm{e}}} = \frac{a}{p}. \tag{25.10}$$

This number appears to be constant for flexible polymers, with the average value $P_{\mathrm{e}} = 20.6(\pm 8\%)$. Table 25.1 shows data for polyolefin melts listing density ρ, plateau modulus G_{e}, melt chain dimensions from SANS $<R^2>_0/M$, entanglement molar mass M_{e} calculated from Eq. (25.6), Kuhn length b, packing length p, tube diameter a, and the overlap parameter for entanglement P_{e}, all at temperature T.

Since P_{e} is apparently a polymer-independent constant, Eq. (25.10) suggests that the tube diameter and packing length are proportional, and the constant of proportionality thus has the empirical temperature dependence [1,2]:

$$a = 14.0 \exp(T/1270)\, p. \tag{25.11}$$

Using Eqs. (25.6), and (25.9)–(25.11), we can obtain useful empirical equations [2] for the entanglement molar mass and the plateau modulus

$$M_{\mathrm{e}} = P_{\mathrm{e}}^2 p^3 \rho N_{\mathrm{Av}} = 200 \exp(T/635)\, \rho p^3 N_{\mathrm{Av}}, \tag{25.12}$$

$$G_{\mathrm{e}} = \frac{\exp(-T/635)}{200} \frac{kT}{p^3}. \tag{25.13}$$

Table 25.1 lists these quantities for polyolefins. Table 25.2 lists these quantities for polydienes while polyacrylics and polymethacrylics are listed in Table 25.3. Table 25.4 lists these quantities for various other flexible linear polymers.

25.3 CRITICAL MOLECULAR WEIGHT

The critical molar mass (M_{c}) parameter [18,19] denotes the transition in the melt viscosity/molar mass relation as the exponents change from ~1 to ~3.4. Table 25.5 presents the polymers for which the M_{c} values are known while Table 25.6 lists the polymers for which, seemingly, $M_{\mathrm{c}}/M_{\mathrm{e}}$ is one. The ratio of $M_{\mathrm{c}}/M_{\mathrm{e}}$ was long taken to be ~2 [18] and thus to be species independent. However, a recent empirical compilation [19] has shown that the ratio is p dependent and varies from ~3.5 (PE; $p = 1.69$) to ~1.4 (*a*-PCHE; $p = 5.59$). Based upon the data of Table 25.5 this ratio is empirically expressed as:

$$\frac{M_{\mathrm{c}}}{M_{\mathrm{e}}} = 3.42 p^{-0.534} = \left[\frac{p^*}{p}\right]^{0.534}. \tag{25.14}$$

M_{c} hence follows the empirical expression:

$$M_{\mathrm{c}} = M_{\mathrm{e}} \left[\frac{p^*}{p}\right]^{0.534}, \tag{25.15}$$

where $M_{\mathrm{c}} = M_{\mathrm{e}}$ at $p = p^* \approx 10$ Å. With M_{c} expressed in this fashion, M_{e} overtakes M_{c} as p approaches p^* in the 10 Å range. At least four polymers exist with $p \cong 10$ Å (see Table

TABLE 25.1. *Molecular characteristics of olefinic polymers and copolymers.*

Polymer	T (K)	ρ (g cm^{-3})	G_e (MPa)	$<R^2>_o/M$ (Å^2)	C_∞	b (Å)	ν_o (Å^3)	M_o	p (Å)	M_e	a (Å)	N_e	P_e
PE	298	0.851	3.5	1.40	8.26	15.4	329	168.3	1.39	602	29.0	3.58	20.8
PE	413	0.785	2.6	1.25	7.38	13.7	318	150.4	1.69	1,040	36.0	6.89	21.3
PEB-2	389	0.802	2.5	1.25	7.70	14.3	339	163.5	1.66	1,040	36.0	6.34	21.7
PEB-2	413	0.785	2.2	1.22	7.51	14.0	338	159.5	1.73	1,220	38.7	7.68	22.3
PEB-5	413	0.788	1.90	1.15	7.47	13.9	353	167.3	1.83	1,420	40.5	8.51	22.1
PEB-7	413	0.789	1.55	1.05	7.08	13.2	347	164.9	1.90	1,750	42.8	10.6	23.0
PEB-10	413	0.791	1.35	1.05	7.53	14.0	391	186.2	2.00	2,010	46.0	10.8	23.0
PEB-12	298	0.860	1.50	1.04	7.72	14.3	382	197.6	1.86	1,420	38.4	7.18	20.7
PEB-12	413	0.793	1.20	0.952	7.06	13.1	379	180.9	2.20	2,270	46.5	12.5	21.1
alt-PEP	298	0.856	1.10	0.924	7.21	13.4	376	194.0	2.10	1,930	42.2	9.93	20.1
alt-PEP	373	0.812	1.03	0.871	6.80	12.6	374	182.9	2.35	2,440	46.1	13.4	19.6
alt-PEP	413	0.790	0.97	0.834	6.51	12.1	368	175.1	2.52	2,790	48.3	16.0	19.2
PEB-18	298	0.860	1.12	0.926	7.42	13.8	396	205.1	2.09	1,900	42.0	9.27	20.1
PEB-18	413	0.797	0.90	0.913	7.31	13.6	421	202.2	2.28	3,040	52.7	15.0	23.1
HPI-16	373	0.812	0.88	0.813	6.51	12.1	368	180.1	2.52	2,860	48.2	15.9	19.2
HPI-20	373	0.812	0.79	0.788	6.45	12.0	372	181.9	2.60	3,190	50.1	17.5	19.3
PEB-25	298	0.864	0.69	0.800	7.08	13.2	416	216.4	2.40	3,100	49.8	14.3	20.7
PEB-25	413	0.799	0.67	0.799	7.07	13.1	449	216.2	2.60	4,090	57.2	18.9	22.0
a-PP	298	0.852	0.48	0.678	6.00	11.2	358	183.4	2.88	4,390	54.6	23.9	19.0
a-PP	348	0.825	0.48	0.678	6.00	11.2	369	183.4	2.97	4,970	58.1	27.1	19.5
a-PP	413	0.791	0.47	0.678	6.00	11.2	385	183.4	3.10	5,780	62.6	31.5	20.2
a-PP	463	0.765	0.42	0.678	6.00	11.2	398	183.4	3.20	7,010	68.9	38.2	21.5
i-PP	463	0.766	0.43	0.694	6.15	11.4	407	187.8	3.12	6,850	69.0	36.5	22.1
s-PP	463	0.766	1.35	1.03	9.12	16.9	604	278.7	2.10	2,180	47.4	7.83	22.5
HHPP	298	0.878	0.52	0.691	6.12	11.4	353	187.0	2.74	4,180	53.8	22.4	19.6
HHPP	413	0.810	0.52	0.691	6.12	11.4	383	187.0	2.97	5,350	60.8	28.6	20.5
HPI-34	373	0.812	0.50	0.703	6.25	11.6	392	192.0	2.91	5,030	59.5	26.2	20.4
alt-PEB	298	0.861	0.58	0.725	6.88	12.8	434	225.2	2.66	3,680	51.6	16.3	19.4
alt-PEB	413	0.800	0.52	0.692	6.57	12.2	446	214.9	3.00	5,280	60.4	24.6	20.1
PEB-32	298	0.863	0.44	0.641	6.22	11.5	400	208.0	3.00	4,860	55.8	23.3	18.6
PEB-32	413	0.802	0.43	0.692	6.71	12.5	465	224.6	2.99	6,400	66.6	28.5	22.2
HPI-50	373	0.812	0.35	0.632	6.21	11.5	430	210.5	3.24	7,190	67.4	34.2	20.8
PEB-40	298	0.864	0.24	0.570	6.06	11.3	427	222.1	3.37	8,910	71.3	40.1	21.1
PEB-40	413	0.805	0.30	0.595	6.32	11.7	478	231.8	3.47	9,210	74.0	39.7	21.3
PIB	298	0.918	0.34	0.570	6.73	12.5	496	274.2	3.18	6,690	61.7	24.4	19.4
PIB	413	0.849	0.30	0.557	6.58	12.2	524	267.9	3.51	9,710	73.6	36.3	20.9
a-PEE	298	0.866	0.18	0.480	5.67	10.5	443	230.9	4.00	11,900	75.6	51.6	18.9
a-PEE	413	0.807	0.20	0.508	6.00	11.1	503	244.3	4.05	13,800	83.9	56.7	20.7
HPI-75	300	0.855	0.12	0.452	6.67	12.4	660	339.7	4.30	17,800	89.6	52.3	20.8
HPMYRC	324	0.832	0.12	0.434	6.73	12.5	720	360.6	4.60	18,700	90.0	51.8	19.6
a-PHEX	273	0.871	0.14	0.542	9.60	17.8	1119	586.6	3.52	14,100	87.5	24.1	24.9
HPMYRC-64	308	0.871	0.10	0.409	7.36	13.7	895	457.5	4.78	21,700	94.3	47.5	19.7
a-PCHE	433	0.920	0.068	0.323	7.49	13.9	1082	599.4	5.59	48,700	125.4	81.2	22.4

TABLE 25.2. *Molecular characteristics of polydiene polymers and copolymers.*

Polymer	T (K)	ρ (g cm^{-3})	G_e (MPa)	$<R^2>_o/M$ (Å^2)	C_∞	b (Å)	ν_o (Å^3)	M_o	p (Å)	M_e	a (Å)	N_e	P_e
cis-PI	298	0.910	0.58	0.679	5.20	9.34	235	128.6	2.69	3,890	51.4	30.2	19.1
PI-7	298	0.900	0.35	0.596	4.70	8.44	221	119.6	3.10	6,370	61.6	53.2	19.9
PI-16	298	0.899	0.35	0.593	4.88	8.82	243	131.2	3.12	6,360	61.4	48.5	19.8
PI-20	298	0.898	0.35	0.591	4.96	8.98	253	136.5	3.13	6,350	61.3	46.5	19.6
PI-29	298	0.896	0.35	0.587	5.20	9.39	279	150.3	3.16	6,340	61.0	42.2	19.3

TABLE 25.2. *Continued.*

Polymer	T (K)	ρ (g cm^{-3})	G_e (MPa)	$<R^2>_o/M$ (Å^2)	C_∞	b (Å)	ν_o (Å^3)	M_o	p (Å)	M_e	a (Å)	N_e	P_e
PI-34	298	0.895	0.35	0.585	5.26	9.58	291	156.9	3.17	6,330	60.9	40.4	19.2
PI-50	298	0.893	0.41	0.528	4.80	8.80	273	146.6	3.52	5,390	53.4	36.8	15.1*
PI-75	298	0.890	0.37	0.563	8.07	15.0	745	399.3	3.32	5,960	57.9	14.9	17.5
cis-PBd	298	0.900	0.76	0.758	4.61	8.28	167	90.5	2.44	2,930	47.1	32.4	19.4
PBd-7	298	0.895	1.15	0.876	5.52	9.93	209	112.5	2.12	1,930	41.1	17.1	19.4
PBd-15	298	0.896	1.10	0.854	5.54	10.0	218	117.7	2.17	2,020	41.5	17.1	19.1
PBd-18	298	0.895	1.05	0.846	5.56	10.1	222	119.8	2.19	2,110	42.3	17.6	19.3
PBd-20	298	0.895	1.07	0.841	5.61	10.1	227	122.4	2.21	2,070	41.7	16.9	18.9
PBd-23	298	0.895	1.05	0.832	5.66	10.2	234	125.9	2.23	2,110	41.9	16.8	18.8
PBd-26	298	0.895	1.00	0.824	5.68	10.3	238	128.0	2.25	2,220	42.7	17.3	19.0
PBd-30	298	0.894	0.98	0.813	5.67	10.3	244	131.2	2.28	2,260	42.9	17.2	18.8
PBd-62	298	0.890	0.81	0.727	6.17	11.3	328	175.9	2.57	2,720	44.5	15.5	17.4
PBd-98	300	0.890	0.57	0.661	7.39	13.7	532	284.8	2.82	3,890	50.7	13.7	18.0
SBR**	298	0.913	0.78	0.818	6.41	11.9	316	173.6	2.22	2,900	48.7	16.7	22.0
PEBd	298	0.891	0.29	0.543	4.85	9.02	279	149.7	3.43	7,610	64.3	50.8	18.7
55-DMBD	348	0.861	0.33	0.640	7.31	13.6	556	288.4	3.01	7,550	69.5	26.2	23.1
PMYRC-0	298	0.892	0.10	0.398	5.30	9.85	454	243.8	4.68	22,100	93.8	90.6	20.0
PMYRC-64	298	0.891	0.071	0.374	5.87	10.9	592	317.5	4.98	31,100	107.8	97.9	21.7

*The low value of P_e likely indicates the real plateau modulus is lower.
**Styrene content 25 wt%.

TABLE 25.3. *Molecular characteristics of poly(acrylics) and poly(methacrylics).*

Polymer	T (K)	ρ (g cm^{-3})	G_e (MPa)	$<R^2>_o/M$ (Å^2)	C_∞	b (Å)	ν_o (Å^3)	M_o	p (Å)	M_e	a (Å)	N_e	P_e
a-PMA	298	1.11	0.25	0.436	7.91	14.7	740	494.6	3.43	11,000	69.2	22.2	20.2
a-PEA	298	1.13	0.36	0.463	9.76	18.1	1,040	710.1	3.17	7,770	60.0	10.9	18.9
a-POA	298	0.98	0.16	0.442	17.1	31.9	3,890	2,295	3.83	15,200	81.9	6.61	21.4
a-PMMA	413	1.13	0.31	0.390	8.22	15.3	880	598	3.77	12,500	69.9	20.9	18.5
a-PEBMA	373	0.988	0.15	0.315	11.3	21.0	2,350	1,396	5.34	20,400	80.2	14.6	15.0*
a-PHMA	373	0.960	0.090	0.366	13.1	24.4	2,800	1,622	4.73	33,100	110.0	20.4	23.3
a-POMA	373	0.923	0.033	0.272	11.4	21.1	2,950	1,635	6.61	86,700	153.6	53.0	23.2
a-PDDMA	298	0.929	0.016	0.254	13.6	25.3	4,500	2,513	7.04	144,000	191.1	57.2	27.1*
a-PAPHMA	393	1.00	0.012	0.167	14.5	26.9	7,220	4,348	9.95	272,000	213.2	62.6	21.4
a-PBPHMA	393	1.00	0.0092	0.154	15.2	28.2	8,600	5,173	10.8	355,000	233.8	68.6	21.7

*These two samples yield P_e values at odds with the value of ~21. This indicates the potential presence of pronounced errors in the chain dimension and/or plateau modulus values. From the trend shown in the chain dimension column the primary error seems to exist with this parameter.

TABLE 25.4. *Molecular characteristics of miscellaneous polymers.*

Polymer	T (K)	ρ(g cm^{-3})	G_e(MPa)	$<R^2>_o/M$ (Å^2)	p (Å)	M_e	a (Å)	P_e
a-PαMS	473	1.04	0.32	0.442	3.61	12,800	75.1	20.8
a-PS	413	0.969	0.20	0.437	3.92	16,600	85.2	21.7
i-PS	413	0.969	0.19	0.420	4.08	17,500	85.7	21.0
a-PtBS	473	0.957	0.10	0.361	4.81	37,600	116.5	24.2
a-PVA	333	1.08	0.35	0.490	3.14	8,540	64.7	20.6
a-PVME	303	1.05	0.41	0.580	2.73	6,450	61.2	22.4
m-AEK	473	1.20	2.2	0.775	1.79	2,140	40.8	22.8
Me-PEEK	463	1.16	3.3	0.834	1.72	1,350	33.6	19.6
PC	473	1.14	2.7	0.864	1.69	1,660	37.9	22.5

TABLE 25.4. *Continued.*

Polymer	T (K)	ρ(g cm^{-3})	G_e(MPa)	$<R^2>_o/M$ (Å^2)	p (Å)	M_e	a (Å)	P_e
PDMS	298	0.970	0.20	0.422	4.06	12,000	71.2	17.5
PET	548	0.989	3.1	0.845	1.99	1,450	35.0	17.6
PN6	543	0.985	1.8	0.853	1.98	2,470	45.9	23.2
PEO	353	1.06	1.8	0.805	1.95	1,730	37.3	19.2
POM	473	1.14	1.7	0.763	1.91	2,640	44.8	23.5
PPO	505	0.998	1.2	0.741	2.24	3,500	50.9	22.7
PSF	523	1.15	2.1	0.756	1.91	2,380	42.4	22.2
PTFE	653	1.46	1.7	0.598	1.90	4,660	52.8	27.7
RADEL-R	555	1.22	3.6	0.821	1.66	1,560	35.8	21.6

TABLE 25.5. *Entanglement and critical molecular weights of miscellaneous polymers.*

Polymer	T (K)	ρ(g cm^{-3})	$<R^2>_o/M$ (Å^2)	p (Å)	M_e	M_c	M_c/M_e
PE	443	0.768	1.21	1.79	980**	3,480	3.5
PBd-7	298	0.895	0.876	2.12	2,000	6,380	3.2
PI-7	243	0.919	0.618	2.92	3,250*	10,000	3.0
PEO	353	1.081	0.805	1.91	2,000	5,870	2.9
SBR	298	0.930	0.708	2.52	2,960	8,210	2.8
a-PVA	428	1.08	0.490	3.14	9,100	24,500	2.7
alt-PEP	373	0.812	0.871	2.40	3,100	8,100	2.6
PI-7	298	0.900	0.625	2.95	6,025	13,100	2.2
a-PMMA	490	1.09	0.425	3.58	13,600	29,500	2.2
PBd-98	300	0.889	0.720	2.59	3,850	8,200	2.1
a-PαMS	459	1.04	0.460	3.47	13,300	28,000	2.1
PDMS	298	0.970	0.422	4.06	12,000	24,500	2.0
PIB	298	0.918	0.570	3.17	6,900	13,100	1.9
a-PS	490	0.959	0.434	3.39	18,100	31,200	1.7
PIB	490	0.817	0.570	3.57	10,500	17,000	1.6
a-PCHE	453	0.920	0.323	5.59	48,750	80,000	1.6

*Calculated value is 6,000.

**Measured value at 413 K. The calculated value (via Eq. (25.12)) at 443 K is 1,150.

TABLE 25.6. *Polymers with large packing lengths.*

Polymer	T (K)	ρ(g cm^{-3})	$<R^2>_o/M$ (Å^2)	p (Å)	M_e	$[M_c/M_e]$
a-PHDEC	418	0.796	0.213	9.79	173,000*	1.01**
a-PAPHMA	393	1.0	0.167	9.94	268,000	1.00
a-PBPHMA	393	1.0	0.154	10.8	355,000	0.96
PMA-CH3	363	1.17	0.123	11.5	485,000*	0.93

*Via Eq. (25.12).

**Via Eq. (25.15).

25.6). Since it seems improbable that $M_e > M_c$ for any polymer, we expect the limiting value for M_c/M_e of 1, independent of p for $p \geq 10$ Å. An unexplained facet of these empirical observations is that as p increases, fewer entanglement events are seemingly required to reach the regime where the melt viscosity becomes proportional to the 3.4 power of molar mass. This is displayed in Table 25.5 where the M_e and M_c data for various flexible polymers are listed. Note that while the relation between M_e and packing length is understood [1], the corresponding state of play between p and M_c remains purely empirical [19].

25.4 TEMPERATURE DEPENDENCE OF CHAIN DIMENSIONS

A feature of chain dimensions is their temperature dependence that is expressed in terms of

$$\kappa \equiv \frac{\mathrm{d}\ \ln \langle R^2 \rangle_0}{\mathrm{d}T} = \frac{f_e/f}{T} \qquad (25.16)$$

where f_e/f denotes the energetic fraction of the temperature-dependent force in a polymer network at constant volume.

TABLE 25.7. *Melt state values of* $\kappa = \mathrm{d}\ln\langle R^2\rangle_0/\mathrm{d}T$.

Polymer samples	$\kappa \times 10^3(\mathrm{K}^{-1})$	
	From SANS	From f_e/f
alt-PEP (PEP)*	−1.1 [25]	−1.5 [26,27]
HPI-50	−0.2 [21]	—
a-PCHE	~0 [21]	—
a-PEE	+0.40 [28,29]	+0.30 [30]
a-PMMA	+0.10 [31]	−0.10 [24]
a-PP	−0.1 [32]	—
a-PS	~0 [31]	+0.17 [33,34]
a-PPEN	—	+0.33 [30]
alt-PEB	0 [21]	—
HHPP	0 [21]	—
i-PP	~0 [35]	—
PBd-7	—	+0.16 [36]
PDMS	—	+0.78 [37]
PEB-2(PE)	−1.2 [38]	−1.2 [39]
PEB-5	−1.3 [29]	—
PEB-7	−0.65 [29]	—
PEB-10	−0.44 [29]	—
PEB-12	−0.44 [29]	—
PEB-18	−0.1 [29]	—
PEB-25	0 [29]	—
PEB-32	+0.63 [29]	—
PEB-40	+0.55 [29]	—
PEO	−0.30 [40]	+0.03 [41]
PIB	—	−0.28 [42]
HPI-75	+1.2 [21]	—
PI-7 (*cis*-PI)	+0.40 [21]	+0.41 [43]

*Ethylene–propylene random copolymer.

The empirical sign of κ can be +, 0, or – (see Table 25.7). The modes of measurement have included theta condition measurements utilizing a family of theta solvents or melt state measurements. The latter include thermoelastic measurements on networks [22] and small angle neutron scattering (SANS) measurements on labeled chains in a polymer melt [23]. Generally, the theta condition approach (multiple theta solvents over a wide temperature range) is recognized to be unreliable [21,24]. An example of this [21] is *a*-PEE, where extensive theta condition work (over the temperature range of ~200 K) led to a negative value of $\kappa = -1.2 \times 10^{-3}$ K^{-1}, as opposed to the two positive values found for the melt state by SANS and thermoelastic measurements; see Table 25.7. The role of κ on the packing length, plateau modulus and entanglement volume can be significant, particularly for cases where the melt rheology is studied over a wide temperature range. A 200 K range is common for amorphous polymers having low glass transition temperatures.

The packing length has two sources of temperature dependence ($\langle R^2\rangle_0$ and ρ, see Eq. (25.5)). For typical temperatures (350 K) the change in density for polymer liquids as a function of temperature is $\mathrm{d}\ln\rho/\mathrm{d}T \approx -6 \times 10^{-4}$ K^{-1}. $\langle R^2\rangle_0$ is the more interesting parameter, in that it can increase, decrease, or remain constant as temperature is changed.

APPENDIX *Alphabetical Listing of Polymers.*

Name	References	Description
alt-PEB	[44,45]	essentially alternating poly(ethylene-*co*-1-butene); hydrogenated PEBd
alt-PEP	[25,46,47]	essentially alternating poly(ethylene-*co*-propylene); hydrogenated PI-7
a-PαMS	[1,17,18,48,49]	atactic poly(α-methyl styrene)
a-PAPHMA	[50,51]	atactic poly[6-{4(anisyloxycarbonyl)phenoxy}-hexyl methacrylate]
a-PBPHMA	[50,51]	atactic poly[6-{4(butoxycarbonyl)phenoxy}-hexyl methacrylate]
a-PCHE	[1,19,21,52]	atactic poly(cyclohexyl)ethylene or poly(vinyl cyclohexane)
a-PDDMA	[53,54]	atactic poly(dodecyl)methacrylate
a-PEA	[53,55]	atactic poly(ethyl)acrylate
a-PEBMA	[17,53,56]	atactic poly(ethyl butyl)methacrylate
a-PEE	[28,57]	atactic poly(ethyl ethylene); also called poly(butene-1);may be made via the hydrogenation of poly(vinyl ethylene)
a-PHDEC	[58]	atactic poly(hexadecene-1)
a-PHEX	[59,60]	atactic poly(hexene-1)
a-PHMA	[53,61]	atactic poly(hexyl)methacrylate
a-PMA	[55,62]	atactic poly(methyl)acrylate
a-PMMA	[17,18,21,31,63]	atactic poly(methyl)methacrylate
a-POA	[55,59]	atactic poly(octyl)acrylate
a-POMA	[17,53,54,64]	atactic poly(octylmethyl)methacrylate
a-PP	[32,65,66]	atactic polypropylene; hydrogenated poly(2-methyl 1,3-pentadiene)
a-PPEN	[59]	atactic poly(pentene-1)
a-PS	[17–19,31,67]	atactic polystyrene
a-PtBS	[1,68]	atactic poly(*t*-butyl styrene)

APPENDIX *Continued.*

Name	References	Description
a-PVA	[17,18,54]	atactic poly(vinyl acetate)
a-PVME	[69,70]	atactic poly(vinyl-methylether)
cis-PBd	[17,71]	1,4-polybutadiene ~ 96% *cis* content.
cis-PI	[17,72,73]	1,4-polyisoprene ~ 100% *cis* content; natural rubber
55-DMBD	[1]	poly-2,3(dimethyl butadiene) 55% 1,4; 45% 3,4 content.
HHPP	[1,21,45]	hydrogenated poly(2,3 dimethyl)butadiene:head-to-head polypropylene (alternating copolymer of ethylene and butene-2).
HPI-*x*	[1,26,74]	hydrogenated polyisoprene where $x = 3,4$ content of parent polyisoprene
HPMYRC-*x*	[1,45]	hydrogenated poly(myrcene) with *x*% 3,4
i-PMMA	[54,63]	isotactic-poly(methylmethacrylate)
i-PP	[35,66]	isotactic polypropylene
i-PS	[54,75]	isotactic polystyrene
m-AEK	[76]	poly(*m*-arylene–ether–ketone)
Me-PEEK	[77,78]	methyl-poly(aryl–ether–ether–ketone); prepared from methyl hydroquinone and 4,4′-difluorobenzophenone.
PBd-*x*	[57,79–82]	polybutadiene, $x =$ vinyl percent; for 100% vinyl content the material is identified as poly(vinyl ethylene) or 1,2-polybutadiene.
PC	[1,54,76,83,84]	polycarbonate of bisphenol A(4, 4’-isopropylidenediphenol)
PDMS	[17,85–87]	poly(dimethylsiloxane)
PE	[17,19,38,88–90]	polyethylene
PEBd	[1,44]	poly(ethyl butadiene) ~ 75/20/5 *cis*/*trans*/3,4
PEB-*x*	[29,57]	poly(ethylene–butene) random copolymer; *x* denotes number of ethyl branches per 100 backbone carbons
PEO	[18,19,40]	poly(ethylene oxide)
PET	[54,91,92]	poly(ethylene terephthalate)
PIB	[17,18,93–95]	polyisobutylene
PI-*x*	[21,47,96–98]	1,4-polyisoprene where $x = 3,4$ content; PI-75 is 75% 3,4, and 25% 1,2 (with essentially no 1,4 addition)
PMA-CH3	[99]	main-chain liquid crystal polyester
PMYRC-*x*	[1,44,45]	poly(myrcene) with *x*% 3,4 [myrcene = 1,6-octadiene-7-methyl-3-methylene]
PN6	[54,100,101]	polycaprolactam-nylon 6
POM	[28,54]	poly(oxymethylene)
PPO	[76,102]	poly(phenylene oxide)
PSF	[76,103]	alternating copolymer of bisphenol A and dichlorodiphenyl sulfone (UDEL)
PTFE	[104,105]	poly(tetrafluoro)ethylene
RADEL-R	[76,103]	alternating copolymer of 4,4′-biphenol and dichlorodiphenyl sulfone
SBR	[17,106]	solution prepared copolymer (anionic polymerization) styrene–butadiene (34% vinyl; 19% *cis* and 47% *trans*) 25 wt% styrene
s-PP	[66,107,108]	syndiotactic polypropylene

REFERENCES

1. Fetters, L. J.; Lohse, D. J.; Richter, D.; Witten, T. A.; Zirkel, A. *Macromolecules* 1994, **27**, 4639.
2. Fetters, L. J.; Lohse, D. J.; Colby, R. H. Ch. 24 of *Physical Properties of Polymers Handbook* (J. E. Mark, editor) AIP Press, Woodbury, NY (1996).
3. Rubinstein, M.; Colby, R. H. *Polymer Physics*, Oxford University Press, Oxford (2003).
4. Graessley, W. W.; Edwards, S. F. *Polymer* 1981, **22**, 1329.
5. Edwards, S. F. *Proc. R. Soc. London A* 1988, **419**, 221.
6. Colby, R. H.; Rubinstein, M.; Viovy, J. L. *Macromolecules* 1992, **25**, 996.
7. de Gennes, P. G. *Scaling Concepts in Polymer Physics*, Cornell University Press, Ithaca, New York (1979).
8. Ronca, G. *J. Chem. Phys.* 1983, **79**, 1031.
9. Lin, Y.-H. *Macromolecules* 1987, **20**, 3080.
10. Kavassalis, T. A.; Noolandi, J. *Phys. Rev. Lett.* 1987, **59**, 2674.
11. Kavassalis, T. A.; Noolandi, J. *Macromolecules* 1988, **21**, 2869.
12. Kavassalis, T. A.; Noolandi, J. *Macromolecules* 1989, **22**, 2709.
13. Ho, J.; Govaert, L.; Utz, M. *Macromolecules* 2003, **36**, 7398.
14. Hiss, R.; Hobeika, S.; Lynn, C.; Strobl, G. *Macromolecules* 1999, **32**, 4390.
15. Flory, P. J. *Statistical Mechanics of Chain Molecules*, Wiley, New York (1969), Chap. II; see Tables 1 and 2.
16. Witten, T. A.; Milner, S. T.; Wang, Z.-G. in *Multiphase Macromolecular Systems* (B. M. Culbertson, editor) Plenum Press New York (1989).
17. Ferry, J. D. *Viscoelastic Properties of Polymers*, 3rd Ed., Wiley, New York (1980); Table 13–1.
18. Berry, G. C.; Fox, T. G *Adv. Polym. Sci.* 1968, **5**, 261.
19. Fetters, L. J.; Lohse, D. J.; Milner, S. T.; Graessley, W. W. *Macromolecules* 1999, **32**, 6847.

20. Graessley, W. W.; Fetters, L. J. *Macromolecules* 2001, **34**, 7147.
21. Krishnamoorti, R.; Graessley, W. W.; Zirkel, A.; Richter, D.; Hadjichristidis, N.; Fetters, L. J.; Lohse, D. J. *J. Polym. Sci., Part B: Polym. Phys.* 2002, **40**, 1768.
22. Price, C. *Proc. R. Soc. London* 1976, **351**, 331.
23. Higgins, J. S.; Benoit. H. C. *Polymers and Neutron Scattering*, Oxford University Press, Oxford (1994).
24. Ciferri, A. *J. Polym. Sci. Part-A* 1964, **2**, 3089.
25. Zirkel, A.; Richter, D.; Pyckhout-Hintzen, W.; Fetters, L. J. *Macromolecules* 1992, **25**, 954.
26. Mark, J. E. *J. Chem. Phys.* 1972, **57**, 2541.
27. Mark, J. E. *J. Polym. Sci., Part B: Polym. Phys.* 1974, **12**, 1207.
28. Zirkel, A.; Richter, D.; Fetters, L. J.; Schneider, D.; Graciano, V.; Hadjichristidis, N. *Macromolecules* 1995, **28**, 5262.
29. Fetters, L. J.; Graessley, W. W.; Krishnamoorti, R.; Lohse, D. J. *Macromolecules* 1997, **30**, 4973.
30. Mark, J. E.; Flory, P. J. *J. Am. Chem. Soc.* 1965, **87**, 1423.
31. Boothroyd, A. T.; Rennie, A. R.; Wignall, G. D. *J. Chem. Phys.* 1993, **99**, 9135.
32. Zirkel, A.; Urban, V.; Richter, D.; Fetters, L. J.; Huang, J. S.; Kampmann, R.; Hadjichristidis, N. *Macromolecules* 1992, **25**, 6148.
33. Orofino, T. A.; Ciferri, A. *J. Phys. Chem.* 1964, **68**, 3136.
34. Dusek, K. *Collect. Czech. Chem. Commun.* 1966, **31**, 1893.
35. Ballard, D. G. H.; Cheshire, P.; Longman, G. W.; Schelten, J. *Polymer* 1978, **19**, 379.
36. Mark, J. E.; Llorente, M. A. *Polym. J.* 1981, **13**, 543.
37. Price, C., Padget, J.; Kirkham, M. C.; Allen, G. *Polymer* 1969, **10**, 573.
38. Boothroyd, A. T.; Rennie, A. R.; Boothroyd, C. B. *Europhys. Lett.* 1991, **15**, 715.
39. Ciferri, A.; Hoeve, C. A. J.; Flory, P. J. *J. Am. Chem. Soc.* 1961, **83**, 1015.
40. Smith, G. D.; Yoon, D. Y.; Jaffe, R. L.; Colby, R. H.; Krishnamoorti, R.; Fetters, L. J. *Macromolecules* 1996, **29**, 3462.
41. Mark, J. E.; Flory, P. J. *J. Am. Chem. Soc.* 1965, **87**, 1415.
42. Allen, G.; Gee, G.; Kirkham, M. C.; Price, C.; Padget, J. *J. Polym. Sci., Part C* 1968, **23** 201.
43. Flory, P. J. *Trans. Faraday Soc.* 1961, **57**, 829.
44. Hattam, P.; Gauntlett, S.; Mays, J. W.; Hadjichristidis, N.; Young, R. N.; Fetters, L. J. *Macromolecules* 1991, **24**, 6199.
45. Fetters, L. J.; Kiss, A. D.; Mays, J. W. unpublished results.
46. Richter, D.; Butera, R.; Fetters, L. J.; Huang, J. S.; Farago, B.; Ewen, B. *Macromolecules* 1992, **25**, 6156.
47. Gotro, J. T.; Graessley, W. W. *Macromolecules* 1984, **17**, 2767.
48. Mays, J. W.; Hadjichristidis, N.; Graessley, W. W.; Fetters, L. J. *J. Polym. Sci., Part B: Polym. Phys.* 1986, **24**, 2553.
49. Fujimoto, T.; Ozaki, N.; Nagasawa, M. *J. Polym. Sci. A-2* 1968, **6**, 129.
50. Kirste, R. G.; Ohm, H. G. *Makromol. Chemie - Rapid Commun.* 1985, **6**, 179.
51. Rubin, S. F.; Kannan, R. M.; Kornfield, J. A.; Boeffel, C. *Macromolecules* 1995, **28**, 3521.
52. Abdel-Goad, M.; Pyckhout-Hintzen, W.; Fetters, L. J. unpublished results.
53. Mays, J. W.; H adjichristidis, N. *J. Macromol. Sci.: Rev. Macromol. Chem. Phys.* 1988, **C28**, 371.
54. Wu, S. *J. Polym. Sci., Polym. Phys. Ed.* 1989, **27**, 723.
55. Janáček, L.; Hrouz, J. *J. Polym. Sci., Polym. Symp.* 1975, **53**, 283.
56. Yin, T. P.; Ferry, J. D. *J. Colloid Sci.* 1961, **16**, 166.
57. Carella, J. M.; Graessley, W. W.; Fetters, L. J. *Macromolecules* 1984, **17**, 2775
58. Pena, B.; Aroca, M.; Perez, E.; Bello, A.; Riande, E.; Benavente, R.; *Macromol. Chem. Phys.* 1997, **198**, 1691.
59. Sundararajan, P. R. in *Physical Properties of Polymers Handbook* (J. E. Mark, Ed.) AIP Press, Woodbury, NY (1996) p. 197.
60. Fetters, L. J.; Lohse, D. J.; Garcia-Franco, C. A.; Brant, P.; Richter, D.; *Macromolecules* 2002, **35**, 10096.
61. Child, Jr., W. C.; Ferry, J. D. *J. Colloid Sci.* 1957, **12**, 389.
62. Fujino, K.; Senshu, K.; Kawai, H. *J. Colloid Sci.* 1961, **16**, 262.
63. Fuchs, K.; Friedrich, C.; Weese, J. *Macromolecules* 1996, **29**, 5893.
64. Dannhauser, W.; Child, Jr., W. C.; Ferry, J. D. *J. Colloid Sci.* 1958, **13**, 103.
65. Xu, Z.; Mays, J. W.; Chen, X.; Hadjichristidis, N.; Schilling, F. C.; Bair, H. E.; Pearson, D. S.; Fetters, L. J. *Macromolecules* 1985, **18**, 2560.
66. Eckstein, A.; Suhm, J.; Friedrich, C.; Maier, R.-D.; Sassmannshausen, J.; Bochmann, M.; Mülhaupt, R. *Macromolecules* 1998, **31**, 1335.
67. Onogi, S.; Masuda, T.; Kitagawa, K. *Macromolecules* 1970, **3**, 109.
68. Mays, J. W.; Ferry, W. M.; Hadjichristidis, N.; Funk, W. G.; Fetters, L. J. *Polymer* 1986, **27**, 129.
69. Kannan, R. M.; Lodge, T. P. *Macromolecules* 1997, **30**, 3694.
70. Choi, S.; Liu, X.; Briber, R. M. *J. Polym. Sci., Part B: Polym. Phys.* 1998, **36**, 1.
71. Brandrup, J.; Immergut, E. H., Eds. *Polymer Handbook*, 3rd Ed., Wiley, New York (1989).
72. Ansorena, F. J.; Revuelta, L. M.; Guzmán, G. M.; Iruin, J. J. *Eur. Polym. J.* 1982, **18**, 19.
73. Sanders, J. F.; Ferry, J. D.; Valentine, R. H. *J. Polym. Sci. A-2* 1968, **6**, 967.
74. Mays, J. W.; Hadjichristidis, N.; Fetters, L. J. *Macromolecules* 1984, **17**, 2723.
75. Guenet, J. M.; Picot, P.; Benoit, H. *Macromolecules* 1979, **12**, 86.
76. Roovers, J. Toporowski, P. M.; Ethier, R. *High Perform. Polym.* 1990, **2**, 165.
77. Hermann-Schönherr, O.; Schneller, A.; Seifert, A. M.; Soliman, M.; Wendorff, J. H. *Makromol. Chem.* 1992, **193**, 1955.
78. Wang, F.; Roovers, J.; Toporowski, P. M. *Macromolecules* 1993, **26**, 3826.
79. Fetters, L. J.; Lohse, D. J.; Graessley, W. W. *J. Polym. Sci., Part B: Polym. Phys.* 1999, **37**, 1023.
80. Roovers, J. *Polym. J.* 1986, **18**, 153.
81. Roovers, J.; Toporowski, P. M. *Rubber Chem. Tech.* 1990, **63**, 734.
82. Colby, R. H.; Fetters, L. J.; Graessley, W. W. *Macromolecules* 1987, **20**, 2226.
83. Hutnik, M.; Argon, A. S.; Suter, U. W. *Macromolecules* 1991, **24**, 5956.
84. Aloisio, C. J.; Boehm, V. W. in *Rheology* Vol.2 (G. Astarita and G. Marrucci, L. Nicholais, Eds.) Plenum Press, New York (1980), p. 513.
85. Kirste, R. G.; Lehnen, B. R. *Makromol. Chem.* 1976, **177**, 1137.
86. Beltzung, M.; Picot, C.; Rempp, P.; Herz, J. *Macromolecules* 1982, **15**, 1594.
87. Plazek, D. J.; Dannhauser, W.; Ferry, J. D. *J. Colloid Sci.* 1961, **16**, 101.
88. Lieser, G.; Fischer, E. W.; Ibel, K. *J. Polym. Sci., Polym. Lett. Ed.*, 1975, **13**, 39.
89. Pearson, D. S.; Fetters, L. J.; Graessley, W. W.; Ver Strate, G.; von Meerwall, E. *Macromolecules* 1994, **27**, 711.
90. Han, J.; Jaffe, R. L.; Yoon, D. Y. *Macromolecules* 1997, **30**, 7245.
91. McAlea, K. P.; Schultz, J. M.; Gardner, K. H.; Wignall, G. D. *Macromolecules* 1985, **18**, 447.
92. Wallach, M. L. *Makromol. Chem.* 1967, **103**, 19.
93. Hayashi, H.; Flory, P. J.; Wignall, G. D. *Macromolecules* 1983, **16**, 1328.
94. Fetters, L. J.; Graessley, W. W.; Kiss, A. D. *Macromolecules* 1991, **24**, 3136.
95. Pyckhout-Hinzen, W.; Fetters, L. J. unpublished data (PIB at 298K).
96. Nemoto, N.; Moriwaki, M.; Odani, H.; Kurata, M. *Macromolecules* 1971, **4**, 215.
97. Nemoto, N.; Odani, H.; Kurata, M. *Macromolecules* 1972, **5**, 531.
98. Abdel-Goad, M.; Pyckhout-Hintzen, W.; Kahle, S.; Allgaier, J.; Richter, D.; Fetters, L. J. *Macromolecules* 2004, **37**, 8135.
99. Fourmaux-Demange, V.; Boué, F.; Brulet, A.; Keller, P.; Cotton, J. P. *Macromolecules* 1998, **31**, 801.
100. Mattiussi, A.; Gechele, G. B.; Francesconi, R. *J. Polym. Sci.* A 1969, **7**, 411.
101. Flory, P. J.; Williams, A. D. *J. Polym. Sci. A-2* 1967, **5**, 399.
102. Cai, H.; Ait-Kadi, A.; Brisson, J. *Polymer* 2003, **44**, 1481.
103. Roovers, J.; Toporowski, P. M.; Ethier, R. *High Perform. Polym.* 1990, **2**, 151.
104. Tuminello, W. H.; Treat, T. A.; English, A. D. *Macromolecules* 1988, **21**, 2606.
105. Chu, B.; Wu, C. *Macromolecules* 1987, **20**, 93.
106. Kraus, G. in *The Stereo Rubbers* (Saltman, W. M. Ed.) Wiley, New York, (1977); p. 613.
107. Wheat, W. R. *ANTEC Proc.* 1995, p. 2275.
108. Jones, T. D.; Chaffin, K. A.; Bates, F. S.; Annis, B. K.; Hagaman, E. W.; Kim, M.-H.; Wignall, G. D.; Fan, W.; Waymouth, R. *Macromolecules* 2002, **35**, 5061.

CHAPTER 26

Temperature Dependences of the Viscoelastic Response of Polymer Systems

K. L. Ngai* and D. J. Plazek†

*Naval Research Laboratory, Washington, D.C. 20375-5320; †Department of Materials Science and Engineering, University of Pittsburgh, Pittsburgh, PA 15216

26.1 THE WLF EQUATION

The most successful temperature dependence for the viscous flow [1,2], viscoelastic response [1], dielectric dispersion [3–5], nuclear magnetic resonance response [6–8] and dynamic light scattering [9–10] of polymers and supercooled liquids with various chemical structures is the Williams, Landel, and Ferry (WLF) equation [11,12]

$$\log\frac{J_s^0(T)\eta(T)}{J_s^0(T_0)\eta(T_0)} \approx \log\frac{\tau(T)}{\tau(T_0)} = \log a_T = -\frac{C_1(T-T_0)}{C_2+T-T_0}, \tag{26.1}$$

where J_s^0 is the steady state recoverable compliance; η is the shear viscosity; τ is a retardation or relaxation time; a_T is the time-scale shift factor; T_0 is the chosen reference temperature; and C_1 and C_2 are characterizing constants. $J_s^0(T)$ is a very weak function of the temperature. In fact in the temperature range where T/T_g varies from 1.2 to 2.0, J_s^0 has been found to be independent of temperature [13]. Therefore its variation is often ignored. It will be ignored in this chapter. Some authors identify magnitude variations with temperature which are reported as $b_T = J_s^0(T)/J_s^0(T_0)$.

Williams, Landel, and Ferry [12] reported that such an expression is valid for polymers over the temperature range $T_g < T < T_g + 100°$. When T_g is chosen as the reference temperature, i.e., when the response curves measured at different temperatures are shifted primarily along the time or frequency scales to superimpose upon the response curve measured at T_g, it was initially noted that the constants C_1^g and C_2^g assume values close to 17.44° and 51.6°, respectively, for 17 polymers [12]. Individual treatment of the data on a wide range of polymers indicates that C_1^g may take values between 15° and 26° and C_2^g between 20° and 130°. The fit extends to temperatures below T_g if the polymer is at its equilibrium density.

The WLF expression has been shown [12] to be related to the Vogel–Fulcher–Tammann–Hesse equation [14–16],

$$\log\tau_i = \log A + \frac{(C/2.303)}{T-T_\infty}, \tag{26.2}$$

for η or τ where A, C and T_∞ are empirical constants. It follows that

$$\log a_T = \frac{C/2.303}{T-T_0} - \frac{C/2.303}{T_0-T_\infty}. \tag{26.3}$$

This is identical to the WLF expression provided the Vogel parameters and the WLF parameters are related as

$$C = 2.303C_1C_2 \tag{26.4}$$

and

$$T_0 - T_\infty = C_2. \tag{26.5}$$

26.2 RELATION OF WLF EQUATION TO FREE VOLUME

The WLF equation for a_T has been rationalized in terms of Doolittle's free volume theory [17]. According to this theory that portion of the volume which is accessible to the kinetic process of interest is considered to be the free volume $v_f = v - v_0$, where v is the measured volume and the inaccessible volume v_0 is called the occupied volume. The Doolittle equation states that the viscosity is an exponential function of the reciprocal of the relative free volume $\phi \equiv v_f/v_0$.

$$\eta = Ae^{b/\phi}, \tag{26.6}$$

where A and b are characterizing constants.

Williams, Landel, and Ferry chose to use the fractional free volume $f = v_f/v$ in place of ϕ. This substitution made no difference in their derivation of the equation for the temperature shift factor a_T

$$\log a_T = \frac{b}{2.303}\left[\frac{1}{f} - \frac{1}{f_g}\right], \tag{26.7}$$

since $[1/f - 1/f_g] = [1/\phi - 1/\phi_g]$.

With the assumption that the fractional free volume is a linear function of temperature

$$f = f_0 + \alpha_f(T - T_0). \tag{26.8}$$

Substituting of Eq. 26.8 in Eq. 26.7 yields

$$\log a_T = -\frac{(B/2.303f_0)(T - T_0)}{f_0/\alpha_f + T - T_0} \tag{26.9}$$

which is identical in form with the WLF equation.

26.3 THERMORHEOLOGICAL COMPLEXITIES

In the frame work of the free volume theory, the molecular mobility at any temperature is assumed to depend primarily on the free volume remaining. It is generally further assumed in this approach that this molecular mobility determines the temperature dependence of the shift factors of *all* different kinds of molecular motions involving various length scales in the polymer melt. Hence free volume approach usually purports that the temperature shift factors of *different* viscoelastic mechanisms are the *same*. This result coming from the free volume theory of molecular mobility is perhaps the justification of the practice of obtaining *the* (meaning that there is only one) shift factor curve, a_T, which is usually derived by superposing curves of viscoelastic functions measured at different temperatures within the time or frequency range of the instrumentation. So long as the curve of the stress relaxation modulus, the creep and recoverable compliance, dynamic moduli or compliance do not change their shape in logarithmic plots, unique reduced curves with extended time or frequency range can be obtained. This will be the case, principally, if all of the molecular mechanisms contributing to the time- and frequency-dependent modulus and compliance functions, have the same temperature dependence. When this is so, the polymer is identified as being thermorheologically simple [18]. This appears to be true, in general, for closely related mechanisms, i.e., those within a group contributing to a single-loss tangent maximum; however mechanisms contributing to different loss peaks inevitably have different temperature dependences. This is widely recognized for the sub-T_g loss peaks, identified by the Greek letters β, γ, and δ. However, it is not as widely recognized that the so-called α mechanism, which is normally seen above T_g involves contributions from possibly three groups of molecular mechanisms with specifically different sensitivities to the variation of temperature [19–21]. In spite of the fact that a single loss peak is generally observed, a growing body of knowledge shows that local mode, sub-Rouse, and Rouse normal modes of chain backbone motions have different temperature dependences [19–24] which are most often different from that of the mechanisms of the terminal zone [19,25–32] which leads to steady-state behavior. Consequently, the temperature dependence of the viscosity is usually different from that of the glass to rubber-softening dispersion.

Therefore, it is important to know from which region or viscoelastic zone the WLF constants C_1 and C_2 were determined. Table 26.1 presents WLF constants and contains such information, when possible.

It should be noted that the shift factors that can be fitted to the WLF equation show positive curvature when plotted logarithmically against the temperature. Quite often, $\log a_T$ values obtained near and below T_g show negative curvature at low temperatures simply is an indication that the lower temperature measurements were made before the density of the material reached its equilibrium value.

26.4 TEMPERATURE DEPENDENCES UNDER PRESSURE

The loss of molecular mobility on approaching the glassy state by decreasing temperature may be due to increased molecular crowding (decrease in free volume) as well as a decrease in thermal energy (decrease in entropy). The relative importance of these two factors, volume (or free volume) and thermal energy (or entropy) has been a controversial issue for many years. It cannot be resolved by temperature variations alone in experimental studies, since the volume, entropy, and thermal energy all depend on temperature. The introduction of pressure, P, as an additional experimental variable makes a difference, because the specific volume, V, can be altered while maintaining temperature, T, constant. By combining the dielectric or light scattering results for polymeric and nonpolymeric glass-formers with the corresponding equation of state (*PVT* data), the volume and temperature dependence of the primary (local segmental for polymers) relaxation times τ_α can be obtained [181–185]. The results indicate that in general neither T (or entropy) nor V is exclusively the appropriate thermodynamic variable for describing the dynamics of glass formers, but rather τ_α is a function of the product variable, $T^{-1}V^{-\gamma}$, where γ is material-dependent, reflecting the nature of the intermolecular potential. Number polymers have been studied thus far, yielding the following

TABLE 26.1. *WLF parameters characterizing temperature dependencies of shift factors for relaxation and retardation times in various polymer systems.*

Polymer	T_0 °K	C_1 °K	C_2 °K	T_g °K	Ref.	Comments
Nonaromatic hydrocarbon backbone polymers						
Poly(acetaldehyde)	243	14.5	24	243	[33]	• $a_{T,\alpha}$ of local segmental motion from dielectric relaxation data.
Polyethylene (solution chlorinated) *Cl content* *= 56.6 w/w, amorphous*	312.3	12.7	63.3	317	[180]	• $a_{T,\alpha}$ of local segmental motion from a combination of dielectric relaxation and dynamic mechanical relaxation data for $\log \tau_\alpha = -12.7 + 804/(T - 249\,\mathrm{K})$.
Poly(hexene-1)	218	17.4	51.6	218	[34]	• The shift factors, $a_{T,S}$, of the softening dispersion with G' ranging from about $10^6 < G' < 10^{9.2}\,\mathrm{dyne/cm^2}$ and temperature T from −27.5 °C to 70 °C.
Polyisobutylene PIB *(the NBS sample with* $M = 1.3 \times 10^6$ *distributed by R.S. Marvin [35–37] on which the most comprehensive studies of viscoelastic properties were carried out in many laboratories)*	298	8.61	200.4	201	[38,39]	• $a_{T,S}$ of the entire softening dispersion, from dynamic mechanical measurement of $J^*(f)$, $10<f<6000$ Hz and $228.4<T<373$°K. Its T-dependence is much weaker than that of $a_{T,G(t)}$ given below.
	197	6.14	56	201	[40–42], [19–20], [43]	• $a_{T,E(t)}$ of the entire viscoelastic spectrum, from glassy state to the terminal zone, from stress relaxation, $E(t)$, between −83 and 25 °C in the time region of about $10^{0.6} < t < 10^{2.6}$ s. Its T-dependence is in agreement with the shift factor obtained from creep data, $J_r(t)$, (to be given below) throughout the softening region.
	228.5	13.18	130.9	201	[20,43]	• $a_{T,\mathrm{Rouse}}$ of Rouse modes in the softening dispersion located in the compliance range $J_N > J_r(t) > 10^{-8}\,\mathrm{cm^2}/\,dyne$, where J_N is the plateau compliance, and resolved as a tan δ peak by a combination of isothermal (i.e., shift factor in this case not obtained from time-temperature superpositioning of viscoelastic curves as commonly done) creep and dynamic mechanical measurements in the wide real time range of $10^6 > t > 3 \times 10^{-4}$ s from −74.2 to −35.8 °C. τ_{Rouse} (−66.9 °C) = 2.74.
	245.3	21.24	147.7		[43,20]	• $a_{T,\alpha}$ of local segmental mode from $G(t)$ and $J_r(t)$ data in the softening dispersion for viscoelastic response with $J_r(t) < J_{e\alpha}$ (where $J_{e\alpha}$ is the relaxed compliance of the local segmental motion and has the value of approximately 5 times the glassy compliance J_g) and combined with data from the resolved local segmental motion obtained by photon correlation spectroscopy. Log $\tau_\alpha(T = -66.9\mathrm{C}) = -0.5$.
	215.3	20.36	117.7		[43,20]	• $a_{T,\text{sub-Rouse}}$ the sub-Rouse modes in the softening dispersion located in the compliance range of $J_{e\alpha} < J_r(t) < 10^{-8}\,\mathrm{cm^2}$ dyne and resolved as a tan δ peak situated at a higher frequency than the Rouse tan δ peak by a combination of isothermal creep and dynamic mechanical measurements in the real time range of $10^6 < t < 3 \times 10^{-4}$ s from −74.2 to −35.8 °C. log $\tau_{\text{sub-Rouse}}$ (−66.9 °C) = 1.63.

TABLE 26.1. *Continued.*

Polymer	T_0 °K	C_1 °K	C_2 °K	T_g °K	Ref.	Comments
PIB	205	14.3	72.5	201	[44]	• $a_{T,\mathrm{Rouse}}$ resolved by a combination of stress relaxation and dynamic birefringence measurements in the range $10^{0.2} < t < 10^{3.8}$ s. Log τ_{Rouse} (-66.9 °C) $=$ 2.13. This result is in fair though not perfect agreement with that obtained by the tan δ peak (see above).
	205	13.7	64.8	201	[44]	• $a_{T,G}$ of the "stress that relaxes through monomer rotation around the chain axis" resolved by a combination of stress relaxation and dynamic birefringence measurements in the range $10^{0.2} < t < 10^{3.8}$ s. Log $\tau_G(-66.9°\mathrm{C}) = 0.1$. This technique has not resolved the sub-Rouse modes possibly because time temperature superposition was used. Hence the result is a compromise between the local segmental mode and the sub-Rouse modes. Log $\tau_G(-68.2°\mathrm{C}) = 0.77$ which is close to the average between τ_α and $\tau_{\text{sub-Rouse}}$ at -66.9 °C obtained from isothermal mechanical data taken over 9 decades of real time (see above).
PIB (*E*-19) *$M = 78\,500$*	198	15.99	62.99	200.4	[45]	• $a_{T,J(t)}$ of the entire viscoelastic spectrum from $J_r(t)$. Its T-dependence is similar to that of viscous flow, η.
PIB	202	16.96	80	202	[47]	• $a_{T,\eta}$ of viscosity η. When extrapolated down to lower temperatures, its temperature dependence remarkably (in the sense that this does not happen in most other polymers) is nearly the same as that of $a_{T,G(t)}$ discussed above [Tobolsky and coworkers, Refs. 40–42].
PIB $2.7 \times 10^4 < M_w < 7 \times 10^5$	298.2	7.49	192	205	[48]	• $a_{T,\eta}$ of the terminal dispersion measured from 243 to 473 K.
PIB ($M = 4900$)	298.2	7.60	184		[49]	• $a_{T,\eta}$ of viscosity from -50 to 170 °C. Its temperature dependence similar to that given above.
Polypropylene PP (*atactic*)	298	7.53	85	262	[29]	• $a_{T,\eta}$ of viscosity measured up to $10^{12.6}$ poise at 266 K. It has a weaker temperature dependence than that of $a_{T,S}$ of the softening dispersion in the temperature range where the viscoelastic response has $J_r(t)$ principally less than $10^{-8}\mathrm{cm}^2/\mathrm{dyne}$.
	298	6.86	65	262	[29]	• $a_{T,S}$ of the softening dispersion from $J_r(t)$. It has a stronger temperature dependence than that of $a_{T,\eta}$.
Same sample as above	267.74	12.9	34.74	262	[50]	• $a_{T,\phi}$ of local segmental motion from correlation functions measured by photon correlation spectroscopy (PCS) carried out in the temperature range of $268 < T < 280$ K. The correlation times determined lie within the range: $10^{-5} < \tau < 10^0$ s.
Same sample as above	262.65	13.14	21.7	262	[51]	• $a_{T,\alpha}$ of local segmental motion from dynamical mechanical data taken in the frequency range of 0.01 to 100 Hz. Its T-dependence is in good agreement with that ($a_{T,\phi}$) obtained from PCS and that ($a_{T,S}$) obtained from creep measurement.
PP (*atactic*)	253	18.2	47.6		[7a]	• $a_{T,\tau(\mathrm{NMR})}$ of local segmental motion from 2D exchange NMR and spin-lattice relaxation data which determined the NMR correlation time in the range $10^{-10} < \tau_{\mathrm{NMR}} < 12$, s. The T-dependence of $\alpha_{T,\tau(\mathrm{NMR})}$ is significantly w3eaker than that of $a_{T,S}$ from creep or $a_{T,\phi}$ from photon correlation spectroscopy, but comparable to that of $a_{T,\eta}$ from creep. The sample may not be totally atactic.
	258	14.5	30	258	[7b]	• $a_{T,\tau(\mathrm{NMR})}$ of local segmental motion in different poly(propylene) samples, $10^{-10} < \tau_{\mathrm{NMR}} < 10^3$ s. $\tau_{\mathrm{NMR}}(T_g) = 10^2$ s.

TABLE 26.1. *Continued.*

Polymer	T_0 °K	C_1 °K	C_2 °K	T_g °K	Ref.	Comments
PP (*atactic prepared by polymerization of 2-methyl-1,3-pentadiene followed by saturation with hydrogen)*	348.2	4.73	123.9	268.5	[52]	• $a_{T,\eta}$ of the terminal relaxation from dynamic mechanical, $G^*(\omega)$, data taken from 25 °C to above 75 °C. Its temperature dependence is slightly stronger than that found by Plazek (see $a_{T,\eta}$ in above) consistent with the sample having a higher T_g by about 6 °C.
Vinyl polymers						
Polystyrene PS	428.9	13.46	28.9	371	[25]	• Shift factors $a_{T,S}$ given here were obtained from recoverable compliance, $J_r(t)$, with the terminal zone excluded from the consideration. Data from samples with molecular weights that range from 1.1×10^3 to 8.0×10^5 were included. Thus the T_g listed here applies to the high molecular weight samples only. At lower temperatures near T_g where the $a_{T,S}$s are for the local segmental motion, the temperature dependence of $a_{T,S}$ is significantly stronger than that of the viscosity η, $a_{T,\eta}$, to be given in the next entry below.
	371	14.63	60	371	[25]	• Shift factor, $a_{T,\eta}J_e$, for the product of the viscosity η and the equilibrium recoverable compliance J_e and samples with molecular weights ranging from 1.1×10^3 to 6×10^5. Thus the T_g listed here applies to the high molecular weight sample only. Also for the high molecular weight samples, J_e is almost temperature independent and the shift factor given here is the same as that for the viscosity, $a_{T,\eta}$. Its temperature dependence is weaker than that of $a_{T,S}$ (see comment in entry immediately above).
PS	373	16.35	52.5	373	[8]	• Shift factor, $a_{T,\tau(\mathrm{NMR})}$ for the local segmental motion from $375<T<443$°K obtained by 2D exchange NMR combined with ^{2}H- spin-lattice measurements covering the correlation time range $10^{-6} < \tau_{\mathrm{NMR}} < 10^3$ s. Temperature dependence of $a_{T,\tau(\mathrm{NMR})}$ agrees closely with that of the $a_{T,S}$ in the low temperature range near T_R where $a_{T,S}$ comes from local segmental motion. Beyond this temperature range $a_{T,\tau(\mathrm{NMR})}$ has a stronger temperature dependence than that of $a_{T,S}$, indicating that the local segmental motion probed by NMR has a more sensitive temperature dependence than the Rouse modes. Reported spectrum of local segmental motion from 2D exchange NMR narrows dramatically with increasing temperature.
PS (*high mol. wt*)	375	12.0	49.9	375	[53]	• $a_{T,\mathrm{Rouse}}$ of the Rouse modes in the softening dispersion resolved by a combination of stress relaxation and dynamic birefringence measurements. $\tau_{\mathrm{Rouse}}(T_g) = 10^{1.4}$ s.
	375	12.0	41.6	375	[53]	• $a_{T,G}$ of the G component in the softening dispersion, which represents the stress that relaxes through monomer rotation around the chain axis, resolved by a combination of stress relaxation and dynamic birefringence measurements. $\tau_G(T_g) = 10^{0.1}$ s.
PS(*A-25*)	373	12.7	49.8	370	[54,55]	• This shift factor, $a_{T,\eta}$, is for viscous flow in a monodisperse sample *(A-25)* with $(M_v)_{av} = 4.7 \times 10^4$ as reported by Ferry in Table 11-II of his book [1]. The shift factor for the softening dispersion, $a_{T,S}$, not reported in Table 11-II has a stronger temperature dependence and is given in the next line.

TABLE 26.1. *Continued.*

Polymer	T_0 °K	C_1 °K	C_2 °K	T_g °K	Ref.	Comments
PS(*A*-25)	373	10.7	29.9	370	[55]	• $a_{T,S}$ from creep in the softening dispersion (see remarks immediately above).
	371	12.95	60	371	[25]	• $a_{T,\eta}$ for viscosity from Berry and Fox [2]. It has even a weaker temperature dependence than that of any of the $a_{T,\eta}$ s determined from creep data described in the above.
PS *(Commercial sample: Hostyrene N-7000, mol. wt. not given.)*	378	9.4	39	363.5 *(from dilatometry at a cooling rate of 3K/h)*	[56]	• $a_{T,S}$ of the entire softening dispersion from creep, $J_r(t)$, data with $10^{-1.8} < t < 10^{3.2}$ s and temperature ranging from −90 to 130 °C. Its temperature dependence is considerably weaker than that of $a_{T,S}$ found by Plazek and O'Rourke [25] by recoverable creep compliance, $J_r(t)$, data with $10^{-0.5} < t < 10^{5.5}$ s. If the difference in T_g of about 7.5° is accounted for (Schwarzl's sample has a lower T_g) then there is reasonable agreement between the the two sets of data.
PS	373	13.7	50.0	373	[57]	
PS (2.5×10^5)					[58]	• Polymer J. **1**, 485 (1970).
PS *M>29 000*	433	7.14	112.1	373	[59]	• $a_{T,\eta}$ of the terminal dispersion measured in the temperature range of 393 to 493 K. Its *T*-dependence is slightly stronger than that of the terminal dispersion determined by Plazek [25,54,55].
Poly(α-methyl styrene)	445	13.7	49.3	445	[60]	
PαMS	441	16.8	53.5	441	[61]	
Poly(4-chloro styrene) P4CS	411.5	11.4	58.0		[62]	• $a_{T,\alpha}$ for local segmental motion from dielectric relaxation data.
Poly(vinyl acetal)	344.1	16.1	77.38		[63–66]	• $a_{T,\alpha}$ of local segmental motion from dielectric relaxation: $10^{-6} < \tau_\alpha < 10^{-3}$ s, $\tau_\alpha(T_0) = 1$ s.
Poly(vinyl acetate) PVAc	349	8.86	101.6	305	[67,68]	• $a_{T,S}$ of the entire softening dispersion from dynamic mechanical $J^*(f)$ with $10<f<6000$ Hz. Sample in equilibrium with ambient moisture and the water absorbed lower the sample's T_g. Its *T*-dependence is considerably weaker than either of the shift factors obtained from creep compliance in dried samples given immediately below.
	310.2	12.0	31.1	310	[27,28]	• $a_{T,S}$ of the softening dispersion obtained from creep compliance $J_r(t)$ data. It has a stronger temperature dependence than that of the shift factor of the terminal dispersion, $a_{T,\eta}$, given immediately below.
	311.1	15.57	60.0	310	[27,28]	• $a_{T,\eta}$ of viscous flow or the terminal dispersion from data of $J_r(t)$.
	373	7.43	125	310	[28]	• a_T of the entire viscoelastic spectrum including the softening and the terminal dispersions obtained when all data ($J_r(t)$, dynamic mechanical, dielectric) are combined together.
PVAc $M_\eta = 8.2 \times 10^4$	316.37	12.67	71.07	308	[4]	• $a_{T,\varepsilon}$ of the local segmental motion from 26.85 to 84.77 °C resolved by dielectric relaxation measurement of $\varepsilon^*(f)$ on dried samples in the range: $10^{-6} < f < 10^6$ Hz. $\tau(34.95\ °\mathrm{C}) = 10^{1.4}$ s. Its *T*-dependence is considerably weaker than that of the local segmental motion, which is $a_{T,S}$ at temperatures close to T_g, as determined from recoverable compliance, $J_r(t)$, data (see above).

TABLE 26.1. *Continued.*

Polymer	T_0 °K	C_1 °K	C_2 °K	T_g °K	Ref.	Comments
PVAc ($M_\eta = 15\,000$)	307.4	14.19	69.40	290.2	[69]	• $a_{T,\alpha}$ of the local segmental motion obtained by PCS data. Its temperature dependence is similar to that found by McKinney and Belcher [174] from dynamic compressibility on another sample with approximately the same T_g.
Poly(vinyl butyral)	336.4	17.24	85.18		[64,66] [70,71]	• $a_{T,\alpha}$ of local segmental motion from dielectric relaxation: $10^{-6} < \tau_\alpha < 10^{-3}$ s, $\tau_\alpha(T_0) = 1$ s.
Poly(vinyl chloroacetate) PVCAc	346	8.86	101.6	296	[72,80]	
Poly(vinyl chloride) PVC	352	19.84	43.89	353	[73]	• $a_{T,\alpha}$ of local segmental motion from tensile stress relaxation (10^{-1} s $< t <$ 1 day) and dynamic mechanical data in the frequency range $10^{-5} < f < 10^4$ Hz from 63 to 123 °C.
PVC	358.7	13.42	28.7	358	[74]	• $a_{T,\alpha}$ of local segmental motion from $365 < T < 410$ K obtained by dielectric relaxation. The relaxation times lie within the range: $10^{-7} < \tau_\alpha < 1$ s. Log $\tau_\alpha(380\,\mathrm{K}) = -4.64$.
PVC (*commercial sample: Solvay & Cie, type Solvic 229)*	346.5	11.2	34.6	338.7 (*from dilatometry at a cooling rate of 3K/h)*	[56]	• $a_{T,S}$ of the softening dispersion from creep, $J(t)$, data. It has a much weaker temperature dependence compared with $a_{T,\alpha}$ from dynamic mechanical and dielectric relaxation given above. This discrepancy between the shift factors of the mechanical data of Schwarzl with the other sets of data may be due to the much lower T_g of the sample used.
Poly(vinyl formal)	381.3	10.33	26.76		[63,64]	• $a_{T,\alpha}$ of local segmental motion from dielectric relaxation data determining the relaxation time in the range: $10^{-7} < \tau_\alpha < 10^{-3}$s. $\tau_\alpha(T_0) = 1$ s.
Poly(vinyl hexanal)	312.6	16.0	85.62		[75]	• $a_{T,\alpha}$ of local segmental motion from dielectric relaxation data determining the relaxation time in the range: $10^{-6} < \tau_\alpha < 10^{-3}$s. $\tau_\alpha(T_0) = 1$ s.
Poly(vinyl methyl ether) PVME	244	14	42	250	[76]	• $a_{T,\alpha}$ of local segmental motion from dielectric relaxation in the range: $10^{-0.5} > \tau_\alpha > 10^{-7}$ s.
PVME	246.5	15.25	47.23		[77,78]	• $a_{T,\alpha}$ from dielectric data of Zetsche *et al.* [78]. Similar to that given above.
Acrylates and methacrylate polymers						
Poly(methyl acrylate) PMA	324	8.86	101.6	276 (*value seems too low*)	[79,80]	• This shift factor was obtained by combining the dynamic mechanical data of the entire softening dispersion ($25 < T < 90$ °C and $30 < f < 3000$ Hz) and early dielectric relaxation data of Mead and Fuoss [79] in a comparable frequency range. Its temperature dependence is weaker than that of the shift factors $a_{T,S}$ and $a_{T,\varepsilon}$ to be described below.
	287.4	11.08	27.9	287	[24]	• $a_{T,S}$ of the entire softening dispersion from $J_r(t)$.
	287.72	12.8	38.2		[5]	• $a_{T,\varepsilon}$ of the local segmental motion from 293 to 373 K by dielectric measurement ($10^{-1} < f < 10^{10}$ Hz). Temperature dependence of $a_{T,\varepsilon}$ is in good agreement with that of $a_{T,S}$ for viscoelastic response principally in the compliance range $J_g > J(t) < 10^{-8}\,\mathrm{cm}^2/\mathrm{dyne}$. Dielectric and creep data are in good agreement.
	326	8.86	101.6		[81]	• a_T of the entire viscoelastic response from relaxation modulus in extension, $E(t)$.

TABLE 26.1. *Continued.*

Polymer	T_0 °K	C_1 °K	C_2 °K	T_g °K	Ref.	Comments
	276	16.67	60	276 (*value seems too low*)	[2]	• $a_{T,\eta}$ of viscosity. It has a weaker temperature dependence than $a_{T,S}$ and $a_{T,\varepsilon}$.
Poly(methyl methacrylate) PMMA (*atactic*)	381	34	80	381	[2]	• $a_{T,\eta}$ for viscosity. Its *T*-dependence similar to that of conventional PMMA given below. If extrapolated down to the temperature regime of $a_{T,S}$ (see next entry) it has a different *T*-dependence than that of $a_{T,S}$.
PMMA (*atactic*)	382.55	9.34	32.5	381	[82]	• $a_{T,S}$ for the softening dispersion determined by $J_r(t)$ from 376 to 404 K. The *T*-dependence of $a_{T,S}$ is stronger than that of the viscoelastic mechanism above the rubbery plateau.
PMMA (*isotactic*)	326.5	9.34	32.5	323	[82–84]	• $a_{T,S}$ for the softening dispersion determined from 29.2 to 159.3 °C.
PMMA (*conventional*)*I*	388	32.2	80	390	[2]	• $a_{T,\eta}$ for viscosity determined in the high temperature range. If extrapolated down to the temperature regime of $a_{T,S}$ (to be given below) it has a different *T*-dependence than that of $a_{T,S}$.
PMMA (*conventional*)	493	7.0	173	378	[85]	• $a_{T,\eta}$ of viscosity. It has a considerably weaker *T*-dependence than that given by Berry and Fox [2].
PMMA (*conventional*)	393.5	9.34	32.5	390	[82]	• $a_{T,S}$ of the softening dispersion obtained by $J_r(t)$ in the range from 387 to 462 K. In good agreement with the *T*-dependence of the shift factors obtained from stress relaxation $E(t)$ data of McLoughlin and Tobolsky [175] in a similar temperature range.
PMMA (*conventional*)	390.5	14.27	63.1		[81]	• $a_{T,S}$ of the softening dispersion. However, the *T*-dependence as reported is weaker than that given in the entry above. The reason for this discrepancy is not clear. We recommended the WLF parameters given in the entry above because they are corroborated by two different experimental measurements.
PMMA (*conventional*)	393.1	12.21	70.1	390	[82]	• $a_{T,\text{plateau}}$ of the viscoelastic mechanism with compliance above the rubbery plateau determined in the same temperature range as $a_{T,S}$, but has weaker *T*-dependence than that of the latter.
PMMA (*commercial, Röhm Plexiglas 240/218*)	396.5	8.0	36.0	380.2 (*from dilatometry at a cooling rate of 3 K/h*)	[56]	• $a_{T,S}$ for the entire softening dispersion from 100 to 145 °C. Its temperature dependence is weaker than that of $a_{T,S}$ obtained by Plazek *et al.* [82–84]. It is possible the discrepancy is caused by the sample studied by Schwarzl *et al.* has a lower T_g. A correction of the difference in T_g of about 3 degrees will bring the two sets of shift factors into agreement.
Poly(ethyl methacrylate) PEMA	373	11.18	103.5	335	[86]	• $a_{T,S}$ of the softening dispersion from dynamic shear compliance $J^*(\omega)$ from 352.7 to 428°K.
Poly(*n*-butyl methacrylate)						
Pn-BMA	373 300	9.7 17.0	169.6 96.6	300 300	[87]	• $a_{T,S}$ of the softening dispersion from dynamic shear compliance $J^*(\omega)$ from 316.7 to 403.1 K.
Pn-BMA	373	8.5	185	300	[88]	• $a_{T,\alpha}$ of local segmental motion from dielectric relaxation: $10^0 < f < 10^7$ Hz and $313 < T < 403$ K. Its *T*-dependence is comparable but slightly weaker than that of $a_{T,S}$ given in the entry above.
Pn-BMA (*M = 250000*)	300	18.2	96.6	300	[89]	• $a_{T,\alpha}$ of local segmental motion from PCS measurement from 35.8 °C to 70.6 °C and $\log\langle\tau\rangle$ from 10 to 10^{-4} s. Its *T*-dependence is similar to that of $a_{T,S}$ from dynamic mechanical data.

TABLE 26.1. *Continued.*

Polymer	T_0 °K	C_1 °K	C_2 °K	T_g °K	Ref.	Comments
Poly(*n*-hexyl methacrylate)						
Pn-HMA	373	9.8	234.4	268	[90]	• $a_{T,S}$ of the softening dispersion from dynamic shear compliance $J^*(\omega)$ from 277.7 to 398 K.
Pn-HMA	268.1	10.95	67.12	268	[91]	• $a_{T,\alpha}$ of local segmental motion from dielectric relaxation: $10^0 < f < 10^6$ Hz and $275 < T < 333$°K. Its *T*-dependence is nearly the same as that of $a_{T,S}$ (see above) within this temperature range.
Poly(*n*-octal methacrylate) Pn-OMA	373	7.6	227.3	253	[92–95]	• $a_{T,S}$ of the softening dispersion from dynamic shear compliance $J^*(\omega)$ from 258.7 to 402.5 K.
Poly(2-ethyl hexyl)	373	11.58	208.9	284	[96]	• $a_{T,S}$ of the softening dispersion from dynamic shear compliance $J^*(\omega)$.
Poly(*n*-lauryl methacrylate)						
Pn-LMA	298.2	8.52	139.2	208?	[97]	• $a_{T,S}$ of the softening dispersion from dynamic shear compliance $J^*(\omega)$ from 232.6 to 318.3 K.
Pn-LMA $M_w = 1.1 \times 10^5$ g/mol	233.8	9.06	62.3	225	[98]	• $a_{T,\alpha}$ of the local segmental motion determined from dielectric relaxation and PCS for the range $10^0 > \tau_\alpha > 10^{-5/2}$ s. It has a weaker *T*-dependence than that of $a_{T,S}$.
Poly(cyclohexyl methacrylate) PCHMA $M_w = 2 \times 10^5$	359.7	14.8	75.67	374	[99]	• $a_{T,\alpha}$ of local segmental motion from data of local density fluctuation observed by PCS, mechanical relaxation and dielectric relaxation. When referenced to the respective T_g s (i.e. plotting $\log(a_{T,\alpha})$ against $(T-T_g)$ the shift factor of PCHMA has a considerably stronger temperature dependence than that of Pn-HMA.
Heterogeneous backbone polymers						
bisphenol A Polycarbonate BPA-PC	418	22.88	78.64		[100]	• $a_{T,S}$ of the entire softening dispersion from dynamic mechanical measurements obtained in the range $405 < T < 426$ K.
BPA-PC	425.7	10.4	52.2	423.6	[101]	• $a_{T,\eta}$ of viscosity from 478 to 597°K obtained on Lexan (General Electric Co.) with $M_w = 72\,600$ and $M_n = 28\,100$.
BPA-PC (*branched*)	425.7	9.61	120.7	425.7	[102]	• $a_{T,\eta}$ from terminal relaxation $G^*(\omega)$ data measured over the temperature range from 473 to 573 K. Its *T*-dependence is nearly the same as that for Lexan given above and is much weaker than that of $a_{T,S}$ for linear BPA-PC given above when the latter is extrapolated to high temperatures and compared at 473 K, the lowest temperature of measurement of $a_{T,\eta}$.
BPA-PC	427.7	12.18	51.97	423	[103]	• $a_{T,E}$ obtained from stress relaxation measurements $(10 < \pm < 10^4$ s) and $(140.5 < T < 172.5$ C) from the glass to the terminal zone.
Poly(dimethyl siloxane)						
PDMS	303	1.90	222	150	[104]	• $a_{T,\eta}$ of viscous flow determined at temperatures significantly higher than T_g. Do not extrapolate down to low temperatures near and above T_g because it shows a *T*-dependence unrealistically much weaker than that of $a_{T,\alpha}$ of the local segmental motion (given below).
PDMS	150	5.08	120	150	[105]	• $a_{T,\eta}$ of viscous flow from creep (remarks given immediately above apply here).

TABLE 26.1. *Continued.*

Polymer	T_0 °K	C_1 °K	C_2 °K	T_g °K	Ref.	Comments
PDMS ($M_n = 10\,370$)	147	10.4	14.24	149.5	[106]	• $a_{T,\varepsilon}$ of local segmental motion from dielectric relaxation in the frequency range $10^{-2} < f < 10^7$ Hz and temperature range $T_g < T < T_g + 20°$ K. If this is extrapolated to higher temperatures, the extrapolated values turns out to agree with $a_{T,\eta}$ throughout the temperature range in which the latter was determined, e.g., $-233 < T < 300$ K.
PDMS ($M_n = 3230$)	145.3	14.12	23.06	148.8	[106]	• Same as above.
PDMS ($M_n = 420$)	136.5	11.46	14.01	135.9	[106]	• Same as above.
PDMS *cyclic* ($M_n = 6920$)	149	11.48	15	150.3	[106]	• Same as above.
PDMS *cyclic* ($M_n = 2120$)	148.2	14.03	23.86	151.6	[106]	• Same as above.
PDMS *cyclic* ($M_n = 410$)	153	13.53	18.05		[106]	• Same as above.
Poly(aryl ether ether ketone) $M_w = 90\,000$; $M_n = 45\,000$ *(450 G.ICI)*	412.9	29.96	53.74	417	[178]	• $a_{T,\alpha}$ of local segmental motion obtained by $G^*(\omega)$ from dynamic mechanical measurements from 1 to 10^{-4} Hz in the temperature range of 412 to 423 K and τ_α ranging from $10^{-0.24}$ to 10^5 s.
methyl-substituted Poly(aryl ether ether ketone) (Me)PEEK	514.1	3.24	132.1	424.1	[107]	• $a_{T,\eta}$ of terminal dispersion measured by $G^*(\omega)$ on a sample with $M_w = 33\,800$. The author has given the shift factor originally as the VFTH form of $\log a_T = B/(T - T_\infty)$ with B=428 ± 30 K and $T_\infty = T_g - 42$°C for samples with different molecular weights.
Poly(oxy-1,4-phenylene sulfoneyl-1,4-phenylene), *also called poly(aryl ether sulfone)* PES	485.2	70.98	241.2	497	[178]	• $a_{T,\alpha}$ of local segmental motion from dynamic mechanical measurement of $G^*(\omega)$ from 1 to 10^{-4} Hz in the temperature range from 485 to 516 K and τ_α ranging from $10^{-2.4}$ to $10^{5.6}$ s.
Poly(ethylene terephthalate)						
PET (*amorphous*)	352.8	9.04	25.5	346.6	[108]	• $a_{T,\alpha}$ of local segmental motion from dielectric relaxation.
PET (*amorphous*)	346.6	17.7	42.63	346.6	[5]	• $a_{T,\alpha}$ of local segmental motion from dielectric relaxation.
Poly(2-hydroxypropyl ether Bisphenol A)						
PH	356.6	14.21	31.6	359	[76]	• $a_{T,\alpha}$ of local segmental motion from dielectric relaxation in the range: $10^{-1} > \tau_\alpha > 10^{-8}$ s.
Poly(methyl phenyl siloxane)						
PMPS (*$M = 5000$*)	181.2	20.4	56.76	223.3	[30]	• $a_{T,S}$ of the softening dispersion from $J_r(t)$ from 23.4 to −50 °C.
PMPS (*$M = 2500$*)	207	18.1	39.8		[109, 110]	• $a_{T,\alpha}$ of the local segmental motion from local density fluctuation in PCS. It has a stronger T-dependence than that of chain diffusion (given below).

TABLE 26.1. *Continued.*

Polymer	T_0 °K	C_1 °K	C_2 °K	T_g °K	Ref.	Comments
PMPS ($M = 2500$)	207	5.6	56.76		[109, 110]	• shift factor of chain diffusion from concentration fluctuation in PCS.
PMPS ($M = 12\,000$)	237.4	23.96	48.8	237.4	[111, 112]	• $a_{T,\alpha}$ of local segmental motion from dynamic mechanical measurement of $G^*(f)$ in the range: $10^{-1.5} < f < 10^{1.5}$ Hz.
	258.4	7.32	32.5	237.4	[111, 112]	• $a_{T,\alpha}$ from dielectric measurement in the range: $10^2 < f < 10^6$ Hz. • Good correspondence to $a_{T,\alpha}$ from mechanical data.
PMPS ($M = 130\,000$)	243.2	17.69	34.71	243.2	[111, 112]	• $a_{T,\alpha}$ from dynamic mechanical (see above).
	261.8	7.47	36.1	243.2	[111, 112]	• $a_{T,\alpha}$ from dielectric relaxation (see above).
PMPS ($M = 28\,500$)	273.2	14.8	66.4	247.2	[113]	• $a_{T,\alpha}$ from PCS.
	248.2	14.8	55.9	248.2		
	273.2	11.8	67.9	247.2	[113]	• $a_{T,\alpha}$ from dielectric relaxation.
	248.2	15.2	49.2	248.2		
	248.2	16.1	53.2	248.2	[177]	• $a_{T,\eta}$ of shear viscosity from $-25°$ to 100 °C and $1 < \eta < 10^{7.7}$ Pa.s.
Poly(methyl-*p*-tolyl siloxane) PMpTS ($M_w = 18\,400$)	262.2	12.9	55.1	262.2	[177]	• a_T of entire viscoelastic response from the glass level to the terminal zone obtained from $G^*(\omega)$.
	259.1	15	45	262.2	[179]	• $a_{T,\alpha}$ of local segmental motion from photon correlation measurement in the range $10^{-6} < \tau_\alpha < 10^1$s and $260 < T < 290$K.Log$[\tau_\alpha(T = 270\text{K})/\text{s}] = -2.9$.
	258.1	12.8	37.8	262.2	[179]	• $a_{T,\alpha}$ of local segmental motion from dielectric relaxation measurement in the range $10^{-9.8} < \tau_\alpha < 10^2$ s and $252 < T < 370$ K. Log $[\tau_\alpha(T = 270\,\text{K})/\text{s}] = -3.06$.
Poly(propylene oxide) PPO	198	16.2	24	198	[114]	• $a_{T,\alpha}$ of the local segmental motion from dielectric relaxation measurements in the frequency range $10^{-4} < f < 10^6$ Hz.
Poly(propylene glycol) PPG (4000, 2000, 1000)	198.8	16.8	48.8		[115]	• $a_{T,\alpha}$ of local segmental motion from dielectric relaxation measurements in the frequency range: $10^6 < f < 10^{-4}$ Hz. It has stronger temperature dependence than that of $a_{T,n}$, the shift factor of the normal modes.
PPG (4000)	216.66	10.1	63.66		[115]	• $a_{T,n}$ of the normal modes from dielectric relaxation measurements (see remarks immediately above).
PPG (40 000)	216.66	8.85	50		[116]	• $a_{T,\eta}$ of the shear viscosity. Its temperature dependence is close to that of $a_{T,n}$, the shift factor of the normal mode from dielectric data.
PPG *linear*, $M_n = 3100$	205.9	9.24	22.93		[117]	• $a_{T,\phi}$ of the local segmental motion from PCS from $-49°$ to -66.7 °C. $\tau_\alpha(-60.7°\text{C}) = 1.00 \times 10^{-2}$s.
Poly(thio-1,4-phenylene), *also called poly(phenylene sulfur) PPS* ($M_w = 37\,000$) *T1. Solvay*	355.3	22.21	49.63	362	[178]	• $a_{T,\alpha}$ of local segmental motion from dynamic mechanical measurement of $G^*(\omega)$ from 1 to 10^{-4} Hz in the temperature range from 355 to 371 K.
Polysulfone PSF	459	15.1	49	459	[118]	• $a_{T,\text{Rouse}}$ of the resolved Rouse modes by the combination of stress relaxation and dynamic birefringence. $\tau_{\text{Rouse}}(T_g) = 10^{0.7}$s.

TABLE 26.1. *Continued.*

Polymer	T_0 °K	C_1 °K	C_2 °K	T_g °K	Ref.	Comments
	459	15.8	43.7	459	[118]	• $a_{T,G}$ of the resolved G-component of the softening dispersion which represents the stress that relaxes through monomer rotation around the chain axis. $\tau_G(T_g) = 1$ s.
Tetra methyl polycarbonate TMPC	456.4	8.9	29.0	456.4	[119]	• $a_{T,\alpha}$ of local segmental motion from dielectric relaxation.
Zinc phosphinate polymer	373	6.94	66.6	324	[120]	
Rubbers						
Butyl rubber (*lightly vulcanized with sulfur*)	298	9.03	201.6	205	[121]	• $a_{T,S}$ of the softening dispersion from dynamic shear measurements.
Ethylene-propylene copolymer *(ethylene:propylene = 16:84 by mole*)	298	5.52	96.7	242	[122]	• $a_{T,S}$ of the softening dispersion from dynamic shear measurements.
(ethylene:propylene = 56:44 by mole)	298	4.35	122.7	216	[122]	• $a_{T,S}$ of the softening dispersion from dynamic shear measurements.
Hypalon-20 *(chloro-sulfonated polyethylene*)	248.5	17.44	51.6	248.5	[123]	• $a_{T,S}$ of the softening dispersion from dynamic shear modulus, $G^*(\omega)$, data in the frequency range of 25 to 2500 Hz from 264.6 to 341.4 °K. Values of G' range from 2×10^9 to 7×10^6 dyne/cm^2 in the glass–rubber region.
Hevea brasiliensis Natural Rubber	248	8.86	101.6	200	[124]	• From dynamic mechanical $G^*(\omega)$ data taken from $10^{-2.2} < \omega < 10^{1.2}$ rad/s in the temperature range of -73 °C to 60 °C. Shift factors are mostly for the entire softening dispersion. G' is about 10^7 dyne/cm^2 in the neighborhood of -30 °C.
	298	5.94	151.6		[125]	• Similar T-dependent as found by Payne and given above.
	211	11.4	37.8		[56]	• $a_{T,S}$ of the entire softening dispersion from creep, $J(t)$, data from 193 to 253 °K. Its T-dependence is similar to that of Payne.
	209	13.5	17.2		[126, 127]	• $a_{T,\alpha}$ of local segmental motion from dynamic mechanical $G^*(\omega)$ data from 203 to 217 °K. It has a much stronger T-dependence than that found by Payne [124] and by Dickie and Ferry [125] in the same temperature range. This large discrepancy may come from different samples being used. The sample studied in this work is of exceptional high grade and substantially masticated.
	210.4	12.26	38.6		[127]	• $a_{T,\alpha}$ of local segmental motion from dielectric relaxation data from 207 to 249 °K in the frequency range of $10^{-2} < f < 10^6$ Hz on the same sample as that used in $G^*(\omega)$ measurement. Its T-dependence is almost the same as, though slightly weaker than, that of $a_{T,\alpha}$ from $G^*(\omega)$ data.
Poly(isoprene) PI *linear 75.7% cis-1,4;18.1% trans-1,4;6.2% vinyl-3,4.* $M_w = 97\,000$	250	6.1	70.9	213.2	[128]	• $a_{T,\alpha}$ from dielectric relaxation data in the range of $10^{-1} < f < 10^9$ Hz.
	300	0.9	57.9	213.2	[128]	• $a_{T,n}$ of the dielectric normal mode which correspond to the terminal relaxation. These WLF parameters for this high mol. wt. sample is probably not reliable because of limited data.

TABLE 26.1. *Continued.*

Polymer	T_0 °K	C_1 °K	C_2 °K	T_g °K	Ref.	Comments
PI *linear* *77.9% cis-1,4* *18.1% tran-1,4* *4% vinyl-3,4* $M_w = 13\,000$	250	5.8	74.3	211.5	[128]	• $a_{T,\alpha}$ from dielectric relaxation data in the range of $10^{-1} < f < 10^9$ Hz.
	300	4.2	128.8	211.5	[128]	• $a_{T,n}$ of the dielectric normal mode which correspond to the terminal relaxation. Its T-dependence is in excellent agreement with that of the viscosity, $a_{T,\eta}$, determined from dynamic mechanical data [Gotro *et al.* Ref. 133] (see below).
PI *linear* *78.8% cis-1,4;* *17.9% trans-1,4* *3.3% vinyl-3,4* $M_w = 5100$	250	5.7	80	207.1	[128]	• $a_{T,\alpha}$ from dielectric relaxation data in the range of $10^{-1} < f < 10^9$ Hz.
	300	4.0	133.9	207.1	[128]	• $a_{T,n}$ of the dielectric normal mode which correspond to the terminal relaxation.
PI *cis-1,4;* $M_w = 2350$	211.4	12.3	40.4	206	[129]	• $a_{T,\alpha}$ of the local segmental motion from a combination of PCS and dielectric relaxation data. $\tau(T_0) = 1$ s.
PI *cis-1,4;* $M_w = 35\,000$	209.4	12.3	37.4	213	[130]	• $a_{T,\alpha}$ of the local segmental motion from $-56 < T < -47$ °C obtained by PCS. $\tau(T_0) = 1$ s.
	210.9	12.85	49.6	210.9	[131]	• $a_{T,\alpha}$ of local segmental motion from 2D deuteron exchange NMR data. Its temperature dependence is in good agreement with that determined from dielectric data.
PI *18 arms star* *76.5% cis-1,4* *17.9% trans-1,4* *5.6% vinyl-3,4* $M_w = 384\,000$	250	6.2	75.0	213.0	[128]	• $a_{T,\alpha}$ from dielectric relaxation data in the range of $10^{-1} < f < 10^9$ Hz.
	300	3.4	100.4	213.0	[128]	• $a_{T,n}$ of the dielectric normal mode which correspond to the terminal relaxation.
PI *4 arms star* *77.6% cis-1,4* *16.8% trans-1,4* *5.6% vinyl-3,4* $M_w = 380\,000$	250	6.2	78.7	212.2	[128]	• $a_{T,\alpha}$ from dielectric relaxation data in the range of $10^{-1} < f < 10^9$ Hz.
	300	2.3	40	212.2	[128]	• $a_{T,n}$ of the dielectric normal mode which correspond to the terminal relaxation.
PI *cis-1,4* $M_w = 2350$	211.38	12.3	40.4	206	[128]	• $a_{T,\alpha}$ of local segmental motion determined by combining PCS and dielectric relaxation data over the frequency range of $10 < f < 10^5$ Hz.
PI *7% vinyl, 84.5% cis-1,4* $1.6 \times 10^5 < M_w < 1.1 \times 10^6$	243.2	8.2	89.5		[132]	• a_T of viscoelastic response in the compliance range of $10^{-9.6} < J_p(t)$ including the terminal relaxation from -70 to 42 °C for $M_w = 6.2 \times 10^5$.
PI *8% 3,4* *high mol. wt.*	298	4.1	122	205	[133]	• $a_{T,\eta}$ of the terminal relaxation determined by dynamic modulus. Its T-dependence is in excellent agreement with that of $a_{T,n}$ obtained from dielectric normal mode data (see above for the 13 000 mol. wt. PI dielectric data). The C_1 and C_2 parameters given here apply also for the other PI microstructures if T_0 is adjusted for the change in T_g: $T_0 = 25 + \Delta T_g$, where ΔT_g is the difference in T_g from 206°K, the value for the 8% 3,4 microstructure.

TABLE 26.1. *Continued.*

Polymer	T_0 °K	C_1 °K	C_2 °K	T_g °K	Ref.	Comments
PI *(70% cis, 23% trans, 7%, 3,4;* $M_w = 63\ 400$)	211.6	12.2	53.7	211.6	[134]	• $a_{T,\eta}$ of terminal dispersion from dynamic mechanical, $G^*(\omega)$, data.
PI *(70% cis, 23% trans, 7%, 3,4;* $M_w = 103\ 000$)	212	11.7	52.9	212	[134]	• $a_{T,\eta}$ of terminal dispersion from dynamic mechanical, $G^*(\omega)$, data.
Hydrogenated polyisoprene						
HPI $4 \times 10^4 < M_w < 3 \times 10^5$						• $a_{T,\eta}$ of terminal dispersion from dynamic mechanical data for T-T_g from ~90 to ~250 °C.
8% 3,4	373	3.91	227	211	[133]	
16% 3,4	376	3.91	227	214	[133]	
20%, 3,4	379	3.91	227	217	[133]	
29% 3,4	386	3.91	227	224	[133]	
34%, 3,4	393	3.91	227	231	[133]	
Poly(vinyl ethylene)						
PVE *97% 1,2*	270.9	14.54	47.39	272.5	[135]	• $a_{T,\alpha}$ of local segmental motion from dielectric relaxation data from 268 to 305°K and $10^{1.2} > \tau_\alpha > 10^{-6}$ s.
	268.2	11.66	23.89	272.5	[136]	• $a_{T,S}$ of the softening dispersion from recoverable creep compliance, $J_r(t)$, data obtained on the same sample as above from −12.6 to 30.1 °C. Same sample as above.
	264.4	13.33	24.33	272.5	[135]	• $a_{T,\alpha}$ of local segmental motion from dynamic mechanical $G^*(\omega)$ data. Same sample as above. Its temperature dependence is in excellent agreement with that for dielectric relaxation data given above.
cross-linked with 0.056 wt % dicumyl peroxide cross-linker	270.0	12.77	24.33		[137]	• $a_{T,\alpha}$ of local segmental motion from dielectric relaxation data from $10^{1.2} > \tau_\alpha > 10^{-6}$ s.
cross-linked with 0.111 wt %dicumyl peroxide cross-linker	277.4	12.1	32.8		[137]	• Same as above
cross-linked with 0.222 wt % dicumyl peroxide cross-linker	276.5	13.36	23.55		[137]	• Same as above.
cross-linked with 0.444 wt % dicumyl peroxide cross-linker	277.6	22.2	52.0		[137]	• Same as above.
cross-linked with 0666 wt % dicumyl peroxide cross-linker	282.9	10.8	13.9		[137]	• Same as above.
PVE *94% 1,2*	271.2	12.3	48.6	271.2	[131]	• $a_{T,\alpha}$ of local segmental motion from 2D deuteron exchange NMR data obtained from 273 to 286°K. Its T-dependence is similar to that determined by dielectric and dynamic mechanical data (see above).
	265.18	13.66	44.72	273	[138]	• $a_{T,S}$ of the terminal relaxation from dynamic stress-optical measurements made in the temperature range from 295 to 353°K.
PVE *(91.5% vinyl)*	298	6.23	72.5	261	[139]	• $a_{T,S}$ Its T-dependence is weaker than the corresponding shift factors obtained in other PVE samples with higher vinyl content and higher T_gs.
PVE (> 99%,1,2; $M_w = 84\ 400$)	279	11.4_5	56.0	279	[134]	• $a_{T,\eta}$ of terminal dispersion from dynamic mechanical, $G^*(\omega)$ data.
PVE (> 99%1,2; $M_w = 204\ 000$)	279.5	11.3	59.2	279.5	[134]	• $a_{T,\eta}$ of terminal dispersion from dynamic mechanical, $G^*(\omega)$ data.

TABLE 26.1. *Continued.*

Polymer	T_0 °K	C_1 °K	C_2 °K	T_g °K	Ref.	Comments
PVE (95% 1,2; $M_w = 19\,000$)	272.2	11.34	28.6	272	[140]	• a_T for the entire viscoelastic response from softening to terminal. This is a compromise of two different temperature dependences of shift factors for the segmental, $a_{T,\alpha}$ and for the terminal motion, $a_{T,\eta}$, found by Zorn *et al.* in PVE, similar to what Plazek and coworkers have seen in PS, a-PP, PVAc, PMPS and etc. [25–32]. However the two shift factors obtained by Zorn *et al.* were determined in two *non*-overlapping temperature regions ($T \leq -0.2$°C for $a_{T,\alpha}$ and $T \geq 40.4$°C for $a_{T,\eta}$), while Plazek and coworkers, using the Leaderman's trick [176] of measuring creep during recovery at a lower temperature, managed to measure both $a_{T,\alpha}$ and $a_{T,\eta}$ over a common temperature range and found them to be different.
Polybutadiene PB						
96% cis, 2% trans, 2% vinyl	298	3.44	196.6	161	[141]	• Softening $a_{T,S}$.
43% cis, 50% trans, 7% vinyl	298	3.64	186.5	172	[142]	• Softening $a_{T,S}$.
27% cis, 37% trans, 36% vinyl	263	5.97	123.2	205	[143]	• Softening $a_{T,S}$.
7% cis, 1.5% trans, 91.5% vinyl	298	6.23	72.5	261	[139]	• Softening $a_{T,S}$.
PB						
20% vinyl-1,2	173.3	10.2	11.32	173.3	[126]	• $a_{T,\alpha}$ of local segmental motion by dynamic mechanical, $E^*(\omega)$, data in the frequency range of 0.01 to 100 Hz and temperatures near but above T_g. The sample is lightly cross-linked to attain dimensional stability for uniaxial extension measurement.
50% vinyl-1,2	200	27.15	64.17	200	[126]	• Same as above.
71% vinyl-1,2	225.5	14.4	25.5	225.5	[126]	• Same as above.
83% vinyl-1,2	249	20.7	42.1	249	[126]	• Same as above.
97% vinyl-1,2	271.5	14.6	24.5	271.5	[126]	• Same as above.
PB						
7% vinyl-1,2, 52% trans-1,4, 41% cis-1,4	177.9	18.0	37.6	178	[140]	• $a_{T,\alpha}$ of local segmental motion by dynamic mechanical, $G^*(\omega)$, data in the frequency range of 0.01 to 100 rads/s and temperatures near but above T_g. The sample is not cross-linked.
52% vinyl-1,2, 29% trans-1,4, 19% cis-1,4	215.6	15.1	38.0	216	[140]	• Same as above.
68% vinyl-1,2, 20% trans-1,4, 12% cis-1,4	238	11.8	38.8	238	[140]	• Same as above.
86% vinyl-1,2, 8% trans-1,4, 6% cis-1,4	249.7	16.6	31.3	250	[140]	• Same as above.
95% vinyl-1,2	272.2	14.9	37.5	272	[140]	• Same as above.
PB						
99% vinyl-1,2	323	5.78	94.8	268	[144]	• $a_{T,\eta}$ of the terminal relaxation from dynamic mechanical, $G^*(\omega)$, data in the T-range of 50 to 150°K above T_g.
x% vinyl-1,2 0.145<x<0.99	55 $+T_g(x)$	5.78	94.8	$T_g(x)$	[144]	• $a_{T,\eta}$ of the terminal relaxation from dynamical mechanical, $G^*(\omega)$, data in the T-range of 50–150°K above T_g for the high-vinyl compositions and of 100–200°K above T_g for the low-vinyl compositions. Results similar to that found by Kraus and Gruver [145].
PB						
35% cis, 54% trans, 10% vinyl $M = 1.30$✓ $\sim 10^5$	298	3.48	163	175	[146]	• a_T of the entire viscoelastic spectrum from dynamic mechanical, $G(\omega)$, data in the T-range of 182 to 398°K.

TABLE 26.1. *Continued.*

Polymer	T_0 °K	C_1 °K	C_2 °K	T_g °K	Ref.	Comments
35% cis, 56% trans, 8% vinyl $M = 6.29 \times 10^3$	298	3.22	160	173.7	[146]	• a_T of the entire viscoelastic spectrum from dynamic mechanical, $G^*(\omega)$, data.
PB *39% cis, 53% trans, 8% vinyl* $2 \times 10^4 < M_w < 2 \times 10^5$	301.2	4.17	196.8	182.2	[147]	• $a_{T,\eta}$ of mainly the terminal relaxation from dynamical mechanical, $G^*(\omega)$, data.
PB *cyclic* *7% cis, 30% trans, 63% vinyl* $3.8 \times 10^4 < M_w < 6.0 \times 10^4$	299.2	5.36	121.2	233	[148]	• $a_{T,\eta}$ of the terminal relaxation from dynamic mechanical, $G^*(\omega)$, data in the T-range of 248 to 361°K.
Polybutadiene crosslinked with dicumyl peroxide						
PB, 40% cis, 50% trans, 10% vinyl *(0.25% DiCup)*	273.2	3.0	120	180.2	[154]	• $a_{T,S}$ of the softening dispersion from creep measurement.
PB, 36% cis, 54% trans, 10% vinyl *(0.80% DiCup)*	273.2	2.95	125	175.2	[154]	• $a_{T,S}$ of the softening dispersion from creep measurement.
Hydrogenated polybutadiene HPB						
99% vinyl-1,2	323	6.35	146	246	[144]	• $a_{T,\eta}$ of the terminal relaxation from dynamic mechanical, $G^*(\omega)$, data in the T-range of 300 to 486°K.
x% vinyl-1,2 *0.145<x<0.99*	77 $+T_g(x)$	6.35	146	$T_g(x)$	[144]	• $a_{T,\eta}$ of the terminal relaxation from dynamic mechanical, $G^*(\omega)$, data in the T-range of about 180–300 °K above T_g for the low-vinyl compositions. Results similar to that found earlier by Arnett and Thomas.
Poly(1,3-dimethyl-1-butenylene) PDMB	348.2	4.88	1119.5	275.4	[150]	• $a_{T,\eta}$ of the terminal relaxation from dynamic mechanical, $G^*(\omega)$, data from 25 °C to 190 °C. Its T-dependence is similar to that of *a- PP* which can be obtained from PDMB by hydrogenation.
Polyurethane PU *(cross-linked)*	283	8.86	101.6	238	[151]	• $a_{T,S}$ of the softening dispersion from rubber to glass from dynamic mechanical data taken over the frequency range of 45–6000 Hz and the T-range of −16–39 °C. The loss tangent exhibits a broad maximum resembling the behavior of PIB.
PU *(network)*	251.1	14.46	33.1		[152]	• $a_{T,\alpha}$ of the local segmental motion from PCS, Brillouin scattering and dielectric relaxation data in the T-range of −14 °C to 105 °C.
PU *(cross-linked)*	228.2	12.5	42.5		[56]	• $a_{T,S}$ of the softening dispersion from creep compliance data.
Styrene-butadiene copolymer *(styrene: butadiene = 23.5:76.5, random, by weight)*	298	4.57	113.6	210	[153]	• $a_{T,S}$
Hydroxy terminated polybutadiene (20% cis, 60% trans, 20% vinyl)						

TABLE 26.1. *Continued.*

Polymer	T_0 °K	C_1 °K	C_2 °K	T_g °K	Ref.	Comments
HTPB-1 *(Mol. wt. per crosslinked unit, $M_x = 1760$)*	273.2	36.79	273.2 *(Arrhenius)*	194.2	[154]	• $a_{T,S}$ of the softening dispersion from creep measurement.
HTPB-2 ($M_x = 2370$)	273.2	41.59	273.2 *(Arrhenius)*	194.2	[154]	• $a_{T,S}$ of the softening dispersion from creep measurement.
HTPB-3 ($M_x = 5930$)	273.2	33.59	273.2 *(Arrhenius)*	194.2	[154]	• $a_{T,S}$ of the softening dispersion from creep measurement.
Hydroxy terminated styrene butadiene rubber						
HTSBR ($M_x = 2980$)	273.2	41.59	273.2 *(Arrhenius)*	194.2	[154]	• $a_{T,S}$ of the softening dispersion from creep measurement.
Fluorinated hydrocarbon elastomers						
Viton 11A(Air) (*Mol. wt. per crosslinked unit, $M_x = 7220$*)	253.2	11.62	37	249	[155]	• $a_{T,S}$ of the softening dispersion from creep measurement.
Viton 10A(Vac) ($M_x = 5220$)	256.2	11.62	37	250.5	[155]	• $a_{T,S}$ of the softening dispersion from creep measurement.
Viton 10B(Air) ($M_x = 3070$)	260.2	11.62	37	253.6	[155]	• $a_{T,S}$ of the softening dispersion from creep measurement.
Viton 10B(Vac) ($M_x = 3070$)	262.0	11.62	37		[155]	• $a_{T,S}$ of the softening dispersion from creep measurement.
Bisphenol A based epoxy resins/4,4′ diamino diphenyl sulfone (DDS) 828/DDS ($M_x = 419$)	478.2	144.4	478.2 (*Arrhenius*)	477.2	[156]	• $a_{T,S}$ of the softening dispersion from creep measurement.
1001/DDS ($M_x = 908$)	403.2	19.26	50.0	400.2	[156]	• $a_{T,S}$ of the softening dispersion from creep measurement.
1004/DDS ($M_x = 1520$)	384.0	21.02	50.0	385.2	[156]	• $a_{T,S}$ of the softening dispersion from creep measurement.
1007/DDS ($M_x = 2870$)	373.9	20.50	50.0	374.2	[156]	• $a_{T,S}$ of the softening dispersion from creep measurement.
Epoxy model networks *from a diepoxy prepolymer, DGEBA, and three different diamines or mixtures of a monoamine and a diamine.*						
DDM *(4,4′ diamino diphenyl methane)* network	457.2	10.9	34.8	457.2 (at 1 Hz)	[149]	• $a_{T,S}$ of the softening dispersion from dynamic mechanical, $E^*(\omega)$.
DDM/Aniline network	394.2	9.5	25.6	394.2 (at 1 Hz)	[149]	• $a_{T,S}$ of the softening dispersion from dynamic mechanical, $E^*(\omega)$.
Hexamethylene diamine *(HMDA)*	391.2	11.0	41.5	391.2 (1 Hz)	[149]	• $a_{T,S}$ of the softening dispersion from dynamic mechanical, $E^*(\omega)$.
HMDA/Hexylamine	336.7	9.9	34.4	336.7 (at 1 Hz)	[149]	• $a_{T,S}$ of the softening dispersion from dynamic mechanical, $E^*(\omega)$.
IPD *(isophorone diamine)*	442.2	12.5	52.9	442.2 (at 1 Hz)	[149]	• $a_{T,S}$ of the softening dispersion from dynamic mechanical, $E^*(\omega)$.
IPD/Trimethylcylcohexy lamine	382.2	9.2	41.9	382.2 (at 1 Hz)	[149]	• $a_{T,S}$ of the softening dispersion from dynamic mechanical, $E^*(\omega)$.

TABLE 26.1. *Continued.*

Polymer	T_0 °K	C_1 °K	C_2 °K	T_g °K	Ref.	Comments
Miscible Blends and Copolymers						
Styrene-*n*-hexyl methacrylate copolymers S-nHMA copolymer *(0.26:0.74)*	373	7.11	192.6	277	[157]	
S-nHMA copolymer *(0.41:0.59p)*	373	6.56	156.4	287	[157]	
Polyisoprene-polyvinylethylene blends (1–*x*)PI-xPVE blends, Resolved component dynamics						
x=0%, PI	210.4	12.26	38.59		[127]	• $a_{T,\alpha}$ of local segmental motion of PI from dielectric relaxation.
x=20%, PVE component	223.9	15.0	85.82		[127]	• $a_{T,\alpha}$ of local segmental motion of the PVE component resolved in the dielectric relaxation spectra which are not thermorheologically simple.
x=25%, PI component	216.7	12.2	38.66		[127]	• $a_{T,\alpha}$ of local segmental motion of the PI component resolved in the dielectric relaxation spectra (not thermorheologically simple).
x=25%, PVE component	255.47	12.2	125.4		[127]	• $a_{T,\alpha}$ of local segmental motion of the PVE component resolved in the dielectric relaxation spectra (not thermorheologically simple).
x=50%, PVE component	235.85	11.64	52.65		[127]	• $a_{T,\alpha}$ of local segmental motion of the PVE component resolved in the dielectric relaxation spectra (not thermorheologically simple).
x=75%, PVE component	255.47	12.2	125.4		[127]	• $a_{T,\alpha}$ of local segmental motion of the PVE component resolved in the dielectric relaxation spectra (not thermorheologically simple).
x=100%, PVE	271.3	12.0	36.8		[127]	• $a_{T,\alpha}$ of local segmental motion of PVE from dielectric relaxation.
(1–*x*)PI-*x*PVE blends, Resolved component dynamics						
x=0%, PI	215.7	10.16	54.14		[131]	• $a_{T,\alpha}$ of local segmental motion of PI from 2D deuteron exchange NMR (2D DE NMR).
x=25%, PI component	218.2	13.0	50.0		[131]	• $a_{T,\alpha}$ of local segmental motion of the PI component resolved by 2D DE NMR.
x=25%, PVE component	227.3	13.32	84.24		[131]	• $a_{T,\alpha}$ of local segmental motion of the PVE component resolved by 2D DE NMR.
x=50%, PI component	226.2	14.43	64.86		[131]	• $a_{T,\alpha}$ of local segmental motion of the PI component resolved by 2D DE NMR.
x=50%, PVE component	236.7	13.83	88.27		[131]	• $a_{T,\alpha}$ of local segmental motion of the PVE component resolved by 2D DE NMR.
x=75%, PI component	236.6	15.15	69.78		[131]	• $a_{T,\alpha}$ of local segmental motion of the PI component resolved by 2D DE NMR.
x=75%, PVE component	253.5	14.1	80.01		[131]	• $a_{T,\alpha}$ of local segmental motion of the PVE component resolved by 2D DE NMR.
x=100%, PVE	273.5	12.3	50.50		[131]	• $a_{T,\alpha}$ of local segmental motion of PVE by 2D DE NMR.
Poly(vinylmethylether)-polystyrene blends 50% PVME/50%PS blend: the PVME *component*	255.9	14.79	44.35		[77, 78]	• $a_{T,\alpha}$ of the local segmental motion of the PVME component in the blend from dielectric spectra, which are not thermorheologically simple. Its T-dependence is stronger than that of pure PVME.

TABLE 26.1. *Continued.*

Polymer	T_0 $^{\circ}$K	C_1 $^{\circ}$K	C_2 $^{\circ}$K	T_g $^{\circ}$K	Ref.	Comments
Diluted Systems						
Cellulose tributyrate in dimethyl phthalate						
(21%)	247	8.86	101.6	188	[158, 159]	• $a_{T,S}$ from creep and dynamic mechanical measurements.
(43%)	251	8.86	101.6	193	[158, 159]	• $a_{T,S}$ from creep and dynamic mechanical measurements.
Cellulose nitrate in diethyl phthalate *(23%)*	298	8.84	165.5	166		• $a_{T,S}$ from creep and dynamic mechanical measurements.
Polyethylene (solution chlorinated) *Cl content = 56.6 w/w, amorphous, in bis(2-ethylhexyl)phthalate*						
(88 polymer)	295.5	11.4	56.5	295	[180]	• $a_{T,\alpha}$ of local segmental motion from dielectric relaxation data for $\log \tau_\alpha = -11.4 + 644/\,(T\text{-}239\,\mathrm{K})$.
(74% polymer)	292.6	12.5	61.6	279	[180]	• $a_{T,\alpha}$ of local segmental motion from dielectric relaxation data for $\log \tau_\alpha = -12.5 + 770/\,(T\text{-}231\,\mathrm{K})$.
(59% polymer)	262.3	12.8	74.3	245	[180]	• $a_{T,\alpha}$ of local segmental motion from dielectric relaxation data for $\log \tau_\alpha = -12.8 + 951/\,(T\text{-}188\,\mathrm{K})$.
Polyisoprene ($M_w = 395\,000$) in Aroclor: *polymer concentration, c.*						
($c = 0.92$ g/ml, 100% PI)	258	7.02	104.5		[161]	• a_T for $J_p(t) > 10^{-8}\,\mathrm{cm}^2/\mathrm{dyne}$ including viscous flow.
($c = 0.849$ g/ml)	258	7.69	107.3		[161]	• a_T of the terminal dispersion. Its T-dependence becomes stronger with addition of Aroclor.
($c = 0.60$ g/ml)	258	10.7	124.6		[161]	• a_T of the terminal dispersion. Its T-dependence becomes stronger with addition of Aroclor.
($c = 0.449$ g/ml)	258	13.1	138.7		[161]	• a_T of the terminal dispersion. Its T-dependence becomes stronger with addition of Aroclor.
($c = 0.30$ g/ml)	258	24.2	197.2		[161]	• a_T of the terminal dispersion. Its T-dependence becomes stronger with addition of Aroclor.
($c = 0.20$ g/ml)	258	21.0	164.6		[161]	• a_T of the terminal dispersion. Its T-dependence becomes stronger with addition of Aroclor.
($c = 0.10$ g/ml)	258	10.3	59.4		[161]	• a_T of the terminal dispersion. Its T-dependence becomes stronger with addition of Aroclor.
PMPS in 1,1-bis(*p*-methoxyphenyl) cyclohexane 90% *(PMPS M = 130 000)*	242.5	12.47	23.23	242.5	[111, 112]	• $a_{T,\alpha}$ of local segmental motion from dynamical mechanical, $G^*(\omega)$, data obtained in the frequency range $10^{-2} < f < 10^2$ Hz. $\tau_\alpha(T_0) = 10^2$ s.
Polystyrene in Decalin 62%	291	8.86	101.6		[162, 163]	• $a_{T,S}$
Polystyrene/Tricresyl phosphate (PS/TCP)						
100% PS	373.2	14.24	66.0	371	[164]	• $a_{T,\eta}$ of the terminal dispersion which has a weaker T-dependence than that of the softening dispersion, $a_{T,S}$ to be given below.
100% PS	373.2	12.09	32.87	371	[164]	• $a_{T,S}$ of the softening dispersion which has a stronger temperature dependence than that of $a_{T,\eta}$.
85% PS	326.2	13.50	38.0		[164]	• $a_{T,S}$ of the softening dispersion.
70% PS	293.2	15.13	60.0		[164]	• $a_{T,\eta}$ of the terminal dispersion which still has a weaker T-dependence than that of the softening dispersion, $a_{T,S}$ to be given below. However, the difference decreases with increasing TCP.
70% PS	293.2	14.96	45.05		[164]	• $a_{T,S}$ of the softening dispersion.
55% PS	268.2	13.8	65.0		[164]	• $a_{T,\eta}$ of the terminal dispersion which has an almost the same though still slightly weaker T-dependence than that of the softening dispersion, $a_{T,S}$ to be given below.

TABLE 26.1. *Continued.*

Polymer	T_0 °K	C_1 °K	C_2 °K	T_g °K	Ref.	Comments
55% PS	268.2	14.75	60.0		[164]	• $a_{T,S}$ of the softening dispersion.
25% PS	212.2	24.46	69.0		[164]	• $a_{T,S}$ of the softening dispersion.
PS in DOP *(70%)*	277	14.43	56.0		[165]	• $a_{T,\alpha}$ of the local segmental motion of PS in the concentrated solution obtained by PCS. $\tau_\alpha(T_0) = 10^2$ s.
PCHMA/di(2-ethylhexyl phthalate (PCHMA/DOP)						
100% PCHMA	359.7	15.5	87.74		[166]	• $a_{T,\alpha}$ of the local segmental motion from PCS data.
95% PCHMA	356.7	15.5	87.74			• $a_{T,\alpha}$ of the local segmental motion from PCS data.
90% PCHMA	342.7	15.5	87.74			• $a_{T,\alpha}$ of the local segmental motion from PCS data.
85% PCHMA	329.7	15.5	87.74			• $a_{T,\alpha}$ of the local segmental motion from PCS data.
PMMA/DOP						
PMMA *plasticized by DOP,* $C_{PMMA} = 0.9\, g/mL$	316.6	15.9	47.6	313 (*T_g of bulk polymer is 351 K*)	[167]	• $a_{T,\alpha}$ of local segmental motion from photon correlation spectroscopy in the range: $10^{-5} < \tau_\alpha < 10^0$ s.
PMMA *plasticized by DOP,* $C_{PMMA} = 0.8\, g/mL$	295	16.9	98	313 (T_g of bulk polymer is 351 K)	[167]	• $a_{T,\alpha}$ of local segmental motion from photon correlation spectroscopy in the range: $10^{-5} < \tau_\alpha < 10^0$ s.
PMMA/toluene						
PMMA $M = 5.4 \times 10^5$, *isotactic rich* 67% PMMA	202.3	11.2	52.7	230	[168]	• $a_{T,\alpha}$ of local segmental motion from dielectric relaxation data from $256 < T < 345$ K and $10^0 < f < 10^{7.5}$ Hz.
30% PMMA	161.6	11.2	53.6	163	[168]	• $a_{T,\alpha}$ of local segmental motion from dielectric relaxation data from $178 < T < 294$ K and $10^0 < f < 10^{7.5}$ Hz.
30% PMMA in Diethyl phthalate	298	7.11	130.1	211	[169]	• $a_{T,S}$ from dynamic mechanical measurement.
Pn-BMA in diethyl phthalate						
(50%)	273	9.98	153.1	206	[170]	• $a_{T,S}$ from dynamic mechanical measurement.
(60%)	273	12.8	157.3	227	[170]	• $a_{T,S}$ from dynamic mechanical measurement.
PVAc in tricresyl phosphate *(50%)*	293	8.86	101.6		[163, 171]	• $a_{T,S}$ from dynamic mechanical measurement.
PVC/tetrahydrofuran (PVC/THF) 100% PVC	355.3	12.4	45.25	344	[172]	• $a_{T,\alpha}$ for the local segmental motion from dielectric relaxation in the frequency range $10^2 < f < 10^6$ Hz. $\tau_\alpha(T_0) = 1$ s.
84% PVC	282.1	11.0	36.1	275		• Same as above.
59% PVC	209.9	11.8	50.85	201		• Same as above.
51% PVC	200.9	10.8	37.87	193		• Same as above.
38% PVC	173.5	11.1	46.5	162		• Same as above.
PMA/toluene 100% PMA	292.4	13.8	48.55	286	[173]	• $a_{T,\alpha}$ for the local segmental motion from dielectric relaxation in the frequency range $10^2 < f < 10^6$ Hz. $\tau_\alpha(T_0) = 1$ s.
75% PMA	235.4	13.8	43.56	225		• Same as above.
60% PMA	209.5	15.9	57.0	201		• Same as above.

results. $\gamma = 1.9$ for poly(vinyl ethylene) with 88% vinyl and $M_w = 3$ kg/mol; $\gamma = 3.0$ for 1,4-polyisoprene with $M_w = 11$ kg/mol; $\gamma = 2.55$ for poly(vinyl methyl ether) with $M_w = 99$ kg/mol; $\gamma = 2.6$ for poly(vinyl acetate) with $M_w = 170$ kg/mol; $\gamma = 2.5$ for poly(propylene glycol) with $M_w = 4$ kg/mol; $\gamma = 5.6$ for poly(methyl phenyl siloxane) with $M_w = 23$ kg/mol; and $\gamma = 5.0$ for poly(methyl tolyl siloxane) with $M_w = 35$ kg/mol. For some low molecular weight glass-formers, the results are $\gamma = 3.3$ for poly[(*o*-cresyl glycidyl ether)-*co*-formaldehyde] with $M_w = 0.87$ kg/mol; $\gamma = 2.8$ for diglycidyl ether of bisphenol *A* with $M_w = 1.8$ kg/mol; and $\gamma = 8.5$ for poly(phenyl glycidyl ether)-*co*-formaldehyde with $M_w = 0.35$ kg/mol. The parameter γ is claimed to be a measure of the relative importance of *V* as opposed to *T*. If the local segmental dynamics were strictly thermally activated and volume does not enter, then γ would be exactly equal to zero. Although $\log(\tau_\alpha)$ is a monotonic increasing function of $T^{-1}V^{-\gamma}$, in general the dependence is not linear. Instead the slope increases with increasing $T^{-1}V^{-\gamma}$, a behavior like the VFTH or the WLF temperature dependence of the τ_α data taken at constant pressure. Thus, a VFTH equation based the variable TV^γ instead of the usual *T* can be constructed to describe the data.

Recently the analysis was extended to the polymer chain dynamics (i.e., the dielectric normal mode) for polymers that have dipole moment parallel as well as normal to the backbone. They are polypropylene glycol (PPG), 1,4-polyisoprene (PI) [186] , and polyoxybutylene (POB) [187]. The normal mode relaxation times (strictly speaking, the longest normal mode relaxation times, τ_n) taken at various combinations of temperature and pressure superpose to a single master curve when plotted against $T^{-1}V^{-\gamma}$, using the same value of γ as for the segmental relaxation times, τ_α. It is paradoxical that τ_n and τ_α are functions of the *same* quantity, $T^{-1}V^{-\gamma}$, yet they have *different* $T^{-1}V^{-\gamma}$-dependences.The dependence of τ_α on $T^{-1}V^{-\gamma}$ is stronger than that of τ_n, similar to the relation between their temperature dependences at ambient pressure [19,25,30,46,115,188–191] or their pressure dependences at constant temperature [192]. The explanation of τ_n and τ_α are functions of the same $T^{-1}V^{-\gamma}$ and yet the dependence of τ_α is stronger than τ_n was given [193] by an application of the Coupling Model [194–197] in the same manner as the explanation given previously for their different *T*-dependences at constant *P* or *P*-dependences at constant *T* [30,46,115,189–191]. These scaling analyses do not constitute a test of the free volume theory stemming from the Doolittle and WLF equations, since these depend on the relative or fractional free volume and not the total volume.

26.5 SOME IMPORTANT SECONDARY RELAXATIONS

Secondary relaxations are commonly found in glass-formers including polymers. Some secondary relaxations involve intramolecular degrees of freedom and have no relation to the α-relaxation such as the motion of a side group of a polymer isolated from the chain backbone. However some secondary β-relaxations are more intriguing. For example, the secondary relaxation found in totally rigid molecules such as chlorobenzene [198–200], and in polymers which have no side groups such as 1,4 polybutadiene [201] and polyisoprene [202] (excluding the very fast rotation of the methyl group). Even in polymers that have side groups such as poly(*n*-ethyl methacrylate) (PEMA), multidimensional ^{13}C solid-state NMR study of the carboxyl moiety [203] found that the β-relaxation involves a π-flip of the side group coupled to a rocking motion around the local chain axis with a ±20° amplitude in the glassy state. The rocking amplitude increases upon raising the temperature above T_g and is as large as ±50° at $T_g + 27$ K. The temperature dependence of the secondary relaxation time, τ_β, of PEMA above T_g is stronger than the Arrhenius dependence extrapolated from the glassy state. In fact, the temperature dependence of τ_β above T_g could be regarded as having another VFTH dependence albeit weaker than that of the α-relaxation. In the research community of nonpolymeric glass-formers, the secondary relaxations which have properties mimicking the α-relaxations are sometimes called the Johari–Goldstein relaxations for the purpose of distinguishing them from secondary relaxations of lesser importance [204]. The properties of these secondary relaxations that bear similarity to that of the α-relaxation include the VFTH temperature dependence and pressure dependence of τ_β in the equilibrium liquid state [203,204]. These secondary relaxations are potentially the originator of the α-relaxation, which is certainly the case of the primitive relaxation of the Coupling Model [194–197]. A remarkable finding is that the primitive relaxation time τ_0 calculated entirely from the parameters of the α-relaxation turns out to be approximately the same as the most probable relaxation time, τ_β, of these secondary relaxation in many polymeric glass-formers, including polybutadiene, polyisoprene, polyvinylacetate, PEMA, and others, as well as many nonpolymeric glass-formers [201,202,205–211]. There is also microscopic experimental evidence for a close connection between the secondary relaxation or the primitive relaxation processes to the α-relaxation. Multidimensional NMR [212,213] experiments have shown that the dynamically heterogeneous molecular reorientations of the α-relaxation (i.e., the primitive relaxation in the coupling model) occurs by relatively small jump angles having an exponential time dependence. Furthermore, from one and two-dimensional 2H NMR studies [214], the secondary relaxations in toluene and polybutadiene are seen to also involve angular jumps of similar magnitude for temperatures above T_g. This similarity in size of the jump angles supports the relation between the secondary and the primitive relaxations, and their role as the origin of the α-relaxation.

Related information can be found in Chapters 23 and 24.

REFERENCES

1. D. J. Ferry, *Viscoelastic Properties of Polymers, 3rd ed.* (John Wiley & Sons, New York, 1980), pp. 277–279.
2. G. C. Berry and T. G. Fox, Adv. Polymer Sci. **5**, 261 (1968).
3. N. G. McCrum, B. E. Read, and G. Williams, *Anelastic and Dielectric Effects in Polymeric Solids* (John Wiley & Sons, London, 1967).
4. R. Nozaki and S. Mashimo, J. Chem. Phys. **84**, 3575 (1986).
5. A. Hoffmann, K. Kremer, E. W. Fischer, *et al.* in *Disorder Effects on Relaxational Processes*, edited by R. Richert and A. Blumen (Springer-Verlag, Berlin and Heidelberg, 1994), p. 309.
6. H. W. Spiess, J. Non-Cryst. Solids **131–133**, 766 (1991).
7. a. D. Schaefer, H. W. Spiess, U. W. Suter, *et al.* Macromolecules **23**, 3431 (1990); U. Pschorn, E. Rössler, H. Sillescu, *et al.* Macromolecules **24**, 398 (1991); (b) K. Zemke, K. Schmidt-Rohr, and H. W. Speiss, Acta Polymer **45**, 148 (1994).
8. S. Kaufmann, S. Wefing, D. Schaeffer, *et al.* J. Chem. Phys. **93**, 197 (1990).
9. G. D. Patterson, in *Dynamic Light Scattering*, edited by R. Pecora, Academic, New York (1986), p. 260.
10. G. Fytas and G. Meier in *Dynamic Light Scattering, the Method and Some Applications*, edited by W. Brown (Clarendon Press, Oxford, 1993), p. 427.
11. M. L. Williams, J. Phys. Chem. **59**, 95 (1955).
12. M. L. Williams, R. F. Landel, and D. J. Ferry, J. Am. Chem. Soc. **77**, 3701 (1955).
13. D. J. Plazek and A. J. Chelko, Jr., Polymer **18**, 15 (1977).
14. H. Vogel, Phys. Z. **22**, 645 (1921).
15. G. S. Fulcher, J. Am. Chem. Soc. **8**, 339, 789 (1925).
16. G. Tamman and W. H. Hesse, Z. Anorg. Allg. Chem. **156**, 245 (1926).
17. A. K. Doolittle, J. Appl. Phys. **22**, 1471 (1951); **23**, 236 (1952).
18. F. Schwarzl and A. J. Staverman, J. Appl. Phys. **23**, 838 (1952).
19. K. L. Ngai and D. J. Plazek, in Rubber Chem. Tech., Rubber Review, **68**, 376 (1995).
20. D. J. Plazek, I.-C. Chay, K. L. Ngai and C. M. Roland, Macromolecules **28**, 6423 (1995).
21. A. K. Rizos, T. Jian, and K. L. Ngai, Macromolecules **28**, 517 (1995).
22. D. J. Plazek, J. Polym. Sci.: Part A-2 **6**, 621 (1968).
23. J. Y. Cavaille, C. Jordan, J. Perez, *et al.* J. Polym. Sci.: Part B: Polymer Phys. **25**, 1235 (1987).
24. D. J. Plazek, M. J. Rosner and D. L. Plazek, J. Polym. Sci.: Part B: Polymer Phys. **26**, 473 (1988).
25. D. J. Plazek and M. V. O'Rourke, J. Polym. Sci. A-2 **9**, 209 (1971).
26. D. J. Plazek, J. Phys. Chem. **69**, 3480 (1965).
27. D. J. Plazek, Polym. J. **12**, 43 (1980).
28. D. J. Plazek, J. Polym. Sci.: Polymer Physics Edition **20**, 729 (1982).
29. D. J. Plazek and D. L. Plazek, Macromolecules **16**, 1469 (1983).
30. D. J. Plazek, C. Bero, S. Neumeister, *et al.* J. Colloid Polymer Sci. **272**, 1430 (1994).
31. D. J. Plazek, J. Non-Cryst. Solids **131–133**, 836 (1991).
32. K. L. Ngai in *Disorder Effects on Relaxational Processes*, edited by R. Richert and A. Blumen (Springer-Verlag, Berlin and Heidelberg, 1994), p. 89.
33. G. Wiliams, Tran. Faraday Soc. **59**, 1397 (1963)
34. S. F. Kurath, E. Passaglia, and R. Pariser, J. Appl. Phys. **28**, 499 (1957).
35. R. S. Marvin and H. Oser, J. Res. Nat. Bur. Stand. **B66**, 171 (1962).
36. R. S. Marvin, *Proceedings of the Second International Congress on Rheology*, edited by V. G. W. Harrison (Butlerworths, London, 1954), p. 156.
37. R. S. Marvin and H. Oser, J. Res. Nat. Bur. Stand. **B66**, 171 (1962)
38. E. R. Fitzgerald, L. D. Grandine, and J. D. Ferry, J. Appl. Phys. **24**, 65 (1953).
39. J. D. Ferry, L. D. Grandine, Jr., and E. R. Fitzgerald, J. Appl. Phys. **24**, 911 (1953).
40. E. Catsiff and A. V. Tobolsky, J. Colloid Sci. **10**, 375 (1955).
41. A. V. Tobolsky and E. Catsiff, J. Polym. Sci. **19**, 111 (1955).
42. A. V. Tobolsky, *Properties and Structure of Polymers* (John Wiley and Sons, New York, 1960), pp. 157–159.
43. K. L. Ngai, D. J. Plazek, and A. K. Rizos (1995), submitted to Macromolecules.
44. H. Okamoto, T. Inoue, K. Osaki, J. Polym. Sci. Phys. Ed. **33**, 417 (1995).
45. D. J. Plazek, X. D. Zheng, and K. L. Ngai, Macromolecules **25**, 4920 (1992).
46. K. L. Ngai, D. J. Plazek, and C. Bero, Macromolecules **26**, 1065 (1993).
47. G. C. Berry and T. G. Fox, Fortschr. Hochpolym. Forsch. (Adv. Polymer Sci.), **5**, 261 (1968).
48. L. J. Fetters, W. W. Graessley, and A. D. Kiss, Macromolecules **24**, 3136 (1991).
49. J. D. Ferry and G. S. Parks, Physics **6**, 356 (1935).
50. G. Fytas and K. L. Ngai, Macromolecules **21**, 804 (1988).
51. P. Santangelo and C. M. Roland, unpublished.
52. D. S. Pearson, L. J. Fetters, L. B. Younghouse, *et al.* Macromolecules **21**, 478 (1988).
53. T. Inoue, H. Hayashihara, H. Okamoto, and K. Osaki, J. Polym. Sci. Part B: Polym. Phys. **30**, 409 (1992).
54. D. J. Ferry, *Viscoelastic Properties of Polymers*, 3rd ed. (John Wiley & Sons, New York), p. 277.
55. D. J. Plazek, J. Phys. Chem. **69**, 3480 (1965)
56. F. R. Schwarzl and F. Zahradnik, Rheol. Acta **19**, 137 (1980).
57. A. J. Barlow, A. Erginsay, and J. Lamb, Proc. R. Soc. **A298**, 481 (1967).
58. N. Nemoto, Polym. J. **1**, 485 (1970).
59. S. Onogi, T. Masuda, and K. Kitagawa, Macromolecules **3**, 110 (1970).
60. H. Endo, T. Fujimoto, and M. Nagasawa, J. Polym. Sci. **7**, 1669 (1960).
61. H. Odani, N. Nemoto, S. Kitimura, M. Kuratas, and M. Tamura, Polym. J. **1**, 356 (1970).
62. K, Yoshimori and R. Work, J. Chem. Phys. **72**, 5909 (1980).
63. B. L. Funt and T. H. Sutherland, Can. J. Chem. **30**, 940 (1952).
64. P. F. Veselovskii, Ber. Tomsk. Polytech. Inst., USSR **91**, 399 (1956).
65. S. P. Kabin, Vysokomol. Soed. **2**, 1324 (1960).
66. G. P. Mikhailov, Usp. Khim. **24**, 875 (1955).
67. J. D. Ferry and R. F. Landel, Kolloid-Z. **148**, 1 (1956).
68. M. L. Williams and J. D. Ferry, J. Colloid Sci. **9**, 479 (1954).
69. G. Fytas, C. H. Wang, G. Meier, and E. W. Fischer, Macromolecules **18**, 1492 (1985); C. H. Wang, G. Fytas, and E. W. Fischer, J. Chem. Phys. **82**, 4332 (1985).
70. B. L. Funt, Can. J. Chem. **30**, 84 (1952).
71. Y. Takahashi, J. Appl. Polym. Sci. **5**, 468 (1961); J. Phys. Soc. Japan **16**, 1024 (1961).
72. J. D. Ferry, M. L. Williams, and E. R. Fitzgerald, J. Phys. Chem. **59**, 403 (1955).
73. W. Sommer, Koll.-Z. **167**, 97 (1959)
74. J. Colmenero, A. Arbe, and A. Alegria, J. Non-Cryst. Solids **172–174**, 126 (1994).
75. T. H. Sutherland and B. L. Funt, J. Polym. Sci. **11**, 177 (1953).
76. A. Alegria, E. Macho, and J. Colmenero, Macromolecules **24**, 5196 (1991); J. Non-Cryst. Solids **131–133**, 860 (1991).
77. C. M. Roland and K. L. Ngai, Macromolecules **25**, 363 (1992).
78. A. Zetsche, F. Kremer, W. Jung *et al.* Polymer **31**, 1883 (1990)
79. M. L. Williams and J. D. Ferry, J. Colloid Sci. **10**, 474 (1955).
80. J. D. Ferry and R. F. Landel, Kolloid-Z. **148**, 1 (1956).
81. K. Fujino, K. Senshu, and H. Kawai, J. Colloid Sci. **16**, 262 (1961).
82. D. J. Plazek, V. Tan, and V. M. O'Rourke, Rheol. Acta **13**, 367 (1974).
83. D. J. Plazek and N. Raghupathi, Polymer Preprints **15**, 53 (1974).
84. D. J. Plazek, in *Relaxations in Complex Systems*, edited by K. L. Ngai and G. B. Wright, Government Printing House, Naval Research Laboratory, Washington, D. C. (1984).
85. T. Masuda, N. Toda, Y. Aoto and S. Onogi, Polym. J. **3**, 315 (1972).
86. J. D. Ferry, W. C. Child, and R. Zand, J. Colloid Sci. **12**, 53 (1957).
87. W. C. Child and J. D. Ferry, J. Colloid Sci. **12**, 327 (1957)
88. G. P. Mikhailov, T. I. Borisova, and A. S. Nigmankhodzhayev, Vysokomol. Soyed. **8**, 969 (1966).
89. G. Meier, G. Fytas, and T. Dorfmüller, Macromolecules **17**, 957 (1984).
90. W. C. Child and J. D. Ferry, J. Colloid Sci. **12**, 389 (1957)
91. G. Meier, F. Kremer, G. Fytas, and A. K. Rizos, J. Polym. Sci., Polym. Phys. Ed. (in press); L. Giebel, G. Meier, G. Fytas, and E. W. Fischer, J. Polym. Sci., Polym. Phys. Ed. **30**, 129 (1992).
92. W. Dannhauser, W. C. Child, and J. D. Ferry, J. Colloid Sci. **13**, 103 (1958).

93. J. W. Berge, P. R. Saunders, and J. D. Ferry, J. Colloid Sci. **14**, 135 (1959).
94. D. M. Stern, J. W. Berge, S. F. Kurath, C. Sakoonkim, and J. D. Ferry, J. Colloid Sci. **17**, 409 (1962)
95. T. E. Newlin, S. E. Lovell, P. R. Saunders, and J. D. Ferry, J. Colloid Sci. **17**, 10 (1962).
96. T. P. Yin and J. D. Ferry, J. Colloid Sci. **16**, 166 (1961).
97. S. F. Kurath, T. P. Yin, J. W. Berge, and J. D. Ferry, J. Colloid Sci. **14**, 147 (1959)
98. G. Floudas, P. Placke, P. Štěpánek, W. Brown, G. Fytas, and K. L. Ngai, Macromolecules **28**, 6799 (1995).
99. G. Fytas, Macromolecules **22**, 211 (1989).
100. W. J. Sichina, American Laboratories, **1**, 42 (1988).
101. D. K. Yoshimura and W. D. Richards, 89CRD211, General Electric Polymer Materials Laboratory Technical Information Series (1989).
102. R. H. Colby, M. G. Hansen, and A. R. Schultz, General Electric Company Corporate REsearch and Development Memo Report MOR-81-069 (1981).
103. J. P. Mercier and G. Groenincks, Rheol. Acta. **8**, 516 (1969).
104. A. J. Barlow, G. Harrison, and J. Lamb, Proc. Royal Soc. **282**, 228 (1964).
105. D. J. Plazek (unpublished).
106. K. U. Kirst, F. Kremer, T. Pakula, and J. Hollingshurst, Colloid Polym. Sci. **272**, 1420 (1994).
107. F. Wang, J. Roovers, and P. Toporowski, Macromolecules **26**, 3826 (1993).
108. J. C. Coburn and R. H. Boyd, Macromolecules **19**, 2238 (1986).
109. G. Fytas, T. Dorfmuller, and B. Chu, J. Polym. Sci., Polym. Phys. Ed. **22**, 1471 (1984).
110. K. L. Ngai and G. Fytas, J. Polym. Sci.: Part B: Polymer Physics **24**, 1683 (1986).
111. C. M. Roland, P. G. Santangelo, K. L. Ngai, and G. Meier, Macromolecules **26**, 6164 (1993).
112. P. G. Santangelo, C. M. Roland, K. L. Ngai, A. K. Rizos, and H. Katerinopoulos, J. Non-Cryst. Solids **172–174**, 1084 (1994).
113. D. Boesse, B. Momper, G. Meier, F. Kramer, and E. W. Fischer, Macromolecules **22**, 4416 (1989).
114. G. Williams, Trans. Faraday Soc. **61**, 1564 (1965).
115. K. L. Ngai, A. Schönhals, and E. Schlosser, Macromolecules **25**, 4915 (1992).
116. J. Cochrane, G. Harrison, J. Lamb, *et al*. Polymer **21**, 837
117. C. H. Wang, G. Fytas, and T. Dorfmüller, Macromolecules **16**, 68 (1983).
118. E. J. Hwang, T. Inoue, and K. Osaki, Polym. Eng. Sci. **34**, 135 (1994)
119. K. L. Ngai, C. M. Roland, J. M. O'Reilley, and J. S. Sedita, Macromolecules **25**, 3906 (1992)
120. J. D. Ferry, L. D. Grandine, Jr., and E. R. Fitzgerald, J. Appl. Phys. **24**, 911 (1953).
121. J. F. Sanders and J. D. Ferry, Macromolecules **7**, 681 (1974).
122. J. R. Richards, R. G. Mancke, and J. D. Ferry, Polym. Lett. **2**, 197 (1964).
123. S. F. Kurath, E. Passaglia, and R. Pariser, J. Appl. Polym. Sci. **1**, 150 (1959).
124. A. R. Payne, in *Rheology of Elastomers*, edited by P. Mason and N. Wookey (Pergamon, London, 1958), p. 86.
125. R. A. Dickie and J. D. Ferry, J. Phys. Chem. **70**, 2594 (1966).
126. C. M. Roland and K. L. Ngai, Macromolecules **24**, 5315 (1992); C. M. Roland, Macromolecules **25**, 7031 (1992); C. M. Roland and K. L. Ngai, Macromolecules **26**, 2688 (1993).
127. A. Allegria, J. Colmenero, K. L. Ngai, and C. M. Roland, Macromolecules **27**, 4486 (1994).
128. D. Boesse, F. Kremers, and L. J. Fetters, Macromolecules **23**, 1826 (1990); J. Non-Cryst. Solids **131–133**, 728 (1991); D. Boesse and F. Kremer, Macromolecules **23**, 829 (1990).
129. J. Kanetakis, G. Fytas, F. Kremer, *et al*. Macromolecules **25**, 3484 (1992).
130. A. K. Rizos (unpublished data).
131. G.-C. Chung, J. A. Kornfield, and S. D. Smith, Macromolecules **27**, 964 (1994).
132. N. Nemoto, M. Moriwaki, H. Odani, and S. Onogi, Macromolecules **4**, 215 (1971).
133. W. Gotro and W. W. Graessley, Macromolecules **17**, 2767 (1984).
134. J. Roovers and P. M. Toporowski, Macromolecules **25**, 3454 (1992).
135. J. Colmenero, A. Alegria, P. G. Santangelo, K. L. Ngai, and C. M. Roland, Macromolecules **27**, 407 (1994).
136. C. Bero and D. J. Plazek, 1994 (unpublished).
137. C. M. Roland, Macromolecules, **27**, 4242 (1994).
138. B. H. Arendt, R. M. Kannan, M. Zewail, and J. Kornfield, Rheol. Acta. **33**, 322 (1994)
139. J. F. Sanders, R. H. Valentine, and J. D. Ferry, J. Polym. Sci. A2 **6**, 967 (1968).
140. R. Zorn, G. B. McKenna, L. Wilner, and D. Richter, Macromolecules **28** (in press) (1995).
141. J. F. Sanders, Ph.D. thesis, University of Wisconsin, 1968.
142. E. Maekawa, R. G. Mancke, and J. D. Ferry, J. Phys. Chem. **69**, 2811 (1965).
143. C. R. Taylor, as referenced by J. D. Ferry (Reference 1, page 320).
144. J. M. Carella, W. W. Graessly, and L. Fetters, Macromolecules **17**, 177 (1984).
145. G. Kraus and J. T. Gruver, J. Appl. Polym. Sci. **9**, 739 (1965).
146. R. H. Colby and W. W. Graessley, Macromolecules **20**, 2226 (1987).
147. M. Baumgaertel, M. E. De Rosa, J. Machado, and H. Winter, Rheol. Acta **31**, 75 (1992).
148. J. Roovers, Macromolecules **21**, 1517 (1988).
149. J. F. Gerard, J. Galy, J. P. Pascault, *et al*. Polym. Eng. Sci. **31**, 615 (1991).
150. D. S. Pearson, L. J. Fetters, L. B. Younghouse, *et al*. Macromolecules **21**, 478 (1988).
151. R. F. Landel, J. Colloid Sci. **12**, 308 (1957)
152. A. K. Rizos, G. Fytas, R. J. Ma, *et al*. Macromolecules **26**, 1869 (1993).
153. R. G. Mancke and J. D. Ferry, Trans. Soc. Rheol. **12**, 335 (1968).
154. D. J. Plazek, G.-F. Gu, R. G. Stacer, *et al*. J. Mat. Sci. **23**, 1289 (1988).
155. D. J. Plazek, I.-C. Choy, F. N. Kelley, *et al*. Rubber. Chem. Tech. **56**, 866 (1983).
156. D. J. Plazek and I.-C. Choy, J. Polym. Sci.: Part B: Polym. Phys. **27**, 307 (1989).
157. A. S. Nigmankhodjaev, L.-K. Bi, C.-P. Wong, J. L. Schrag, and J. D. Ferry, J. Polym. Sci. A-2 **8**, 1927 (1970).
158. R. F. Landel and J. D. Ferry, J. Phys. Chem. **60**, 294 (1956).
159. D. J. Plazek, J. Colloid Sci. **15**, 50 (1960).
160. M. N. Vrancken and J. D. Ferry, J. Polym. Sci. **24**, 27 (1957).
161. N. Nemoto, T. Ogawa, H. Odani, and S. Onogi, Macromolecules **5**, 641 (1972).
162. L. D. Grandine and J. D. Ferry, J. Appl. Phys. **24**, 679 (1953).
163. J. D. Ferry and R. F. Landel, Kolloid-Z. **148**, 1 (1956).
164. D. J. Plazek, E. Riande, H. Markovitz, *et al*. J. Plym. Sci.: Polym. Phys. Edition **17**, 2189 (1979).
165. A. K. Rizos, R. M. Johnsen, W. Brown, and K. L. Ngai, Macromolecules **28**, 5450 (1995).
166. G. Floudas, G. Fytas, and K. L. Ngai, Macromolecules **24**, 1955 (1991).
167. G. Floudas, A. Rizos, W. Brown, and K. L. Ngai, Macromolecules **27**, 2719 (1994).
168. K. Adachi and T. Kotaka, Polymer J. **13**, 687 (1981).
169. D. M. Stern, J. W. Berges, S. F. Kurath, and J. D. Ferry, J. Colloid Sci. **17**, 409 (1962).
170. P. R. Saunders, D. M. Stern, S. F. Kurath, and J. D. Ferry, J. Colloid Sci. **14**, 222 (1959).
171. M. L. Williams and J. D. Ferry, J. Colloid Sci. **10**, 1 (1955)
172. K. Adachi and Y. Ishida, J. Polym. Sci.: Polymer Physics edition **14**, 2219 (1975).
173. K. Adachi and Y. Ishida, Polym. J. **3**, 233 (1972).
174. J. E. McKinney and H. V. Belcher, Res. Natl. Bur. Stand., Section A **67A**, 43 (1963).
175. J. R. McLoughlin and A. V. Tobolshy, J. Colloid Sci. **7**, 555 (1952).
176. H. Leaderman, R. G. Smith, and R. W. Jones, J. Polym. Sci. **14**, 47 (1954).
177. B. Momper, Doctoral Dissertation, Chemistry Department, Johannes Gutenberg Universität Mainz, Germany (1989).
178. L. David, A. Sekkat, and S. Etienne, J. Non-Cryst. Solids **172–174**, 214 (1994).
179. T. Kanaya, A. Patkowski, E. W. Fischer, J. Seils, H. Gläser, and K. Kaji, Macromolecules (1995), in press.
180. G. Floudas, J. S. Higgins, F. Kremer, and E. W. Fischer, Macromolecules **25**, 4955 (1992).

181. R. Casalini and C.M. Roland, Colloid Polym. Sci. **283**, 107 (2004).
182. R. Casalini and C.M. Roland, Phys. Rev. E **69**, 062501 (2004).
183. C. Alba-Simionesco, A. Cailliaux, A. Alegria A, and G. Tarjus Europhys. Lett. **68**, 58 (2004).
184. C. Dreyfuss, A. Aouadi, J. Gapinski, M. Matos-Lopes, W. Steffen, A. Patkowski, and R.M. Pick, Phys. Rev. E **68**, 011204 (2003).
185. C. Dreyfus, A. Le Grand, J. Gapinski, W. Steffen, and A. Patkowski, Europhys. J. B **42**, 309 (2004).
186. C.M. Roland, R. Casalini, M. Paluch, J. Polym. Sci. Polym. Phys. Ed. **42**, 4313 (2004).
187. R. Casalini and C.M. Roland, Macromolecules, **38**, 1779 (2005).
188. A. Schönhals, Macromolecules **26,** 1309 (1993).
189. C.M. Roland, K.L. Ngai, P.G. Santangelo, X.H. Qiu, M.D. Ediger, and D.J. Plazek, Macromolecules, **34**, 6159 (2001).
190. C.M. Roland, K.L. Ngai, and D.J. Plazek, Macromolecules, **37**, 7051 (2004).
191. K.L. Ngai, Chapter 2 in *Physical Properties of Polymers*; 3rd edition, (Cambridge University Press, Cambridge, England, 2004).
192. G. Floudas and T. Reisinger, J. Chem. Phys. **111**, 5201 (1999).
193. K.L. Ngai, R. Casalini, and C.M. Roland, Macromoelcules, **38**, 4363 (2005).
194. K.L. Ngai, D.J. Plazek and R.W. Rendell. Rheol. Acta, **36**, 307 (1997).
195. K.L. Ngai and K. Y. Tsang, Phys. Rev. E **60,** 4511 (1999).
196. K.L. Ngai and R.W. Rendell, in *Supercooled Liquids, Advances and Novel Applications*, edited by J.T. Fourkas, D. Kivelson, U. Mohanty, K. Nelson, ACS Symposium Series Vol. 676; American Chemical Society: Washington, DC (1997); Chapter 4, p 45.
197. K. L. Ngai, IEEE Trans. Dielectr. Electr. Insul. **8,** 329 (2001).
198. G. P. Johari and M. Goldstein, J. Chem. Phys. **53**, 2372 (1970).
199. G. P. Johari, J. Chem. Phys. **58**, 1766 (1973).
200. G. P. Johari, Ann. N.Y. Acad. Sci. **279,** 117 (1976).
201. K. L. Ngai, J. Phys.: Condens. Matter **15,** S1107 (2003).
202. C.M., Roland, M.J. Schroeder, J.J. Fontanella, and K.L. Ngai, Macromolecules, **37**, 2630 (2004).
203. A. S. Kulik, H. W. Beckham, K. Schmidt-Rohr, D. Radloff, U. Pawelzik, C. Boeffel, and H. W. Spiess, Macromolecules **27**, 4746 (1994).
204. K. L. Ngai and M. Paluch, J. Chem. Phys. **120,** 857 (2004).
205. K. L. Ngai and C.M. Roland, Polymer **43,** 567 (2002).
206. K. L. Ngai, J. Chem. Phys. **109,** 6982 (1998).
207. K.L. Ngai, Macromolecules, **32,** 7140 (1999).
208. D. Prevosto, S. Capaccioli, M. Lucchesi, P. A. Rolla, and K. L. Ngai, J. Chem. Phys. **120**, 4808 (2004).
209. K.L. Ngai and M. Beiner, Macromolecules, **37**, 8123 (2004).
210. K.L. Ngai, in AIP Conference Procedings Vol. 708, p. 515 (2004), Amer. Inst. Phys, Melville, NY.
211. K.L. Ngai and S. Capaccioli, Phys. Rev. E **69,** 031501 (2004).
212. R. Böhmer, G. Diezemann, G. Hinze, and E. Rössler, Prog. Nucl. Magn. Res. Spectrosc. **39**, 191 (2001).
213. H. Sillescu, R. Böhmer, G. Diezemann, and G. Hinze, J. Non-Cryst. Solids **307–310**, 16 (2002).
214. M. Vogel, C. Tschirwitz, G. Schneider, C. Koplin, and P. Medick, J. Non-Cryst. Solids **307–310**, 326 (2002).

CHAPTER 27

Adhesives

Alphonsus V. Pocius

3M Corporate Research Materials Laboratory, St. Paul, MN 55144–1000

The term "adhesive" applies to a wide range of materials that are used to join other materials together by means of surface attachment. Thus, an "adhesive" joins "adherends" together to generate an "adhesive joint" or an "adhesively bonded assembly." Adhesive technology is a joining technology in much the same sense that rivets, screws, nuts and bolts, welding and brazing are joining technologies. Most materials that we recognize as adhesives are based upon organic materials that are either polymers or react to form polymers. There are also inorganic adhesives, such as Portland cement and solder, which will not be discussed in this chapter.

27.1 ADHESION AND POLYMERS

Adhesives are joining systems based upon surface attachment, i.e., adhesion. Adhesion is the physical attraction of the surface of one material for the surface of another. These physical attractions are the same physical attractions that one normally associates with descriptions of the states of matter, i.e., van der Waals forces and electrostatic forces. In general, van der Waals forces play a significant role in the adhesion processes of polymeric materials. In addition, adhesives can be synthesized such that they can chemically interact with a surface through the formation of donor–acceptor bonds, hydrogen bonds, and covalent bonds.

The science of polymeric adhesion is concerned with the description of two distinct steps: the formation of the adhesive bond ("adhesive bond making") and the physical strength of the adhesive bond ("adhesive bond breaking"). The bulk of this chapter is associated with the latter topic, that is, the strength of joints made with adhesives. For this first section, we deal primarily with the former topic.

Polymeric materials are "van der Waals solids." That is, the forces of attraction between chains can be described, for most polymeric materials, by van der Waals attractions. Thus, the cohesive energy density of a polymer and, hence, the surface energy of a polymer, is low relative to most inorganic materials where other intermolecular forces may dominate. The room temperature surface energy of polymers varies from about $12\,\mathrm{mJ/m^2}$ to about $70\,\mathrm{mJ/m^2}$. By comparison, the surface energy of aluminum oxide is $638\,\mathrm{mJ/m^2}$.

In order to obtain maximum adhesion, one needs to have intimate contact between the adhesive and the adherend. The attainment of intimate contact is termed "complete wetting." In the 1950s, Zisman and coworkers codified this concept using contact angle measurements and the definition of a parameter related to the surface energy of a polymer, the "critical wetting tension [1]." Table 27.1 provides a list of critical wetting tensions of a number of polymers. The Zisman wetting criterion states that the surface energy of an adhesive must be less than the critical wetting tension of the adherend in order for the adhesive to exhibit complete wetting of an adherend. For the most part, polymeric materials are lower in surface energy than most clean inorganic surfaces and would be expected to wet most of them completely. The situation becomes more complicated when discussing adhesion between polymers. In that case, whether or not the polymer is the adhesive or the adherend becomes very important.

In the case of polymer-polymer adhesion, one can have another basis for providing a strong joint between two materials. This is the phenomenon of interdiffusion. In general, it is difficult for two high polymeric materials to interdiffuse because of poor entropy gain. Entropic effects are overcome in the case when the two polymers interact

TABLE 27.1. *Critical wetting tension of some common polymeric materials [1].*

Polymer	Critical wetting tension (mJ/m^2)
Poly(tetrafluoroethylene)	18
Poly(dimethylsiloxane)	21
Poly(propylene)	28
Poly(ethylene)	31
Poly(vinyl chloride)	38
Cured epoxy resin	43
Poly(ethylene terephthalate)	45

exothermically or in the case when the two polymers have very similar or identical solubility parameters. One can also describe this situation in terms of the χ-parameter.

The work of adhesion is defined by the following equation:

$$W_A = \gamma_1 + \gamma_2 - \gamma_{12} \tag{1}$$

where W_A is the thermodynamic work of adhesion, the γ_1 are the surface energies of materials 1 and 2 γ_{12} and is the interfacial energy between them. Realizing that interfacial energies are usually less than surface energies, one can easily see that the work of adhesion is a relatively small number, usually on the order of a few hundreds of mJ/m^2. In the case of applying a polymer to an inorganic surface or in the case of an incompatible polymeric adherend, one can obtain higher adhesion by means of chemical interactions at surfaces. These chemical interactions include acid-base interactions (which include donor-accepter, Bronsted-Lowrey acid-base, and hydrogen-bonding interactions) and covalent bonding. Providing covalent bonding at an interface can lead to levels of interfacial interaction that are in the tens of J/m^2.

The energy necessary to break a polymer-based adhesive joint is almost always much higher than the energy of interaction at an interface. A natural rubber-based pressure sensitive adhesive (*vide infra*) has only van der Waals interactions available to it for adhering to a surface. Despite that, the energy to break an adhesive joint made with such an adhesive at room temperature and a rate of about 2.54 cm/min is on the order of 100 J/m^2. The discrepancy between interfacial energetics and the energy necessary to break a joint is due to dissipative processes in the materials making up the joint.

The ability to dissipate mechanical energy is the key to the ability of polymers to perform as adhesives. One can imagine the following scenario. A polymer is tethered to a surface by one or more attachments each having an energy of interaction with the surface on the order of a van der Waals energy. That same polymer is also entangled with and associated with segments of itself or other polymers in the adhesive. As long as the energy of interaction of the polymer with the surface is higher than the energy of interaction between polymer segments, the polymer will tend to disentangle and dissipate mechanical energy as heat, rather than separate from the surface. If the energy of interaction between the polymer and the surface is less than the energy necessary to disentangle, the polymer will likely separate from the surface. Also, if the polymer has no mobility (such as in the case of a glassy material) the energy of interaction with the surface must be significant. Examples of efforts to model adhesives by molecular dynamics can be found in the work of Baljon [2] and Robbins [3].

If the energy of interaction with the surface cannot be made to exceed the segment–segment interaction energy then other means can be used to improve the interaction with the surface. In general, this means that the adherend surface has to be made mechanically rough by some type of surface preparation. If the adhesive has the correct viscosity, it will wet into the nooks and crannies of such a surface. When the adhesive hardens, it will be mechanically interlocked with the adherend. Now the energy required to remove the adhesive becomes equal to the plastic deformation energy of either the adherend or the adhesive. In this way, even stiff polymers such as thermoset epoxy adhesives can be used as adhesives, providing an energy to fail a joint in excess of 1,000 J/m^2.

27.2 PHYSICAL PROPERTY TESTING

Adhesive test methods and their test results are related to but are not the same as other polymer property tests described in this handbook. In general, adhesive property tests are ultimate properties measured at the failure load of an adhesive joint. Adhesive joint properties are certainly related to adhesion (vide supra) but are primarily due to the physical properties of the adhesive and the physical properties of the adherends. In addition, the design of the adhesive joint has a major effect on the measured strength. Indeed, a properly designed adhesive joint will always lead to failure of the adherend. In addition, adhesive joint properties are as temperature- and rate-dependent as the properties of the polymers used to make the adhesive. Unfortunately, in many cases in the literature, the rate of test is not described. In this chapter, the type of adherend or backing will be described, if at all possible.

A primary method used to characterize adhesives is the lap shear test. A diagram of the test is shown in Fig. 27.1 and is described in Standard Test Method ASTM D1002 [4]. The specimen is usually 1 in. (2.54 cm) wide. The lap shear test places the adhesive in normal as well as shear stress [5]. This type of test is used for many types of adhesives, with the exception of pressure-sensitive adhesives (PSAs, defined below). In the tables presented later, lap shear strength is presented in units of mega Pascal (MPa) and pounds per square inch (psi). The latter is shown in parenthesis. The temperature of the test will always be room temperature.

FIGURE 27.1. Diagram of an ASTM D1002 lap shear specimen. The adherends are usually 2.54 cm wide and 10.16 cm long. The thickness of the adherend depends upon the adherend material. If the adherend is aluminum, that thickness is usually 0.16 cm thick.

A T-peel test is shown in Fig. 27.2. The specimen is usually 1 in. (2.54 cm) wide and is described in Standard Test Method ASTM D1876 [6]. This specimen is symmetrical (both adherends are the same thickness). Other peel test specimens are not symmetrical, such as the floating roller peel test [7] or the climbing drum peel test [8]. The test measures the fracture resistance of an adhesive under conditions in which the adherends may plastically deform. In the tables presented later, the peel strength is given in Newtons per centimeter of width (N/cm) and in units of pounds per inch width (piw). The latter is shown in parenthesis. In some cases, the peel strength is derived from climbing drum peel measurements in which the results are presented in torque, in. lb/in. For pressure sensitive adhesives, the testing procedures are somewhat different and this is described below. Rubber-based adhesives are often evaluated using a modification of the PSA-type peel tests in which a piece of canvas is used as the flexible adherend.

The last important test for evaluating adhesive properties is a cleavage or fracture test. Figure 27.3 shows an example of such a test, the double cantilever beam test. The adherends are usually 1 in. (2.54 cm) wide and the thickness depends on the adherend modulus. Described in Standard Practice ASTM D3433 [9], the test is meant to measure fracture resistance (strain energy release rate) under conditions in which the adherends do not plastically deform. The units of fracture resistance (strain energy release rate) are joules per square meter and this quantity is given the symbol $\mathcal{G}_{IC}$.

FIGURE 27.2. Diagram of an ASTM D1876 T-peel specimen.

FIGURE 27.3. Diagram of an ASTM D3433 double cantilever beam specimen. The load is usually applied by attaching a fixture to holes located near the front of the specimen. In general, the initial portion of the specimen is not bonded in order to provide an initial crack.

27.3 TYPES OF ADHESIVES AND THEIR PHYSICAL PROPERTIES

Adhesives can be classified in a number of ways. Thy can be classified according to chemistry (e.g., epoxy versus neoprene), according to application method (e.g., hot melt versus spray applied), or according to strength. It is important to note that, in adhesive technology, high strength is not necessarily related to "best." Rather, having the correct strength along with the most appropriate and economical application conditions is usually equated with "best." The choice of adhesive for a particular end use is based upon criteria of modulus, ultimate strength, fracture resistance, compatibility with the adherend, resistance to adverse environments, and considerations of economy. The adhesives described in the following paragraphs are presented in order of decreasing strength.

27.3.1 Structural Adhesives

Structural adhesives are a class of adhesives, usually thermosets, that can bond high strength materials such as metals and composites and sustain a high load (often defined as being in excess of 1,000 psi) for long periods of time. Another definition includes the criterion that the adhesive must sustain a significant load without measurable creep. Materials ranging from naturally occurring proteins to epoxy resins to acrylic resins have been used as structural adhesives. The properties of a structural adhesive depend not only upon the properties of the base resin but also on the type of cross-linker and the kinds of modifiers that are added to enhance performance. Especially important are the elastomeric modifiers that have been added to increase the fracture resistance of otherwise brittle thermoset resins. Table 27.2 provides a representative listing of room tem-

TABLE 27.2. *Representative physical properties of adhesive bonds made with structural adhesives.*

Adhesive	Adherend	Lap shear strength, MPa (psi)	Peel stength, N/cm (piw)	$\mathcal{G}_{IC}$, J/m^2
Methyl cyanoacrylate	Aluminum	22 (3,190) [10]		
Ethyl cyanoacrylate	Aluminum	17 (2,465) [10]		
300 series surface-activated acrylic	Steel	15 (2,175) [10]		
	Aluminum		12 (7) [10]	
Modern two-part acrylic adhesive	Steel	29.6 (4,300) [11]	51 (29) [11]	
Toughened two-part acrylic	Aluminum	32.6 (4,727) [12]	78 (45) [12]	3,600 [12]
Two-part acrylic adhesive for low surface energy plastics	Polyethylene	5.5 (799) [13][a]		
	Polypropylene	6.9 (993) [13][a]		
FM73 (rubber modified 120 °C curing film adhesive)	Etched aluminum			2,107 [14]
EA946 two-part epoxy	Steel			1,150 [15]
EA913NA two-part epoxy	Steel			375 [15]
FM1000 (nylon epoxy film adhesive)	Aluminum	48.9 (7,090) [16]	175 in. lb/in. [16][b]	
Diglycidyl ether of bisphenol-A cured with dicyandiamide	Aluminum	13.8 (2,000) [17]	19 (11) [17]	
Thermoplastic polyimide	Titanium	41.4 (6,000) [18]		
LARC-13 (polyimide adhesive)	Titanium		2.3 (1.3) [19]	70 [19]
LARC-13 modified with aromatic amine terminated acrylonitrile–butadiene copolymer	Titanium	25.2 (3,650) [19]	9.6 (5.5) [19]	371 [19]
Bis-maleimide-based adhesive	Aluminum	20 (2,900) [20]		
Bis-maleimide-based adhesive mdofied with carboxy terminated acrylonitrile–butadiene copolymer	Steel	24 (3,480) [21]		776 [22]
X-PQ (crosslinkable poly(phenyl quinoxaline)	Titanium	26.6 (3,650) [23]	11.7 in. lb/in [23][b]	
Poly(vinyl formal)-phenolic	Aluminum	27.6–34.5 (4,000–5,000) [16]	14–18 in. lb/in [16][b]	
Nitrile-phenolic	Aluminum	24.1 (3,500) [16]	20 in. lb/in. [16][b]	1,000–1,500 [14]
Phenol/formaldehyde/resorcinol	Wood	6.9 (1,000) [24]		
EC-3549 B/A (two-part polyurethane adhesive)	Aluminum	13.8 (2,000) [25]	43 (25) [25]	

[a] Adherends yielded and elongated, bond did not fail, adherend yield strength is quoted.
[b] Climbing drum peel results are given in values of torque (in. lb/in).

perature lap shear, peel strengths, and strain energy release rates for a number of structural adhesives. Trade names for several structural adhesives are also listed in Table 27.2 and the generic chemistry for that product is also given in parenthesis following the trade name.

Table 27.2 lists a wide range of chemistries including phenolics, epoxies, bis-maleimides, and polyimides. Most of these adhesives are considered to be heat curing although epoxies and phenolics can be made to be room temperature curing. Urethanes and acrylics are often formulated to be two-part, room temperature-curing adhesives. Cyanoacrylates cure at room temperature as a one-part system. Of the chemistries used to formulate structural adhesives, the epoxies offer the widest range of formulation possibilities and resultant performance. For example, epoxy curing conditions can be tuned for almost any temperature between room temperature and 200+ °C. Lap shear strengths from 10 to 48 MPa are available as are peel strengths from about 9 to 175 N/cm. Cross-linked epoxies are brittle. A cross-linking system is chosen such that the cured epoxy resin "matrix" has some level of ductility (low enough yield strength). In addition, an elastomeric modifier is added in order to provide internal stress concentrators to yield the matrix, thus providing a means for internal energy absorption. Cross-linking agents are usually polyamines (such as dicyandiamide) although other reactive ingredients such as phenolics, anhydrides, and imidazoles have been used. An elastomeric modifier that is widely referenced in the literature is the butadiene–acrylonitrile copolymer, in particular, telechelic, epoxy reactive, low molecular weight butadiene–acrylonitrile copolymers. Epoxy adhesives are used in a wide range of applications, too great to list. Of particular interest is their use in the aircraft construction industry as well as in electronic components and assemblies.

Epoxy adhesives are limited to about 171 °C long-term service conditions. Phenolic adhesives, bis-maleimides, and polyimides exceed epoxies in terms of heat resistance. Phenolic resins are either self-curing (resoles) or they require a curing agent (novolacs). A standard heat-curing agent for a novolac phenolic is hexamethylene tetraamine ("hexa"). Cured, unmodified phenolic resins are brittle and would be very poor adhesives. As with epoxy resins, elastomeric modifiers have been used to improve the fracture resistance of phenolics. High molecular weight butadiene–acrylonitrile rubbers and poly(vinyl acetal)s have been used to modify phenolics. These adhesives are used in a number of demanding applications such as friction surface bonders in automobile brake and clutch assemblies.

Table 27.2 lists a variety of very-high-temperature-resistant structural adhesives such as the bis-maleimides, polyimides, and polyphenyl quinoxolines. These adhesives can give reasonable lap shear performance at temperatures as high as 220 °C. These materials are also brittle when cured. Despite many attempts to improve their performance by the addition of various modifiers, their use is limited to their lack of fracture resistance. LARC-13 is given as an example of this situation in Table 27.2. It is thought that the reason for the lack of ability to obtain fracture resistance in these adhesives is the high yield strength (low ductility) of the cured matrix.

Room temperature-curing structural adhesives include epoxies, acrylics, and urethanes. Acrylic systems offer very rapid cure but in much the same manner as described above, they are brittle after cure. Chlorosulfonated polyethylene has been used as a modifier for acrylic adhesives to achieve fracture resistance. Acrylic adhesives can be two-part systems in which the free-radical generating species are kept separate from each other. Typical free-radical initiator systems include cumene hydroperoxide plus saccharin and *N*,*N*′- dimethyl-*p*-toluidine. An example of a new technology in this area is a two-part acrylic adhesive that bonds to polyolefins without surface preparation of the adherend. In light of the section on wetting on adhesion, acrylic adhesives with surface energies in excess of $35\,\mathrm{mJ/m^2}$ should not be able to wet and adhere to polyethylene (critical wetting tension of $31\,\mathrm{mJ/m^2}$). The new technology adhesives adhere so well to unprepared polyolefins that the adherend breaks before the bond does. Tables 27.2 provides an example of that adhesive. Acrylics are also used in so-called anaerobic cures in which adhesive polymerization is inhibited by the presence of oxygen but the polymerization is promoted in its absence. Thread-locking adhesives are an example of this type of acrylic structural adhesive. Cyanoacrylates cure by the action of ambient moisture. Even though these materials appear to cure, the resultant material is a thermoplastic unless cross-linking agents are added. Polyurethanes are typically used as two-part adhesives in which the isocyanate and polyol are kept in separate containers. Cure is effected upon mixing. Polyurethane performance is dependent upon the type of isocyanate, polyol, and catalyst. Organotin compounds are often used to catalyze these reactions. Polyurethane performance is typified by high peel strength but relatively low shear strength.

27.3.2 Hot-Melt Adhesives

Hot-melt adhesives are materials that are applied from the melt state and are capable of producing moderate strength bonds upon cooling. The properties of hot-melt adhesives are heavily dependent upon the primary polymeric formulation material, which is generally based upon a polyolefin or a poly(vinyl acetate-*co*-ethylene) copolymer. Properties are optimized by formulation with materials such as crystalline waxes and tackifiers. Crystalline waxes are used to decrease the melt viscosity and the surface tension of the molten adhesive. Properly formulated, the wax might also increase the strength of the solidified adhesive. Tackifiers are unique low-molecular weight materials that are typically high glass temperature solids. They have the interesting property of conferring increased compliance at low rates of strain application but increasing stiffness at high rates of strain application. That is, tackifiers decrease the plateau modulus but increase the glass temperature of a formulation. Hot-melt adhesives also include an antioxidant in the formulation, as the adhesive may have to sit for long periods of time at high temperature in an applicator. Melt temperatures are often in excess of 120 °C. Much of hot-melt adhesive performance is dependent upon the melt-flow index (inversely proportional to molecular weight) of the primary polymer as well as the surface energy of the molten adhesive. Thus, high melt-flow index adhesives, while having easy application, will have poor properties due to the low molecular weight (sometimes below or only approaching the entanglement molecular weight of the polymer). Low melt-flow index adhesives will have better performance due to the higher molecular weight but are often difficult to apply. Base polymers with high vinyl acetate content will have higher cohesive strength (and higher surface energy) but will wet poorly on low surface energy adherends. The formulator must balance these properties by having appropriate melt-flow index, and the appropriate content of vinyl acetate, tackifier, and wax.

A distinct set of hot-melt adhesives are designed through synthetic rather than formulation means. Thus, polyesters and polyamides are synthesized with appropriate monomers to provide the desired performance. The polyester chemistry used to make these hot-melt adhesives is the same as that used to make polyester film and fiber but the molecular weight is usually lower and the mixtures of diols and diesters are chosen to control crystallinity and flexibility. One class of monomers used to make polyamide amide hot melts is based on dimer acids that are made from natural products.

Representative physical properties of some hot-melt adhesives are shown in Table 27.3. Note that some of the synthetic hot-melt adhesives are almost structural in strength but, because they are thermoplastic, they would likely creep under load. Hot-melt adhesives are increasing in usage due to the lack of volatile emissions during application. They are used in packaging, bookbinding, furniture manufacture, and other applications.

27.3.3 Elastomer-Based Adhesives

Rubber-Based Adhesives

Rubber-based adhesives are moderate strength materials whose primary formulation ingredient is a rubber. Neoprene (chloroprene) is widely used in these adhesives. Other elastomers used in the formulation of rubber-based cements are natural rubber, styrene–butadiene rubber, and nitrile rubber. Rubber-based adhesive formulations may include phenolic resins, tackifiers, and, sometimes, cross-linking agents. When neoprene is used, the formulation must also contain an acid acceptor such as ZnO or MgO in order to guard against dehydrohalogenation. Formulations are optimized to obtain a balance between shear and peel properties. These adhesives are most often tacky when applied but are not tacky after solvents and carriers evaporate. This makes these materials distinct from pressure-sensitive adhesives (vide infra), which must remain aggressively and permanently tacky. A particular form of rubber-based adhesive, known as a ‘‘contact cement,’’ must remain tacky during the bonding operation. This control of tack is known as the ‘‘open time’’ between application of the adhesive and closing of the bond. The choice of elastomer, tackifier and, in particular, the solvent, controls the ‘‘open time.’’ Rubber-based adhesives have been sold in a solvent vehicle for decades. Recent regulations controlling levels of solvent emissions have forced the industry to provide water-thinned rubber-based adhesives or, alternatively, have forced users to switch to hot-melt adhesives.

Rubber based adhesives are used in a myriad of applications which are familiar to the consumer. Tile and paneling adhesives are examples of these adhesives used in home construction. The largest use of rubber-based adhesives is in laminated furniture manufacture. Representative physical properties of rubber-based adhesives are shown in Table 27.4. The adhesives are characterized as having low to moderate shear strength and high peel strength.

TABLE 27.3. *Representative physical properties of adhesive bonds made with hot-melt adhesives.*

Adhesive	Adherend	Lap shear strength, MPa (psi)	Peel strength, N/cm (piw)
Co-polyetheramide from polyetherdiamine and dimer acid	Aluminum	11 (1,600) [26]	16 (9) [26]
Low-melt-flow index dimer acid-based polyamide (Versamide)	Aluminum	1.4–6.8 (200–1,000) [27]	
Low-melt-flow index dimer acid-based polyamide (Milvex)	Aluminum	25.2 (3,660) [27]	61 (35) [27]
Ethylene–vinyl acetate copolymer modified with tackifier and microwax	Wood	2.8 (400) [28]	
	ABS	1.7 (245) [28]	
Co-polyester	Aluminum	24.5 (3,550) [29]	
Crystallizable co-polyester-amide	Reinforced plastic	16.7 (2,421) [30]	1.5 (0.9) [30]
Co-polyester modified with 2,2′-bis [4′-(β-hydroxyethoxy)phenyl]propane	Unspecified metal	16.9 (2,450) [31]	2–3 (1–2) [31]
Poly(vinyl acetate) (unmodified)	Aluminum	3.9 (570) [32]	1.9 (1.1) [32]

TABLE 27.4. *Representative properties of adhesive bonds made with rubber-based adhesives.*

Adhesive	Adherends	Lap shear strength, MPa (psi)	Peel strength, N/cm (piw)
Acrylic/styrene latex formulated with plasticizers, to provide a solvent-free mastic adhesive	Mahogony to mahogany	1.2 (172) [33]	
Polyurethane elastomer construction adhesive (EC-5230)	Douglas fir to Douglas fir	1.6 (236) [34][a]	
Acrylic latex/phenolic dispersion (2/1)	Canvas to cold rolled steel		35 (20) [35]
Neoprene latex/phenolic dispersion (2/1)	Canvas to cold rolled steel		3.5 (2) [35]
Neoprene latex/butylated phenolic resin/MgO	Canvas to painted steel	0.34 (50) [36]	52.5 (30) [36][b]
Solvent-based neoprene, Fastbond$^{\text{TM}}$ 5	Canvas to steel		33 (19) [25]
	Birch to Birch	3.3 (482) [25]	
Solvent-based neoprene contact bond adhesive, EC-1357	Canvas to steel		40.3 (23) [25]
	Birch to birch	3.7 (536) [25]	
Solvent-based nitrile EC-1099	Aluminum to aluminum	9 (1306) [25]	
	Canvas to steel		53 (30) [25]

[a] Block shear according to ASTM D143.
[b] Canvas to canvas peel at 140 °F after 2 weeks of aging.

Pressure-Sensitive Adhesives

Pressure-sensitive adhesives (PSAs) are a class of elastomer-based materials that have the following characteristics: they are aggressively and permanently tacky, they adhere without the need of more than finger pressure, they require no heat or activation, they adhere "well," and they can be removed without leaving a visible residue. PSAs are considered low strength materials. The shear strength values are on the order of a few to ten pounds per square inch and the peel strengths are on the order of a few ounces to ten pounds per inch width. PSAs are usually sold on a backing as a tape and are very familiar to the consumer as Scotch$^{\text{TM}}$ Brand tape. The properties of the tape are dependent not only on

Table 27.5. *Representative physical properties of pressure-sensitive adhesives and bonds made with them.*

Adhesive chemistry	Backing	Adherend	Peel strength, N/cm (piw)	Shear holding power (min)	Tack (g/cm^2)
Emulsion polymerized copolymer of butyl acrylate, styrene, acrylic acid, and acrylamide	Polyester	Stainless steel	42 (24) [39][a]	190 [39][b]	370 [39][c]
Kraton 107 block copolymer tackified with Wingtack 95	Polyester	Aluminum	24 (13) [40]		1,500 [40][c]
Acrylic latex tackified with Staybelite ester 10 (50/50 blend)	?	?	5.4 (3.1) [41]	>6,000 [41]	830 [41]
Carboxylated styrene–butadiene rubber	Polyester	Stainless steel	0.4 (0.24) [42][a]	60 [42][b]	248 [42][c]
Carboxylated styrene (46%)–butadiene rubber tackified with Foral 85 (50/50 blend)	Polyester	Stainless steel	5.9 (3.4) [42][a]	10,000 [42][b]	492 [42][c]
Waterborne acrylic PSA for box sealing tape	Poly(propylene)	Stainless steel	2.8–3.3 (1.6–1.9) [43][a]	6,000 [43][b]	
Acrylic hot-melt	Polyester	Stainless steel	2.6 (1.5) [43][a]	190 [43][b]	
Natural rubber tackified with Piccolyte 85 (50/50 blend), aqueous	Polyester	Stainless steel	4.4 (2.5) [44][a]	>6,000 [44][b]	1,200 [44][c]
Poly(*iso*-butylene)-based PSA (6×10^5 Daltons)	?	Stainless steel	2.6–4.4 (1.5–2.5) [45]	1,100 [45][d]	100–300 [45][c]
Acrylic foam tape "VHB 4929"	Aluminum foil	Stainless steel	35 (20) [46][e]	10,000 [46][f]	

[a] 180° peel, Pressure Sensitive Tape Council Method 1.
[b] 1 kg weight for a 0.5 in.^{2} lap, Pressure Sensitive Tape Council Method 7.
[c] Polyken Probe Tack Test, ASTM D2979.
[d] 500 g weight for a 0.5 in.^{2} lap otherwise similar to Pressure Sensitive Tape Council Test Method 7.
[e] 90° Peel.
[f] 1.5 kg weight for a 0.5 in.^{2} lap, Pressure Sensitive Tape Council Method 7.

the adhesive but the backing as well. PSAs are usually formulated by using an elastomeric material such as natural rubber in combination with a tackifier resin such as a rosin ester. The balance of peel and shear properties is obtained by the rubber to resin ratio. Other elastomer chemistries important to PSA technology are acrylics, nitriles, styrene–isoprene block copolymers, silicones, vinyl ethers, and butyl rubber. Of these, all have to be externally tackified with the exception of the acrylics. Tackifiers include the rosin esters (mentioned above), terpene resins, the so-called C-5 and C-9 resins, which are low molecular weight polymers formed from petroleum streams. Silicone PSAs are made tacky by the addition of unique silicate resins known as "MQ." MQ resin is material of unspecified structure made by the reaction of monofunctional trimethyl silane ("M") with quadrafunctional silicon tetrachloride ("Q").

Instead of the normal lap shear strengths that we have described for other adhesives, PSAs are evaluated for their "shear holding power [37]." In this test, a piece of tape is applied to a clean surface and a known weight is attached to the end of the tape. The time to failure is determined. As shown in Table 27.5, this value is given in minutes. Shear holding power is determined not only by the choice of elastomer, tackifier, and their ratio but also by the level of cross-linking. When styrene–isoprene block copolymers are used as the PSA elastomer, the system does not need to be cross-linked. The unique structure of these elastomers induces phase separation of the styrene blocks. The phase-separated segments act as virtual cross-links. There are also special tapes having an acrylic foam core which provide properties having exceptional peel and shear holding power that approach that of rubber-based adhesives.

For peel testing of PSAs, the usual configuration differs from that shown in Fig. 27.2. That is, one adherend is usually rigid while the other is the backing for the tape. The peel test can be conducted in such a fashion that the tape is peeled at 90° or 180° with respect to the rigid adherend.

Another important property of PSAs is their tack or response to light pressure. Bringing a probe of known composition in contact with the adhesive with a specified force for a specified time and then measuring the amount of force necessary to remove the probe from the adhesive at a specified rate measures tack [38]. Peel strength and tack are dependent upon the rubber to resin ratio and are inversely dependent upon the cross-link density. Representative physical propertied of PSA tapes are provided in Table 27.5.

REFERENCES

1. W. A. Zisman, Ind. Eng. Chem., **55**(10), 19 (1963).
2. A. R. C. Baljon, J. Vorselaars and T. R. Depuy, Macromolecules, **37**, 5800 (2004).
3. A. R. C. Baljon, and M. O. Robbins, Science, **271**, 482 (1996).
4. ASTM D1002, American Society for Testing and Materials, Philadelphia, PA.
5. M. Goland and E. Reissner, J. Appl. Mech. Trans. Am. Soc. Eng., **66**, A17 (1944).
6. ASTM D1876, American Society for Testing and Materials, Philadelphia, PA.
7. ASTM D3176, American Society for Testing and Materials, Philadelphia, PA.
8. ASTM D1781, American Society for Testing and Materials, Philadelphia, PA.
9. ASTM D3433, American Society for Testing and Materials, Philadelphia, PA.
10. F. R. Martin, in *Developments in Adhesives-1*, edited by W. C. Wake (Applied Science, London, 1977), Ch. 6.
11. P. C. Briggs, U. S. Patent 4,536,546, assigned to Illinois Tool Works, Aug 20, 1985.
12. C. Burrows, N. Sammes, G. Stables, M. H. Stone and C. Tempest, in *Adhesion-8*, edited by K. W. Allen (Applied Science, Essex, England,1984), Ch. 7.
13. A. V. Pocius and E. J. Deviney, U.S. Patent 5,935,711, Assigned to 3M Company, Issued Aug. 10, 1999.
14. R. Y. Ting and R. L. Cottington, Adhes. Age, **24**(6), 35 (1981).
15. G. L. Anderson, J. Adhes., **41**, 129 (1993).
16. L. T. Eby and H. P. Brown, in *Treatise on Adhesion and Adhesives*, edited by R. L. Patrick, (Marcel Dekker, New York, 1969), vol. 2, pp. 77–171.
17. Y. Lee, S. Wang and W. Chin, J. Appl. Polym. Sci., **32**, 6317 (1986).
18. A. K. St. Clair and T. L. St. Clair, NASA Technical Memorandum No. 84516, June 1982.
19. A. K. St. Clair and T. L. St. Clair, U. S. Patent 4,497,935, assigned to the United Staes Government, issued February 5, 1985.
20. S. J. Shaw, Mater. Sci. Technol., **3**, 589 (1987).
21. S. J. Shaw and A. J. Kinloch, in *Proceedings of the International Adhesion Conference, 1984* (The Plastics and Rubber Institute, London, 1984), pp. 3.1–3.4.
22. H. Stenzenberger, in *Structural Adhesives: Developments in Resins and Primers*, edited by A. J. Kinloch (Elsevier Applied Science, London and New York, 1986), Ch. 4.
23. C. L. Hendicks, S. G. Hill and J. N. Hale, NASA Contractor Report No. 177936, October, 1985, p. 33.
24. R. T. Hood and R. L. Bender, U. A. Patent 4,608,408, assigned to Koppers Company, issued Aug. 26, 1986.
25. 3M Product Literature, Industrial Adhesives and Tapes, St. Paul MN and www.3M.com
26. A. T. Hu, R. Tsai and Y. Lee, J. Appl. Polym. Sci., **37**, 1863 (1989).
27. R. D. Dexheimer and L. R. Vertnik, Adhes. Age, **15**(8), 39 (1972).
28. P. R. Lakshmanian and B. J. Monachino, Adhes. Age, **24**(9), 27 (1981).
29. F. Eichhorn, Schweissen Schneiden, **35**, 116 (1983).
30. D. D. Donermeyer, J. G. Martins,J. C. Martins, U. S. Patent 4,581,410, assigned to Monsanto Company, issued April 8, 1986.
31. L. Buxbaum and R. Hugl, British Patent 2,000,790, assigned to Ciba-Geigy AG, issued January 17, 1979.
32. Y. Hatano, B. Tomita and H. Mizumachi, Holzforschung, **40**, 255 (1986).
33. J. Bax, Adhes. Age, **24**(10) 22 (1981).
34. R. J. Hoyle, Adhes. Age, **24**(7), 43 (1981).
35. R. G. Azrak, B. L. Joesten and W. F. Hale, in *Adhesion Science and Technology*, edited by L-H. Lee (Plenum, New York, 1975), pp. 233–248.
36. J. Keramedjian, Adhes. Age, **5**(6), 34 (1962).
37. PSTC-7, Pressure Sensitive Tape Council, Chicago, IL.
38. ASTM D2979, American Society for Testing and Materials, Philadelphia, PA.
39. M. J. Skoglund, PCT WO 91/18739, applied for by Ashland Chemical Co., published December 12, 1991.
40. N. Nakajima, R. Babrowicz and E. R. Harrell, J. Appl. Polym. Sci., **44**, 1437 (1992).
41. K. F. Foley and S. G. Chu, Adhes. Age, **29**(10), 24 (1986).
42. A. Midgley, Adhes. Age, **29**(10), 14 (1986).
43. W. J. Sparks, Adhes. Age, **25**(3), 38 (1982).
44. S. G. Chu, in *Adhesive Bonding*, edited by L-H. Lee (Plenum press, New York, 1991), pp. 97–138.
45. M. A. Krenceski and J. F. Johnson, Polym. Eng. Sci., **29**, 36 (1989).
46. 3M Data Sheet "VHB Double Coated Acrylic Foam", April 2001.

CHAPTER 28

Some Mechanical Properties of Typical Polymer-Based Composites

Jianye Wen

ALZA Corporation, 1900 Charleston Rd., Mountain View, CA 94039

28.1 INTRODUCTION

Composite materials have a variety of definitions and there is no universally accepted one. The definition in the literature differ widely [1–6]. In the broadest definition, any material composed of two or more distinct components is a composite, but this definition is too broad to be useful. To be more inclusive, the level of definition, the forms and composition of constituents have to be considered together. For many of the materials now commonly considered composites, a working definition can be given as follows:

A composite is a multiphase material brought about by combining materials which differ in composition or form on a macroscale in order to obtain specific characteristics and properties. The constituents retain their identities and properties such that they exhibit an interface between one another and act in concert to achieve improved synergistic properties not obtainable by any of the components acting alone.

Even this definition needs to be classified [7, 8]. To some researchers it is still too broad because it includes many materials that are not usually thought of as composites such as concrete, copolymers and blends, reinforced plastics, and carbon-black-filled rubber. On the other hand, some of the more recent composites are excluded from the category of composites if this definition is strictly applied. For example, many particulate-type composites such as dispersion-hardened alloys and cermets have composite structures that are microscopic rather than macroscopic [2,8]. In some cases, the composite structures are nanoscopic, with the physical constraint of several nanometers as the minimum size of the components [9–16]. The terms ‘microcomposite’, ‘‘nanocomposite’’, or ‘molecular composite’’ are suggested instead. They differ from traditional composites in the smaller sizes of the component phases and exhibit unique behaviors due to the smaller size effect, the large interface effect, and the quantum confining effect.

Composite structures open up a whole new dimension of design freedom which is not available with traditional homogeneous materials. Composite can be designed to provide us with an almost unlimited selection of properties to meet the demands of different environments as well as any other specific needs. The behavior and properties of composites are determined by three factors: the intrinsic properties of constituents, the form and structural arrangement of the constituents, and the interaction between the constituents. The properties of constituents determine the general order or range of the properties of composite. The form (shape and size), the structural arrangement, and the composition and distribution of constituents give composites their versatility and contribute to the overall performance. The interaction between the constituents also plays a critical role in improving the mechanical properties of composites.

The constituents of a composite are generally arranged in such a way so that one or more discontinuous phases are embedded in a continuous phase. The continuous phase is the matrix. The discontinuous phase are called reinforcement and generally much stronger and stiffer than the matrix although exception dose exist (such as the use of rubber particles). The matrix of composite could be polymer, ceramics, or metal. The main thrust of this chapter will be directed at polymeric matrix composites. These materials usually have exceptional mechanical properties and often termed high performance composites. They can be classified on the basis of the form of their structural components: (1) fibrous (composed of fibers in a matrix), (2) laminar (layers of materials), (3) particulates (composed of particles, skeletal, or flakes in a matrix), (4) hybrid (combination of any of the above). In general, the reinforcing agents can be either fibers, particles, laminae, whiskers, or flakes and either an organic, metallic, inorganic, or ceramic material. They are structural constituents. They determine the internal structure of composite and provide the high strength and modulus. Composite strength is directly proportional to the basic reinforcing agent and can be improved at the expense of stiffness. The polymeric matrices can be either thermoplastics (capable of being repeatedly hardened and softened by increasing and decreasing temperature) or thermoset (changing into an infusible and insoluble material after cured by applying heat or by chemical means). Although the properties of the matrix are not directly related to the composite strength, the matrix does play an important role. They are the body constituents and serve to enclose the composite and give them their bulk forms, spread the load as well as offering resistance to weathering and corrosion. Typical thermoplastic resins include ABS, polyethylene, polypropylene, polycarbonate, nylon, polysulfone, and polyetheretherketone (PEEK). The most used thermosetting resins include epoxy, polyester, phenolic, vinyl ester, polyimide, and silicone. At present, the use of fibrous reinforcing agent combined with thermosetting resins predominates [2]. In this chapter, the mechanical and some physical properties of most used reinforcing agents, thermoplastic and thermosetting resins used as composite matrix, and high performance polymeric matrix composites were summarized in Tables 28.1–28.4.

28.2 TERMINOLOGY

(1) Elastic modulus (ASTM-D638, D759, D-1708)

It is the ratio of nominal tensile stress to corresponding strain below the proportional limit of a material.

Units: psi; kgf cm^{-2}; Nm^{-2}

(2) Tensile strength (ASTM-D638, D759, D-1708)

At break: maximum tensile stress sustained by the specimen at break.

At yield: maximum tensile stress sustained by the specimen at the yield point.

Units: psi; kgf cm^{-2}; Nm^{-2}

(3) Elongation (ASTM-638)

The elongation of a specimen at break expressed as a percentage of the original length.

Units: %

(4) Impact strength (ASTM D-256, ASTM D-758, ISO R 180, BS 2782)

In pendulum-impact methods: energy expended by a standard pendulum-impact tester to break a test specimen

TABLE 28.1. *Physical properties of reinforcing agents—fiber, particulate.*

Material	Elastic modulus GPa	Tensile strength MPa	Density g cm^{-3}	Specific stiffness MJ kg^{-1}	specific strength MJ kg^{-1}	Reference
Synthetic inorganic						
E-glass fiber	72.4	3450	2.54	28.5	1.36	[2,17,18]
S-glass fiber	85.5	4820	2.49	34.3	1.94	[2,17,18]
M-glass fiber	110	3500	—	—	—	[19,20]
Boron fiber	441	3450	2.30	192	1.50	[17,18]
Carbon	200	2760	1.76	114	1.57	[17]
Graphite fiber						
high-strength	253	4500	1.8	140	2.5	[2,18]
high-modulus	520	2400	1.85	281	1.3	[2,18]
intermediate	186	2482	1.74	107	1.43	[18]
Alumimum oxide	323	689	3.97	81.4	0.174	[17]
Aluminum silicate	100	4130	3.90	25.6	1.06	[17]
Beryllium oxide	352	517	3.03	116	0.171	[17]
Quartz (fuses silica)	70	—	2.2	31.8		[17]
Tungsten	414	4200	—	—	—	[19,20]
Natural inorganic						
Asbestos	172	1380	2.50	68.8	0.552	[17]
Synthetic organic						
Aramid fiber*						
Kevlar 29	59	3500	1.44	41.0	2.43	[2,18]
Kevlar 49	124	3600	1.44	86.11	2.50	[2,18]

*Chemical structure:

TABLE 28.2. *Physical properties of most used unreinforced thermosets and thermoplastics.*

	Property	Elastic modulus	Tensile strength	Elongation	Impact strength Izod, notched	Specific gravity (Density)	Specific stiffness	Specific strength	
	Units	GPa	MPa	%	J m^{-1}	g cm^{-3}	MJ kg^{-1}	MJ kg^{-1}	
Material	Methods of determination	D638	D638	D638	D256	D792			Reference
Polyester		4.1	689	1.40	2.93	0.492			[17]
Polyamide		2.8	827	1.14	2.46	0.725			[17]
Polyacrylonitrile		200–390	2,100–3,400	—	—	—			[19,20]
Thermoplastics									
Acetal		2.83	60.28	40.0	50	1.41	2.01	0.043	[7,21]
ABS		2.07	41.10	5.0	270	1.03	2.01	0.040	[7,21]
Nylon 6		2.62	80.83	30.0	30	1.12	2.34	0.072	[7,21,22]
Nylon 66		2.76	78.78	60.0	40	1.13	2.44	0.069	[7,21,23]
Polycarbonate		2.34	65.08	110.0	850	1.20	1.95	0.054	[7,21]
Polyester (PBT)		1.93	56.17	50.0	40	1.31	1.47	0.042	[7,21]
Polyester (PET)		2.76	58.23	50.0	10–30	1.34	2.06	0.044	[7,21]
Polyetheretherketone (PEEK)		3.6	92	50	—	1.32	2.73	0.070	[24, 25]
Polyetherketoneketone (PEEK)		4.5	102	4	—	—	—	—	[26,27]
Polyethylene									
LDPE		—	20	350	—	0.925	—	0.022	[28]
HDPE		—	27	100	133	0.95	—	0.028	[28]
Polyphenylene oxide (PPO)		2.62	53.43	50.0	270	1.080	2.43	0.050	[7,21]
Polyphenylene sulfide		0.31	65.08	1.0	<30	1.30	2.55	0.050	[7,21]
Polypropylene		0.69	34.25	200.0	100–1,010	0.89	0.775	0.039	[7,21]
Polystyrene acrylonitrile (SAN)		2.76	65.08	0.5	20	1.05	2.63	0.065	[7,21]
Polyurethanes		–	42.76	480	—	1.23	—	0.035	[29]
Polyvinyl Chloride		—	34.48–62.07	1–25	—	1.33–1.45	—	0.03–0.062	[30]
Thermosets									
Unsaturated polyester resins									
rigid		2–4.4	40–90	<5.0	16–32	1.10–1.46	1.83–3.01	0.036–0.062	[31]
flexible		—	3.4–21	40–310	370	1.01–1.20	—	0.003–0.018	[31]
Vinyl ester resins*									
MW = 500		3.3	80.7	4.5	—	—	—	—	[32]
MW = 900		3.2	79.9	5.0	—	—	—	—	[32]
MW = 1200		3.0	78.6	5.5	—	—	—	—	[32]
Vinyl ester resins**									
phenolic novolac		0.4	75.8	3.5	—	—	—	—	[32]
tetrabromo bisphenol A		—	73.1	4.0	—	—	—	—	[32]
bisphenol A		3.4	84.1	5.0	—	—	—	—	[32]
Polybutadiene resins		—	235	600	—	0.86–0.90	—	—	[33,34]
Epoxy resins		2.8–4.2	55–130	—	5.3–53	1.2–1.3	2.33–3.23	0.046–0.10	[2,35]
Polyimides		3.2	55.8	—	—	1.43	2.24	0.039	[2]

*Bisphenol A epoxy-based vinyl ester resins containing 50 wt% styrene.

**Vinyl ester resins containing 40 wt% styrene.

TABLE 28.3. *Physical properties of most used reinforced thermosets and thermoplastics.*

Material	Property	Elastic modulus	Tensile strength	Elongation	Flexural Strength	Flexural Modulus	Impact strength Izod notched	Specific gravity (Density)	Specific stiffness	Specific strength	Reference
	Unit	GPa	MPa	%	MPa	GPa	J m^{-1}	g cm^{-3}	MJ kg^{-1}	MJ kg^{-1}	
	Methods of determination	D638	D638	D638	D790	D790	D256	D792			
Reinforced Thermoplastics											
ABS											
glass fiber											
10 wt%		4.6	65	3.0	102	4.5	64	1.10	4.18	0.0591	[7]
20 wt%		5.1	76	2.0	107	4.9	59	1.22	4.18	0.0623	[7]
30 wt%		6.3	90	1.4	116	6.4	53	1.28	4.92	0.0703	[7]
asbestos fiber											
30 wt%		—	96	—	—	7.8	—	—	—	—	[36]
carbon fiber											
16.6 wt%		—	42	—	—	5.8	—	—	—	—	[36]
Acetal											
glassfiber											
10 wt%		6.6	72	2.4	107	6.1	53	1.54	4.29	0.0468	[7]
30 wt%		7.7	83	2.0	114	7.2	43	1.63	4.72	0.0509	[7]
Ethylene tetrafluoroethylene (ETFE)											
graphite fiber											
30 wt%		—	103	2–3	138	1.65	213–267	1.73	—	0.0509	[37]
Nylon 6											
glass fiber											
15 wt%		5.9	104	4.0	159	5.4	80	1.25	4.72	0.0832	[7]
30 wt%		7.2	166	3.0	200	6.9	117	1.37	5.26	0.121	[7]
30 wt%		—	159	3–4	234	8.3	123	1.37	—	0.116	[22]
Nylon 6/6											
glass fiber											
13 wt%		6.2	97	4.0	173	4.5	53	1.23	5.041	0.0789	[7]
30 wt%		9.0	173	3.0	235	9.0	107	1.37	6.569	0.126	[7]
aluminum flake											
30 wt%		—	69	2–3	121	7.6	54	1.38	—	0.050	[38]
35 wt%		—	69	2–3	121	7.6	54	1.43	—	0.048	[38]
Nylon 6/12											
glass fiber											
30 wt%		8.3	135	4.0	193	7.6	117	1.30	6.39	0.104	[7]
kevlar											
20 vol%		8.55	151.7	2.8	—	—	—	—	—	—	[39]

TABLE 28.3. *Continued*

	Property	Elastic modulus	Tensile strength	Elongation	Flexural Strength	Flexural Modulus	Impact strength Izod notched	Specific gravity (Density)	Specific stiffness	Specific strength	
	Unit	GPa	MPa	%	MPa	GPa	J m^{-1}	g cm^{-3}	MJ kg^{-1}	MJ kg^{-1}	
Material	Methods of determination	D638	D638	D638	D790	D790	D256	D792			Reference
Polycarbonate											
glass fiber											
10 wt%		5.2	83	9.0	110	4.1	107	1.26	4.13	0.0659	[7]
30 wt%		8.6	121	2.0	141	6.9	128	1.43	6.01	0.0846	[7]
kevlar 49											
20 vol%		9.8	163.4	2.1	—	—	—	—	—	—	[40]
graphite		12.6	176.5	1.7	—	—	—	—	—	—	[41]
aluminum flake											
30 wt%		—	46	2–3	93	4.8	80	1.44	—	0.0032	[38]
40 wt%		—	44	2	86	6.6	70	1.54	—	0.0029	[38]
Polyethertherketone (PEEK)											
63 Vf% AS4*		140	2,040	1.4	2,280	135	—	—	—	—	[26]
Polyetherketoneketone (PEKK)											
58 Vf% AS4*		129.6	1,675	—	1,620	—	—	—	—	—	[42]
Polyetherketonesetherketoneketone (PEKEKK)											
60 Vf% AS4*		130	1,724	—	1,759	112	—	—	—	—	[26]
Thermoplastic polyester											
PBT											
glass fiber											
30 wt%		8.3	131	3.0	193	7.9	80	1.52	5.46	0.0862	[7]
PET											
glass fiber											
30 wt%		9.0	144	2.0	221	8.6	60	1.56	5.77	0.0923	[7]
Polyethylene											
glass fiber											
10 wt%		2.5	36	4.0	46	2.5	75	1.04	2.40	0.0346	[7]
30 wt%		5.0	59	3.0	89	4.9	91	1.18	4.24	0.0496	[7]
kevlar 49		10.6	131.7	2.3	—	—	—	—	—	—	[39]
graphite		19.3	110.3	0.7	—	—	—	—	—	—	[39]
Poly(methyl methacrylate)											
kevlar 49											
20 Vol%		11.1	207.5	2.0	—	—	—	—	—	—	[39]

TABLE 28.3. *Continued*

	Property	Elastic modulus	Tensile strength	Elongation	Flexural Strength	Flexural Modulus	Impact strength Izod notched	Specific gravity (Density)	Specific stiffness	Specific strength	
	Unit	GPa	MPa	%	MPa	GPa	J m^{-1}	g cm^{-3}	MJ kg^{-1}	MJ kg^{-1}	
Material	Methods of determination	D638	D638	D638	D790	D790	D256	D792			Reference
Poly(phenylene oxide), modified											
glass fiber											
20 wt%		6.4	100	5.0	128	5.2	96	1.21	5.29	0.0826	[7]
Poly(phenylene sulfide)											
glass fiber											
40 wt%		14.1	152	3.0	255	13.0	80	1.64	8.60	0.0927	[7]
Polypropylene											
glass fiber											
10 wt%		2.5	43	4.0	54	2.4	43	0.98	2.55	0.0439	[7]
20 wt%		3.7	45	3.0	57	3.6	59	1.04	3.56	0.0433	[7]
30 wt%		4.4	47	2.0	63	4.3	69	1.12	3.93	0.0420	[7]
talc**											
20 wt%		—	40***	4.1****	—	2.7	22	—	—	—	[41]
40 wt%		—	37***	3.1****	—	4.1	15	—	—	—	[41]
50 wt%		—	34***	2.4****	—	4.8	37	—	—	—	[41]
Polysulfone											
glass fiber											
20 wt%		6.0	97	2.5	138	5.9	64	1.38	4.35	0.0703	[7]
40 wt%		11.6	124	1.5	173	10.7	80	1.55	7.484	0.080	[7]
Thermoplastic Polyurethane											
glass fiber											
10 wt%		0.7	33	48.0	43	0.6	747	1.22	0.574	0.027	[7]
PVC											
glass fiber											
20 wt%		0.8	97	3.0	145	6.9	80	1.58	0.506	0.0614	[7]
SAN											
glass fiber											
20 wt%		8.6	100	1.8	131	7.6	64	1.22	7.05	0.082	[7]
35 wt%		10.4	110	1.4	155	9.3	53	1.35	7.70	0.0815	[7]
Reinforced Thermosets											
Epoxy											
E-glass fiber		45	1,100	—	—	—	—	(2.1)	21.4	0.52	[2]
S-glass fiber		55	2,000	—	—	—	—	(2.0)	27.5	1.0	[2]

TABLE 28.3. *Continued*

	Property	Elastic modulus	Tensile strength	Elongation	Flexural Strength	Flexural Modulus	Impact strength Izod notched	Specific gravity (Density)	Specific stiffness	Specific strength	
	Unit	GPa	MPa	%	MPa	GPa	J m^{-1}	g cm^{-3}	MJ kg^{-1}	MJ kg^{-1}	
Material	Methods of determination	D638	D638	D638	D790	D790	D256	D792			Reference
glassfiber*****											
80 wt%		28	548	1.6	690	1.33	34.5	(1.91)	14.4	0.289	[7,21]
boron fiber		207	1,600	—	—	—	—	(2.1)	99	0.76	[2]
graphite fiber											
–high strength		145	2,300	—	—	—	—	(1.6)	90.6	1.42	[2]
–high modulus		290	1,000	—	—	—	—	(1.63)	178	0.61	[2]
aramid fiber											
(Kevlar)		80	2,000	—	—	—	—	(1.38)	58	1.45	[2]
Kevlar 49											
50 vol%		31	517	1.7	345	27.6	—	1.33	23.3	0.39	[39]
Unsaturated polyester											
woven cloth		10.3–31.0	206–344	0.5–2.0	276–550	172–344	267–1,600	1.5–2.1	6.9–14.8	0.14–0.16	[31]
chopped roving		5.5–13.8	103–206	0.5–5.0	69–276	103–206	107–1,070	1.35–2.3	4.1–6	0.08–0.08	[31]
Corezyn polyester											
Kevlar 49											
40 vol%		24	414	—	207	20	—	1.30	18.5	0.32	[39]
Polyester SMC											
glass fiber											
20 wt%		11.72	36.31	0.4	110.32	9.65	430	(1.772)	6.61	0.021	[7,21]
30 wt%		11.72	82.20	<1.0	179.27	11.03	850	(1.827)	6.41	0.045	[7,21]
50 wt%		15.65	157.55	1.7	310.28	13.79	1030	(2.000)	7.83	0.080	[7,21]
Polyurethane											
glass fiber											
13 wt%		—	19.18	140.0	—	0.26–0.27	—	(1.052)	—	0.018	[7,21]
23 wt%		—	30.21	38.9	—	1.03	110	(1.163)	—	0.026	[7,21]

*Continuous carbon fibres from Hercules

**Talc is a fine-ground product consisting of thin platelets, preferably white in color.

***Tensile strength at yield.

****Tensile elongation at yield.

*****Filament wound.

TABLE 28.4. *Mechanical properties of glass fiber unidirectional lamina.*

	Property	Elastic moduli			Strengths					
		E_L	E_T	G_{LT}	F_L	F_T	F'_L	F'_T	F_LT	
Composite	Unit	GPa	GPa	GPa	GPa	GPa	GPa	GPa	GPa	Reference
Epoxy										
E-glass fiber		45	12	5.5	1,100	40	620	140	70	[2]
S-glass fiber		55	16	7.6	1,600–2,000	40	690	140	80	[2]
graphite fiber										
–high strength		145	10	4.8	1,240–2,300	41	1,200	170	80	[2]
–high modulus		220–290	6.2–6.9	4.8	900–1,200	21	620	170	60–70	[2]
Kevlar 49		80	5.5	2.1	2,000	20	280	140	40	[2]

(plain or notched) under stipulated conditions of specimen mounting, notching, and pendulum velocity at impact. There are two pendulum methods in common use: Izod method and Charpy method.

In falling-weight methods: the minimum value of the product of fall height and mass to cause fracture of a test specimen.

Units: J/m, ft lb, cm kgf

(5) Specific gravity (ASTM D-792)

The ratio of the mass in air of a unit volume of the material at 23 °C to the mass (determined in identical conditions) of an equal volume of gas-free distilled water.

Units: gcm^{-3}, $lbft^{-3}$

(6) Flexural strength (ASTM D-790, ISO R 178, BS 2782, DIN 53 452)

At break: maximum stress in the outer fiber of the specimen at the moment of break in bending.

At yield: stress at yield (calculated from formulae appropriate to the test method).

Units: psi; $kgfcm^{-2}$; $N\ m^{-2}$

(7) Flexural modulus (ASTM D-790, ISO R 178, BS 2782, DIN 53 452)

The ratio of stress to corresponding strain in bending within the elastic limit, calculated by the appropriate theory.

Units: psi; $kgf\ cm^{-2}$; $N\ m^{-2}$

(8) Specific stiffness

The ratio of elastic modulus to density or specific gravity.

Units: $MJ\ kg^{-1}$

(9) Specific strength

The ratio of tensile strength to density or specific gravity.

Units: $MJ\ kg^{-1}$

(10) Lamina

The simplest representative form of high performance composites which consists of fibers oriented in a single direction and bonded together by a resin.

(11) Thermoplastics

A material that can be melted by heating and then resolidified by cooling.

(12) Thermoset

A material which hardens or sets by heat, chemical, or radiation cross-linking techniques and which, once set, cannot be resoftened by heating.

4. REFERENCES

1. G. Lubin, Handbook of Fiberglas and Advanced Composites, Van Nostrand Reinhold, New York, 1982.
2. Frank P. Gerstle, Jr., Encyclopedia of Polymer Science and Technology, John Wiley & Sons, New York, 1985, Volume 3, pp. 776–820.
3. Reference Book for Composites Technology, Ed. by Stuart M. Lee, Technomic Publishing Company, Inc., Lancaster, PA, 1989.
4. G. H. Staab, Laminar Composites, Elservier Science Ltd, Amsterdam 1999.
5. S. T. Peter, Handbook of composites (2nd edition), Kluwer Academic Publishers, London, 1998.
6. D. D. L. Chang, Carbon Fiber Composites, Elsevier Science Ltd, Amsterdam 1994.
7. D. V. Rosato, International Encyclopedia of Composites, Ed. by Stuart M. Lee, VCH Publishers, New York, 1990, pp. 148–180.
8. Mel M. Schwartz, Composite Materials Handbook, McGraw-Hill, Inc., New York, 1992.
9. H. Schmidt and H. Wolter, *J. Non-Cryst. Solids*, 121, 428, 1990.
10. G. L. Wilkes, H. H. Huang, R. H. Glaser, American Chemical Society, Washington DC, 1990, p. 207.
11. E. J. A. Pope, M. Asami, J. D. Mackenzie, *J. Mater. Rev.* 4, 1018, 1989.
12. J. Wen and J. E. Mark, *Polym. Prepr.* 34, 362, 1993.
13. J. Li, "Nanocomposites" in Handbook of Nanophase and Nanostructured Materials, 4, 69, 2003.
14. J. Wen and G. L. Wilkes, *Chem. Mater.* 8, 1667, 1996.
15. G. l. Wilkes and J. Wen, The Polymeric Encyclopedia: Synthesis, Properties and Applications, CRC Press, FL, USA 1996, Vol. 6, p. 4782.

16. J. Wen, Encyclopedia of Materials: Science & Technology, Elsevier Science Ltd, Amsterdam 2001, p. 7610.
17. Dominick V. Rosato, Handbook of Composites, Ed. by George Lubin, Van Nostrand Reinhold, New York, 1982, Chapt. 1, p. 1.
18. Dusan C. Prevorsek, Reference Book for Composites Technology, Ed. by Stuart M. Lee, Technomic Publishing Company, Inc., Lancaster, PA, 1989, Chapt. 9, p. 168.
19. C. C. Evans, Whiskers, Mills & Boon Limited, London, 1972.
20. B. D. Agarwal and L. J. Broutman, Analysis and Performance of Fiber Composites, John Wiley & Sons, New York, 1980.
21. Fiberglas Plus Design: A Comparison of Materials & Process for fiber Glass Composites, Owens-Corning Fiberglas Corporation, Grandville, OH, 1987.
22. W. V. Titow and B. J. Lanham, Reinforced Thermoplastics, John Wiley & Sons, New York, 1975, p. 55.
23. W. V. Titow and B. J. Lanham, Reinforced Thermoplastics, John Wiley & Sons, New York, 1975, p. 54.
24. L. S. Penn and J. D. Muzzy, Handbook of Composites, Ed. by George Lubin, Van Nostrand Reinhold, New York, 1982, Chapt. 5, p. 57.
25. Raymond B. Seymour, Polymeric Composites, VSP BV, The Netherland, 1990, p. 146.
26. A. S. Wood, "Unmatched Performance Sparks a Buildup in Ketone Resins", Modern Plastics, pp. 46–48, April 1987.
27. I. Y. Chang and J. K. Lee, J. Thermoplastic Composite Materials, Vol. 1, pp. 277–296, July 1988.
28. Raymond B. Seymour, Polymeric Composites, VSP BV, The Netherland, 1990, pp. 126–127.
29. W. V. Titow and B. J. Lanham, Reinforced Thermoplastics, John Wiley & Sons, New York, 1975, p. 69.
30. W. V. Titow and B. J. Lanham, Reinforced Thermoplastics, John Wiley & Sons, New York, 1975, p. 68.
31. H. Updegraff, Handbook of Composites, Ed. by George Lubin, Van Nostrand Reinhold, New York, 1982, Chapt. 2, p. 19.
32. M. B. Launikitis, Handbook of Composites, Ed. by George Lubin, Van Nostrand Reinhold, New York, 1982, Chapt. 3, p. 38.
33. Raymond B. Seymour, Polymeric Composites, VSP BV, The Netherland, 1990, p. 112.
34. M. Stander, Handbook of Composites, Ed. by George Lubin, Van Nostrand Reinhold, New York, 1982, Chapt. 4, p. 50.
35. L. S. Penn and J. D. Muzzy, Handbook of Composites, Ed. by George Lubin, Van Nostrand Reinhold, New York, 1982, Chapt. 5, p. 57.
36. W. V. Titow and B. J. Lanham, Reinforced Thermoplastics, John Wiley & Sons, New York, 1975, p. 55.
37. D. M. Riggs, R. J. Shuford, R. W, Lewis, Handbook of Composites, Ed. by George Lubin, Van Nostrand Reinhold, New York, 1982, Chapt. 11, p. 196.
38. Vincent Sussman, Handbook of Fillers for Plastics, Ed. by Harry S. Katz and John V. Milewski, Van Nostrand Reinhols Company, New Yowk, 1987, Chapt. 13, p. 262.
39. C. C. Chiao and T. T. Chiao, Handbook of Composites, Ed. by George Lubin, Van Nostrand Reinhold, New York, 1982, Chapt. 12, p. 272.
40. C. Wittman and G. D. Shock, Handbook of Composites, Ed. by George Lubin, Van Nostrand Reinhold, New York, 1982, Chapt. 13, p. 321.
41. J. A. Radosta and N. C. Trivedi, Handbook of Fillers for Plastics, Ed. by Harry S. Katz and John V. Milewski, Van Nostrand Reinhols Company, New York, 1987, Chapt. 11, pp. 224–228.
42. Y. Chang, "PEKK as a New Thermoplastic Matrix for High Performance Composites", SAMPE Quarterly, pp. 29–34, July 1988.

CHAPTER 29

Polymer Networks and Gels

Ferenc Horkay* and Gregory B. McKenna†

*National Institutes of Health, National Institute of Child Health and Human Development, Laboratory of Integrative and Medical Biophysics, Section on Tissue Biophysics and Biomimetics, Bethesda, MD 20892
†Department of Chemical Engineering, Texas Tech University, Lubbock, TX 79409-3121

Abstract: When long polymer molecules are chemically linked together to form a three-dimensional network, the resulting material exhibits a unique set of properties that have come to be referred to as "rubberlike." Among these are large deformation elasticity which has important consequences for mechanical behavior and resistance to solvent attack. As for the latter, when solvent molecules penetrate into the polymer it undergoes swelling rather than dissolution, and the diluted network is referred to as a chemically crosslinked gel. A survey of the thermodynamics and mechanics of crosslinked gels is presented. Subjects include the phenomenological description of crosslinked networks within the framework of finite elasticity theory and continuum thermodynamics. Particular emphasis is placed on the Valanis–Landel form of the strain energy density function. Several statistical mechanical models of rubber elasticity are also presented. Of particular usefulness are the affine and phantom network models, which are commonly used to derive information about the molecular parameters of the gel from swelling or mechanical measurements. Techniques for using these models and the more modern Flory–Erman constrained junction model and its most recent modifications are described. The application of Scaling Theory to polymer gels is also considered.

Key Words: Crosslinked Rubber, Flory–Rehner Hypothesis, Gels, Networks, Polymer, Rubber Elasticity, Scaling Theory, Solution Thermodynamics, Swelling, Valanis–Landel Function.

29.1 INTRODUCTION

Polymer networks and gels have a wide range of technical and biological applications. Crosslinked polymers are the building blocks of systems as different as rubber tires and scaffolds for tissue engineering. Morphology, molecular and supermolecular structures play important roles, especially when considering processing and final properties. While such materials have been the subjects of experimental and theoretical investigations for more than six decades, their understanding still presents a challenge. Gels exhibit both solid-like and liquid-like properties. The three-dimensional network structure obtained by joining long flexible polymer strands at junction points is the most important molecular characteristic required to achieve "rubberlike" behavior. Numerous models have been proposed to develop a rigorous molecular description of polymer gels. Statistical mechanical theories along these lines encounter serious mathematical difficulties. Rubber elasticity theories, therefore, omit a detailed description of the conformation of polymer chains. Earlier models focus on the effects of topological constraints on the crosslinks. Modern theories are made more realistic by applying the constraints to other parts of the chains. As a result, it is of great interest and importance to understand the structure–property relationships that determine network and gel behaviors.

To begin, when long polymer molecules are chemically linked together to form a three-dimensional network, the resulting material exhibits a unique set of properties that have come to be referred to as rubberlike. Among these are large deformation elasticity which has important consequences for mechanical behavior and resistance to solvent attack. As for the latter, when solvent molecules penetrate into the polymer it undergoes swelling rather than dissolution, and the diluted network is referred to as a chemically crosslinked gel. While there are several structures that exhibit gellike behavior, e.g., (1) covalent networks of large chain molecules, (2) physical networks formed by aggregation of polymer chains (gelatin, agarose), (3) lamellar, fibrillar, or reticular systems exhibiting partially ordered structures (clays, surfactants, etc.), the focus of this work is solely on elastomeric polymer networks containing a three-dimensional permanent structure of high molecular weight chain molecules swollen in a low molecular weight diluent as depicted in Fig. 29.1.

The covalent network, composed of long flexible chains capable of adopting large conformational changes (chain deformations), extends throughout the sample providing the ability to undergo large and reversible (elastic) deformations and a corresponding ability to swell rather than dissolve. Though the molecular origins of rubber elasticity were recognized as early as the 1930s and 1940s [1–5], a complete theoretical description of the swelling behavior of rubberlike polymers has yet to be achieved. The result is that, while there is a general understanding of the behavior of crosslinked materials within the framework of some "classical" models of rubber elasticity, there are still several unresolved problems. For example, even the fundamental assumption, originally put forth by Frenkel [5], Flory and Rehner [2,4] that the free energy of mixing of a solvent and rubber network can be separated into an elastic term for the network and a mixing term for the solvent and polymer has been a subject for much research and discussion over the years [6–32].

There is a diversity of theroetical models used to elucidate the relationships between the molecular parameters of the network and the various experimental results [33–57]. Hence, the resulting deduction of the molecular structure of the network can depend on the model chosen for data analysis. Additionally, the structure of the networks at the supermolecular level is a function of the preparation conditions (temperature, concentration at crosslinking, chemical nature of the crosslinker, etc.). During network formation imperfections in the structure may also develop. In many cases the crosslinking process leads to fixation of otherwise nonequilibrium states. A wide variety of molecular superstructures may be produced within networks prepared from the same starting materials. This makes comparisons of experimental results from different literature sources extremely complicated. Consequently, a simple tabulation of previously published data is not particularly useful.

The present work is intended to survey briefly the basic thermodynamic considerations of rubber elasticity and

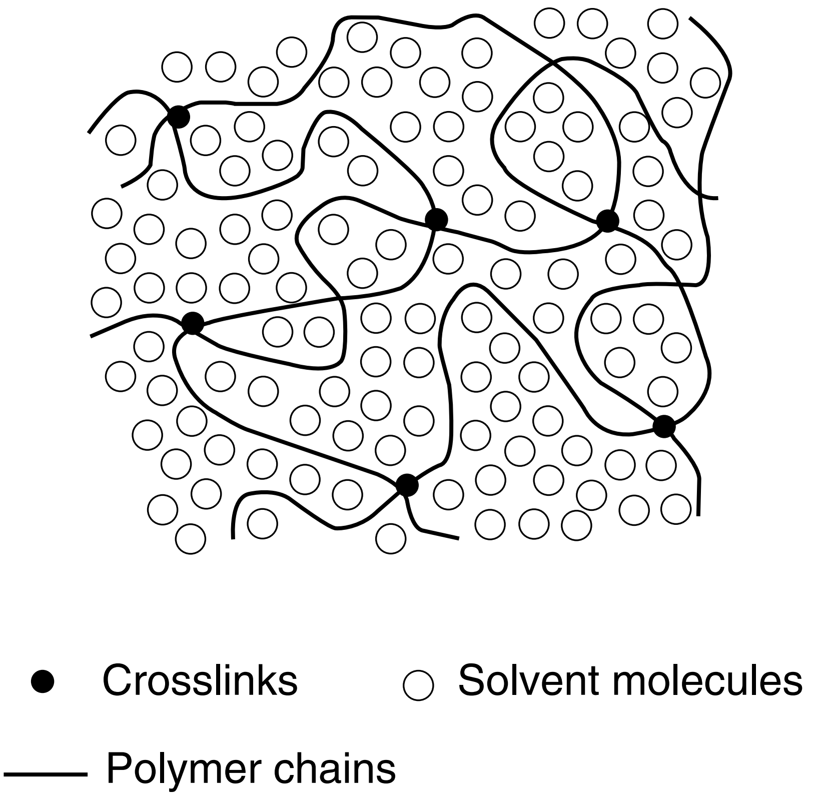

FIGURE 29.1. Schematic representation of a chemically crosslinked polymer network swollen by a low molecular weight solvent.

swelling from both a continuum point of view and with regard to existing network models. Our goal is to illustrate the range of applicability and the limitations of the different approaches for the description of experimental data. The main emphasis is to discuss the structure–property relationships of amorphous polymer networks and gels. We briefly summarize what we believe are the most important ideas of the theories, and compare them with experimental observations made on well-defined networks. For details of each model the reader is referred to the original literature. We focus exclusively on the equilibrium properties of model networks in the dry and swollen states, and the relationships between macroscopically measurable physical quantities. We do not deal with the consequences of the morphology and supermolecular architecture of the polymer network, which can be revealed by scattering measurements. Certain fundamental topics (e.g., effect of charged groups, finite chain extensibility, contribution of filler particles, dynamic properties such as relaxation behavior) are not discussed here.

Additionally, this work should provide the reader with the ability to use the models to obtain estimates of the molecular structure of the gel through analysis and interpretation of typical sets of experimental data. Conversely, the swelling and mechanical responses of new networks should be able to be estimated from a chemist's knowledge of the molecular parameters of the network.

29.2 THEORETICAL BACKGROUND

29.2.1 General Considerations

In thinking about the behavior of rubber networks and gels, there are two features of behavior that we will consider in the following. First, the fundamental nature of the elastomeric network itself in the undiluted state needs to be weighed. This will be done using both the phenomenological theories of rubber elasticity and the molecular (statistical mechanical) models. Both approaches result in forms of the free energy function (Helmholtz) of the network and ultimately need to give the same descriptions of the phenomenological behavior of the dry network. Second, we will consider the specific behavior of the swollen network or gel from similar considerations. In the latter case the formulation of a mixing free energy as a function of the swelling ratio is also required in addition to the elastic free energy. We also remark that the mere presence of the crosslink sites may alter the expressions for the free energy of mixing.

Laboratory measurements, for the most part, record the macroscopic behavior of the material. Depending on the purposes of the experimenter, the link between the molecular models and the phenomenological models provides a basis for either deducing molecular parameters from the measurements or for predicting future measurements from known molecular structures. The latter is primarily important to estimate the physical properties of a given gel whose molecular structure is known. The background provided in what follows should permit one to do both within the limitations of current knowledge.

29.2.2 The Strain Energy Density Function—The Mechanical Contribution to the Helmholtz Free Energy

Continuum Description

There is an extensive body of literature describing the stress–strain response of rubberlike materials that is based upon the concepts of Finite Elasticity Theory which was originally developed by Rivlin and others [58,59]. The reader is referred to this literature for further details of the relevant developments. For the purposes of this paper, we will discuss the developments of the so-called Valanis–Landel strain energy density function, [60] because it is of the form that most commonly results from the statistical mechanical models of rubber networks and has been very successful in describing the mechanical response of cross-linked rubber. It is resultingly very useful in understanding the behavior of swollen networks.

Here we begin with a sample of rubber having initial dimensions l_1, l_2, l_3. We deform it by an amount $\Delta l_1, \Delta l_2, \Delta l_3$ and define the stretch (ratio) in each direction as $\lambda_i = (l_i + \Delta l_i)/l_i = l/l_i$. The purpose of Finite Elasticity Theory has been to relate the deformations of the material to the stresses needed to obtain the deformation. This is done through the strain energy density function, which we will describe using the Valanis–Landel formalism as $W(\lambda_1, \lambda_2, \lambda_3)$. Importantly, as we will see later, this is the mechanical contribution to the Helmholtz free energy. Valanis and Landel assumed [60] that the strain energy density function is a separable function of the stretches λ_i:

$$W(\lambda_1, \lambda_2, \lambda_3) = w(\lambda_1) + w(\lambda_2) + w(\lambda_3) + a \ln(\lambda_1 \lambda_2 \lambda_3). \tag{29.1}$$

While the term $a \ln(\lambda_1\lambda_2\lambda_3)$ is not important in the mechanical response, because of the incompressibility assumption, it may be important in swelling [61]. We also note that some of the molecular models include this logarithmic term. Then, the principal stresses σ_{ii} in any deformation can be related through the strain energy function and deformations as follows:

$$\sigma_{ii} - \sigma_{jj} = \lambda_i\, w'(\lambda_i) - \lambda_j\, w'(\lambda_j), \tag{29.2}$$

where $w'(\lambda) = \mathrm{d}w(\lambda)/\mathrm{d}\lambda$ is the derivative of the VL function $w(\lambda)$. We note that the stresses are the true stresses in that they are referred to the deformed sample geometry. In the dry, unswollen rubber, the material is generally assumed to be incompressible, meaning that the distortional or shape changing deformations are much more easily made than are the volume changing ones, so the latter are negligible. Hence Eq. (29.2) is written in terms of the principal stress differences. In the case of a uniaxial deformation $\lambda = \lambda_1$ in the 1 direction Eq. (29.2) becomes:

$$\sigma_{11} - \sigma_{22} = \lambda_1\, w'(\lambda_1) - \lambda_2\, w'(\lambda_2) \tag{29.3}$$

and because of the incompressibility condition that $\lambda_1\lambda_2\lambda_3 = 1$ we find that $\lambda_2 = \lambda_1^{-1/2}$ and Eq. (29.3) becomes:

$$\sigma_{11} - \sigma_{22} = \lambda\, w'(\lambda) - \lambda^{-1/2} w'(\lambda^{-1/2}), \tag{29.4}$$

where $\lambda = \lambda_1$. For uniaxial extension $\lambda > 1$ while for uniaxial compression $\lambda < 1$.

From a practical viewpoint, Eq. (29.4) can be used to describe the stress–strain relation of a material if $w'(\lambda)$ is known. $w'(\lambda)$ can be obtained in the laboratory in various ways, such as pure shear experiments as described by Valanis and Landel [60], by torsional measurements as described by Kearsley and Zapas [62] and by a combination of tension and compression experiments as also described by Kearsley and Zapas [62]. Treloar and co-workers [63] have also shown that the VL function description of the mechanical response of rubber is a very good one. The reader is referred to the original literature for these methods.

Another point to keep in mind here is that, in most models, the description of rubber elasticity given from statistical mechanical models results in a Valanis–Landel form of strain energy density function. This will be important in the following developments. We now look at some common representations of the strain energy density function used to describe the stress–strain behavior of crosslinked rubber.

There are two common phenomenological strain energy functions that have been used to describe the stress–strain response of rubber [58,59,64]. These are referred to as the Neo-Hookean form and the Mooney–Rivlin form and both can be written as Valanis–Landel forms, although they represent truncated forms of more general strain energy density functions. The Neo-Hookean form is a special form of the Mooney–Rivlin form, so we will begin with the latter. For a Mooney–Rivlin material the strain energy density function is written as:

$$W(\lambda_1,\lambda_2,\lambda_3) = C_1(\lambda_1^2 + \lambda_2^2 + \lambda_3^2 - 3) + C_2(\lambda_1^{-2} + \lambda_2^{-2} + \lambda_3^{-2} - 3) \tag{29.5}$$

and we see that the VL function for this is of the form $w(\lambda_i) = C_1\lambda_i^2 + C_2\lambda_i^{-2}$ and the VL derivative is given as:

$$w'(\lambda_i) = 2C_1\lambda_i - 2C_2\lambda_i^{-3}, \tag{29.6}$$

where C_1 and C_2 are material constants, often referred to as the Mooney–Rivlin Coefficients.

For uniaxial deformations of magnitude λ one then writes Eq. (29.4) for the Mooney–Rivlin stress–strain response as:

$$\sigma_{11} - \sigma_{22} = (\lambda^2 - 1/\lambda)\{2C_1 + 2C_2/\lambda\}. \tag{29.7}$$

Equation (29.7) makes obvious the reasons for the representation of experimental data in the so-called Mooney–Rivlin plot. If the material has a Mooney–Rivlin strain energy density function then a plot of $(\sigma_{11} - \sigma_{22})/(\lambda^2 - 1/\lambda)$ vs.$1/\lambda$ results in a straight line with the slope and intercept at $\lambda = 1$ determining $2C_2$ and $(2C_1 + 2C_2)$, respectively.

For the Neo-Hookean material, the strain energy density function is the same as the Mooney–Rivlin material but with $C_2 = 0$:

$$W(\lambda_1,\lambda_2,\lambda_3) = C_1(\lambda_1^2 + \lambda_2^2 + \lambda_3^2 - 3). \tag{29.8}$$

The VL derivative is:

$$w'(\lambda_i) = 2C_1\lambda_i. \tag{29.9}$$

The corresponding reduced stress σ_R is:

$$\sigma_R = (\sigma_{11} - \sigma_{22})/(\lambda^2 - 1/\lambda) = 2C_1. \tag{29.10}$$

Hence, in the Mooney–Rivlin plot, the stress–strain data are reduced to a line of slope zero.

A point worth noting here is that several of the molecular models that will be described in the subsequent sections are Neo-Hookean in form. Normally, dry rubbers do not exhibit Neo-Hookean behavior. As for the Mooney–Rivlin form of strain energy density function, rubbers may follow such behavior in extension, yet they do not behave as Mooney–Rivlin materials in compression. In Fig. 29.2, we depict typical experimental data for a polydimethylsiloxane network [39] and compare the response to Mooney–Rivlin and Neo-Hookean behaviors. The horizontal lines represent the affine and the phantom limits (see "Network Models" in Section 29.2.2). The straight line in the range $\lambda^{-1} < 1$ shows the fit of the Mooney–Rivlin equation to the experimental data points.

Statistical Theories

Structural Characteristics of Polymer Networks

In this section we discuss the most important structural parameters characteristic of an ideal polymer network. The structure of a real network always displays deviation from that of an ideal network. Network defects, such as unreacted functionalities, cyclic structures and entanglements, arise from the statistics of the crosslinking process. The crosslinking reaction, in general, results in a length distribution for the network chains. In addition to the molecular imperfections, real networks always contain inhomogeneities, i.e., regions in which the polymer concentration is permanently higher than the average concentration. The topological structure of any real network can be very complex and treatment of the topology is beyond the scope of the present work. (The reader is referred to [56,66–69] for discussions of this topic.) It is worthwhile, however, to define the structural parameters for a perfect network because it allows us to treat any real network by reference to these parameters.

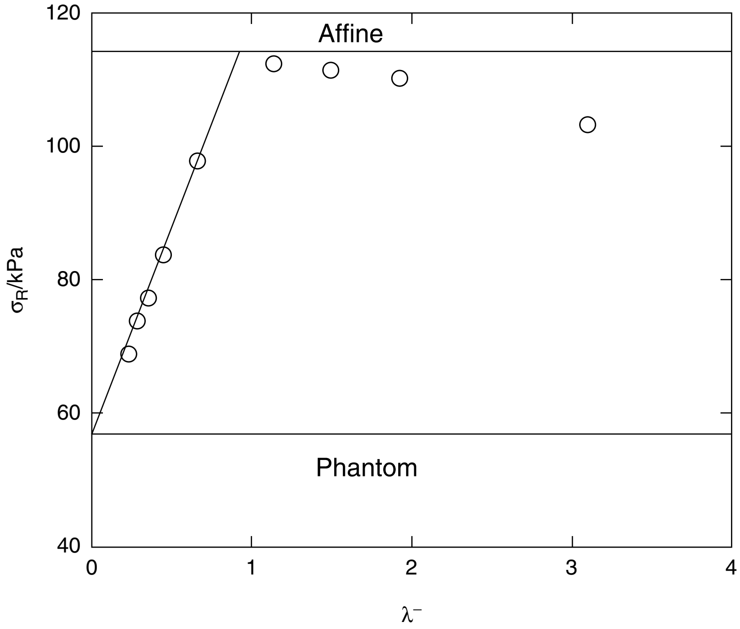

FIGURE 29.2. Comparison of typical stress–strain data for PDMS rubber [39] in a "Mooney–Rivlin" plot with "Neo-Hookean" and "Mooney–Rivlin" strain energy function descriptions. (See text for discussion).

Statistical models yield explicit expressions for the relation between the molecular structure of the network and the elastic properties.

The most important molecular parameter characteristic of a polymer network is the concentration of the elastic chains or that of the crosslinks connecting the macromolecules. An active junction is joined by at least three paths to the polymer network and an active chain is defined as one terminated by active junctions at both ends. There are several ways to express the extent of crosslinking: (1) the concentration of the elastically active chains, ν_{el}/V_0, where ν_{el} is the number of chains connecting two elastically active junctions and V_0 is the volume of the dry network, (2) the molecular weight of the polymer chains between the junctions

$$M_{\mathrm{c}} = \rho(V_0 N_{\mathrm{A}}/\nu_{\mathrm{el}}), \qquad (29.11)$$

where ρ is the density of the polymer and N_{A} is Avogadro's number, (3) the crosslink density, μ_{el}/V_0, where μ_{el} is the number of the crosslinks and (4) the cycle rank density, ξ/V_0, where ξ is the cycle rank, i.e., the number of the independent circuits in the system. Naturally, these quantities are not independent. The relationship between ν_{el}, μ_{el}, and ξ for a perfect network is given by [35]

$$\xi = \nu_{\mathrm{el}} - \mu_{\mathrm{el}} + 1. \qquad (29.12)$$

In Fig. 29.3 a network structure is shown with $\xi = 4$, $\nu_{\mathrm{el}} = 12$, and $\mu_{\mathrm{el}} = 9$.

Another important parameter is the crosslink functionality, f, which is the number of chains emanating from a network junction. Only junctions with functionality higher than 2 are elastically active. For perfect networks, i.e., crosslinked polymers containing no defects, ν_{el} and μ_{el} are connected by the functionality of the crosslinks [70]

$$\mu_{\mathrm{el}} = (2/f)\nu_{\mathrm{el}}. \qquad (29.13)$$

Real networks always contain molecular imperfections, such as pendant chains bound to the network at one end only, intramolecular loops formed by linking of two units of the same chain, and intermolecular entanglements. For an imperfect tetrafunctional network Flory [4,65] proposed a simple formula for correction for pendant chains

$$\nu_{\mathrm{el}} = \nu_0(1 - 2M_{\mathrm{c}}/M_{\mathrm{n}}), \qquad (29.14)$$

where ν_0 is the total number of chains in the network and M_{n} is the number average molecular weight of the primary molecules.

The extent to which entanglements contribute to network elasticity is not yet fully resolved. In the model of Langley[45], Dossin and Graessley [46–49] a contribution to the equilibrium modulus is associated with the plateau modulus of viscoelasticity. On the other hand, Flory [36] and Erman [38–40] assume that interpenetration of chains is solely reflected by suppression of the fluctuations of junctions.

Another type of network defect occurs due to the presence of inhomogeneities. Clustering of chains or network junctions causes permanent departures from the homogeneous distribution of the polymer throughout the gel. Regions of higher polymer concentration build up that appear as permanent departures from uniformity. They are specific to the given system and dependent upon the condition of crosslinking. The effects of inhomogeneities on the elastic and swelling behavior of the networks has not been considered

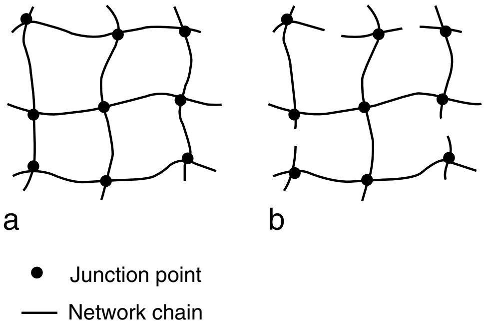

FIGURE 29.3. Schematic representation of a network structure with $\nu_{\mathrm{el}} = 12$, $\mu_{\mathrm{el}} = 9$, and $\xi = 4$ (a). Note that the cycle rank is the number of cuts needed to reduce the network to a tree (b).

quantitatively in any theoretical models of rubber elasticity. The reader is referred to several relevant papers in references [71–74].

Network Models

The primary goal of a general statistical theory is to derive an equation of state for the elastomeric molecular network which will hold for any deformation including swelling. Since the major contribution to the elasticity is entropic the molecular interpretation depends on how the stress affects the conformational distribution of an assembly of chains. The successful statistical model will provide predictive relationships between the molecular structure and topology of the network and its macroscopic behavior, e.g., mechanical and swelling responses.

The classical theories of rubber elasticity rest on two basic assumptions [4]:

1. The elastic free energy of the network is the sum of the elastic free energies of the network chains, i.e., the interactions between the constituent chains are independent of the state of deformation, and do not make any contribution to the elastic free energy; and
2. The end-to-end distribution of the network chains is Gaussian, i.e., the excluded volume interactions are ignored.

The affine and the phantom models derive the behavior of the network from the statistical properties of the individual molecules (single chain models). In the more advanced constrained junction fluctuation model the properties of these two classical models are bridged and interchain interactions are taken into account. We remark for completeness that other molecular models for rubber networks have been proposed [32,57,75–87], however, these are not nearly as widely used and remain the subject of much debate. Here we briefly summarize the basic concepts of the affine, phantom, constrained junction fluctuation, diffused constraint, tube and slip-tube models.

The Affine Model. In the early version of this model it was assumed that the components of length at all scales are deformed affinely [88,89], i.e., local deformations are the same as the macroscopically imposed deformation. Later this view was revised to treat only the displacement of the mean positions of the junctions and the end-to-end vectors of the chains as transforming affinely [6]. Fluctuations of the network junctions are completely suppressed by intermolecular entangling with neighboring coils sharing the same region of space. The elastic free energy of the affine network is given by [35,88–90]

$$\begin{aligned}\Delta F_{\mathrm{el}}^{\mathrm{aff}}/kT &= (\nu_{\mathrm{el}}/2V_0)(\lambda_1^2+\lambda_2^2+\lambda_3^2-3)\\ &\quad-(\mu_{\mathrm{el}}/V_0)\ln(\lambda_1\lambda_2\lambda_3),\end{aligned} \tag{29.15}$$

where ν_{el} and μ_{el} are the number of elastic chains and junctions in the network, respectively. λ_1, λ_2, and λ_3 are the principal deformation ratios, k is the Boltzmann constant and T is absolute temperature. Here we note that the affine model is of the Neo-Hookean form with $C_1 = \nu_{\mathrm{el}}/2V_0$, if there is no volume change upon deformation. Note also the presence of a logarithmic term in the free energy expression.

The Phantom Model. In this model polymer chains are allowed to move freely through one another and the network junctions fluctuate around their mean positions [3,91–93]. The conformation of each chain depends only on the position of its ends and is independent of the conformations of the surrounding chains with which they share the same region of space. The junctions in the network are free to fluctuate around their mean positions and the magnitude of the fluctuations is strain invariant. The positions of the junctions and of the domains of fluctuations deform affinely with macroscopic strain. The result is that the deformation of the mean positions of the end-to-end vectors is not affine in the strain. This is because it is the convolution of the distribution of the mean positions (which is affine) with the distribution of the fluctuations (which is strain invariant, i.e., nonaffine). The elastic free energy of deformation is given by

$$\Delta F_{\mathrm{el}}^{\mathrm{ph}}/kT = (\xi/2V_0)(\lambda_1^2+\lambda_2^2+\lambda_3^2-3) \tag{29.16}$$

and again the free energy function is of the Neo-Hookean form, with $C_1 = \xi/2V_0$.

The Constrained Junction Fluctuation Model. The affine and phantom models are two limiting cases on the network properties and real network behavior is not perfectly described by them (recall Fig. 29.2). Intermolecular entanglements and other steric constraints on the fluctuations of junctions have been postulated as contributing to the elastic free energy. One widely used model proposed to explain deviations from ideal elastic behavior is that of Ronca and Allegra [34] and Flory [36]. They introduced the assumption of constrained fluctuations and of affine deformation of fluctuation domains.

In the constrained junction fluctuation model [36,38–40] developed by Flory and Erman the spatial fluctuations of junctions are inhibited from the large values allowed in the phantom network by restrictions due to neighboring chains. The effect of conformational constraints is assumed to be imposed solely on the network junctions. The situation is illustrated by Fig. 29.4. The mean position of the network junction is located at point A. In a phantom network (Fig. 29.4(a)) the radius of the circle shows the average root-mean-square fluctuation $\langle(\Delta R)^2\rangle^{1/2}_{\mathrm{ph}}$ around the mean position. The domain of constraints due to intermolecular interactions with neighboring chains and to steric requirements is represented by the smaller circle in Fig. 29.4(b). This latter is centered at point B. Because of the effect of constraints, the mean position of the junction (i.e., the equilibrium position in the unstrained network) is removed from point A to point C. The instantaneous position of the junction may differ significantly, however, from the equilibrium position because the junction fluctuates around its mean position. Thus, in addition to the phantom network contribution to the free energy, an important new parameter in this model is the measure of the severity of the constraints relative to those imposed by a phantom network $\kappa = {<}\Delta R^2{>}_{\mathrm{ph}}/{<}\Delta s^2{>}_0$ where ${<}\Delta R^2{>}_{\mathrm{ph}}$ is the mean-squared fluctuation in the positions of junctions from their mean locations in the phantom model, and ${<}\Delta s^2{>}_0$ is the mean-squared fluctuation of junctions from their mean positions under the action of constraints. The range of κ therefore is from 0 (phantom limit) to ∞ (affine limit). The size of the domains of constraints is assumed to decrease with increasing strain so that the junction fluctuations become larger. If the network is deformed the fluctuations become anisotropic in the stretching direction because the constraints become smaller.

The elastic free energy is given by

$$\Delta F_{\mathrm{el}} = \Delta F^{\mathrm{ph}}_{\mathrm{el}} + \Delta F^{\mathrm{c}}_{\mathrm{el}} \qquad (29.17)$$

where $\Delta F^{\mathrm{c}}_{\mathrm{el}}$ is the contribution to the elastic free energy arising from entanglement constraints relative to those in the phantom network $\Delta F^{\mathrm{ph}}_{\mathrm{el}}$ (see Eq. 29.16). This term can be written

$$\frac{\Delta F^{\mathrm{c}}_{\mathrm{el}}}{kT} = \frac{\mu_{\mathrm{el}}}{2V_0}\sum_{t=1}^{3}[(1+g_t)B_t - \ln((B_t+1)(g_tB_t+1))] \qquad (29.18a)$$

with

$$B_t = (\lambda_t - 1)(1 + \lambda_t - \zeta\lambda_t^2)(1 + g_t)^{-2}, \qquad (29.18b)$$

$$g_t = \lambda_t^2[\kappa^{-1} + \zeta(\lambda_t - 1)], \qquad (29.18c)$$

where the parameter ζ characterizes the nonaffine transformation of the domains of constraint with deformation.

Importantly, the model spans the behavior between the phantom and affine models. When $\kappa = \infty$ and $\zeta = 0$ we recover the affine network behavior. In this case the junction fluctuations are completely suppressed, i.e., ${<}\Delta s^2{>}_0 = 0$. When $\kappa = 0$, i.e., the junctions are free to fluctuate, we recover the phantom network model.

The constrained junction fluctuation theory was modified by Erman and Monnerie [94]. The fundamental difference between the modified and the original models is the adoption of the assumption that constraints affect the centers of mass of the chains rather than the junction points only. They considered two different cases: (1) the fluctuations of all points along the chains in the phantom network are independent of macroscopic strain (constrained chain scheme, CC) and (2) the fluctuations of the points in the phantom network are dependent on the macroscopic strain, only the junctions are invariant to strain (modified constrained chain

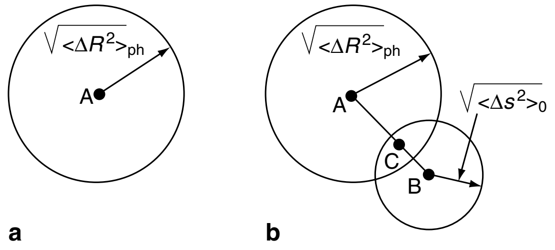

FIGURE 29.4. Effect of constraints on the fluctuations of network junctions. (a) Phantom model and (b) constrained junction fluctuation model. Note that the domain boundaries (circles in the figures) are diffuse rather than rigid. The action of domain constraint is assumed to be a Gaussian function of the distance of the junction from B similar to the action of the phantom network being a Gaussian function of ΔR from the mean position A.

scheme, MCC). The important consequence is that κ of the constrained junction fluctuation theory has been replaced by the function [94]

$$h(\lambda_x) = \kappa_G[1 + (\lambda_x^2 - 1)\Phi]^{-1}, \qquad (29.19a)$$

where κ_G is a parameter corresponding to κ, and

$$\Phi = (1 - 2/f)^2/3 \quad \text{(CCmodel)}, \qquad (29.19b)$$

$$\Phi = (1 - 2/f)^2 \quad \text{(MCCmodel)}. \qquad (29.19c)$$

Both constrained chain models predict that the elastic modulus exceeds the value obtained from the phantom model, and according to the MCC scheme it exhibits a more sensitive dependence upon elongation or swelling than given by the original Flory–Erman theory. The effect of constraints is represented by a single parameter κ_G instead of the two parameters κ and ζ in the previous model, which makes the new theory more straightforward for the interpretation of the experimental stress–strain-swelling data.

We note that the free energy function in the Flory–Erman model is a specific form of the Valanis–Landel strain energy density function. McKenna and Hinkley [61] determined the Valanis–Landel function for the junction constraint model

$$w'(\lambda_t) = \xi kT\lambda_t + (\mu_{\mathrm{el}}kT/2)\{B_t^*(1 + g_t) + g_t^*B_t - B_t^*(B_t + 1)^{-1} - (g_tB_t^* + B_tg_t^*)(g_tB_t + 1)^{-1}\}, \qquad (29.20)$$

where

$$B_t^* = B_t\{[2\lambda_t(\lambda_t - 1)] - 1 + (1 - 2\zeta\lambda_t)[2\lambda_t(1 + \lambda_t - \zeta\lambda_t^2)]^{-1} + 2g_t^*(1 + g_t)^{-1}\} \qquad (29.21)$$

and

$$g_t^* = \kappa^{-1} - \zeta(1 - 3\lambda_t/2). \qquad (29.22)$$

We will come back to these models subsequently.

Diffused Constraint Model of Polymer Networks. This model, which is an extension of the Erman–Monnerie model, is more realistic in that the constraints are assumed to act continuously along the chains, instead of allowing the constraints to affect only the fluctuations of the junctions or the centers of mass of the network chains. Because the constraints affect fluctuations of all points along the macromolecule, the elastic energy of constraints must be averaged over all segments of the chain. Following a similar argument used by Flory [36] in the original constrained-junction theory, Kloczkowski, Mark, and Erman [95] derived the elastic free energy of the constraints

$$\Delta F_{\mathrm{el^c}} = \frac{1}{2}\nu kT\sum_{t=1}^{3}\int_0^1 W(\theta)[B_t(\theta) + D_t(\theta) - \ln[B_t(\theta) + 1] - \ln[D_t(\theta) + 1]]\mathrm{d}\theta \qquad (29.23)$$

with

$$B_t(\theta) = \frac{\kappa^2(\theta)(\lambda_t^2 - 1)}{[\lambda_t^2 + \kappa(\theta)]^2} \qquad (29.23a)$$

and

$$D_t(\theta) = \frac{B_t(\theta)\lambda_t^2}{\kappa(\theta)}. \qquad (29.23b)$$

In Eq. (29.23) $W(\theta)$ is the distribution of constraints among different points along the network chain and $\theta = i/n$ is the position of the ith segment of the chain as a fraction of the contour length between two crosslinks. If the distribution is uniform, then $W(\theta) = 1$ inside the integrand of Eq. (29.23). In the case when constraints are assumed to affect only fluctuations of junctions (as in the constrained-junction theory), θ is limited to $\theta = 0$ or $\theta = 1$ only. [95] It is important to note that this theory does not reduce identically to the constrained-chain theory, because the latter characterizes the deformation-dependent fluctuations of the centers of mass of the chains and not the deformation-independent fluctuations of the midpoints [95].

In summary, the common feature of all constrained chain models is that they impose only limited constraints on chain fluctuations. [101] The constrained-junction fluctuation model restricts fluctuations of junctions and of the center of mass of network chains. The diffused constraint model restricts fluctuations of a single randomly chosen monomer for each network strand. Consequently, all these models can only represent the crossover between the phantom and affine limits. [101] The phantom limit corresponds to a weak constraining case, while the affine limit corresponds to a very strong constraining potential.

Tube Models. Several versions of the tube models have been developed. These models take into account the fact that constraints act along the whole chain and restrict the fluctuations of all monomers of the chain. The tube models consider that each network strand is confined within a configurational tube with a harmonic potential modeling topological constraints of entanglements. [101,120] The field is described as an uncrossable tube of constraints the centerline of which is the primitive path of the strand. The constraining field of force penalizes excursions of a strand [126] from its primitive path, i.e., a random-walk trajectory running from one network junction to the other. [126] The free energy penalty increases with excursion amplitude. The elastic free energy is given by the sum of two terms. One has the Gaussian form due to chain connectivity, while the other represents the loss of the degrees of freedom of the chains due to their spatial localization originating from entanglements. [120]

In the Edwards tube model [80] the topological potential is applied to every monomer of the chain restricting its fluctuations to a confining tube with the diameter $a \approx bN_{\mathrm{e}}^{1/2}$ where N_{e} is the degree of polymerization between network entanglements. [101] In the model this potential is independent of the network deformation and the tube diameter changes affinely with the macroscopic deformation of the network, $a \sim \lambda$. However, this assumption is unrealistic and disagrees with the experimental observations. [97,101]

In the Gaylord–Douglas model [57,81] the chains are localized in a tube defined by the interactions with neighboring chains. The first term of the elastic free energy is the same as that of a phantom network model, while the second term accounts for the loss of degrees of freedom of the chains due to chain localization. In the dry network the cross-sectional dimension of the tube is of the order of the hard-core cross-sectional radius of the polymer chain, and the volume of the tube is comparable with the chain molecular volume. The tube volume is considered to be invariant with macroscopic strain, since the molecular volume of the chains is independent of the deformation. The elastic free energy is given by

$$\Delta F_{\mathrm{el}} = (G_{\mathrm{net}}/2)(\lambda_1^2 + \lambda_2^2 + \lambda_3^2 - 3) + G_{\mathrm{e}}(\lambda_1 + \lambda_2 + \lambda_3 - 3), \qquad (29.24)$$

where

$$G_{\mathrm{net}} = \nu_{\mathrm{el}} kT/(2V_0) \qquad (29.24\mathrm{a})$$

and

$$G_{\mathrm{e}} = \gamma G_{\mathrm{net}} + G_{\mathrm{N}}. \qquad (29.24\mathrm{b})$$

G_{N} is the plateau modulus of the polymer melt, V_0 is the volume of the dry network, and γ is a constant. In the absence of localization interactions, $G_{\mathrm{e}} = 0$, and Eq. (29.24) reduces to the result obtained for the phantom model. Since the constraining effect of the surrounding network chains diminishes upon swelling, G_{e} is predicted to depend on swelling as well as the conditions under which the network was formed [32,96]. The concentration dependence of G_{e} is especially large for lightly crosslinked gels (roughly linear in the concentration), however, the concentration dependence for highly crosslinked networks is relatively weak (comparable to that of the phantom model).

A challenging problem in the theory of rubber elasticity is to determine how the macroscopic deformation of the network affects the conformation of the polymer chains. At macroscopic length scales polymer networks behave as elastic solids, while at microscopic length scales the network chains move relatively freely. The elasticity is mainly entropic and is governed by deformations occurring on short length scales. Therefore, it is important to distinguish between affine and nonaffine length scales. [97] The affine length is the shortest length scale at which the network deformation is the same as that of the macroscopic deformation of the sample. At smaller length scales the deformation of the network chains is nonaffine. [97]

The nonaffine tube model developed by Rubinstein and Panyukov [97] captures the basic features of the phantom and affine models. In this model the amplitude of fluctuations that defines the tube diameter changes proportionally with the deformation of the network. The network deforms affinely on length scales larger than the affine length, R_{aff}. However, on length scales smaller than R_{aff} the confining potential has little effect on the conformation of the individual chains. The most important feature of this model is that the tube diameter a changes nonaffinely with network deformation $a \sim \lambda^{1/2}$. The prediction for the elastic free energy and the reduced force of the nonaffine tube model is [97]

$$\Delta F^{\mathrm{el}} = \Delta F^{\mathrm{el}}_{\mathrm{ph}} + \frac{ckT}{2N_{\mathrm{e}}} \sum_{\alpha} \left(\lambda_\alpha + \frac{1}{\lambda_\alpha} \right), \qquad (29.25)$$

$$f^*(\lambda^{-1}) = G_{\mathrm{ph}} + \frac{G_{\mathrm{e}}}{\lambda - \lambda^{1/2} + 1}, \qquad (29.26)$$

where c is the monomer concentration, G_{ph} is the phantom modulus, G_{e} is the entanglement contribution to the modulus, and N_{e} is the number of monomers between entanglements.

A more advanced version of this model combines the ideas of slip-link [98] and tube models. The "slip-tube" model allows slippage of the network chains and redistribution of the monomers between different sections of the tube [101]. The idea of slippage of the chain along the contour of the tube was originally proposed by de Gennes [105] in the reptation model of polymer melts, and the analysis of the redistribution of stored length was made by Doi [100]. The basic concept of the slip-link models is that permanent entanglements act as slip-links connecting neighboring chains. The slip-links are allowed to pass through each other, but each of them can slide along the chain only up to a limited distance. [101] If this distance is equal to the chain length, the slip-link model reduces to the phantom network model. In the opposite limit, when the sliding distance of the slip-links is small compared to the average distance between neighboring slip-links, the model is reduced to the affine model.

In the slip-tube model [101] the topological constraints imposed by the neighboring network chains are represented by virtual chains attached to the elastic nonfluctuating background at one end and ending with slip-links at the other. The network chains pass through these slip-links but they are not allowed to pass through each other. [101] The amplitude of the slip-link fluctuations depends on the density of the slip-links. At high density the slip-links are located at every monomer and the fluctuations are completely suppressed. In this limit the slip-tube model reduces to the nonaffine tube model. If slippage along the tube is allowed the network chains redistribute their lengths along the contour of their confining tubes. [101] In the anisotropically deformed network the number of monomers in a given direction α will be changed due to the slippage.

The elastic free energy of the network is given as [101]

$$\Delta F^{\mathrm{el}} = \Delta F^{\mathrm{el}}_{\mathrm{ph}} + \frac{kT\nu L}{2}\sum_{\alpha}\left(\frac{\lambda_\alpha}{g_\alpha^{1/2}} + \frac{g_\alpha^{1/2}}{\lambda_\alpha}\right) - \nu TS\{g_\alpha\}, \qquad (29.27)$$

where L is the number of slip-links per network chain and g_α is the "redistribution parameter" that depends on the number of monomers along the axis α in the deformed network relative to that in the undeformed network. The function $S\{g_\alpha\}$ is related to the entropy of the degrees of freedom corresponding to different positions of slip-links along the chains.

Numerical solution of the slip-tube model yields for the reduced stress [101]

$$f^*(\lambda^{-1}) = G_{\mathrm{ph}} + \frac{G_{\mathrm{e}}}{0.74\lambda + 0.61\lambda^{1/2} - 0.35}. \qquad (29.28)$$

In this equation the deformation ratio λ appears only in the entanglement contribution. Thus, the experimental data can be analyzed in the form of a universal plot. Moreover, Eq. (29.28) allows one to separate the phantom and entanglement contributions to the elasticity of the network.

The Mixing Contribution to the Free Energy

So far we have discussed the behavior of networks in the dry state. In the case of a swollen network additional effects must be taken into account. The thermodynamics of mixing is governed by the interaction between the polymer and the solvent molecules. As we have seen in "Network Models" in Section 29.2.2 in gels the fluctuations of the network junctions are significantly altered by the presence of crosslinks. The formulation of a mixing free energy for the swollen network would require the detailed knowledge of the effect of osmotic forces on the size and shape of the fluctuation domains. This is beyond the scope of the existing molecular theories.

Because of the lack of an explicit molecular theory which accounts for the effect of crosslinking on the structure of a polymer solution, it is generally assumed that the functional dependence of the free energy of mixing in the swollen network is the same as in a polymer solution. Although this is a strong approximation, the application of the theoretical free energy functions derived for polymer solutions provides a simple and straightforward way to interpret the results of mechanical and swelling measurements performed on swollen polymer networks. There are two essentially different ways to describe the thermodynamics of polymer solutions: classical (mean field) theories [4] including recent renormalized models [102,103] and asymptotic scaling theories [104,105] based on the analogy found between critical phenomena and polymer chain statistics.

Flory–Huggins Theory of Polymer Solutions

The classical treatment of polymer solution thermodynamics due to Flory and Huggins [4] is based on a lattice model which assumes a uniform polymer segment concentration throughout the entire system. The free energy of mixing of a polymer solution is given by

$$\Delta F_{\mathrm{mix}} = RT[n_1 \ln(1-\varphi) + n_2 \ln\varphi + \chi n_1 \varphi)], \qquad (29.29)$$

where φ is the volume fraction of the polymer, χ is the Flory–Huggins interaction parameter, and n_1 and n_2 are the numbers of moles of solvent and polymer, respectively. The chemical potential of the solvent is defined as the derivative of the free energy of mixing with respect to amount of solvent

$$\begin{aligned}(\Delta\mu_1)_{\mathrm{mix}} &= (\partial\Delta F_{\mathrm{mix}}/\partial n_1)\\ &= RT[\ln(1-\varphi) + (1-\mathrm{N}^{-1})\varphi + \chi\varphi^2], \qquad (29.30)\end{aligned}$$

where N is the degree of polymerization. For a crosslinked polymer $N = \infty$. In general, χ depends on the polymer concentration [106], i.e.,

$$\chi = \chi_0 + \chi_1\varphi + \ldots, \qquad (29.30a)$$

where χ_0 and χ_1 are constants.

Scaling Theory

In the 1970s a new theory of polymers, taking account of correlations between monomers, was developed based on the analogy found between polymer statistics and critical phenomena [105]. For the chemical potential of mixing in the semidilute region scaling theory yields

$$(\Delta\mu_1)_{\mathrm{mix}} = ART\varphi^n \quad (\varphi^* < \varphi \ll 1), \qquad (29.31)$$

where the prefactor A is characteristic of the polymer/solvent system and the value of the exponent n depends on the thermodynamic quality of the solvent. In a good solvent $n \approx 2.31$, and in the theta condition $n=3$. φ^* is the polymer volume fraction above which the domains of the coils start to overlap, i.e., the volume fraction of the polymer inside a separate coil

$$\varphi^* \propto N/R^3 \propto N^{1-3\nu}, \qquad (29.32)$$

where ν is the excluded volume exponent, the value of which is $\nu \approx 3/5$ (good solvent condition) or $\nu = 1/2$ (theta condition).

De Gennes proposed a description of the properties of swollen polymer networks based on the analogy found between the swollen network and semidilute polymer solutions (φ^* theorem) [105]. The fully swollen gel is expected to maintain a polymer volume fraction, φ_{e}, which is proportional to the overlap concentration. In good solvent condition

$$\varphi_{\mathrm{e}} = z(f)\varphi^* \propto z(f)(1/2-\chi)^{-3/5}N^{-4/5}, \qquad (29.33)$$

where $z(f)$ is a constant factor of the order of unity and f is the crosslink functionality.

Many attempts to explain the results of osmotic and mechanical measurements on swollen polymer networks have invoked analogies with semidilute polymer solutions. Scaling forms for different physical quantities have been derived from the φ^* theorem.

For example, the elastic (shear) modulus of a gel is given by [99,105]

$$G = B(\varphi_e/N_c), \tag{29.34}$$

where φ_e is the volume fraction of the polymer in the fully swollen gel, N_c is the degree of polymerization between crosslink points and B is a constant which depends on the polymer/solvent system. From Eqs. (29.32) and (29.34) it follows that

$$G = B\varphi_e^n, \tag{29.35}$$

where $n = 3\nu/(3\nu - 1)$. Equation (29.35) predicts that the concentration dependence of the elastic moduli of gel homologues (chemically similar gels having different crosslinking densities) follows a simple power law behavior. The value of n depends on the thermodynamic quality of the solvent: in good solvent condition $n \approx 2.31$, in theta condition $n=3$.

Here we note that in the simple scaling theory used earlier, the polymer is considered as an infinitely thin chain possessing length but not volume. At higher polymer concentration, however, the finite volume of the structural elements may no longer be neglected. Advanced scaling theories [102,103] using the Flory–Huggins lattice model as a starting point are able to incorporate the polymer volume into their formalism.

Swelling of Polymer Networks—The Frenkel–Flory–Rehner Hypothesis

A crosslinked polymer exposed to a thermodynamically compatible diluent absorbs solvent molecules. The driving force of the mixing process is mainly entropic. As the volume increases the network chains are deformed and an elastic retractive force develops. The chain deformation causes a decrease in the entropy, because the extended configuration of the chains is less probable. Equilibrium is achieved when these opposing forces are balanced.

The basic assumption in the Frenkel–Flory–Rehner theory describing the swelling of a crosslinked polymer is that the elastic (ΔF_{el}) and mixing (ΔF_{mix}) contributions in the free energy that accompanies the swelling of the dry network are separable and additive [2,4,5]

$$\Delta F = \Delta F_{el} + \Delta F_{mix}, \tag{29.36}$$

where ΔF is the total free energy of the polymer–solvent system. At equilibrium with the pure solvent (at constant temperature and pressure) the free energy is at minimum with respect to any changes in composition, i.e.,

$$\begin{aligned}(\partial \Delta F/\partial n_1) &= \mu_1 - \mu_1^0 = 0 \\ &= (\mu_1 - \mu_1^0)_{mix} + (\mu_1 - \mu_1^0)_{el},\end{aligned} \tag{29.37}$$

where n_1 is the number of moles of solvent, μ_1 is the chemical potential of solvent in the gel and μ_1^0 is the chemical potential of the pure solvent. The subscripts mix and el refer to the mixing and elastic contributions to the chemical potential, respectively. How the Frankel–Flory–Rehner model can be used to relate macroscopic swelling observations to the molecular structure of the network is developed subsequently.

Experimental Characterization of Swollen Polymer Networks

Molecular theories of rubber elasticity (see "Network Models" in Section 29.2.2) allow the interpretation of the experimental data obtained for elastomeric materials in terms of structural characteristics of the network. The most frequently used experimental techniques are stress–strain measurements and swelling measurements.

Stress–Strain Isotherms

Uniaxial stress–strain measurements are often used to characterize polymer networks both in the dry state and in equilibrium with a diluent. The analysis of the stress–strain isotherms is usually performed in terms of the reduced force

$$[f^*] = f^*\varphi^{1/3}/(\alpha - \alpha^{-2}), \tag{29.38}$$

where f^* is the force per unit unstrained cross-section of the unswollen network and α is the deformation ratio relative to the undeformed swollen state of volume V. The relationship between α and λ is given by

$$\lambda_1 = \alpha(V/V_0)^{1/3} \tag{29.39a}$$

and

$$\lambda_2 = \lambda_3 = \alpha^{-1/2}(V/V_0)^{1/3}. \tag{29.39b}$$

In both the phantom and affine models the reduced force is identified with the elastic modulus. In the affine limit the shear modulus is expressed as

$$G_{aff} = [f^*]_{aff} = kT(\nu_{el}/V_0), \tag{29.40}$$

while in the phantom limit

$$G_{ph} = [f^*]_{ph} = kT(\xi/V_0). \tag{29.41}$$

In general, experimental stress–strain isotherms differ from the predictions of the simple statistical theories.

The constrained junction fluctuation theory provides a description of the network behavior which lies between the affine and phantom limits [36,38–40]. According to this theory the elastic force, f, is the sum of two contributions

$$f = f_{\mathrm{ph}} + f_{\mathrm{c}}, \tag{29.42}$$

where f_{ph} is the phantom network contribution and f_{c} arises from the entanglement constraints. The reduced stress $[f^*]$ is given by

$$[f^*] = kT(\xi/V_0)(1 + f_{\mathrm{c}}/f_{\mathrm{ph}}) \tag{29.43}$$

and the expression for $f_{\mathrm{c}}/f_{\mathrm{ph}}$ in uniaxial deformations is

$$f_{\mathrm{c}}/f_{\mathrm{ph}} = (\mu/\xi)[\alpha K(\lambda_x^2) - \alpha^{-2} K(\lambda_y^2)](\alpha - \alpha^{-2})^{-1}, \tag{29.44}$$

where $\lambda_1 = \lambda$ and $\lambda_2 = \lambda^{-1/2}$. The function K is defined by

$$K(\lambda_t^2) = B_t[B_t^*(B_t + 1)^{-1} + g_t(g_t B_t^* + g_t^* B_t)(g_t B_t + 1)^{-1}], \tag{29.45}$$

where B_t,B_t^* and g_t are the same as in Eqs. (29.18), (29.21) and (29.22).

The ratio $f_{\mathrm{c}}/f_{\mathrm{ph}}$ is expected to decrease with increasing deformation, and at $\alpha^{-1} = 0$ the modulus approaches the phantom limit.

The Flory theory considers topological interactions among junctions and chains only in that they restrict junction fluctuations. Ferry [107], Langley [45], Dossin [46] and Graessley [49] assume that these interactions are also present in the small-strain limit. Their argument is based on the existence of a rubbery plateau modulus, G_{N}^0, which is observed in the viscoelastic properties of high molecular weight linear polymers. The plateau modulus is assumed to be a measure of the entanglement interactions between the chains. In a permanent network the interchain entanglements are fixed due to the presence of the chemical bonds. Dossin and Graessley [46] proposed that

$$G = \nu kT(1 - 2h/f)(V/V_0)^{2/3}/V + T_{\mathrm{e}} G_{\mathrm{e}}^{\max}, \tag{29.46}$$

where G is the small-strain modulus, T_{e} is the fraction of the maximum concentration of topological interactions which are permanently trapped by the network, $G_{\mathrm{e}}^{\max}$ is the maximum possible contribution of entangled chains to the modulus, and h is an empirical constant, the value of which is between 0 and 1, depending on the extent to which the junction fluctuations are impeded in the network (h=0 in the affine limit and h=1 in the phantom limit). Thus Eq. (29.46) predicts a small-strain modulus greater than that predicted by the Flory–Erman theory and greater than that of the affine model.

The apparent discrepancy between the Flory theory and the entanglement concept of Dossin and Graessley has been addressed by Gottlieb and Macosco [55]. They pointed out that the two parameters h and κ, both measuring the severity of constraints are related. For the case of a perfect, incompressible, unswollen network the analytical relationship is given by

$$h = 1 - (\kappa^2 + 1)(\kappa + 1 - p/2)^2(\kappa + 1)^{-4}, \tag{29.47}$$

where p is a constant. For the case of the Flory theory p=2. Importantly the Flory–Erman theory has been developed for finite (large) deformations, which is not true of the trapped entanglement model, which resultingly limits the latter's usefulness in terms of making quantitative estimates of experimental results, particularly in large deformation experiments, including swelling.

Swelling Measurements

In addition to mechanical measurements, swelling measurements are frequently used to characterize rubber networks. Of particular interest is the relationship between the molecular weight between crosslinks and the degree of swelling. Unfortunately, the numerical values of the molecular parameters obtained by elastic and swelling measurements strongly depend upon the particular theoretical model used to evaluate the experiments. The model behaviors are described in the following paragraphs. The swelling equation for a phantom network is given as [44,108]:

$$\ln(1 - \varphi_{\mathrm{e}}) + \varphi_{\mathrm{e}} + \chi\varphi_{\mathrm{e}}^2 = -(\xi/N_{\mathrm{A}}V_0)V_1\varphi_{\mathrm{e}}^{1/3}, \tag{29.48}$$

while for an affine network

$$\ln(1 - \varphi_{\mathrm{e}}) + \varphi_{\mathrm{e}} + \chi\varphi_{\mathrm{e}}^2 = -(\xi/N_{\mathrm{A}}V_0)V_1\varphi_{\mathrm{e}}^{1/3}[1 + (\mu/\xi)(1 - \varphi_{\mathrm{e}}^{2/3})], \tag{29.49}$$

where N_{A} is Avogadro's number and the complexity in Eq. (29.49) arises due to the logarithmic contribution to the free energy in the affine network model (see Eqs. (29.1) and (29.15)).

The corresponding equation according to the Flory–Erman constrained junction fluctuation model is

$$\ln(1 - \varphi_{\mathrm{e}}) + \varphi_{\mathrm{e}} + \chi\varphi_{\mathrm{e}}^2 = -(\xi/N_{\mathrm{A}}V_0)V_1\varphi_{\mathrm{e}}^{1/3}[1 + K(\lambda^2)], \tag{29.50}$$

where $K(\lambda^2)$ was defined previously (see Eq. (29.45)). Queslel *et al.* [108] made a comparison between the values of the molecular network parameters calculated through Eqs. (29.48)–(29.50). The highest value of M_{c} (chain molecular weight) is obtained by the affine model. The phantom model yields lower M_{c} than the affine model, because in the former junction fluctuations decrease the impact of chain entropy changes. Using Eq. (29.49) the same elastic contribution as that of an affine network is thus achieved if ξ is higher (or correspondingly M_{c} is smaller). The value of M_{c} determined from the Flory–Erman model lies between these limiting values. It is worth mentioning that Eqs. (29.48) and (29.49) enable one to estimate a range for M_{c} without any prior knowledge of the network structure.

Both the affine and the phantom network models predict that the reduced stress, $[f^*]$, measured in uniaxial deformation is independent of the deformation ratio. However, it became clear from early studies of rubber elasticity that real networks, in general, exhibit significant departures from this prediction: the reduced stress decreases with elongation and also with increasing swelling. It was recognized that the limiting value of the reduced stress at high elongation or swelling ratio is a characteristic quantity of the network.

The detailed calculations according to the constrained junction fluctuation model and other advanced models can only be performed numerically. The fitting of the stress–strain (or swelling) data to the Flory–Erman model, in principle, requires three parameters: $[f^*]_{\mathrm{ph}}$, κ and ζ. Here we briefly outline the steps of the fitting procedure [113,114]:

1. In many cases it is reasonable to take the initial value of $[f^*]_{\mathrm{ph}} = 2C_1$, where $2C_1$ is the first Mooney–Rivlin constant. An alternative possibility is to estimate $[f^*]_{\mathrm{ph}}$ from the stoichiometry of the chemical reaction using Eqs. (29.12)–(29.14) and (29.41).

2. The initial value of κ can be obtained from the Flory–Erman theory on the basis of the following argument [109]. Since κ is assumed to be proportional to the number of chains sharing the volume occupied by one chain, it is the measure of the degree of interpenetration of the network chains, i.e.,

   $$\kappa = I{<}r^2{>}_0^{3/2}(\nu/V_0), \qquad (29.51)$$

   where ${<}r^2{>}_0$ is the unperturbed dimension of a chain and I is a proportionality constant. Expressing Eq. (29.51) in terms of measurable quantities one gets [109]

   $$\kappa = A(2C_1)^{-1/2}\varphi_c^{(4/3)+m}, \qquad (29.52)$$

   where φ_c is the volume fraction of the polymer at crosslinking and $A = I({<}r^2{>}_{0/M})^{3/2}(1-2/f)N_A^{3/2}\rho^{3/2}/(kT)^{1/2}$, where N_A is Avogadro's number, ρ is the density of the polymer and f is the crosslink functionality. The experimental value of A is the order of unity (for PDMS networks Erman and Mark [110] reported $A{=}1.29$ and $m{=}0.385$).

3. In a first approximation the parameter ζ can be assumed to be zero.

4. Using these initial values the differences between theory and experiment should be minimized. In order to achieve this the value of κ obtained in step (2) is used to calculate $[f^*]_{\mathrm{ph}}$ from Eqs. (29.43) and (29.44). Then $2C_1$ in Eq. (29.52) is replaced by $[f^*]_{\mathrm{ph}}$ to obtain a new value of κ. These steps are iterated until κ converges. Using the new values of $[f^*]_{\mathrm{ph}}$ and κ the function $[f^*]$ vs. α^{-1} is calculated from Eq. (29.43).

5. The procedure described in 4 is repeated for a new value of m (and A), and the values of $[f^*]_{\mathrm{ph}}$ and κ are recalculated. The calculation is continued until the error between the experimental and the calculated data reaches a minimum.

6. If the agreement between calculated data and experiment is still not satisfactory, the value of ζ can be varied to match theory and experiment. The values of ζ giving the best agreement with experiments are usually close to zero.

29.3 ANALYSIS OF EXPERIMENTAL RESULTS

29.3.1 General Comments

The primary goal of the molecular theories is to derive the structure–property relationships for polymeric networks. A quantitative understanding of the dependence of the physical properties upon the network structure is essential to deduce molecular parameters (e.g., molecular weight between crosslinks) from measurements. This is also required to synthesize new polymer networks having desired physical properties.

To test the validity of different network theories is particularly difficult because the structure of the network, at the molecular level, is unknown. Usually crosslinks are introduced in a less perfectly controlled manner than desired. The extent of imperfections depends on the mechanism of the crosslinking process, e.g., clustering of chains or junctions may lead to deviations from the complete randomness assumed in the theories. In many cases, the distribution of the network chains and junctions is not uniform throughout the sample.

Analysis of the experimental data obtained for model networks having known structure provides a straightforward way of understanding the structure–property relationships. Such model networks can be synthesized by specific chemical reactions, e.g., by end-linking of well-characterized polymer chains through a controlled chemical reaction. The characteristics of the chains, prior to crosslinking, can be determined using the usual solution characterization techniques (gel chromatography, viscometry, etc.). In this way the average molecular weight between crosslinks (M_c) and the distribution of M_c can be varied in a controlled manner. The crosslink functionality (f) is known from the chemistry of the crosslinking reaction. Since ν_{el} and f are known. $\xi = \nu_{\mathrm{el}} - \mu_{\mathrm{el}} + 1$ is also known. Assuming that the chemical reaction between the end-groups of the chains and the crosslinking agent is stoichiometric, and that the effects of entanglements and network imperfections (cycles, pendent chains) are negligible, the elastic properties of the gel can be predicted. Equations (29.40) and (29.41) allow the elastic modulus both in the phantom and the affine limits to be calculated. The decrease of the modulus with λ depends on the values of κ and ζ in the Flory–Erman theory. Unfortunately, this theory does not make an a priori prediction for these parameters. Since no independent information is available about the actual size of fluctuation domains of junctions and about the anisotropy of these domains, the values of κ and ζ can only be determined empirically using a fitting procedure such as that described in "Swelling Measurements" in Section 29.2.2

The testing of the network models with regard to the prediction of the equilibrium swelling degree of the crosslinked polymer as a function of the thermodynamic activity of the diluent requires further assumptions concerning the mixing free energy contribution. This term is supposed, firstly, to be separable from the total change in the free energy (see Eq. 29.36) and, secondly, to be identical for the gel and for the solution of the uncrosslinked polymer of infinite molecular weight. The latter assumption presumes that the polymer solvent interaction parameter is unaffected by the presence of crosslinks. Thus, the only difference between the swollen network and the polymer solution is the existence of a permanent elastic modulus and the theoretical dependence of the equilibrium volume fraction upon the molecular parameters is predicted by Eqs. (29.48)–(29.50).

The structure of any real network exhibits departures from that of the ideal (model) network. A comparison between the experimental and theoretical values of the network parameters provides quantitative information on the deviation from the behavior of the hypothetical model system, and allows one to treat real networks by reference to the structural parameters of a perfect network.

In the following sections typical experimental results obtained for different network systems and analyzed using several of the theoretical approaches are briefly reviewed. For a more extensive discussion, we refer the reader to a work by Han, Horkay, and McKenna [111] where a critical evaluation of many of the modern theories of molecular rubber elasticity was performed. Based on an analysis of carefully selected data sets reported in the literature, these authors concluded that, of the tested models, the Flory–Erman theory and its modified versions provided the best agreement with the stress–strain data in both the dry and the swollen states for polymer networks.

29.3.2 Determination of the Model Parameters from Stress–Strain Measurements

A large amount of experimental work has been reported on the stress–strain behavior of swollen polymeric networks. Fitting of stress–strain data measured at different degrees of dilution to Eqs. (29.43)–(29.45) enables one to determine ξ,κ, and ζ.

Erman and Flory [39] reanalyzed the data of Allen *et al.* [112] on swollen natural rubber samples crosslinked with dicumyl peroxide. It was found that the shape of the $[f^*]$ vs. α^{-1} curves in a wide range of dilution in *n*-decane ($0.24<\varphi<1$) can be well reproduced using a single set of parameters $[f^*]_{\text{ph}} = 0.166\,\text{Nmm}^2$, $\kappa = 8$, and $\zeta = 0.12$. Similar analysis of the data of Flory and Tatara [33] for radiation crosslinked PDMS samples swollen in benzene yields the values $[f^*]_{\text{ph}} = 0.136\,\text{MPa}$, $\kappa = 6$, and $\zeta = 0.12$. For poly(ethyl acrylate) networks [37] having different crosslink densities swollen in bis(2-ethoxyethyl)ether κ varied in the range 1.8–16.0, and ζ varied between 0.0 and 0.1. It was also found that the stress–strain isotherms for the same networks in the unswollen state and in swelling equilibrium with a diluent are consistently described by the same set of parameters, κ and ζ. Typical $[f^*]$ vs. α^{-1} data set along with the fit of the Flory–Erman theory is shown in Fig. 29.5.

Swelling equilibrium measurements provide an independent route to determine $[f^*]_{\text{ph}}$. At swelling equilibrium the sum of the contributions to the chemical potential from

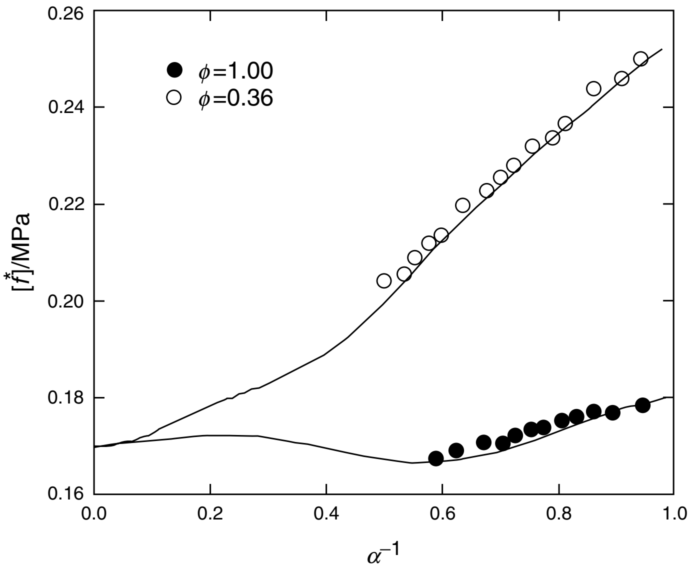

FIGURE 29.5. "Mooney–Rivlin" reduced stress plot showing comparison of experimental data with modified constrained chain model (MCC) predictions for dry (○) and swollen (●) natural rubber networks [112, 117]. Swelling agent: *n*-Decane. continuous lines are theoretical curves calculated with paremeters $\xi kT/V_0 = 0.17\,\text{MPa}$ and $\kappa_{\text{G}} = 2.0$.

mixing and from the elastic deformation of the network should be zero (see Eq. 29.37). Thus

$$0 = \ln(1-\varphi) + \varphi + \chi\varphi^2 + (V_1\xi/N_A V_0)\lambda^{-1} [1 + K(\lambda^2)], \quad (29.53)$$

where N_A is the Avogadro number. Substitution for ξ/V_0 according to Eq. (29.41) yields

$$[f^*]_{ph} = -(RT/V_1)[\ln(1-\varphi) + \varphi + \chi\varphi^2]\lambda / [1 + K(\lambda^2)], \quad (29.54)$$

where $K(\lambda^2)$ is defined by Eq. (29.45).

Using Eq. (29.54) Erman and Flory [39] analyzed the results of Mark and Sullivan [113] on end-linked PDMS networks swollen in benzene as well as the data from Erman, Wagner, and Flory [37] on poly(ethyl acrylate). They compared the values of $[f^*]_{ph}$ obtained from stress–strain isotherms and swelling measurements with data calculated from the chemistry of crosslinking. The $[f^*]_{ph}$ values derived from elasticity measurements were slightly higher than those calculated from the known molecular weights of the primary chains on the basis of stoichiometry. The deviation was attributed to possible departures from equilibrium in the force measurements. The most pronounced departure was observed for networks of low degrees of crosslinking in which the approach of equilibrium is protracted. No such deviation was detected for $[f^*]_{ph}$ obtained from swelling measurements. The satisfactory agreement between the experimental and the calculated values of $[f^*]_{ph}$ led the authors to the conclusion that trapped entanglements do not have a significant contribution to the elastic response of the network. If the effective degree of interlinking is enhanced by discrete entanglements, the values of $[f^*]_{ph}$ deduced from elastic or swelling measurements should exceed the chemical values of $kT\xi/V_0$ calculated from the chemistry of crosslinking.

Gottlieb *et al.* [54] reached the opposite conclusion by the analysis of data on PDMS from different sources, including the same data set of Mark and Sullivan [113]. They argue that trapped entanglements contribute substantially to the stress. Erman and Flory [39] criticized this interpretation on several grounds. Their main criticism was that Gottlieb *et al.* [54] confined their attention to stresses at small strains and did not deduct the contribution to the reduced stress from restraints on junction fluctuations. In the analysis of Gottlieb *et al.* such fluctuations are assumed to be totally suppressed at small strains, as if $\kappa = \infty$ for all networks, and the contribution arising from the constraints is treated as a constant fraction of the reduced stress. This procedure may enhance the reduced forces by factors that increase with decreasing crosslink density, and lead to a finite value of $[f^*]_{ph}$ at $\xi = 0$. According to Flory and Erman [39] the large entanglement contribution in the analysis conducted by Gottlieb *et al.* [54] is largely a fiction of their data treatment.

A comprehensive analysis of previously reported stress–strain data for five different elastomers both in the swollen and unswollen states was performed on the basis of the Flory–Erman theory by Brotzman and Mark [114] (Table 29.1). They found that, in most cases, as the polymer volume fraction decreases, the value of κ required to describe the experimental data also decreases. The analysis also revealed that when ζ is set to zero the high-extension intercept of the $[f^*]_{ph}$ vs. α^{-1} curves is practically independent of the degree of swelling. In Table 29.2 the values of $2C_1$ and $2C_1 + 2C_2$ obtained for the same networks by using the linear Mooney–Rivlin equation of the reduced force, $[f^*] = 2C_1 + 2C_2\alpha^{-1}$, are listed. The $2C_1$ values are in reasonable agreement with the $[f^*]_{ph}$ data given in Table 29.1, indicating that the Mooney–Rivlin treatment can yield similar estimates of the cycle rank of the network as does the more detailed theoretical approach. Poorer agreement was found between $[f^*]_{ph}$ and $2C_1$ by Sharaf and Mark [115]. These authors re-examined the small-strain modulus data reported for unswollen PDMS model networks (Table 29.3). The values $[f^*]_{ph}$ were found two- or threefold lower than the corresponding values of $2C_1$. For comparison in Table 29.4 the characteristic quantities of the same PDMS model networks are given in terms of the entanglement model (see Eq. (29.46)).

Fontaine *et al.* [116,117] compared the prediction of the constrained chain models with the results of elongation measurements performed on dry and swollen natural rubber, poly(ethylene oxide), polybutadiene, poly(dimethylsiloxane) and *cis*-1,4-polyisoprene networks. In Table 29.5 the parameters obtained by analysis of the same network systems using both the CC and the MCC models are listed. It was found that the strong dependence of the reduced force on extension and swelling, observed in all the experiments, can be satisfactorily described by the constrained chain models. The value of the parameter, κ_G, varies between 0.9 and 6.0 for all five network systems investigated. (The other parameter, $\xi kT/V_0$, required to describe the strain and swelling dependence of the data is obtained directly from the experimental stress–strain isotherms at $\alpha^{-1} = 0$.) In the framework of the Flory–Erman model quantitative agreement between the theory and the data for the polybutadiene and poly(ethylene oxide) networks has been achieved only when both κ and the phantom modulus $\xi kT/V_0$ were allowed to be dependent on φ. The formulation according to the constrained chain models, however, does not require φ dependent values of $\xi kT/V_0$ and κ_G.

Kloczkowski, Mark, and Erman [95] compared the prediction of the diffused constraint model with the results of the Flory constrained-junction fluctuation theory [36] and the Erman–Monnerie constrained chain theory [94]. They found that the shapes of the $[f^*]$ vs. α^{-1} curves for all three theories were very similar. Rubinstein and Panyukov [101] reanalyzed the data of Pak and Flory [118] obtained for uniaxially deformed crosslinked PDMS samples. They concluded that the fit of the experimental data by the diffused

TABLE 29.1. *Parameters of the stress–strain isotherms calculated from the fit of the Flory–Erman model for different networks systems [114].*

Polymer[a]	Diluent	f	Crosslinker	T (°C)	φ	$[f^*]_{ph}$ (MPa)	κ	ζ
PDMS [134]	Lin. PDMS	4	γ-Irradiation	30	1.00	0.0325	7.66	0.00
					0.80	0.0317	4.79	0.00
					0.60	0.0317	4.10	0.00
					0.40	0.0318	3.96	0.00
					1.00	0.0355	6.75	0.05
					0.80	0.0334	4.91	0.05
					0.60	0.0330	5.02	0.05
					0.40	0.0333	4.69	0.05
					1.00	0.0366	6.94	0.10
					0.80	0.0341	6.09	0.10
					0.60	0.0335	7.72	0.10
					0.40	0.0343	9.96	0.10
PDMS [134]	Lin. PDMS	4	γ-Irradiation	30	1.00	0.0245	14.3	0.00
					0.80	0.0238	4.74	0.00
					0.60	0.0232	4.63	0.00
					0.40	0.0221	4.35	0.00
PDMS [134]	Lin. PDMS	4	γ-Irradiation	30	1.00	0.0146	15.3	0.00
					0.80	0.0139	8.23	0.00
					0.60	0.0129	10.8	0.00
					0.40	0.0130	4.77	0.00
PBD-S [135]	1,2,4-Trichlorobenzene	4	1% Sulfur	25	1.00	0.222	7.93	0.00
					0.80	0.213	6.43	0.00
					0.60	0.204	6.74	0.00
					0.40	0.192	8.07	0.00
					0.20	0.212	5.21	0.00
					1.00	0.245	6.83	0.05
					0.80	0.232	6.04	0.05
					0.60	0.227	5.47	0.05
					0.40	0.219	7.68	0.05
					0.20	0.231	12.0	0.05
					1.00	0.250	10.3	0.10
					0.80	0.237	7.77	0.10
					0.60	0.232	8.12	0.10
					0.40	0.229	25.0	0.10
					0.20	0.240	4.81	0.10
PBD-G [135]	1,2,4-Trichlorobenzene	4	γ-Irradiation	10	1.00	0.107	20.2	0.00
					0.80	0.097	16.4	0.00
					0.60	0.98	9.77	0.00
					0.40	0.93	8.11	0.00
					0.20	0.93	6.78	0.00
		24		10	1.00	0.162	24	0.00
					0.80	0.135	20	0.00
					0.60	0.127	22.8	0.00
					0.40	0.111	27.2	0.00
					0.20	0.101	29.7	0.00
PBDG-P [135]	1,2,4-Trichlorobenzene	4	1% BPO	10	1.00	0.147	2.96	0.00
					0.80	0.143	2.16	0.00
					0.60	0.142	1.42	0.00
					0.40	0.142	0.84	0.00
					0.20	0.140	1.07	0.00
		24		10	1.00	0.164	18.2	0.00
					0.80	0.153	16.1	0.00
					0.60	0.143	17.7	0.00
					0.40	0.138	25.4	0.00
					0.20	0.136	23.0	0.00

TABLE 29.1. *Continued.*

Polymer[a]	Diluent	f	Crosslinker	T (°C)	φ	$[f^*]_{\mathrm{ph}}$ (MPa)	κ	ζ
PIB [136]	1,2,4-Trichlorobenzene	4	Disulfide	30	1.00	0.082	10.0	0.00
					0.80	0.083	2.44	0.00
					0.60	0.073	3.98	0.00
					0.40	0.070	2.65	0.00
				20	1.00	0.166	3.22	0.00
					0.80	0.104	3.74	0.00
					0.60	0.104	2.75	0.00
					0.40	0.095	3.14	0.00
				15	1.00	0.131	3.95	0.00
					0.80	0.123	4.11	0.00
					0.60	0.119	2.16	0.00
					0.40	0.107	1.21	0.00
POE [137]	Phenylacetate	3	Triisocyanate	25	1.00	0.721	1.14	0.00
					0.597	0.637	1.58	0.00
					0.565	0.549	2.26	0.00
					0.488	0.337	14.8	0.00
					0.390	0.608	1.58	0.00
POE [137]	Phenylacetate	3	Triisocyanate	25	0.429	0.608	1.56	0.00
					0.325	0.240	2.52	0.00
					0.220	0.259	0.960	0.00
POE [137]	Phenylacetate	3	Triisocyanate	25	0.457	0.314	1.29	0.00
					0.341	0.345	1.19	0.00
					0.291	0.314	1.29	0.00
					0.488	0.337	14.8	0.00
					0.390	0.608	1.58	0.00
POP [138]	Benzene		Tris(*p*-phenylisocyanate)	60	0.216	0.285	2.0	0.00
					0.216	0.315	2.2	0.00
			$M_c = 3{,}000$		0.286	0.400	1.5	0.00
			$M_c = 2{,}000$		0.286	0.417	1.7	0.00
					0.273	0.376	1.7	0.00
			$M_c = 1{,}025$		0.406	0.805	0.5	0.00
					0.421	0.773	0.5	0.00
			$M_c = 725$		0.464	0.750	0.5	0.00
					0.456	0.769	0.5	0.00
			$M_c = 730$		0.473	0.725	0.4	0.00
					0.477	0.758	0.4	0.00
					0.440	0.755	0.4	0.00
			$M_c = 740$		0.522	0.695	0.5	0.00
					0.519	0.645	0.4	0.00
			$M_c = 725$		0.480	0.850	0.5	0.00
					0.510	0.829	0.4	0.00

[a] PDMS: poly(dimethylsiloxane); PDB: *cis*-1,4-polybutadiene; PIB: polyisobutylene; POE: poly(oxyethylene); POP: poly(oxypropylene).

constraint model was significantly better than by the Mooney–Rivlin expression or by the nonaffine tube model [97].

Urayama *et al.* [119–121] tested the diffused constraint model using both uniaxial compression and equibiaxial elongation data for end-linked PDMS networks in which trapped entanglements were dominant in number relative to chemical crosslinks. The parameter κ was used as an empirical fitting parameter, and the best-fit procedure yielded $\kappa = 2.9$. The structural parameters (ν, ξ, μ, f) were estimated from the stoichiometry using the Miller–Macosko model [56] in conjunction with the measured sol fraction. They concluded that the diffused constraint model successfully reproduced the reduced stress–strain data over a wide range of deformations, but the model underestimated the modulus, G, because it did not consider trapped entanglements as additional crosslinks contributing to G. The theoretical value of G calculated using $\kappa = 2.9$ was approximately one order of magnitude smaller (G=5.22 kPa) than the experimental value (G=64.9 kPa).

TABLE 29.2 *Mooney–Rivlin parameters of the stress–strain isotherms for different networks systems [114].*

Polymer	Diluent	f	Crosslinker	T (°C)	φ	$2C_1$ (MPa)	$2C_1 + 2C_2$ (MPa)
PDMS	Lin. PDMS	4	γ-Irradiation	30	1.00	0.0304	0.0571
					0.80	0.0298	0.0476
					0.60	0.0299	0.0433
					0.40	0.0305	0.0398
PDMS	Lin. PDMS	4	γ-Irradiation	30	1.00	0.0218	0.0533
					0.80	0.0220	0.0365
					0.60	0.0218	0.0324
					0.40	0.0208	0.0290
PDMS	Lin. PDMS	4	γ-Irradiation	30	1.00	0.0118	0.0364
					0.80	0.0121	0.0255
					0.60	0.0117	0.0230
					0.40	0.0126	0.0168
PBD-S[a]	1,2,4-Trichlorobenzene	4	1% Sulfur	25	1.00	0.203	0.406
					0.80	0.202	0.343
					0.60	0.202	0.302
					0.40	0.196	0.272
					0.20	0.204	0.254
PBD-G	1,2,4-Trichlorobenzene	4	γ-Irradiation	10	1.00	0.0904	0.280
					0.80	0.0864	0.210
					0.60	0.0915	0.167
					0.40	0.0933	0.135
					0.20	0.0878	0.117
		24		10	1.00	0.0904	0.28
					0.80	0.0868	0.210
					0.60	0.0915	0.167
					0.40	0.0933	0.135
					0.20	0.0878	0.117
PBDG-P	1,2,4-Trichlorobenzene	4	1% BPO	10	1.00	0.142	0.228
					0.80	0.140	0.178
					0.60	0.138	0.160
					0.40	0.138	0.150
					0.20	0.142	0.144
		24		10	1.00	0.164	0.168
					0.80	0.140	0.178
					0.60	0.138	0.160
					0.40	0.138	0.150
					0.20	0.135	0.144
PIB	1,2,4-Trichlorobenzene	4	Disulfide	30	1.00	0.072	0.159
					0.80	0.083	0.103
					0.60	0.074	0.0953
					0.40	0.073	0.0777
				20	1.00	0.113	0.165
					0.80	0.0976	0.148
					0.60	0.104	0.131
					0.40	0.0905	0.115
				15	1.00	0.128	0.194
					0.80	0.123	0.170
					0.60	0.114	0.145
					0.40	0.108	0.114
POE	Phenylacetate	3	Triisocyanate	25	1.00	0.744	0.934
					0.597	0.660	0.795
					0.565	0.613	0.722
					0.488	0.575	0.732
					0.390	0.593	0.715
POE	Phenylacetate	3	Triisocyanate	25	0.429	0.251	0.320
					0.325	0.231	0.296
					0.220	0.263	0.266

TABLE 29.2 *Continued*

Polymer	Diluent	f	Crosslinker	T (°C)	φ	$2C_1$ (MPa)	$2C_1 + 2C_2$ (MPa)
POE	Phenylacetate	3	Triisocyanate	25	0.457	0.280	0.390
					0.341	0.329	0.402
					0.291	0.310	0.348
POP	Benzene		Tris(*p*-phenylisocyanate)	60	0.216	0.322	0.423
					0.216	0.328	0.477
			$M_c = 3{,}000$		0.286	0.450	0.546
			$M_c = 2{,}000$		0.286	0.448	0.594
					0.273	0.398	0.537
			$M_c = 1{,}025$		0.406	0.839	0.899
					0.421	0.839	0.859
			$M_c = 725$		0.464	0.810	0.835
					0.456	0.847	0.851
			$M_c = 730$		0.473	0.779	0.785
					0.477	0.796	0.832
					0.440	0.814	0.817
			$M_c = 740$		0.522	0.723	0.776
					0.519	0.647	0.713
			$M_c = 725$		0.480	0.861	0.959
					0.510	0.891	0.904

It should be noted that the effect of G is cancelled when reduced stress–strain data are analyzed. This explains the success of this model in describing the shape of the experimental curves. On the basis of the diffused constraint theory a detailed comparison between theory and experiment on swollen polymer networks has not yet been made.

TABLE 29.3. *Parameters of the stress–strain isotherms calculated from the Flory–Erman model for unswollen PDMS model networks[115].*

M_n(g mol^{-1})	f	$[f^*]_{ph}$(MPa)	κ	$2C_1$(MPa)	$2C_2$(MPa)
32,900	3	0.013	19.4	0.033	0.034
25,600	3	0.014	18.2	0.043	0.052
18,500	3	0.021	15.0	0.066	0.061
9,500	3	0.053	9.5	0.093	0.057
4,700	3	0.075	7.9	0.148	0.011
4,000	3	0.101	6.8	0.192	0.015
45,000	4	0.008	22.3	0.038	0.030
32,900	4	0.015	16.4	0.058	0.042
25,600	4	0.028	11.9	0.084	0.055
18,500	4	0.023	13.3	0.089	0.040
9,500	4	0.062	8.0	0.167	0.050
4,700	4	0.119	5.8	0.353	0.031
4,000	4	0.195	4.5	0.395	0.021
18,500	4	0.020	14.3	0.096	0.043
18,500	4	0.020	14.3	0.089	0.043
18,500	4	0.020	14.3	0.089	0.040
11,300	4	0.082	7.0	0.196	0.083
11,300	4	0.079	7.1	0.169	0.115
11,300	4	0.084	6.9	0.199	0.076
11,300	4	0.064	7.9	0.188	0.092
11,300	4	0.060	8.2	0.178	0.098
11,300	4	0.062	8.1	0.165	0.120
21,500	4	0.038	10.3	0.142	0.098
11,100	4	0.086	6.8	0.207	0.087
8,800	4	0.104	6.2	0.244	0.084

TABLE 29.4. *Parameters of the stress–strain isotherms for PDMS model networks calculated from the entanglement model (Eq. (29.46)) [54].*

M_n(g mol^{-1})	f	T (K)	$10^{-5}G$(Pa)	$10^{-5}(\nu RT)$(Pa)	T_e
32,900	3	298	0.699	0.286	0.467
25,600	3		0.947	0.377	0.474
18,500	3		1.27	0.508	0.467
9,500	3		1.50	1.41	0.641
4,700	3		1.59	2.00	0.467
4,000	3		2.07	2.66	0.536
45,000	4	298	0.68	0.185	0.278
32,900	4		1.00	0.335	0.38
25,600	4		1.40	0.618	0.571
18,500	4	298	1.29	0.517	0.324
9,500	4		2.17	1.38	0.466
4,700	4		3.84	2.63	0.439
4,000	4		4.16	4.185	0.625
18,500	4		1.35	0.45	0.278
11,300	4	298	2.79	1.72	0.744
11,300	4		2.84	1.68	0.723
11,300	4		2.75	1.77	0.769
11,300	4		2.75	1.50	0.804
11,300	4		2.76	1.41	0.752
11,300	4		2.85	1.44	0.771
21,600	4	298	2.40	0.871	0.774
11,100	4		2.94	1.87	0.866
8,800	4		3.28	2.28	0.783

29.3.3 Determination of the Model Parameters from Swelling Measurements

Swelling of elastomers in a solvent is a relatively simple technique for the characterization of polymer networks. Empirical information, such as the degree of swelling and the elastic modulus, can be obtained by direct measurements. Equilibrium swelling measurements and stress–strain measurements are the most frequently used methods for determining the relative degree of crosslinking. A quantitative analysis of the swelling data, however, requires further considerations.

According to the Frenkel–Flory–Rehner hypothesis the elastic and mixing contributions to the free energy are additive, and the mixing free energy for the network is the same as that of the corresponding uncrosslinked polymer. It follows from these assumptions that the thermodynamic activity of the solvent in the network contains two separable contributions, $a_{1,c}$ and $a_{1,u}$, representing the diluent activities in the crosslinked and the uncrosslinked polymers, respectively, and the ratio $a_{1,c}/a_{1,u}$ at identical concentrations yields the elastic component of the solvent activity. Experimental tests of this prediction have been performed by differential sorption measurements first conducted by

TABLE 29.5. *Network parameters calculated by the constrained chain (CC) and modified constrained chain (MCC) models [116,117].*

System	Crosslinker[a]	φ	$\xi kT/V_0$ (MPa)		κ_G	
			CC	MCC	CC	MCC
cis 1,4-	DCP 1.3%	0.197	0.312	0.325	1.1	0.9
Isoprene/	DCP 0.75%	0.165	0.215	0.220	1.6	1.6
benzene	DCP 0.30%	0.133	0.115	0.125	3.0	2.5
T=25 °C	DCP 0.20%	0.112	0.083	0.092	3.8	3.0
	DCP 0.10%	0.081	0.043	0.045	5.0	6.0
NR/*n*-decane	DCP	0.24–1.0	0.150	0.170	3.0	2.0
PEO/phenylac.	isocyanate	0.22–1.0	0.260	0.275	1.5	1.6
PBD/chl.benz.	sulfur	0.2–1.0	0.235	0.235	2.0	2.6
PDMS/benzene	el.radiation	0.32–1.0	0.125	0.135	2.5	2.0

[a] DCP: dicumyl peroxide.

Gee *et al.* [122]. In this experiment on natural rubber/benzene system the vapor pressure of the solvent and the amount of solvent absorbed by the crosslinked and uncrosslinked rubbers were determined simultaneously by using a sensitive microbalance housed in a vacuum system. Similar experiments were performed by Yen and Eichinger [6], Brotzman and Eichinger [7–9], Neuburger and Eichinger [10], Zhao and Eichinger [11] and McKenna *et al.* [13–16]. Conventionally the results of these measurements are given in term of the dimensionless swelling activity parameter [15] (or dilation modulus [6–11])

$$S = \lambda \ln(a_{1,\mathrm{c}}/a_{1,\mathrm{u}}). \tag{29.55}$$

Typical theoretical and experimental S vs. $\varphi^{-1/3}(=\lambda)$ curves are shown in Fig. 29.6. The phantom network theory predicts constancy while the affine network model predicts a monotonic increase of S with increasing $\varphi^{-1/3}$. Many of the experimental S vs. $\varphi^{-1/3}$ curves, including that of Gee *et al.* [122] exhibit a maximum. This behavior is consistent with the Flory–Erman theory, although the experimental peak is, in general, much sharper and of significantly greater magnitude than that predicted by the model. Neuburger and Eichinger [10] determined the swelling activity parameter for poly(dimethylsiloxane) networks in benzene and cyclohexane at 20 and 30 °C. They found that the benzene data at 20 °C can be reasonably well described by the Flory–Erman model with the parameters: $\xi/(N_\mathrm{A}V_0) = 4.09\times 10^{-4}$ mol/cm^3, $\kappa = 1.0$, and $\zeta = 90$ (this value of ζ is much bigger than that required to fit the stress strain data). The value of the molecular weight between crosslinks, M_c, calculated from the equation $\xi/(N_\mathrm{A}V_0) = \rho/2M_\mathrm{c}$ was $M_\mathrm{c} = 1{,}190$ g/mol. It is significantly smaller than the actual $M_\mathrm{c} = 26{,}000$ g/mol. Even larger discrepancies were found between the calculated and the actual values of M_c for the PDMS/cyclohexane system. In this case the best fit was obtained using the phantom network model with $\xi/(N_\mathrm{A}V_0) = 0.0012$ mol/cm^3 corresponding to $M_\mathrm{c} = 406$ g/mol. The authors concluded that the deviation is the consequence of the breakdown of the Frenkel–Flory–Rehner theory, namely the hypothesis that the elastic and mixing free energies are separable.

McKenna *et al.* [13–16] performed similar investigations on natural rubber networks swollen in different diluents. They assumed that the elastic free energy contribution is adequately described by the phenomenological Valanis–Landel function (see Eq. (29.1)) and for the measured degree of swelling they calculated it from the values of $w'(\lambda_\mathrm{s})$ determined in the unswollen state. Comparing these data with the mixing contribution obtained by using Eq. (29.24) they came to the conclusion that the value of the interaction parameter for the crosslinked polymer, χ_c, exceeds that of the solution of the uncrosslinked polymer, χ_u. This conclusion has been supported by lattice model calculations of Freed and Pesci [123], who pointed out that the effective interaction parameter depends on the crosslink density.

McKenna *et al.* [13–16] use the following relation for the swelling activity parameter:

$$S = \lambda \ln(a_{1,\mathrm{c}}/a_{1,\mathrm{u}}) = (\chi_\mathrm{c} - \chi_\mathrm{u})\lambda^{-5} + V_1 w'(\lambda)/RT\lambda. \tag{29.56}$$

The important point to note from this equation is the assumption that $\chi_\mathrm{c} = \chi_\mathrm{u}$ often found in the use of the Frenkel–Flory–Rehner hypothesis, has been suppressed. Hence the first term on the right hand side of Eq. (29.56) provides insight into the thermodynamics of swelling and in particular is in accord with the experimental observation that $S \neq 0$ as $\lambda \to 1$, i.e., no swelling. A typical value for $\chi_\mathrm{c} - \chi_\mathrm{u}$ of

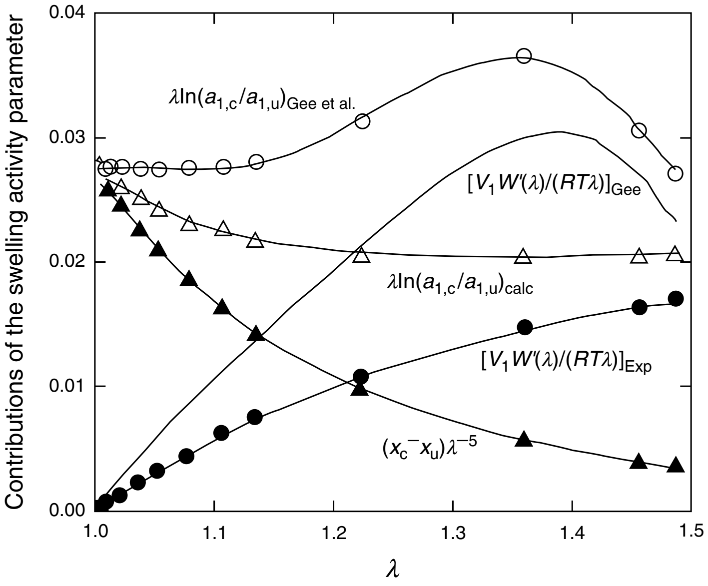

FIGURE 29.6. Thermodynamic parameters that contribute to the swelling activity parameter S vs. the swelling deformation $\lambda_\mathrm{s} = \varphi^{-1/3}$. (After Ref. 15 see text for discussion).

0.027 can be obtained by examining the curve labeled $\lambda \ln(a_{1,c}/a_{1,u})_{\text{Gee } et\ al.}$ of Fig. 29.6 and taking the value at $\lambda = 1$.

In Fig. 29.6 we show the thermodynamic parameters from Eq. (29.56) and a comparison with the swelling data of Gee *et al* [122]. The curve labeled $\lambda \ln(a_{1,c}/a_{1,u})_{\text{Gee } et\ al.}$ refers to the data obtained by Gee *et al.* for *S*. The curve labeled $\lambda \ln(a_{1,c}/a_{1,u})_{\text{calc}}$ refers to a calculation of *S* from Eq. (29.56) using the values of $(\chi_c - \chi_u)\lambda^{-5}$ depicted in the plot on the curve so labeled summed with the values of $[V_1 w'(\lambda)/RT\lambda]_{\text{Exp}}$ determined experimentally by measurements on a rubber similar to that used by Gee *et al.* [122] and depicted with solid circles. The solid line without points labeled $[V_1 w'(\lambda)/RT\lambda]_{\text{Gee}}$ represents the value of the elastic contribution that would have been needed to have in order to agree with the Gee *et al.* [122] results for *S*, i.e., when added to the measured values of $(\chi_c - \chi_u)\lambda^{-5}$. The deviation between the measured and calculated curves is significant, i.e., the crosslink dependence of the interaction parameter does not provide an adequate explanation for the anomalous behavior of the swelling activity parameter. The reader is referred to McKenna *et al.* [13–16] for further discussion.

McKenna and Crissman [16] also investigated the effect of temperature on the shape of the *S* vs. $\varphi^{-2/3}(=\lambda^2)$ curves. In the polyisoprene/benzene system they did not observe a maximum in *S* at 30 and 40 °C, rather a rapid decrease occurred which was followed by a plateau region above $\lambda^2 = 1.2$. At 50 °C, however, a pronounced maximum was found at $\lambda^2 = 1.13$. Neuburger and Eichinger [10] reported similar changes in the swelling behavior for the PDMS/benzene system in the temperature range between 20 and 30 °C. Similar results were reported for changing solvent quality by Zhao and Eichinger [11]. Such abrupt changes in behavior imply significant changes in the free energy of the network over a narrow range of temperatures (or solvent qualities). None of the existing network theories predicts such a possibility.

Sivasailam and Cohen [124] studied the effect of swelling on the elastic modulus of end-linked polydimethyl siloxane networks synthesized at the theta condition from a series of molecular weight precursors ($9{,}900 < M < 101{,}700$) at polymer concentrations from 100% to 40%. These networks exhibited a minimal number of defects as they were prepared from low polydispersity chains at an optimal ratio of crosslinks to precursor chains. The optimum ratio was chosen as the one that produced the network with the highest elastic modulus, the minimum equilibrium swelling, and the minimum soluble fraction. The wide range of precursor molecular weights allowed the investigation of the effect of trapped entanglements as a function of the molecular weight. Equilibrium swelling concentrations were determined in PDMS oligomer ($M_n = 3{,}900$ g/mol), and the elastic modulus was measured at three different states: in swelling equilibrium (fully swollen state), at the concentration at which the network was formed (reference state), and in the unswollen (dry) state (Table 29.6 and Table 29.7). The dependence of the modulus after cure, the dry modulus

TABLE 29.6. *Elastic modulus of end-linked PDMS networks made at different precursor concentrations [124,126].*

Molecular weight (g/mol)	Diluent	Volume fraction φ_{ref}	*Sol fraction w%	G_{ref} (kPa)
101,700		1.00	2.60	111
	PDMS	0.89	2.50	95
	oligomer	0.79	1.28	72
		0.74	2.10	62
		0.67	2.99	50
71,500		1.00	0.28	176
	PDMS	0.89	−1.41	143
	oligomer	0.78	−0.75	98
		0.49	−1.84	48
		0.40	−1.67	27
30,200		1.00	0.26	210
	PDMS	0.89	0.12	168
	oligomer	0.78	0.13	150
		0.70	−0.05	106
		0.59	−0.96	85
		0.50	−2.50	61
		0.40	−4.90	39
9,900		1.00	0.25	343
	PDMS	0.89	−0.07	277
	oligomer	0.80	−0.05	251
		0.69	−0.98	193
		0.57	−3.04	147
		0.51	−6.90	123

*The negative value indicates that solvent is expelled from the swollen network by syneresis. In these gels the amount of uncrosslinked polymer is practically negligible.

TABLE 29.7. *Experimental and calculated values of the elastic modulus of end-linked PDMS networks swollen in PDMS oligomer (M=3,900 g/mol, theta solvent) and in the dry state [124,126].*

	Polymer volume fraction		G_{sw} (kPa)		G_{dry} (kPa)	
Molecular weight (g/mol)	φ_{ref}	φ_θ	Exp.	Calc.	Exp.	Calc.
101,700	1.00	0.38	59	37	111	111
	0.89	0.37	62	32	105	87
	0.79	0.34	45	27	82	68
	0.74	0.32	36	23	71	60
	0.67	0.23	16	16	57	49
71,500	1.00	0.48	129	84	175	191
	0.89	0.44	110	70	148	150
	0.78	0.37	61	52	105	116
	0.50	0.30	36	29	77	51
30,200	1.00	0.51	153	121	210	229
	0.89	0.47	130	101	172	185
	0.78	0.45	109	87	159	148
	0.59	0.37	67	59	98	95
	0.50	0.33	48	48	72	74
9,900	1.00	0.62	280	258	342	363
	0.89	0.59	240	228	286	310
	0.80	0.56	212	203	263	270
	0.69	0.52	161	175	208	226
	0.57	0.47	133	141	172	182

after solvent extraction, and the degree of equilibrium swelling on precursor concentration during cure were compared to scaling predictions. The experimental scaling exponents were found to be strong functions of the molecular weight of the precursor chains and for high molecular weight precursors their values approached the theoretical prediction by Obukhov *et al.* [125] for entanglement-dominated networks. The authors concluded that for networks made of high molecular weight chains a major contribution to the modulus is from trapped entanglements. They also pointed out that at molecular weights below the entanglement molecular weight the modulus of the network is affected by the mutual interpenetration of interspersed chains.

The data of Sivasailam and Cohen were reanalyzed by Graessley [126] in terms of the entanglement model. According to this model the shear modulus at the reference state $G_{\rm ref}$ is the sum of crosslink and entanglement contributions

$$G_{\rm ref} = \nu_{\rm ref} kT + T_0 G_{\rm N}^0 \varphi_{\rm ref}^{2.3}, \qquad (29.57)$$

where $G_{\rm N}^0$ is the plateau modulus of the polymer melt (for PDMS $G_{\rm N}^0 = 0.2\,MPa$), T_0 is the entanglement trapping factor, and $\varphi_{\rm ref}$ is the volume fraction of the polymer at crosslinking. Assuming that the first term (crosslink contribution) in Eq. (29.57) varies with the concentration as in the phantom network, and the second term (entanglement contribution) varies like the Mooney–Rivlin term C_2, the following equations can be derived

$$G_{\rm ref} = G_0 \varphi_{\rm ref} + T_0 G_{\rm N}^0 \varphi_{\rm ref}^{2.3}, \qquad (29.58a)$$

$$G_{\rm swollen} = G_0 \varphi_{\rm ref}^{2/3} \varphi^{1/3} + T_0 G_{\rm N}^0 \varphi_{\rm ref} \varphi^{1.3}, \qquad (29.58b)$$

$$G_{\rm dry} = G_0 \varphi_{\rm ref}^{2/3} + T_0 G_{\rm N}^0 \varphi_{\rm ref}^{2.3}, \qquad (29.58c)$$

where $G_0(=\nu kT)$ is the crosslink contribution in the dry state (this excludes trapped entanglement effects). Using Eqs. (29.58a–c) in conjunction with empirically obtained data for T_0 and the sol fraction, the elastic moduli of these gels were calculated (Table 29.7). No systematic deviation can be observed between the predicted and measured moduli.

Urayama *et al.* [127,128] made similar investigations on end-linked PDMS networks cross-linked in solution. The elastic moduli of gels made from M=29,400g/mol and M=4,400 g/mol precursor chains were measured in the fully swollen state in toluene (good solvent), and in the reference state (Table 29.8). The sol fraction of these gels was less than 10%. The same analysis described above indicates that at high polymer volume fractions the calculated and experimental values agree fairly well, while at high swelling ratios the deviation is pronounced [126]. The discrepancy may be the consequence of structural and chemical changes accompanied by the crosslinking process.

In general, the reasonable agreement between the predicted and measured values of the elastic modulus suggests that the effect of swelling on the elastic properties can be approximated as a sum of two distinct contributions: one due to the chemical crosslinks and the other due to the entanglements. The latter in polymer melts is independent of chain lengths and represent an entanglement contribution

TABLE 29.8. *Elastic modulus and polymer volume fraction of end-linked PDMS networks at the preparation state and in the fully swollen state in toluene (good solvent) [127,128].*

Molecular weight (g/mol)	Diluent	Polymer volume fraction		G_{ref} (kPa)	G_{sw} (kPa)
		φ_{ref}	φ_{sw}		
29,400	toluene	1.0	0.187	113	33
		0.852	0.155	93	27
		0.709	0.126	63	17
		0.544	0.093	30	73
		0.411	0.078	19	47
		0.281	0.055	9	2.3
		0.179	0.038	3	0.9
4,400	toluene	1.0	0.275	680	251
		0.777	0.216	423	149
		0.654	0.208	330	137
		0.601	0.194	297	119
		0.584	0.195	301	113
		0.504	0.180	241	100
		0.381	0.140	150	53
		0.298	0.109	61	29

when the network is formed. [126] Chemical crosslinks trap a fraction of this contribution into the structure that governs the elastic response of the network.

29.3.4 Analysis of the Experimental Results on the Basis of the Scaling Theory

The validity of scaling laws has been tested on several swollen network systems (Table 29.9). Munch *et al.* [99] studied the concentration dependence of the shear modulus for polystyrene model networks synthesized by copolymerization of styrene and divinylbenzene and swollen to equilibrium in benzene (good solvent for polystyrene). It was found that the modulus obeys a scaling law with equilibrium concentration, similar to that obtained for semidilute polymer solutions. The best fit to the equation $G = B\varphi_e^n$ yields B=4,200 kPa and n=2.28. Hild *et al.* [129] compared the concentration dependence of the shear moduli of poly(ethylene oxide) networks crosslinked by aliphatic pluriisocyanate in two diluents: dioxane and water. The corresponding scaling laws were found: $G = 8{,}430\varphi_e^{2.30}$ kPa (in 1,4-dioxane) and $G = 10{,}400\varphi_e^{2.51}$ kPa (in water). The exponent obtained in 1,4-dioxane is in excellent agreement with the prediction of the scaling theory. However, for the same networks swollen in water a significantly higher exponent, n=2.51, was obtained. They assumed that the deviation from the theoretical exponent is due to the insolubility of the urethane linkages in water, which may induce inhomogeneities in the gels at the molecular level. Hecht and Geissler [130] investigated the elastic properties of polyacryamide gel homologs in a theta solvent (water–methanol mixture, 3:1 by volume). They found that in the concentration range $0.07<\varphi<0.3$ the longitudinal elastic modulus, E_L, obtained

TABLE 29.9. *Power law exponents for the concentration dependence of the elastic modulus in swollen network homologs.*

System	T (°C)	φ	A (kPa)	n	r	Ref.
NR/*n*-decane	20	0.06–0.40	4,500	2.06	0.992	[139, 140]
PS/benzene	20	0.05–0.20	4,200	2.28	0.955	[99]
PS/benzene	25	0.05–0.50	4,140	2.35	0.993	[99]
PS/cyclohexane	37	0.12–0.28	1,750	3.14	0.980	[28]
PEO/dioxane	25	0.03–0.35	8,430	2.30	0.984	[129]
PEO/water	25	0.03–0.30	10,401	2.51	0.992	[129]
PHPMA	25	0.08–0.35	2,590	2.59	0.995	[129]
PDMS/toluene	25	0.10–0.40	2,650	2.20	0.988	[23]
PVAC/toluene	25	0.06–0.30	2,430	2.27	0.990	[22]
PVAC/acetone	25	0.05–0.25	4,420	2.25	0.992	[22]
PVAC/isopropanol	70	0.10–0.60	3,388	2.31	0.977	[132]
PAA/water	25	0.03–0.30	4,880	2.23	0.991	[141]
PVA/water	25	0.03–0.30	3,500	2.11	0.993	[139]

NR: natural rubber; PS: polystyrene; PEO: poly(ethylene oxide); PHPMA: poly(hydroxi-ethyl-methacrylate); PDMS: polydimethylsiloxane; PVAC: poly(vinyl acetate); PAA: poly(acryamide); PVA: poly(vinyl alcohol); r: correlation coefficient.

from light scattering observations, obeys a scaling law $E_L = 8.090\varphi_e^{3.07}$ kPa in reasonable agreement with the theoretical prediction. Richards and Davidson [131] determined the shear moduli of randomly crosslinked polystyrene networks swollen in cyclohexane at the theta (Θ) temperature and also in toluene (good solvent condition). The power law exponent, n=3.7, reported for the theta system exceeds that of the theoretical value. In good solvent condition (toluene, 20 °C) they found the value n=2.25. A comprehensive study of the dependence of the elastic (shear) modulus on the polymer concentration was performed by Zrínyi and Horkay [132] on poly(vinyl acetate) gels swollen to equilibrium in isopropylalcohol. The thermodynamic quality of the solvent was varied by changing the temperature in the range from 30 °C to 70 °C. Isopropylalcohol is a theta solvent for poly(vinyl acetate) at 52°C and a good solvent at 70 °C. It was found that G vs. φ exhibits a simple power law behavior at each temperature. The exponent n varies between the values of 2.32 (good solvent condition, 70 °C) and 14.1 (poor solvent condition, 30 °C) [133]. At the theta temperature (52 °C) the best fit to the experimental data yields n=3.10.

The osmotic response of swollen polymeric networks was studied on the basis of the scaling theory by Horkay *et al.* [17–19,22,23,133]. They measured both the swelling pressure, ω, and the shear modulus of gels, G, at different stages of dilution. The swelling pressure vs. polymer volume fraction data were analyzed according to the equation [22]

$$\omega = \Pi - G = A\varphi^n - G_v{}^e(\varphi/\varphi_e)^m, \tag{29.59}$$

where Π is the "osmotic" pressure of the swollen network and G_v^e is the value of the volume elastic modulus at equilibrium with the pure solvent ($\omega = 0$) and the constant A depends on the polymer/solvent system. The exponents n and m were iteratively adjusted to minimize the variance of ω for each set of data points. The resulting values of A, n, m, and G_v^e for poly(vinyl acetate) gels are displayed in Table 29.10. The n values are consistent with the scaling prediction for the mixing term. Also displayed in Table 29.10 are the values of the shear modulus, G_s^e, measured at the swelling equilibrium condition. The agreement between the numerical values of the shear and the volume elastic moduli provides experimental evidence that in highly swollen networks the separability of the elastic and mixing terms is a reasonable approximation.

29.4 SUMMARY

A survey of the thermodynamics and mechanics of crosslinked gels has been presented. Subjects include the phenomenological description of crosslinked networks within the framework of finite elasticity theory and continuum thermodynamics. Particular emphasis is placed on the Valanis–Landel form of the strain energy density function. Several statistical mechanical models of rubber elasticity are also presented. Of particular usefulness are the affine and phantom network models, which are commonly used to derive information about the molecular parameters of the gel from swelling or mechanical measurements. Techniques for using these models and the more modern Flory–Erman constrained junction model and its most recent modifications are described. Experimental data from the literature are presented and used to deduce molecular parameters for the networks using the different models. The application of Scaling Theory to polymer gels is also considered.

ACKNOWLEDGMENTS

FH acknowledges the support of the Intramural Research Program of the NIH, NICHD. GBM would like to acknowledge the support of the National Science Foundation for partial support of this work under grant DMR-0307084. We also thank J. Wang for help with the figures.

TABLE 29.10. *Swelling pressure and shear modulus parameters of PVAc networks in toluene and acetone [22].*

Sample	φ_e	A	n	m	G_v^e(kPa)	G_s^e(kPa)
Toluene 25 °C						
3/50	0.089	2171	2.28	0.342	8.6	8.9
6/50	0.146	2613	2.29	0.331	31.6	32.4
6/200	0.078	2072	2.22	0.340	7.2	6.9
9/50	0.208	2481	2.27	0.355	70.8	70.3
9/100	0.141	2350	2.25	0.336	28.6	28.3
9/200	0.112	2374	2.27	0.326	16.6	16.7
9/400	0.074	2273	2.27	0.315	6.16	6.26
12/50	0.229	3100	2.35	0.383	95.7	99.8
12/200	0.133	2425	2.26	0.335	25.5	25.2
Acetone 25 °C						
9/100	0.103	4264	2.24	0.321	24.9	25.9
9/200	0.078	4731	2.26	0.346	14.9	14.8
9/400	0.051	4262	2.24	0.369	5.44	5.24

REFERENCES

1. Guth, E. and Mark, H. *Monatshefte*, **65**, 93 (1934).
2. Flory, P.J. and Rehner, J. *J. Chem. Phys.*, **11**, 521 (1943).
3. James, H.M. and Guth, E. *J. Chem. Phys.*, **15**, 651 (1947).
4. Flory, P.J. *Principles of Polymer Chemistry*; Cornell University. Press, Ithaca, NY, 1953.
5. Frenkel, J. *Rubber Chem. Technol.*, **13**, 264 (1940).
6. Yen, L.Y. and Eichinger, B.E. *J. Polym. Sci. Polym. Phys. Ed.* **16**, 121 (1978).
7. Brotzman, R.W and Eichinger, B.E. *Macromolecules* **14**, 1445 (1981).
8. Brotzman, R.W. and Eichinger, B.E. *Macromolecules* **15**, 531 (1982).
9. Brotzman, R.W. and Eichinger, B.E. *Macromolecules* **16**, 1131 (1983).
10. Neuburger, N.A. and Eichinger, B.E. *Macromolecules* **21**, 3060 (1988).
11. Zhao, Y. and Eichinger, B.E. *Macromolecules* **25**, 6988 (1992).
12. Gottlieb, M. and Gaylord, R.J. *Macromolecules* **17**, 2024 (1984).
13. McKenna, G.B., Flynn, K.M. and Chen, Y. *Polym. Commun.* **29**, 272 (1988).
14. McKenna, G.B., Flynn, K.M. and Chen, Y. *Macromolecules* **22**, 4507 (1989).
15. McKenna, G.B., Flynn, K.M. and Chen, Y. *Polymer* **31**, 1937 (1990).
16. McKenna, G.B. and Crissmann, J.M. *J. Polym. Sci B. Polym. Phys.* 35, 817 (1997).
17. Horkay, F. and Zrinyi, M. *Macromolecules*, **15**, 1306 (1982).
18. Horkay, F. and Zrinyi, M. *J. Macromol. Sci. Phys.* **B25**, 307 (1986).
19. Horkay, F., Geissler, E., Hecht, A.M. and Zrinyi, M. *Macromolecules*, **21**, 2589 (1988).
20. Geissler, E., Horkay, F., Hecht, A.M. and Zrinyi, M. *J. Chem. Phys.* **90**, 1924 (1989).
21. Horkay, F., Hecht, A.M. and Geissler, E. *Macromolecules*, **22**, 2007 (1989).
22. Horkay, F., Hecht, A.M. and Geissler, E. *J. Chem. Phys.* **91**, 2706 (1989).
23. Horkay, F., Zrinyi, M., Geissler, E., Hecht, A.M. and Pruvost, P. *Polymer*, **32**, 835 (1991).
24. Horkay, F., Hecht, A.M., Mallam, S., Geissler, E. and Rennie, A.R. *Macromolecules*, **24**, 2896 (1991).
25. Hecht, A.M., Horkay, F., Geissler, E. and Benoit, J.P. *Macromolecules*, **24**, 4183 (1991).
26. Geissler, E., Horkay, F. and Hecht, A.M. *Macromolecules*, **24**, 6006 (1991).
27. Hecht, A.M., Guillermo, A., Horkay, F., Mallam, S., Legrand, J.F. and Geissler, E. *Macromolecules*, **25**, 3677 (1992).
28. Hecht, A.M., Horkay, F., Mallam, S. and Geissler, E. *Macromolecules*, **25**, 6915 (1992).
29. Horkay, F., Burchard, W., Geissler, E. and Hecht, A.M. *Macromolecules*, **26**, 1296 (1993).
30. Horkay, F., Burchard, W., Hecht, A.M. and Geissler, E. *Macromolecules*, **26**, 3375 (1993).
31. Geissler, E., Horkay, F. and Hecht, A.M. *Phys.Rev.Lett.* **71**, 645 (1993).
32. Douglas, J.F. and McKenna, G.B. *Macromolecules*, **26**, 3282 (1993).
33. Flory, P.J. and Tatara, Y. *J. Polym. Sci., Polym. Phys. Ed.*, **13**, 683 (1975).
34. Ronca, G. and Allegra, G. *J. Chem. Phys.*, **63**, 4990 (1975).
35. Flory, P.J. *Proc. R. Soc. Lond.* **A351**, 351 (1976).
36. Flory, P.J. *J. Chem. Phys.*, **66**, 5720 (1977).
37. Erman, B. Wagner, W. and Flory, P.J. *Macromolecules* **13**, 1554 (1980).
38. Flory, P.J. and Erman, B. *Macromolecules* **15**, 800 (1982).
39. Erman, B. and Flory, P.J. *Macromolecules* **15**, 806 (1982).
40. Erman, B. and Flory, P.J. *Macromolecules* **16**, 1600 (1983).
41. Mark, J.E. *Adv. Polym. Sci.*, **44**, 1 (1982).
42. Queslel, J.P. and Mark, J.E. *J. Polym. Sci., Polym. Phys. Ed.* 22, 49 (1984).
43. Queslel, J.P. and Mark, J.E. *Adv. Polym. Sci.*, **65**, 135 (1984).
44. Queslel, J.P. and Mark, J.E. *Adv. Polym. Sci.* **71**, 229 (1985).
45. Langley, N.R. *Macromolecules* **1**, 348 (1968).
46. Dossin, L.M. and Graessley, W.W. *Macromolecules* **12**, 123 (1979).
47. Pearson, D.S. and Graessley, W.W. *Macromolecules* **11**, 528 (1978).
48. Pearson, D.S. and Graessley, W.W. *Macromolecules* **13**, 1001 (1980).
49. Graessley, W.W. *Adv. Polym. Sci.*, **47**, 67 (1982).
50. Marucci, G. *Rheol. Acta* **18**, 193 (1979).
51. Marucci, G. *Macromolecules* **14**, 434 (1981).
52. Gottlieb, M. and Gaylord, R.J. *Polymer* **24**, 1644 (1983).
53. Gottlieb, M., Macosco, C.W. and Lepsch, T.C. *J. Polym. Sci., Polym. Phys. Ed.* **19**, 1603 (1981).
54. Gottlieb, M., Macosco, C.W., Benjamin, G.S., Meyers, K.O. and Merrill, E.W. *Macromolecules* **14**, 1039 (1981).
55. Gottlieb, M. and Macosco, C.W. *Macromolecules* **15**, 535 (1982).
56. Miller, D.R. and Macosco, C.W. *Macromolecules* **9**, 206 (1976).
57. Gaylord, R.J. and Douglas, J.F. *Polym. Bull.* **23**, 529 (1990).
58. Rivlin, R.S. *Philos. Trans. R. Soc.* **A241**, 379 (1948).
59. Treloar, L.R.G. *The Physics of Rubber Elasticity*, Clarendon, Oxford, 1975.
60. Valanis, K.C. and Landel, R.F. *J. Appl. Phys.*, **38**, 2997 (1967).
61. McKenna, G.B. and Hinkley, J.A. *Polymer* **27**, 1368 (1986).
62. Kearsley, E.A. and Zapas, L.J. *J.Rheol.* **24**, 483 (1980).
63. Jones, D.F. and Treloar, L.R.G. *J. Phys. D. (Appl. Phys.)* **8**, 1285 (1975).
64. Mooney, M. *J. Appl. Phys.*, **11**, 582 (1940).
65. Flory, P.J. *Chem. Rev*. 35, 51 (1944).
66. Vega, D.A., Villar, M.A., Alessandrini, J.L. and Valles, E.M. *Macromolecules*, **34**, 4591 (2001).
67. Edwards, S.F. and Muller-Nedebock, K.K. *J. Phys. A—Math. Gen.*, **32**, 3301 (1999).
68. Sommer, J.U., Vilgis, T.A. and Heinrich, G. *J. Chem. Phys.*, **100**, 9181 (1999).
69. Ryzmski, W.M. and Walska, B. *Polimery*, **48**, 246 (2003).
70. Graessley, W.W. *Macromolecules* **8**, 186 (1975).
71. Horkay, F., McKenna, G.B., Deschamps, P. and Geissler, E. *Macromolecules*, **33**, 5215 (2000).
72. Jackson, C.L. and McKenna, G.B. *Rubber Chem. Technol.*, **64**, 760 (1991).
73. Madkour, T. and Mark, J.E. *Polym. Bull.*, **31**, 615 (1993).
74. Saalwachter, K., Kleinschmidt, F. and Sommer, J.U. *Macromolecules*, **37**, 8556 (2004).
75. Ball, R.C., Edwards, S.F. and Warner, M. *Polymer* **22**, 1010 (1981).
76. Ball, R.C. and Edwards, S.F. *Macromolecules* **13**, 748 (1980).
77. DiMarzio, E.A. *J. Chem. Phys.*, **36**, 1563 (1962).
78. DiMarzio, E.A. *Polymer* **35**, 1819 (1994).
79. Deam, R.T. and Edwards, S.F. *Philos. Trans. R. Soc. Lond., A*, **280**, 378 (1978).
80. Edwards, S.F. *Proc. Phys. Soc.*, **92**, 9 (1967).
81. Gaylord, R.J. and Douglas, J.F. *Polym. Bull.*, **18**, 347 (1987).
82. Edwards, S.F. and Vilgis, Th. *Polymer* **27**, 483 (1986).
83. Kilian, H.G. *Polymer* **22**, 209 (1982).
84. Enderle, H.F. and Kilian, H.G. *Prog. Colloid Polym. Sci.*, **75**, 55 (1987).
85. Gao, J. and Weiner, J.H. *Macromolecules* **20**, 2520 (1987).
86. Gao, J. and Weiner, J.H. *Macromolecules* **22**, 979 (1989).
87. Deloche, B. and Samulski, E.T. *Macromolecules* **21**, 3107 (1988).
88. Wall, F.T. *J. Chem. Phys.*, **11**, 527 (1943).
89. Flory, P.J. and Wall, F.T. *J. Chem. Phys.*, **19**, 1435 (1951).
90. Hermans, J.J. *Trans. Faraday Soc.* **43**, 591 (1947).
91. James, H.M. and Guth, E. *J. Chem. Phys.*, **15**, 669 (1947).
92. James, H.M. and Guth, E. *J. Chem. Phys.*, **21**, 1039 (1953).
93. Guth, E. *J. Polym. Sci., Pt. C*, **12**, 89 (1966).
94. Erman, B. and Monnerie, L. *Macromolecules* **22**, 3342 (1989).
95. Kloczkowski, A., Mark, J.E. and Erman, B. *Macromolecules* **28**, 5089 (1995).
96. Douglas, J.F. and McKenna, G.B. in *Elastomeric Polymer Networks*, edited by J.E. Mark and E. Burak, Prentice Hall, Englewood Cliffs, NJ, 1993.
97. Rubinstein, M. and Panyukov, S. *Macromolecules* **30**, 8036 (1997).
98. Doi, M. and Edwards, S.F. *The Theory of Polymer Dynamics*, Clarendon Press, Oxford, England, 1986.
99. Munch, J.P., Candau, S., Herz, J. and Hild, G. *J. Phys.*, **38**, 971 (1977).
100. Doi, M. *J. Polym. Sci., Polym. Phys. Ed.* **21**, 667 (1983).
101. Rubinstein, M. and Panyukov, S. *Macromolecules* **35**, 6670 (2002).
102. Muthukumar, M. and Edwards, S.F. *J. Chem. Phys.*, **76**, 2720 (1982).
103. Muthukumar, M. *J. Chem. Phys.*, **85**, 4722 (1986).
104. des Cloiseaux, J. *J. Phys. (Les Ulis)* **36**, 281 (1973).

105. de Gennes, P.G. *Scaling Concepts in Polymer Physics*, Cornell, Ithaca, NY, 1979.
106. Flory, P.J. *Discuss Faraday. Soc.*, **49**, 7 (1970).
107. Ferry, J.D. *Viscoelastic Properties of Polymers*, Wiley, New York, 1970.
108. Queslel, J.P., Fontaine, F. and Monnerie, L. *Polymer* **29**, 1086 (1988).
109. Erman, B. and Mark, J.E. *Macromolecules* **20**, 2892 (1987).
110. Erman, B. and Mark, J.E. *Macromolecules* **25**, 1919 (1992).
111. Han, W.H., Horkay, F. and McKenna, G.B. *Math. Mech. Solids*, **4**, 139 (1999).
112. Allen, G., Kirkham, M.J., Padget, J. and Price, C. *Trans. Faraday Soc.*, **67**, 1228 (1971).
113. Mark, J.E. and Sullivan, J.L. *J. Chem. Phys.*, **66**, 1006 (1977).
114. Brotzman, R.W. and Mark, J.E. *Macromolecules* **19**, 667 (1986).
115. Sharaf, M.A. and Mark, J.E. *Polymer* **35**, 740 (1994).
116. Fontaine, F., Morland, C., Noel, C., Monnerie, L. and Erman, B. *Macromolecules* **22**, 3348 (1989).
117. Fontaine, F., Noel, C., Monnerie, L. and Erman, B. *Macromolecules* **22**, 3352 (1989).
118. Pak, H. and Flory, P.J. *J. Polym. Phys.,* **17**, 1845 (1979).
119. Kawamura, T., Urayama, K. and Kohjiya, S. *Macromolecules*, **34**, 8252 (2001).
120. Urayama, K., Kawamura, T. and Kohjiya, S. *Macromolecules*, **34**, 8261 (2001).
121. Urayama, K., Kawamura, T. and Kohjiya, S. *J. Chem. Phys.*, **118**, 5658 (2003).
122. Gee, G., Herbert, J.B.M. and Roberts, R.C. *Polymer* **6**, 541 (1965).
123. Freed, K.F. and Pesci, A.I. *Macromolecules* **22**, 4048 (1989).
124. Sivasailam, K. and Cohen, C. *J. Rheol.*, **44**, 897 (2000).
125. Obukhov, S.P., Rubinstein, M. and Colby, R.H. *Macromolecules,* **27**, 3191 (1994).
126. Graessley, W.W. *Polymeric Liquids and Networks: Structure and Properties*, Garland Science, New York, 2004.
127. Urayama, K. and Kohjiya, S. *J. Chem. Phys.*, **104**, 3352 (1996).
128. Urayama, K., Kawamura, T. and Kohjiya, S. *J. Chem. Phys.*, **105**, 4833 (1996).
129. Hild, G., Okasha, R., Macret, M. and Gnanou, Y. *Makromol. Chem.* **187**, 2271 (1986).
130. Hecht, A.M. and Geissler, E. *J. Phys.* **39**, 631 (1978).
131. Richards, R.W. and Davidson, N.S. *Macromolecules* **19**, 1381 (1986).
132. Zrinyi, M. and Horkay, F. *Macromolecules* **17**, 2805 (1986).
133. Horkay, F. and Zrinyi, M. *Macromolecules* **21**, 3260 (1988).
134. Chiu, D.S. and Mark, J.E. *Colloid Polym. Sci.* **255**, 644 (1977).
135. Chiu, D.S., Su, T.K. and Mark, J.E. *Macromolecules* **10**, 1110 (1977).
136. Rahalkar, R.R. and Mark, J.E. *Polym. J. (Tokyo)* **12**, 835 (1980).
137. Sung, P.H. and Mark, J.E. *J. Polym. Sci. Polym. Phys. Ed.* **19**, 507 (1981).
138. Andrady, A.L. and Llorente, M.A. *J. Polym. Sci. Polym. Phys. Ed.* **25**, 507 (1987).
139. Horkay, F. and Zrinyi, M. *Polym. Bull.* **4**, 21, 361 (1981).
140. Bristow, G.M. *J. Appl. Polym. Sci.* **9**, 1571 (1965).
141. Geissler, E., Hecht, A.M., Horkay, F. and Zrinyi, M. *Macromolecules* **21**, 2594(1988).

CHAPTER 30

Force Spectroscopy of Polymers: Beyond Single Chain Mechanics

Xi Zhang, Chuanjun Liu, and Weiqing Shi

Department of Chemistry, Tsinghua University, Beijing 100084, P. R. China

Abbreviations

AFM	atomic force microscopy
SMFS	single molecule force spectroscopy
Force curve	force-extension curve
FJC	freely jointed chain
WLC	worm-like chain
PDDA	poly(diallyldimethylammonium chloride)
PFDMS	poly(ferrocenyldimethylsilane)
THF	tetrahydrofuran
M-FJC	modified freely jointed chain
l_k	Kuhn length
L_c	contour length
k_B	Boltzmann constant
l_p	persistence length
CM-amylose	carboxymethyl amylose
CM-cellulose	carboxymethyl cellulose
PFS	poly(ferrocenylsilane)
PDMA	poly(dimethylacrylamide)
PDEA	poly(diethylacrylamide)
FTIR	the Fourier transform infrared spectrum
PEG	poly(ethylene glycol)
PVA	poly(vinyl alcohol)
PS	polystyrene
PNIPAM	poly(*N*-isopropylacrylamide)
PNIPAM-*seg*-PS	poly(*N*-isopropylacrylamide-*seg*-styrene)
F_{MPD}	the most probable desorption force
V_{stretch}	stretching velocity
pN	piconewton
PAMPS	poly(2-acrylamido-2-methylpropane-sulfonic acid)

The mechanical property of polymer materials is a classical topic in polymer science, however it is very difficult to be studied at a single chain level. To study and manipulate single polymer chain become possible because of the appearance of AFM [1]. Actually, AFM is not only a tool for the imaging of surfaces with high resolution, but also a high sensitive force sensor. SMFS, a new technique based on AFM, has become a platform for studying the minute force in polymers as well as in supramolecular systems [2–5]. The force signals versus extension curves can provide new insight into traditional aspects of polymer science, and moreover, some new information which is not accessible by conventional methods.

Besides AFM based SMFS, there are several other nanotechnologies which have also been used to measure the minute force in molecular scale, including magnetic beads [6], optical tweezers [7], glass microneedles [8], and biomembrane force probe [9]. These different methods can offer force signals with different timescale and sensitivity. The AFM based SMFS becomes popularized in single polymer chain experiment, because it is relatively easy to be handled. Till now, many elegant experiments have been done, such as the force–extension relationship of a normal random coil [10–21], for which force curves are fitted well by using the FJC or WLC model; the unfolding force of the titin Ig-domain [22–34], seen as a zigzag-like force curve; the chair-to-boat conformational transition of individual glucopyranose rings [35–43], which may be identified by a plateau in the force curves; the splitting or unwinding force of helical structure [10,11,37,38,44–47], for which a plateau or a kink has been observed in the force curve; and the detachment of single polymer chains from the substrate [48–57], for which a saw-tooth pattern or a long plateau has been achieved; based on the force fingerprint of amylose, the rupture force of silicon–carbon and sulfur–gold bonds has been measured [58].

Here we attempt to briefly introduce the principle of the AFM based SMFS and then focus on using SMFS to address three main questions: force induced conformation transition, interaction between small molecules and polymers, and the interfacial conformation and adhesive energy of polymers.

30.1 THE BASIC PRINCIPLE OF AFM BASED SMFS

30.1.1 The SMFS Methodology

The experiment of SMFS can be described as follows and the schematic drawing is shown in Scheme 30.1. In brief, the polymer chains are physisorbed or chemisorbed onto a solid substrate from their solutions. Then the sample is mounted onto the instrument. A drop of liquid, acting as the buffer, is injected between the substrate and the cantilever holder, and both the substrate and the cantilever are immersed in the buffer. By the movement of the piezo tube, the sample approaches the AFM tip. During this process, when there are no strong long-range interactions, the cantilever stays in its relaxed state, as shown in step 1, so only a base line, part a in graph A, is recorded. When the sample is brought into contact with the AFM tip, there exist a strong repulsion force between the tip and the solid substrate. As a result, the cantilever bends against the substrate, as shown in step 2. This repulsive signal is recorded and converted in the b region, which is perpendicular to the base line. The curve in graph A is called an approaching force curve. During step 2, polymer chains adsorb onto the AFM tip to form bridge structure between the AFM tip and substrate. That bridge structure will be stretched when the tip and substrate separate, resulting in the bending of cantilever toward the substrate, as shown in step 3. This process is traced and shown in region c in graph B. When the bridge structure is stretched further, the weakest part in it will break. At the same time the bent cantilever will go back to its relaxed state rapidly, resulting in a sudden drop of the force, seeing region d. The deflection of the cantilever and the displacement of the piezo tube are recorded at the same time. Then the deflection is converted into force signal, and the relationship between the force and the extension is obtained. More attention is paid to the retracting force curve, since it contains more information about the polymer chain being stretched.

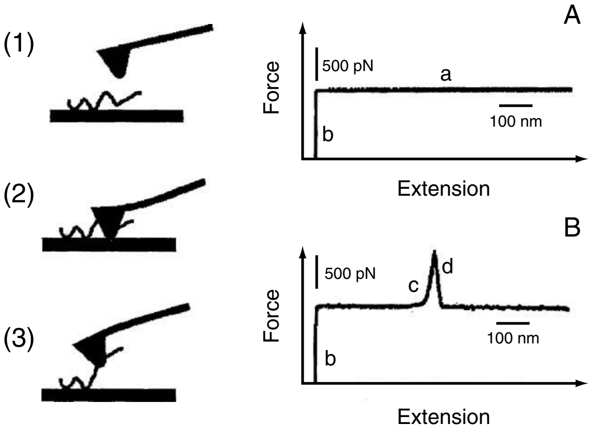

SCHEME 30.1. Schematic drawing of the principle of AFM based SMFS.

One of the key issues of the AFM based SMFS is to build a polymer bridge between the AFM tip and the substrate. The polymer chain can be immobilized onto the substrate by physical or chemical adsorption. In the physical adsorption, the polymer chains are simply adsorbed onto the substrate from their dilute solution. The physical adsorption is not that weak as expected, and actually the multipoint interaction between the polymers and the tip or substrate is strong enough to form a polymer bridge [4,5]. To obtain the single chain stretching, it is important to use a dilute polymer solution during the sample preparation. So the density of molecules at the solid–liquid interface will be low enough to suppress intermolecular entanglement and knotting, simplifying the explanation of the experimental data. However, the paucity of polymers on the substrate creates difficulty in obtaining a force signal. The optimal concentration of the polymer solution for the sample preparation varies for different polymer systems [5,16].

In the chemical adsorption, polymers bearing reactive groups react with the substrate or AFM tip, forming covalent bonds, as shown in Scheme 30.2. Two chemical modification methods are utilized frequently for the covalent bonding based anchoring of molecules on the solid substrate or AFM tip, including gold–thiol [14,58,59] and silanization chemistry [51,58]. When a chemical modification method is adopted during the immobilization process, one can decrease the surface density of polymers by incorporating ‘‘dilute molecules’’, such as short alkyl or hydroxy-silane, into the film [14]. The specific interaction, such as ligand–receptor interaction, can also be used in the immobilization of the polymer chains onto the substrate [35]. Recently, a new method is proposed to isolate polymer chains individually at the quartz surface by utilizing the defects in the self-assembled monolayers of organosilane. This method makes it possible to measure the desorption force of a single PDDA chain from a substrate directly [53].

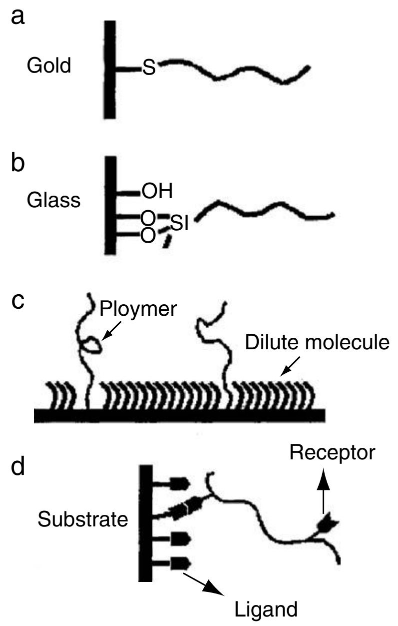

SCHEME 30.2. Schematic drawing of the immobilization of polymers on the solid support: (a) the gold–thiol chemistry; (b) silanization; (c) incorporating the dilute molecules; (d) ligand–receptor interaction.

30.1.2 Evidence on Single Chain Elongation

How can we confirm that the force extension curves are from the single polymer chains? We take single chain elongation of PFDMS as an example. The force curves of PFDMS in THF contain one force signal in each curve, as shown in Fig. 30.1, indicating that it is likely a single polymer chain elongation [21]. The contour length of the polymer chain is varied because the molecular weight of polymers is polydisperse, and the anchor points that attach to the tip or the surface is stochastic. To scale the contour length, the force curves of PFDMS are divided by the relative extension under the same force value, which is called normalizing process. The force signals from individual polymer chain should superimpose after the normalization, since the measured stretching force is linearly proportion with the relative extension [4]. The inset of Fig. 30.1 shows that the normalized force curves of PFDMS in THF superimpose well, which indicates the single chain stretching in the experiment. Moreover, if the stretching force can be controlled well below the rupture force, the PFDMS polymer chain can be stretched and relaxed repeatedly. There is no hysteresis between the stretching and relaxing force curves, as shown in Fig. 30.2, which suggests that the elongation of PFDMS polymer chain is in equilibrium condition and the elongation is reversible [21]. Fitting the force curves with the theoretical models, e.g., FJC and WLC models, is another way to check whether the force curves show the properties of the individual polymer chains. The details of the two models are described as follows. If all the force curves can be fitted well with similar parameters, it provides a further evidence of single chain experiment. Only after the above analysis we can conclude whether the force signals represent single chain characteristics or not.

30.1.3 M-FJC and WLC Models

The M-FJC is used to describe the extension of the polymer and the entropic restoring force generated. The M-FJC model treats a macromolecule as a chain of statistically independent segments of Kuhn lengths l_k, and the segment can be deformed under stress, as shown in Scheme 30.3a. The relationship between the extension and external force acting on the polymer chain is based on the extended Langevin function [13,60]:

$$x(F) = \{\coth[(Fl_k)/(k_BT)] - (k_BT)/(Fl_k)\}\,(L_c + nF/K_s). \tag{30.1}$$

In Eq. (30.1), F is the external force, x is the extension of polymer under external force (end to end distance), L_c is the

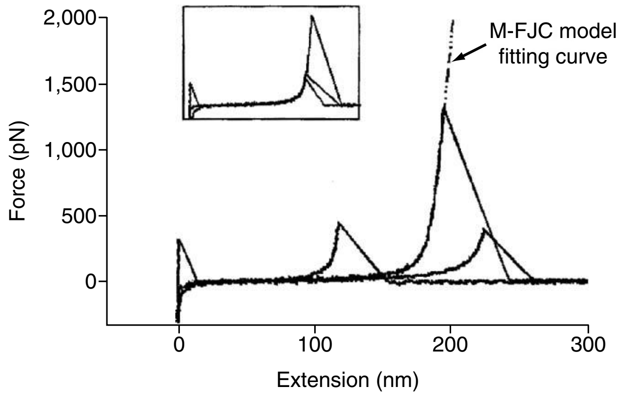

FIGURE 30.1. Several typical force curves of PFDMS in THF buffer. One of the force curves is fitted by the M-FJC model curve, shown in the dashed line. Inset: superposition of the normalized force curves. Reproduced from Macromolecules (2004) with permission from American Chemical Society [21].

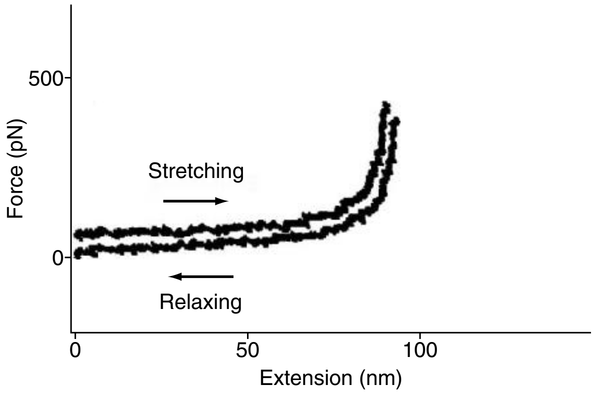

FIGURE 30.2. Successive manipulation of a PFDMS single chain, suggesting that the elongation of the polymer chain in the experiment is reversible. The stretching force curve is shifted. Reproduced from Macromolecules (2004) with permission from American Chemical Society [21].

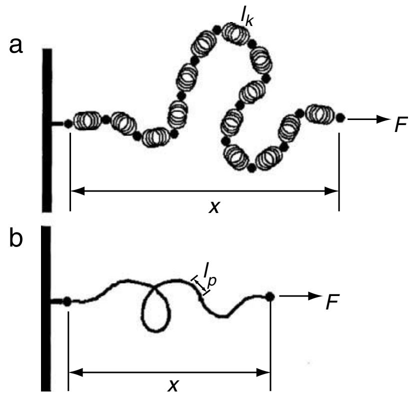

SCHEME 30.3. Schematic drawing of M-FJC and WLC models: (a) M-FJC model; (b) WLC model.

contour length of the polymer chain, n is the number of segments being stretched, k_B is the Boltzmann constant, and T is the temperature. The deformability of segments is characterized by a specific parameter, the segment elasticity, K_s. The elasticity of an M-FJC is dominated by the entropic contribution at low force region, and at high force region the elasticity is dominated by enthalpy as well as entropy.

Another model frequently used to describe the polymer chain is WLC. In WLC model, a polymer is treated as a homogenous string of constant bending elasticity. Both entropic and enthalpic contributions are combined in this model [6,61]. Scheme 30.3b shows the WLC model and the relationship between force and the extension of a WLC is shown as follows:

$$F(x) = [(1 - x/L_c)^{-2}/4 - 1/4 + x/L_c]k_BT/l_p. \qquad (30.2)$$

In Eq. (30.2), l_p is the persistence length.

Although the M-FJC and WLC models fit many systems investigated so far, it needs to be pointed out that the two models fail to describe the elastic behavior of polymers containing complex structures [12,13,16].

30.2 FORCE INDUCED CONFORMATION TRANSITION

Synthetic and natural polymers may undertake conformation transition upon external force. Different spectroscopic methods, e.g., FTIR and Raman spectroscopy, can be used to monitor their conformation transition the process, and with these methods the structure change can be revealed. However, it is rather difficult to manipulate a single polymer chain, and to determine the energy barrier that is needed to induce the conformation transition by conventional methods.

30.2.1 Fingerprinting Property of Polysaccharides

Polysaccharides are essential components of all living organisms and are the most abundant classes of biological polymers. Under an external force, the chair conformation, the most stable conformation of the glucopyranose ring, transforms into a boat conformation after passing over an energy barrier. A set of polysaccharides have been investigated by SMFS focusing on the unique transition has been reported [35–43]. For example, Rief *et al.* have studied the single chain elongation of dextran and observed that there are shoulder-like plateaus at 700–850 pN in the force curves, caused by a flip of the C5–C6 bond in the pyranose ring [35].

The various linkages of the glucose residues, such as α-(1,4) and β-(1,3)-linked, can influence the transitional energy during the elongation of the polysaccharides. CM-amylose and CM-cellulose are two isomers, and their primary structures only differ in the linkage of the glucose residues: CM-amylose is linked by α-D-(1,4)-glucosidic bonds, while CM-cellulose is β-(1,4)-linked. Li *et al.* and Marszalek *et al.* have independently found that the small difference in the primary structure induces a great difference in their chain elongation properties [36,39]. For CM-amylose, a marked shoulder-like plateau on the force curves is observed at about 300 pN. The plateau shows a 0.08 nm elongation of each glucose residue and the estimated energy to induce this conformational transition is about 7.3 kT per glucose residue [39]. For CM-cellulose, the force curves of the single chain elongation only show a sharp increase in force with the extension, and no plateau is present, as shown in Fig. 30.3. The different linkage influences the mechanical property of the polysaccharide chain greatly: each successive β-(1,4)-linked glucose residue can easily flip 180° to a extended conformation under external force; however, α-(1,4)-linked residues can easily adopt a chair–boat transition to achieve a extended conformation during the elongation. Hence the force induced conformational transition is a unique property of CM-amylose. Similar shoulder-like plateau is also observed in the force curves of heparin, which is another type of the familiar polysaccharides with the α-(1,4)-linkage [39]. This finding further confirms the fingerprint of the α-(1,4)-linked residues. In order to understand the physical nature of the force induced conformation transition, molecular dynamic simulation is needed to provide the molecular details: a chair–boat transition of the pyranose ring in CM-amylose will happen under external force; elongation of the β-(1,4)-linked pyranose ring induces only slight rotations which do not notably affect its elastic properties [62].

The force induced conformational transition of the pyranose ring will not arise if an oxygen bridge is introduced over the ring, as predicted by theory [63]. This interesting speculation can be confirmed by the experiments of single-chain force spectroscopy. Zhang and his coworkers have done the control experiment using a set of carrageenans bearing oxygen bridges or not and clearly found the influence of the oxygen bridge during the conformational transition [42]. As shown in Fig. 30.4, the primary structure of λ-, κ-, and ι-carrageenan are identical in one part of the repeating unit,

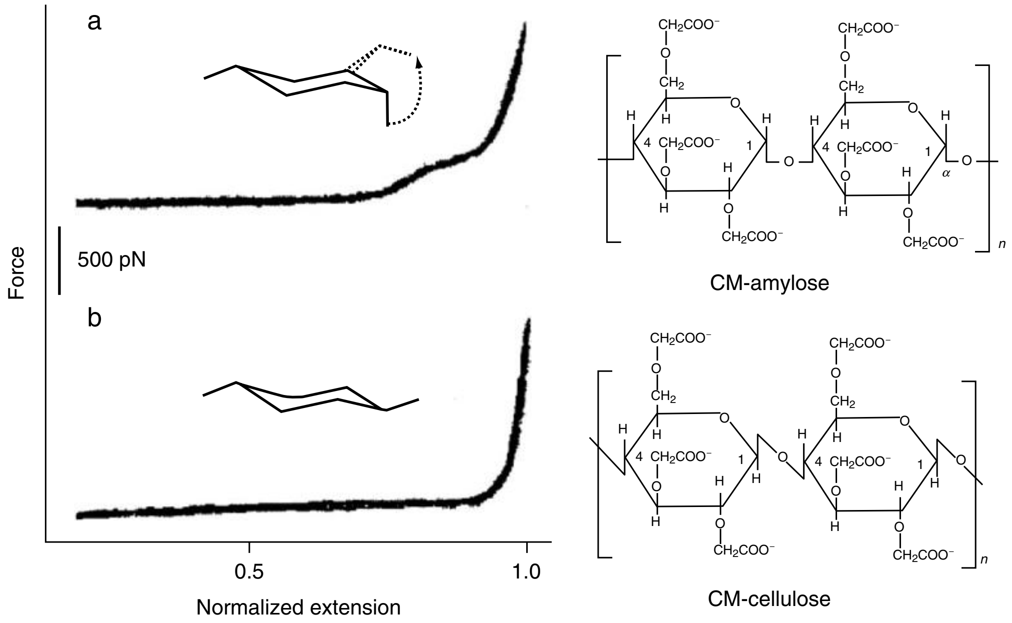

FIGURE 30.3. Comparison of normalized force curves of CM-amylose and CM-cellulose.

the 1,3-linked β-D-pyranose ring; however, there is an oxygen bridge over the 1-4-linked α-D-galactopyranose ring in the other part of the repeating unit of κ- and ι-carrageenan. The typical shoulder-like plateau about 300 ± 50 pN high appears in the force curves of λ-carrageenan, as shown in Fig. 30.4. This shoulder-like plateau indicates that force induced conformational transition can still take place in the elongation of the λ-carrageenan single chain if there are no oxygen bridges. But for κ- and ι-carrageenan, the shoulder-like plateaus disappear in the force curves and the M-FJC model can fit the force curves of κ- and ι-carrageenan well. These results suggest that the conformational transition of the galactopyranose rings is inhibited efficiently due to the additional barrier of the oxygen bridges.

30.2.2 Single-Molecule Optomechanical Cycle

SMFS has also proven to be a useful tool in the investigation of "molecular machine," whose working principle is based on the energy conversion cycle of stimuli-responsive

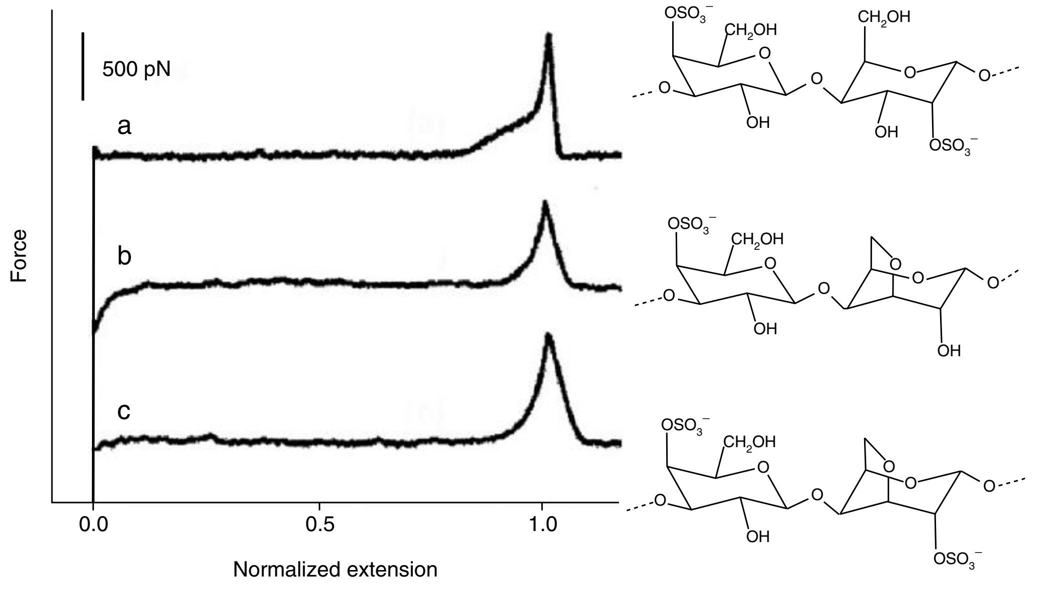

FIGURE 30.4. Primary structures of λ,κ,ι-carrageenan and the typical normalized force curves obtained on (a) λ-, (b) κ-, and (c) ι-carrageenan.

polymers. Gaub and his coworkers firstly demonstrate an example of the optomechanical energy conversion at single molecule level [64,65]. They utilize a stimuli-responsive polymer of synthetic polypeptide with multiple photoactive azobenzene groups incorporated into the backbone. The contour length of the polymer could be selectively lengthened or shortened by switching between the *trans*- and *cis*-azo configurations with 420 and 365 nm wavelength lights, respectively. In their experiment, the polymer end groups were covalently coupled to both the AFM tip and a supporting glass slide by heterobifunctional chemistry. As Fig. 30.5 shows, an individual azopolymer is first lengthened by five pulses with $\lambda = 420\,\text{nm}$ at a force of 80 pN (I) and then expanded mechanically to a restoring force of 200 pN (II). Then five pulses at $\lambda = 365\,\text{nm}$ are applied, resulting in a contraction of the polymer against the external force (III). Then the force on the polymer is reduced to 85 pN (IV). Finally, the cycle is completed by applying five pulses at $\lambda = 420\,\text{nm}$, resulting in an optical expansion of the molecule to its original length. From which, a new cycle can be started by switching the shortened configuration to the extended state.

Besides the optomechanical energy conversion, PFS can be used as a model system for the realization of an electrochemically powered molecular motor as proposed by Vancso *et al.* [66]. Surface immobilized PFS macromolecules are reversibly oxidized and reduced in situ by applying an electrochemical potential or chemically oxidized by addition of tetracyanoethylene. The entropic elasticity of the neutral PFS chains is found to be larger compared to the oxidized PFS in the lower force region, whereas the segment elasticity can be reversibly controlled in situ by adjusting the applied potential in electrochemical SMFS experiments. For a defined single PFS molecule operating cycle, a work of about 3.4×10^{-19} J is estimated based on the single chain experimental data. The efficiency is estimated as 5%, and it could be improved further if reducing the input energy [67].

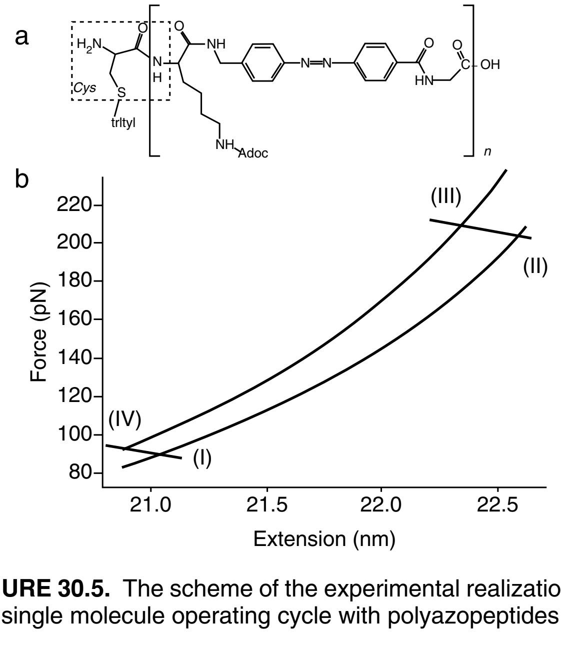

FIGURE 30.5. The scheme of the experimental realization of the single molecule operating cycle with polyazopeptides.

30.3 INTERACTION BETWEEN SMALL MOLECULES AND POLYMERS

Since the SMFS experiments are carried out at a solid–liquid interface in a liquid cell, it allows for studying the interaction between small molecules and polymers by easily changing buffers. The difference of the single chain elasticity before and after the addition of small molecules can indicate whether there exists interaction between the polymer and small molecules or not. Zhang *et al.* have employed PDMA and PDEA for studying their interaction with urea molecules [17]. It is well understandable that the single polymer chain of PDEA is stiffer than that of PDMA in deionized water because of the different substitutes, as shown in Fig. 30.6. The elasticity of the two polymers increases when using urea aqueous solution instead of the deionized water. In order to understand how the urea molecules affect the elasticity of the polymer, FTIR is used to identify the interaction between PDMA and urea molecules. The band at approximately $1{,}639\,\text{cm}^{-1}$ is attributed to the carbonyl stretching mode in the FTIR spectrum of PDMA film, while there is a shoulder at approximately $1{,}610\,\text{cm}^{-1}$ region in the spectrum of PDMA and urea mixture. These experimental data suggest the formation of hydrogen bonds between urea molecules and carbonyl groups of PDMA. Due to the formation of hydrogen bonds, urea can enlarge the enthalpic elasticity of the polymer backbone by binding to the side groups directly. In addition, the elasticity of PDMA chain is dependent on the concentration of urea, as shown in Fig. 30.7. The urea molecules have a similar influence on the elasticity of PDEA chain.

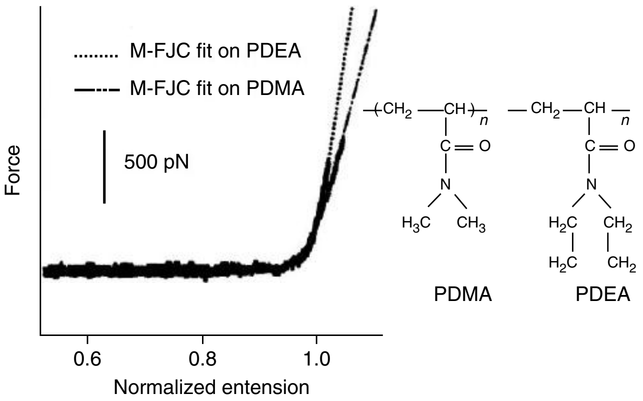

FIGURE 30.6. Primary structures of PDMA and PDEA, and a comparison of the normalized curve of PDMA and PDEA in water. The two dotted lines are the modified FJC fitting curves. Reproduced from Nano Letters (2002) with permission from American Chemical Society [17].

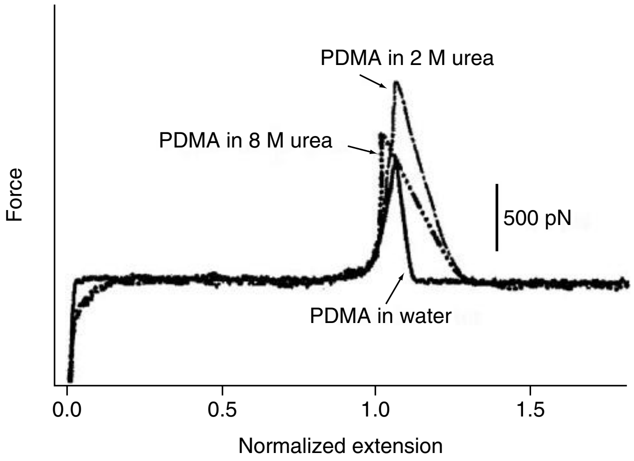

FIGURE 30.7. Comparison of normalized force curves of PDMA in water, 2 and 8 M urea aqueous solutions. Reproduced from Nano Letters (2002) with permission from American Chemical Society [17].

Of interest is that the effects of urea molecules on the elasticity of single PDMA and PDEA chains depend on the urea concentration. When comparing the elasticity between PDMA and PDEA in the 2 M urea buffer solution, the elasticity of PDEA is still greater than that of PDMA, similar to the situation in water. The discrepancy in the high force region may also be attributed to the effects of different side groups. However, in the 8 M urea buffer solutions, as shown in Fig. 30.8, no discrepancy is seen. This result indicates that when the concentration of urea solution is sufficiently high to become the dominating factor in determining the elasticity of a single polymer chain, the discrepancy in the elasticity between PDMA and PDEA is shielded completely.

There exists hydrogen bonding governed elasticity in many water-soluble polymers, such as PEG, and PVA [11–13]. The single chain elongation of PEG is like the behavior of an ideal entropic string in hexadecane, and can be described well with M-FJC model. However, in aqueous solution an evident deviation in the middle force region of the force curves is observed, indicating the deformation of a suprastructure within the polymer. The binding free energy is estimated as 3.0 ± 0.3 kT [13]. Further analysis of the force curves based on the Markovian two-level systems, agreeing well with the ab initio calculations, identifies the nonplanar suprastructure, water bridges, between the PEG chain and the water molecules.

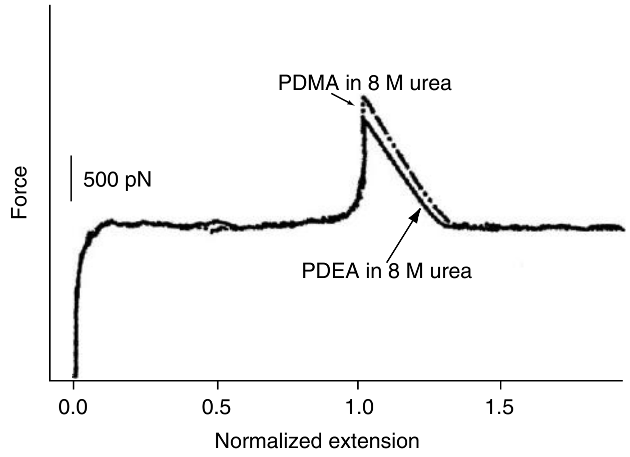

FIGURE 30.8. Comparison of normalized force curves of PDMA and PDEA in 8 M urea aqueous solution. Reproduced from Nano Letters (2002) with permission from American Chemical Society [17].

30.4 INTERFACIAL CONFORMATION AND ADHESIVE ENERGY OF POLYMERS

Polymers generally interact strongly with surfaces. Even if the gain of energy per monomer is weak, once a monomer is adsorbed, there is a strong probability that other monomers will also be adsorbed [68]. This energy gain must be compared to the entropy loss of the chain in order to predict its conformation [69]. So both enthalpy and entropy can drive the adsorption process. It has been generally known that the conformation of a long polymer chain adsorbed on a surface is in the form of a "train", "loop", or "tail", though lack of direct experimental evidence [70]. Let's take a few model systems to discuss the possibility by using AFM based SMFS to reveal the macromolecular conformation and the adhesive energy.

30.4.1 Saw-Tooth Pattern and The Loop Structure

For a homopolymer or statistically random copolymer chain, the adsorption normally results in a mixture of trains, loops, and tails on a surface. Therefore, one has no control over the number of monomer units adsorbed on each site. One can only measure the average interaction strength per chain, not per monomer unit, adsorbed on the substrate. To bridge the gap between force profile and interfacial conformation, Zhang and Wu have used a segment copolymer as a model system, in which short hydrophobic PS segments are more uniformly inserted into a linear PNIPAM chain backbone [71]. The structure and composition of such a copolymer chain are schematically shown in Scheme 30.4a. As this segment copolymer chains adsorb onto the PS substrate in water, it is reasonable to expect that the adsorption of insoluble short PS segments onto the PS substrate results in many PNIPAM loops, as shown in Scheme 30.4b. Therefore, the typical force curves of the segment copolymer on PS substrate exhibit a similar characteristic, saw-tooth pattern, as shown in Fig. 30.9. The analysis of the distance between each two adjacent peaks in the force curves, as shown in Fig. 30.10a, shows an average distance of about 114 nm. This value is very similar to the average length of the "repeat unit", i.e., one long PNIPAM segment plus one short PS segment, in the copolymer chain. These results suggest that the copolymer chain does form loops with a similar size on

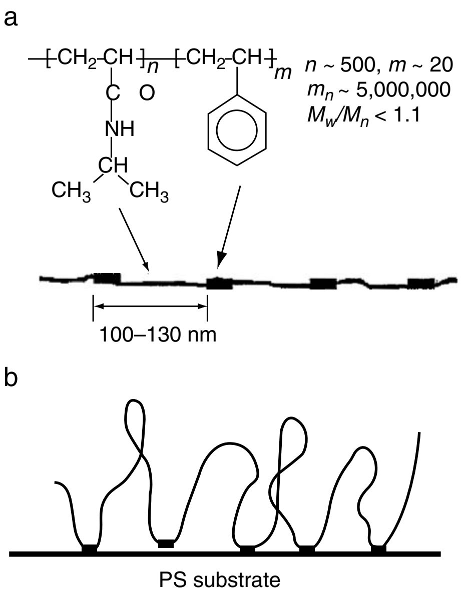

SCHEME 30.4. (a) Schematic of a linear segment PNIPAM-*seg*-PS prepared by micelle copolymerization, in which short PS segments are relatively evenly distributed on the chain backbone. (b) A possible adsorption conformation of a linear PNIPAM-*seg*-PS chain on a hydrophobic PS substrate in water. Reproduced from Macromolecules (2003) with permission from American Chemical Society [50].

the PS substrate. Therefore, the saw-tooth pattern corresponds to the detachment of the adsorbed segments in a single chain from the substrate. Moreover, the force curves obtained on a quartz substrate have single peak force signals, which is similar to PNIPAM [16]. This result is reasonable since short hydrophobic PS segments cannot adsorb onto the hydrophilic quartz substrate. This finding further confirms that the weak rupture force obtained on the PS substrate corresponds to the desorption of short PS segments from the PS substrate [50].

The most probable desorption force at a given stretching velocity, which is obtained from the histogram of desorption force, is about 41 pN, as shown in Fig. 30.10b. Such a distribution varies with the stretching velocity. The linear dependence of the most probable desorption force on the logarithm of the stretching velocity experimentally reveals that the adsorption and desorption of the PS segments on the PS substrate is a dynamic process [50]. Since it is known that each PS segment contains 20 monomer units on average, the desorption force for per PS monomer unit from the PS substrate in water is estimated in the range 1.3–2.1 pN, depending on the imposed stretching velocity.

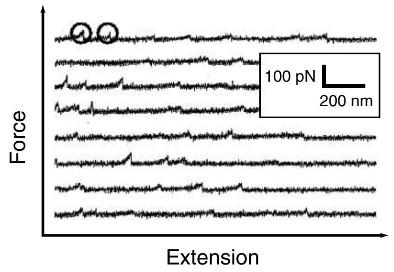

FIGURE 30.9. Measured force curves of linear segment PNIPAM-*seg*-PS chains adsorbed on a hydrophobic polystyrene substrate in water. Reproduced from Macromolecules (2003) with permission from American Chemical Society [50].

Besides the physical adsorption, the stable covalent attachment of a single or a small number of polymer molecules to AFM cantilever tip is a most important prerequisite in order to employ individual polymer molecules as interfacial, analytical probes for the identification and measurement of various types of polymer-surface interactions [54]. Recently, Haschke *et al.* have covalently attached polyacryamide molecule to the AFM cantilever tip. By approaching and retracting the tip with the molecule to the surface of interest, they have obtained force curves with multipeaks [72]. The covalent attachment of the chain to the tip ensures that any detachment measured in the force spectroscopy experiment is the force between the molecule and the sample surface. Therefore, the multipeaks of force curves correspond to detachment of multiple loops that are formed by the physisorption of polyacryamide at interface, as shown in Fig. 30.11.

30.4.2 Long Plateau Versus Train-like Structure

Provided that the polymer forms a train-like conformation at interface, the desorption force should be similar when detaching each adsorption point during the polymer chain elongation. As a result, the force curves should show a characteristic plateau. Seitz and his coworkers have used chemisorption to immobilize polyvinylamine polymer chain and studied the elasticity of the single polymer chain as a function of polymer's charge density and electrolyte concentration [51]. Their results indicate that, in addition to electrostatic interaction between polyvinylamine and negatively charged silica substrate which depends linearly on the Debye screening length and the polymer's line charge density, a constant nonelectrostatic interaction plays an important role in the desorption process [51].

PAMPS and its random copolymer containing 18-crown-6 (PAMPS-*co*-crown), are used to further study the nonelectrostatic contribution to desorption force [56]. The primary structures of polymers are shown in Scheme 30.5. As shown in Fig. 30.12, the typical force curves of PAMPS with a plateau are obtained from amino-modified quartz in the buffer of water. The long plateau suggests that the desorption process of the PAMPS chain from the substrate is smooth and that it adopts a train-like conformation at the interface and the desorption force remains about 120 pN. The desorption–adsorption process is in equilibrium in the experimental time scale, which is confirmed by the constant desorption force when changing the stretching velocity. The desorption force of PAMPS from the amino-modified quartz has been

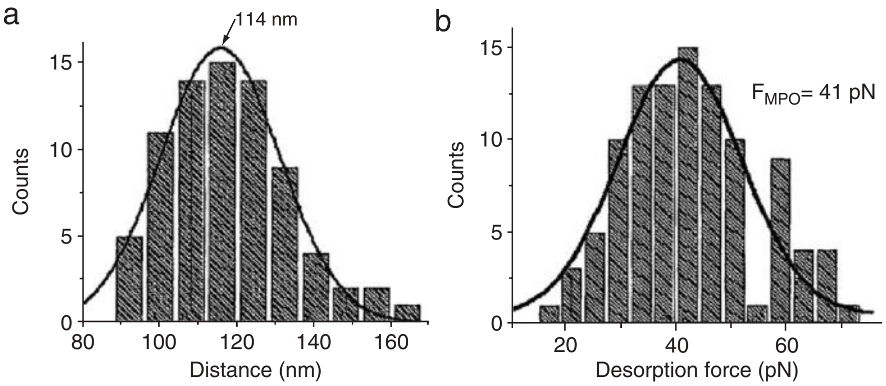

FIGURE 30.10. (a) Statistics of the distance between two adjacent peaks in the measured force curves. (b) Distribution of the measured desorption force for linear PNIPAM-*seg*-PS chains adsorbed on hydrophobic polystyrene substrate, where the stretching velocity is kept at 4,600 nm/s. Reproduced from Macromolecules (2003) with permission from American Chemical Society [50].

studied using different concentration of electrolyte as buffer. A series of experiments show that the external salt does not influence the desorption force of PAMPS.

In experiments, when the sample is immersed in the salt solution, the ion screening effect would influence largely on the electrostatic interaction but little on the nonelectrostatic interaction between the polyelectrolyte and the substrate [4,51]. It is possible for both the hydrophobic backbone and the charged groups of PAMPS to adsorb onto the substrate, since the static contact angle of amino-modified substrate is about 67°. It is reported that there is a "zero charge contribution" by about 38 pN in the ionic strength sensitive desorption force for the polyelectrolyte without spacer [51,54]. In the case of PAMPS, the introduced spacer between the charged groups and the backbone effectively enhances the nonelectrostatic contribution to the interfacial interaction, making the interfacial interaction insensitive to the ionic strength. These results together reveal the nonelectrostatic origin for the adsorption of the polyelectrolytes [56].

The force curves of PAMPS-*co*-crown obtained from amino-modified substrate are resembled to the curves shown in Fig. 30.12, which also show a long plateau with a height of about 120 pN. The long plateau indicates that PAMPS-*co*-crown chains also assume a train-like conformation at the interface. Similar to PAMPS, the desorption force of PAMPS-*co*-crown is independent of the concentration of electrolyte and the stretching velocity. The result indicates that the 20% content of crown ether side groups in the copolymer chain does not influence the desorption force. In other words, the interaction between PAMPS-*co*-crown chain and the substrate could be mainly dominated by the hydrophobic interaction. Based on the above discussion, SMFS allows to measure adhesive forces on the single molecule level and to gain new insight into the fundamental interactions in polymer adsorption.

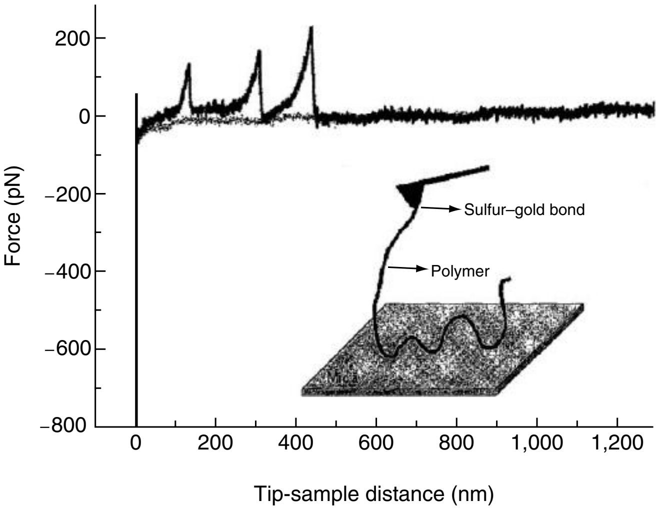

FIGURE 30.11. Force curve with a polyacrylamide molecule end-grafted to a gold-coated cantilever tip obtained on mica in water. Reproduced from Macromolecules (2004) with permission from American Chemical Society [72].

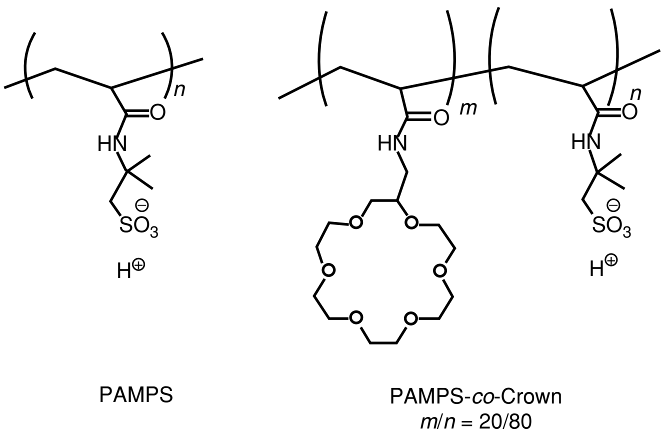

SCHEME 30.5. Primary structures of PAMPS and PAMPS-*co*-crown.

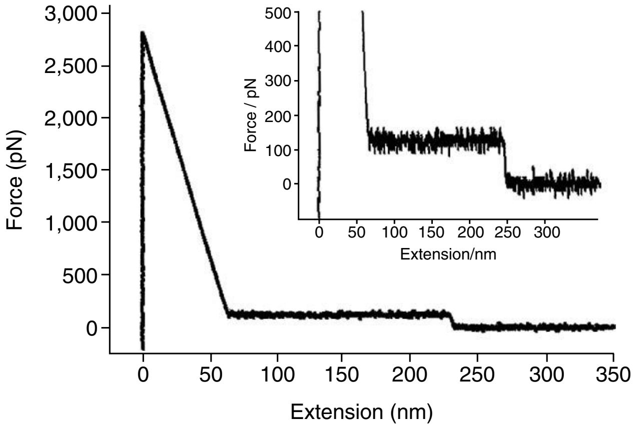

FIGURE 30.12. Typical force curve of PAMPS in water that shows a long plateau with a height of about 120 pN. Reproduced from Macromolecules (2004) with permission from American Chemical Society [56].

30.5 OUTLOOK

AFM based SMFS is a powerful tool in studying the intermolecular and intramolecular interaction in polymer systems, leading to opening a new field of nanomechanics of polymers. Although many elegant experiments have been performed, it must be point out that SMFS is still in the nascent stage. The technique itself can be improved and introduce new functions. For example, introduction of force clamp mode allow for following the dynamic process of the folding or unfolding probability of proteins [73]. It will be necessary to combine SMFS with other spectroscopic methods in order to link the force signal with structure change. In addition, theoreticians and experimenters need collaborate to realize the full potential of SMFS. After accumulating enough data in her information storeroom and in combination with other detection methods, SMFS will provide us new insight into the basic problems in polymer science and life science.

ACKNOWLEDGMENTS

This research was supported by the Major State Basic Research Development Program (G2000078102), National Natural Science Foundation of China (20474035), and Ministry of Education.

REFERENCES

1. Binnig G, Quate CF, Gerber C (1986) Phys. Rev. Lett. 56:930
2. Weisenhorn AL, Hansma PK, Albrecht TR, Quate CF (1989) Appl. Phys. Lett. 54:2651
3. Janshoff A, Neitzert M, Oberdorfer Y, Fuchs H (2000) Angew. Chem., Int. Ed. 39:3212
4. Hugel T, Seitz M (2001) Macromol. Rapid Commun. 22:989
5. Zhang WK, Zhang X (2003) Prog. Polym. Sci. 28:1271
6. Smith SB, Finzi L, Bustamante C (1992) Science (Washington, DC, US) 258:1122
7. Ashkin A, Schütze K, Dziedzic JM, Euteneuer U, Schliwa M (1990) Nature (London, UK) 348:346
8. Kishino A, Yanagida T (1988) Nature (London, UK) 334:74
9. Evans E, Ritchie K, Merkel R (1995) Biophys. J. 68:2580
10. Li HB, Liu BB, Zhang X, Gao CX, Shen JC, Zou GT (1999) Langmuir 15:2120
11. Li HB, Zhang WK, Zhang X, Shen JC, Liu BB, Gao CX, Zou GT (1998) Macromol. Rapid Commun. 19:609
12. Li HB, Zhang WK, Xu WQ, Zhang X (2000) Macromolecules 33:465
13. Oesterhelt F, Rief M, Gaub HE (1999) New J. Phys. 1:6.1
14. Ortiz C, Hadziioannou G (1999) Macromolecules 32:780
15. Bemis JE, Akhremitchev BB, Walker GC (1999) Langmuir 15:2799
16. Zhang WK, Zou S, Wang C, Zhang X (2000) J. Phys. Chem. B 104:10258
17. Wang C, Shi WQ, Zhang WK, Zhang X, Katsumoto Y, Ozaki Y (2002) Nano Lett. 2:1169
18. Zhang WK (2002) PhD Thesis, Jilin University
19. Zhang WK, Xu QB, Zou S, Li HB, Xu WQ, Zhang X, Shao ZZ, Kudera M, Gaub HE (2000) Langmuir 16:4305
20. Yamamoto S, Tsujii Y, Fukuda T (2000) Macromolecules 33:5995
21. Shi WQ, Cui SX, Wang C, Wang LY, Zhang X, Wang XJ, Wang L (2004) Macromolecules 37:1839
22. Rief M, Gautel M, Oesterhelt F, Fernandez JM, Gaub HE (1997) Science (Washington, DC, US) 276:1109
23. Rief M, Gautel M, Schemmel A, Gaub HE (1998) Biophys. J. 75:3008
24. Tskhovrebova L, Trinick J, Sleep JA, Simmons RM (1997) Nature (London, UK) 387:308
25. Oberhauser AF, Marszalek PE, Erickson HP, Fernandez JM (1998) Nature (London, UK) 393:181
26. Marszalek PE, Lu H, Li HB, Carrion-Vazquez M, Oberhauser AF, Schulten K, Fernandez JM (1999) Nature (London, UK) 402:100
27. Oberhauser AF, Marszalek PE, Carrion-Vazquez M, Fernandez JM (1999) Nat. Struct. Biol. 6:1025
28. Carrion-Vazquez M, Marszalek PE, Oberhauser AF, Fernandez JM (1999) Proc. Natl. Acad. Sci. USA. 96:11288
29. Carrion-Vazquez M, Oberhauser AF, Fowler SB, Marszalek PE, Broedel SE, Clarke J, Fernandez JM (1999) Proc. Natl Acad. Sci. USA. 96:3694
30. Li HB, Oberhauser AF, Fowler SB, Clarke J, Fernandez JM (2000) Proc. Natl Acad. Sci. USA. 97:6527
31. Carrion-Vazquez M, Oberhauser AF, Fisher TE, Marszalek PE, Li HB, Fernandez JM (2000) Prog. Biophys. Mol. Biol. 74:63
32. Yang GL, Cecconi C, Baase WA, Vetter IR, Breyer WA, Haack JA, Matthews BW, Dahlquist FW, Bustamante C (2000) Proc. Natl Acad. Sci. USA. 97:139
33. Li HB, Linke WA, Oberhauser AF, Carrion-Vazquez M, Kerkviliet JG, Lu H, Marszalek PE, Fernandez JM (2002) Nature (London, UK) 418:998
34. Linke WA, Kulke M, Li HB, Fujita-Becker S, Neagoe C, Manstein DJ, Gautel M, Fernandez JM (2002) J. Struct. Biol. 137:194
35. Rief M, Oesterhelt F, Heymann B, Gaub HE (1997) Science (Washington, DC, US) 275:1295
36. Marszalek PE, Oberhauser AF, Pang YP, Fernandez JM (1998) Nature (London, UK) 396:661
37. Li HB, Rief M, Oesterhelt F, Gaub HE (1998) Adv. Mater. (Weinheim, Germany) 10:316
38. Li HB, Rief M, Oesterhelt F, Gaub HE (1999) Appl. Phys. A 68:407
39. Li HB, Rief M, Oesterhelt F, Gaub HE, Zhang X, Shen JC (1999) Chem. Phys. Lett. 305:197
40. Marszalek PE, Pang YP, Li HB, Yazal JE, Oberhauser AF, Fernandez JM (1999) Proc. Natl Acad. Sci. USA. 96:7894
41. Marszalek PE, Li HB, Fernandez JM (2001) Nat. Biotechnol. 19:258
42. Xu QB, Zhang WK, Zhang X (2002) Macromolecules 35:871
43. Marszalek PE, Li HB, Oberhauser AF, Fernandez JM (2002) Proc. Natl Acad. Sci. USA. 99:4278
44. Rief M, Calusen-Schaumann H, Gaub HE (1999) Nat. Struct. Biol. 6:346
45. Clausen-Schaumann H, Rief M, Tolksdorf C, Gaub HE (2000) Biophys. J. 78:1997
46. Xu QB, Zou S, Zhang WK, Zhang X (2001) Macromol. Rapid Commun. 22:1163
47. Krautbauer R, Rief M, Gaub HE (2003) Nano Lett. 3:493

48. Zhang WK, Cui SX, Fu Y, Zhang X (2002) J. Phys. Chem. B 106:12705
49. Haupt BJ, Ennis J, Sevick EM (1999) Langmuir 15:3886
50. Cui SX, Liu CJ, Zhang WK, Zhang X, Wu C (2003) Macromolecules 36:3779
51. Hugel T, Grosholz M, Clausen-Schaumann H, Pfau A, Gaub HE, Seitz M (2001) Macromolecules 34:1039
52. Chatellier X, Senden TJ, Joanny JF, di Meglio JM (1998) Europhys. Lett. 41:303
53. Cui SX, Liu CJ, Zhang X (2003) Nano Lett. 3:245
54. Seitz M, Friedsam C, Jostal W, Hugel T, Gaub HE (2003) Chem. Phys. Chem. 4:986
55. Friedsam C, del Campo BA, Jonas U, Seitz M, Gaub HE (2004) New J. Phys. 6:9
56. Cui SX, Liu CJ, Wang ZQ, Zhang X, Strandman S, Tenhu H (2004) Macromolecules 37:946
57. Friedsam C, del Campo BA, Jonas U, Gaub HE, Seitz M (2004) Chem. Phys. Chem. 5:388
58. Grandbois M, Beyer M, Rief M, Clausen-Schaumann H, Gaub HE (1999) Science (Washington, DC, US) 283:1727
59. Oesterhelt F, Oesterhelt D, Pfeiffer M, Engel A, Gaub HE, Muller DJ (2000) Science (Washington, DC, US) 288:143
60. Smith SB, Cui YJ, Bustamante C (1996) Science (Washington, DC, US) 271:795
61. Senden TJ, di Meglio JM, Auroy P (1998) Eur. Phys. J. B 3:211
62. Heymann B, Grubmüller H (1999) Chem. Phys. Lett. 305:202
63. Eliel E, Allinger NL, (1974) Topics in Stereochemistry, Interscience: New York, Vol.8 p. 159
64. Hugel T, Holland NB, Cattani A, Moroder L, Seitz M, Gaub HE (2002) Science (Washington, DC, US) 296:1103
65. Holland NB, Hugel T, Neuert G, Cattani-Scholz A, Renner C, Oesterhelt D, Moroder L, Seitz M, Gaub HE (2003) Macromolecules 36:2015
66. Zou S, Ma YJ, Hempenius MA, Schonherr H, Vancso GJ (2004) Langmuir 20:6278
67. Zou S (2005) PhD Thesis, University of Twente
68. Levy R, Maaloum M (2004) J. Phys.: Condens Matter 16:7199
69. de Gennes PG (1979) Scaling concepts in polymer physics, Cornell University Press, New York
70. Conti M, Bustanji Y, Falini G, Ferruti P, Stefoni S, Samor B (2001) Chem. Phys. Chem. 2:610
71. Zhang GZ, Winnik FM, and Wu C (2003) Phys. Rev. Lett. 90: 035506
72. Haschke H, Miles MJ, Koutsos V (2004) Macromolecules 37:3799
73. Fernandez JM, Li HB (2004) Science (Washington, DC, US) 303: 1674